



**HAL**  
open science

## Definition of bifunctional theranostic molecules for cancer treatment

Tao Jia

► **To cite this version:**

Tao Jia. Definition of bifunctional theranostic molecules for cancer treatment. Cellular Biology. Université Grenoble Alpes, 2016. English. NNT : 2016GREAV086 . tel-01686187

**HAL Id: tel-01686187**

**<https://theses.hal.science/tel-01686187>**

Submitted on 17 Jan 2018

**HAL** is a multi-disciplinary open access archive for the deposit and dissemination of scientific research documents, whether they are published or not. The documents may come from teaching and research institutions in France or abroad, or from public or private research centers.

L'archive ouverte pluridisciplinaire **HAL**, est destinée au dépôt et à la diffusion de documents scientifiques de niveau recherche, publiés ou non, émanant des établissements d'enseignement et de recherche français ou étrangers, des laboratoires publics ou privés.

## THÈSE

Pour obtenir le grade de

### **DOCTEUR DE LA COMMUNAUTÉ UNIVERSITÉ GRENOBLE ALPES**

Spécialité : **Biologie Cellulaire**

Arrêté ministériel : 23 septembre 2016

Présentée par

**« Tao JIA »**

Thèse dirigée par « **Jean-Luc COLL** »

préparée au sein du **Laboratoire Institut Albert Bonniot,  
INSERM U1209, UMR CNRS 5309**  
dans **l'École Doctorale Chimie et Science du Vivant**

## Définition de molécules théranostiques bifonctionnelles pour le traitement du cancer

Thèse soutenue publiquement le « **date de soutenance** »,  
devant le jury composé de :

**Mme, Muriel, BARBERI-HEYOB**

Professeur, Nancy, France, Rapporteur

**M, Stephen, ROBINSON**

Group leader, Norwich, UK, Rapporteur

**M, Gilles, SUBRA**

Professeur, Montpellier, France, Examineur

**Mme, Eva, FAUROBERT**

Habilitation à diriger des recherches, Grenoble, France, Examineur

**Mme, Nadia, CHERRADI**

Habilitation à diriger des recherches, Grenoble, France, Président

**M, Jean-Luc, COLL**

Directeur de recherche, Grenoble, France, Directeur de THÈSE



# Acknowledgements

I want especially to thank my supervisor Dr. **Jean-Luc COLL** who provided me a strict but also tolerant research environment. Without your encouragement, great support and care neither my families nor I could enjoy four years staying in France.

To chemists Prof. **Gilles SUBRA** and Dr. **Jeremy CICCIONE**, you really deserve my special acknowledgements. Without your excellent and efficient work, I could not take charge of this huge, ambitious, and exciting project. I feel very happy and lucky to work with you. Thanks also to Prof. **Didier BOTURYN** and champion guy Mr. **Fabien THOREAU**, I enjoyed the discussion with you.

To Dr. **Beatrice EYMIN**, I send special thanks for your invaluable suggestions, understanding and help. I also enjoy the discussion with you.

To Prof. **Muriel BARBERI-HEYOB** and Dr. **Stephen ROBINSON**, great thanks for your valuable time to review my thesis. I would like also to thank Dr. **Eva FAUROBERT** and Prof. **Gilles SUBRA** for being the examiners of my PhD work.

To Dr. **Nadia CHERRADI**, great thanks for accepting to examine my thesis with the act of the committee's president. I also appreciate your advices and constructive criticism in the first two years of annual meeting of "Committee following PhD thesis".

To Dr. **Anastassia KARAGEORGIS**, I owe a huge debt of gratitude for your continued help and moral support, especially when arriving France in the beginning time.

I send huge thanks to the people of the Institute Albert Bonniot for your warmth and generosity, and especially to Dr. **Veronique JOSSERAND**, Ms. **Michelle KERAMIDAS**, Ms. **Laetitia VANWONTERGHEM**, Ms. **Celine BARRIAL**, Dr. **Amandine HURBIN**, Dr. **Julien GRAVIER**, Dr. **Sandrine DUFORT**, Miss. **Cherine ABOU FAYCAL**, Miss. **Anne-Sophie HATAT** and all the team 5 and 2 members. Thanks also to Mr. **Maxime Henry**, Ms. **Laetitia VANWONTERGHEM** and the members of FACS and Confocal platform (IAB), Ms. **Mylene PEZET**, Mr. **Jacques MAZZEGA**, Mr. **Alexei GRICHINE** for your excellent technical support.

To my families, **Mingsheng JIA** (Father), **Yuying LU** (Mother), **Hongmei CHEN** (Mother in Law) and my wife **Ruirui HU**, as well as my dear daughter **Chloé**, you are all staying in my deep heart. A special thank-you for your tolerance and belief in me.

I would like to acknowledge the financial support from **China Scholarship Council (CSC)** for 4 years that made my Ph.D study abroad possible.

Finally, thanks Grenoble, my families' and my second hometown!

# Preface

This work has been accomplished in team "Cancer Targets and Experimental Therapeutics" of the research center UGA / Inserm U1209 / CNRS 5309 in the Institute Albert Bonniot. It was realized under the supervision of **Jean-Luc COLL**.

This work gave reason for the following publications and presentations.

## Publications:

- Ciccione J\* & **Jia T\***, Coll J-L. *et al.* Unambiguous and controlled synthesis of multi-ligands silica nanoparticles. *Chem. Mater.*, 2016, 28 (3), pp 885–889 (\* Co-first author)
- **Jia T**, Ciccione J. *et al.* Dual targeting of integrins and Neuropilin 1 promotes endothelial cell proliferation and survival despite inhibiting VEGF/VEGFR2 . *Nature communications*, submission

## Poster Communication:

- Bifunctional Macromolecules: pros and cons for the definition of theranostic anticancer agents. **Jia Tao**, Ciccione Jérémie, Choi Jungyoon, Muriel Amblard, Said Jebors, Mehdi Ahmad, Martinez Jean, Gilles Subra, Jean-Luc Coll, EMBL Symposia: Tumour Microenvironment and Signalling, April/2016
- Development of multifunctional particles for diagnostic & targeted delivery in cancer therapeutics. **Tao Jia**, Jérémie Ciccione, Gilles Subra, Mickael Claron, Fabien Thoreau, Didier Boturyn, Jean-Luc Coll, Journée de la Recherche Médicale, Oct/2013

## Oral Presentation:

- Development of bifunctional theranostic molecules targeting tumor angiogenesis. **Jia Tao** Cancéropôle Lyon Auvergne-Rhône-Alpes (CLARA), Oct/2016
- Definition of bifunctional theranostic molecules for cancer treatment. **Jia Tao**, French Alternative Energies and Atomic Energy Commission (CEA), April/2016
- Bifunctional Nanoparticles: pros and cons for the definition of theranostic anticancer agents. **Jia Tao**, Ciccione Jérémie, Choi Jungyoon, Muriel Amblard, Said Jebors, Mehdi

*Ahmad, Martinez Jean, Gilles Subra, Jean-Luc Coll, European Nanomedicine Meeting 2015, Dec/2015*

- Screening of bifunctional nanoparticles for diagnostic & targeted delivery in cancer therapeutics. **Tao Jia, Jérémie Ciccione, Gilles Subra, Mickael Claron, Fabien Thoreau, Didier Boturyn, Jean-Luc Coll, ERC BIOMIM MEETING 2015 : At the Frontier between Materials and Biology, March/2015**

Honors And Awards:

- 2016 FRENCH AMERICAN DOCTORAL EXCHANGE PROGRAM 2016 TRAVEL GRANT
- 2015 Prize Sanofi: Best oral presentation in European Nanomedicine Meeting
- 2015 Two Minute Thesis Winner: Best oral presentation in annual meeting of Institute Albert Bonniot
- 2012-2016 National Scholarship for 4 years

# Abbreviations

---

AKT/PKB	Protein kinase B
BsAbs	Bispecific Antibodies
BMP2	Bone Morphogenetic Protein 2
CendR	C-terminal consensus R/KXXR/K sequence
CPPs	Cell-penetrating Peptides
cRGD	cyclic RGD
DAPI	4', 6-DiAmidino-2-PhenylIndole
DMSO	Dimethyl Sulfoxide
ECM	Extracellular Matrix
ECs	Endothelial Cells
EGF	Epidermal Growth Factor
eNOS	endothelial Nitric Oxide Synthase
EPR	Enhanced Penetration and Retention
ERK	Extracellular signal-regulated Kinase
FACS	Fluorescence Activated Cell Sorting
FAK	Focal Adhesion Kinase
FBP	Folate Binding Protein
FDA	Food and Drug Administration
FGF	Fibroblast Growth Factor
FITC	Fluorescein Isothiocyanate
GAG	glycosaminoglycan
GSK-3 $\beta$	Glycogene Synthase Kinase-3 $\beta$
Hg	Hedgehog
HRP	Horse Radish Peroxidase

---

---

i.v	Intravenous
ID	Injected Dose
IGF-1	Insulin-like Growth Factor-1
ILK	Integrin-linked Kinase
IR	Insulin Receptor
$k_a$	Association rate constant
$k_d$	Dissociation rate constant
$K_D$	Dissociation constants
MAPK	Mitogen-activated Protein Kinase
MFI	Mean Fluorescence Intensity
NP	Nanoparticle
NRP1	Neuropilin-1
OD	Optical Density
OS	Overall Survival
PBS	Phosphate Buffered Saline
PDGF	Platelet-derived Growth Factor
PDZ	Post synaptic density protein, Drosophila disc large tumor suppressor, Zonula occludens-1 protein
PEG	Polyethylene glycol
PI3K	Phosphoinositide 3-kinase
PK	Pharmacokinetic
PKC	Protein Kinase C
RTK	Receptor Tyrosine Kinase
SFK	Src-family Kinase
SPR	Surface Plasmon Resonance
TME	Tumor Microenvironment
VEGF	Vascular Endothelial Growth Factor

---

---

vSMCs

Vascular Smooth Muscle Cells

---

## Table of contents

<b>1</b>	<b>Overview</b>	<b>11</b>
<b>2</b>	<b>Introduction</b>	<b>12</b>
2.1	Tumor angiogenesis	12
2.2	Integrins and cancer	14
2.2.1	Presentation of integrins	14
2.2.2	Integrin signaling	16
2.2.3	Integrin $\alpha_v\beta_3$ as a target for cancer therapies	21
2.3	VEGFRs, Neuropilins and cancer	23
2.3.1	Presentation of VEGFRs	23
2.3.2	Presentation of Neuropilins	25
2.3.3	VEGFR2 signaling	29
2.4	Crosstalks among VEGFR2 and NRP1 as well as integrin $\alpha_v\beta_3$	32
<b>3</b>	<b>Angiogenesis and cancer targeted therapies</b>	<b>35</b>
3.1	Anti-angiogenic therapies targeting integrin $\alpha_v\beta_3$	35
3.2	Anti-angiogenic therapies targeting VEGF-VEGFR	37
3.3	Anti-angiogenic therapies targeting NRP1	39
3.4	Pros and cons of anti-angiogenesis therapies	43
<b>4</b>	<b>Nanoparticles and cancer therapy</b>	<b>46</b>
4.1	Passive targeting of nanoparticles to cancer	46
4.2	Active targeting of nanoparticles	50
4.2.1	Interest of ATWLPPR for cancer targeted therapies	52
4.2.2	Interest of RGD for cancer targeted therapies	54
4.3	Multifunctional targeting of tumors	56
4.3.1	Multivalent targeting for drug delivery	56
4.3.2	Pro and cons of heteromultivalent targeting	58
<b>5</b>	<b>Results Part 1</b>	<b>63</b>
5.1	Design of NPs	63
5.1.1	Design of the NPs A, B, C and D	63
5.1.2	Different chemical synthesis (FITC, Fluorine)	65
5.1.3	Characterization of receptor expression in the selected cell lines	65
5.1.4	Binding efficiency of naked-NP on endothelial and tumor cells	67
5.2	Binding of type A NP on endothelial and tumor cells	69
5.2.1	Binding of type A NP with increasing amount of peptides/NP	69
5.2.2	Binding of type A NP on tumor cells as a function of peptide ratios and concentrations	71
5.3	Binding of type A Fluorinated-NP on HUVEC and tumor cells	79
5.3.1	Interest of the presence of Fluorine	79
5.3.2	Results published in CM	81
5.3.3	Supplementary data attached to the CM publication	86
5.4	Conclusion:	88
<b>6</b>	<b>Results Part 2: Type A NPs on primary ECs</b>	<b>90</b>
6.1	NPs' binding efficiency	90
6.2	VEGFR2 blocking activity and NRP1 internalization	93
6.3	AKT signaling	96
6.4	MAPK/ERK signaling	102
6.5	RGD/ATW-NP protects HUVEC from cell death	106

6.5.1	RGD/ATW-NP prevents caspase-3 activation .....	106
6.5.2	RGD/ATW-NP prevents HUVEC cell death.....	108
<b>6.6</b>	<b><i>In vivo</i> evaluation .....</b>	<b>111</b>
<b>6.7</b>	<b>RGD/ATW-NP activates EGFR, IGF1-R/Insulin R and Met on HUVEC.....</b>	<b>118</b>
<b>6.8</b>	<b>Proposed model of action.....</b>	<b>121</b>
<b>6.9</b>	<b>Confirmation of these results on HDMEC .....</b>	<b>121</b>
<b>7</b>	<b>Results Part 3: Signaling on tumor cells .....</b>	<b>124</b>
7.1	Study of VEGF response on the tumor cell lines.....	124
7.2	At 100pM, ATW-NP blocks VEGF and AKT on PANC-1 cells.....	125
7.3	At 1nM, RGD/ATW-NP activates AKT on PANC-1 cells.....	126
7.4	PANC-1 cells proliferation is not affected .....	127
7.5	Conclusion and Discussion:.....	127
7.6	Supplementary data:.....	129
<b>8</b>	<b>Results Part 4: Comparative studies of type A, B and C NPs.....</b>	<b>132</b>
8.1	Binding of A, B and C-NP on HUVEC.....	132
8.2	Phosphorylation of AKT .....	133
8.3	Signaling pathways activated by type A, B or C NPs .....	136
8.4	Binding of A, B and C-NP on tumor cell lines.....	138
8.4.1	Impact of the number of peptide/NP .....	138
8.4.2	Binding of B NPs on 9 different cell lines.....	140
8.5	Conclusion and discussion:.....	144
8.6	Supplementary data:.....	146
<b>9</b>	<b>Final conclusion and perspective:.....</b>	<b>152</b>
<b>10</b>	<b>Materials and Methods.....</b>	<b>161</b>
<b>11</b>	<b>Appendix .....</b>	<b>171</b>
<b>12</b>	<b>References:.....</b>	<b>175</b>

# 1 Overview

Tumor angiogenesis refers to the ability of a tumor to stimulate new blood vessels formation. Angiogenesis strongly depends on cell surface receptors and integrin activation to promote tumor progression, local invasion and dissemination.

Intensive efforts have been made to block tumor angiogenesis by inhibiting integrins and VEGFR2 or its co-receptor Neuropilin-1 (NRP1) function. However, patients usually benefit modestly from this mono-therapy strategy, and their response varies greatly according to the dosage. These results can be understandable according to the biological complexity of tumors, which implies in particular the existence of several crosstalks among the different receptors and of numerous bypass systems.

The aim of my PhD project is to generate bi-functional macromolecules targeting the integrin  $\alpha_v\beta_3$  and NRP1 simultaneously. We generated different kinds of silica-based NPs and targeted peptides (Fig. 1).

My work is summarized in four parts.

- ❖ **Affinity** of the different molecules for selected cell lines
- ❖ **Selectivity** toward endothelial and tumor cells
- ❖ Biological response and **characterization of the** molecular cascades
- ❖ **Anti-angiogenic and antitumoral activities**

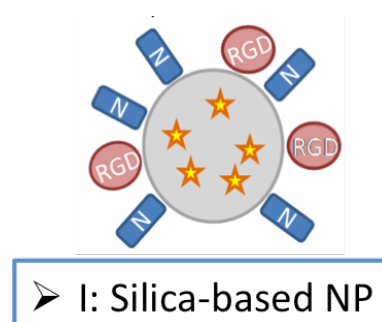


Fig.1 Schematic presentation of the molecule

## 2 Introduction

The vascular system has the critical function of supplying tissues with nutrients and clearing waste products. In the presence of a rapidly growing tumor, the formation of new blood vessels is necessary. The tumor will thus reactivate a physiological process called angiogenesis in emergency to form a new network of vessels for its irrigation. During angiogenesis, endothelial cells become activated, degrade local basement membranes, and the vessel begins to “sprout” with migrating tip cells leading a column of proliferating stalk cells.

### 2.1 Tumor angiogenesis

Tumor angiogenesis is very important to promote tumor initiation, progression and dissemination, and was initially listed as one of the six hallmark of cancer by R. A. Weinberg [1]. Like normal tissues, tumor cells also need blood to provide nutrients and oxygen as well as to evacuate metabolic wastes and carbon dioxide. When compared to the “well controlled” physiologic angiogenesis, important during development, wound healing and female reproductive cycling, the “angiogenesis switch” activated during tumor progression is constitutively activated and remains “on”.

Due to the specific hostile tumor microenvironment (hypoxia, low pH and high interstitial fluid pressure), the structure and function of tumor vessels are different from those of normal vessels (Fig. 2). Tumor neo-vasculature is marked by precocious capillary sprouting, convoluted and excessive vessel branching, distorted and enlarged vessels, erratic blood flow, micro-hemorrhaging, leakiness, inflammatory cells’ infiltration, and abnormal levels of cell proliferation and apoptosis as well as variable cellular plasticity of endothelial cells and pericytes [2, 3]. Notably, the tumors’ blood vessels themselves are also strikingly heterogeneous regarding their organization, structure, and function. An excellent review about the classification of tumor vessel types is presented by H. F. Dvorak and coworkers [4].

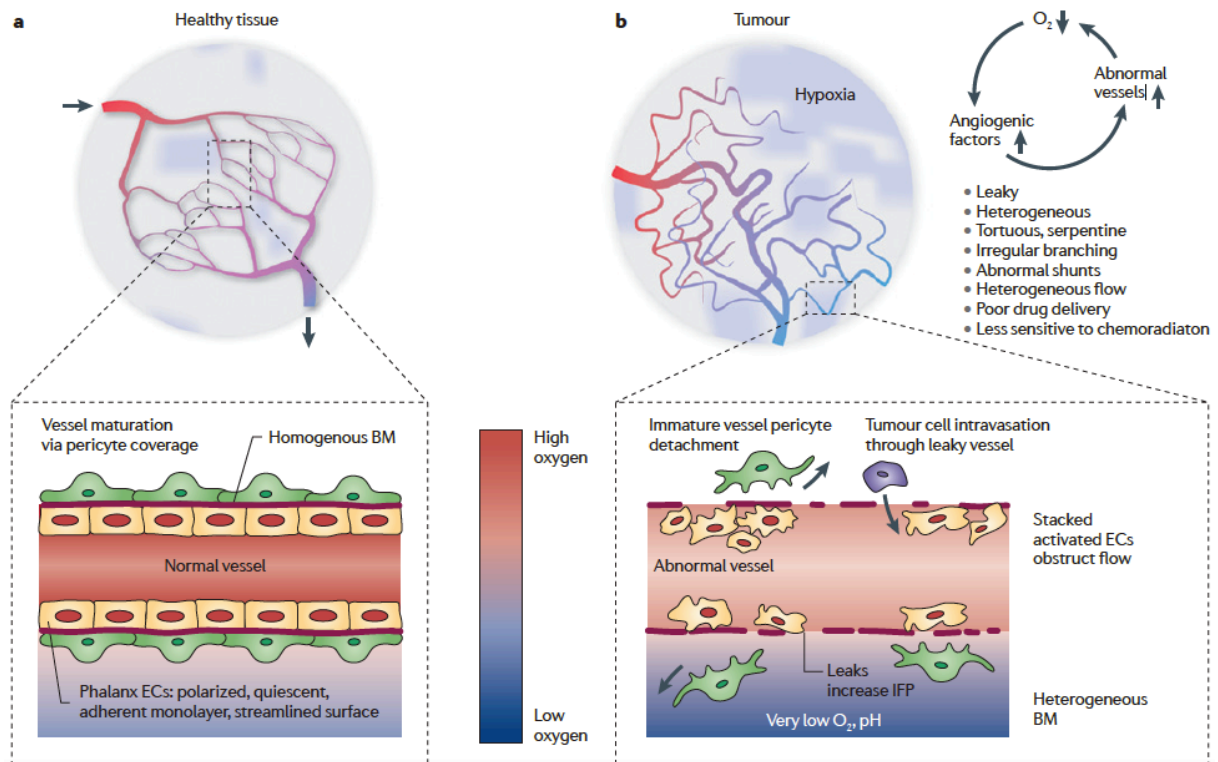


Fig. 2 Tumor vessels are structurally and functionally abnormal. A) In healthy tissues, a regularly patterned and functioning vasculature is formed (upper panel), with a normal vessel wall and endothelium (lower panel). B) In established tumors, the vasculature (upper panel), as well as the endothelium and vessel wall (lower panel) exhibit structural and functional abnormalities, leading to regions of severe hypoxia (represented by blue shading) [3].

Tumor angiogenesis is triggered and results from the activity of two groups of factors: activators and inhibitors. Activators include members of the vascular endothelial growth factor (VEGF) and fibroblast growth factor (FGF) families. Inhibitors include in particular thrombospondin-1 (TSP-1), interferons, angiostatin, endostatin, and many others [2]. When the balance between activators and inhibitors is in favor of endothelial cells activation, these activated cells will “sprout”. To do so, these cells must be capable of “sensing” their micro-environment and will modify their pattern of cell surface receptors accordingly. This is true in particular for the VEGF receptors and for integrins that are transmembrane receptors necessary for cell adhesion and mobility. These changes in the presentation and quantities

of receptors present on the surface of tumor-activated endothelial cells make perfect targets for the design of anti-angiogenic and anti-tumor drugs.

## 2.2 Integrins and cancer

### 2.2.1 Presentation of integrins

Integrins are heterodimeric cell adhesion receptors that bind to extracellular matrix ligands, cell-surface ligands, and soluble ligands. There are at least 18 $\alpha$  and 8 $\beta$  subunits that can dimerize to form more than 24 combinations that yield functional cell surface receptors. According to the ligand specificity, integrins can be classified in 4 groups: leukocyte-specific receptors, collagen receptors, laminin receptors and RGD receptors [5]. Individual integrins have unique ligand specificities (Table 1).

Integrins	Ligands
$\alpha_1\beta_1$	Laminin, collagen
$\alpha_2\beta_1$	Laminin, collagen, thrombospondin, E-cadherin, tenascin
$\alpha_3\beta_1$	Laminin, thrombospondin, uPAR
$\alpha_4\beta_1$	Thrombospondin, MAdCAM-1, VCAM-1, fibronectin, osteopontin, ADAM, ICAM-4
$\alpha_5\beta_1$	Fibronectin, osteopontin, fibrillin, thrombospondin, ADAM, COMP, L1
$\alpha_6\beta_1$	Laminin, thrombospondin, ADAM, Cyr61
$\alpha_7\beta_1$	Laminin

---

$\alpha_8\beta_1$	Tenascin, fibronectin, osteopontin, vitronectin, LAP-TGF- $\beta$ , nephronectin
$\alpha_9\beta_1$	Tenascin, VCAM-1, osteopontin, uPAR, plasmin, angiostatin, ADAM, VEGF-C, VEGF-D
$\alpha_{10}\beta_1$	Laminin, collagen
$\alpha_{11}\beta_1$	Collagen
$\alpha_V\beta_1$	LAP-TGF-en fibronectin, osteopontin, L1
$\alpha_L\beta_2$	ICAM, ICAM-4
$\alpha_M\beta_2$	ICAM, iC3b, factor X, fibrinogen, ICAM-4, heparin
$\alpha_X\beta_2$	ICAM, iC3b, fibrinogen, ICAM-4, heparin, collagen
$\alpha_D\beta_2$	ICAM, VCAM-1, fibrinogen, fibronectin, vitronectin, Cyr61, plasminogen
$\alpha_{IIb}\beta_3$	Fibrinogen, thrombospondin,, fibronectin, vitronectin, vWF, Cyr61, ICAM-4, L1, CD40 ligand
$\alpha_V\beta_3$	Fibrinogen, vitronectin, vWF, thrombospondin, fibrillin, tenascin, PECAM-1, fibronectin, osteopontin, BSP, MFG-E8, ADAM-15, COMP, Cyr61, ICAM-4, MMP, FGF-2, uPA, uPAR, L1, angiostatin, plasmin, cardiotoxin, LAP-TGF- $\beta$ , Del-1
$\alpha_6\beta_4$	Laminin
$\alpha_V\beta_5$	Osteopontin, BSP, vitronectin, CCN3, LAP-TGF- $\beta$

---

---

$\alpha_V\beta_6$	LAP-TGF-LA fibronectin, osteopontin, ADAM
$\alpha_4\beta_7$	MAdCAM-1, VCAM-1, fibronectin, osteopontin
$\alpha_E\beta_7$	E-cadherin
$\alpha_V\beta_8$	LAP-TGF-i

---

Table 1 Ligand-binding specificities of human integrins (modified from [6])

Integrins are among the most abundant cell surface receptors and are expressed in all cell types apart from erythrocytes [7], but the expression of different types of integrins is specifically limited to certain cell types or tissues. A special attention was paid in mammals to particular integrins such as  $\alpha_{IIb}\beta_3$  in platelets,  $\alpha_6\beta_4$  on keratinocytes;  $\alpha_E\beta_7$  for T cells, dendritic cells and mast cells in mucosal tissues,  $\alpha_4\beta_1$  on leukocytes,  $\alpha_4\beta_7$  in a subset of memory T cells [6]. In the present work, we will focused largely on integrin  $\alpha_v\beta_3$ , known as the vitronectin receptor, because it is selectively overexpressed on the surface of endothelial cells of growing blood vessels.

It must be emphasized that the expression of integrins varies spatially and temporally according to the cell type and lesion site. There are unique integrin profiles in myocytes versus fibroblasts or endothelial cells, in fetal versus adult myocytes [8]. For example, the  $\alpha_5$  and  $\alpha_7$  subunits are significantly more expressed in ischemic conditions. As well aortic constriction can increase  $\alpha_1$ ,  $\alpha_5$ ,  $\alpha_7$  and  $\beta_{1D}$  expression [9]. Differential splicing can also occur and adds an additional level of complexity in the integrins' repertoire. The  $\beta_1$  integrin has four isoforms, two of which are expressed in myocytes ( $\beta_{1A}$  and  $\beta_{1AD}$ ). The A form is predominantly detected in embryos, while the D form is highly expressed in adult myocytes [8]. They take different, but important functions in the development of the heart.

### 2.2.2 Integrin signaling

Integrin receptors have been well studied. They play vital functions in cell adhesion, signal transduction and cytoskeletal organization. Since they are presented on the cell membrane, they form a network of molecular signaling machinery between the cells and their environment through bi-directional signaling transmission. During their internalization, integrins associated trafficking is directly linked to molecular signaling cascades. This plays major roles in a number of pathological conditions, such as cancer [7]. How integrins orchestrate such a complex repertoire of functions is still a big and difficult question. For example, the exact nature of the conformational changes following the interaction of their cytoplasmic tail with intracellular activating proteins still remains controversial. A considerable variability in the composition of integrin-containing adhesion plaques is reported, and it is still unclear how the dynamics of integrins' assembly and turnover are determined [10]. Recently, Pere *et al.* emphasized that mechanical molecular pathways are also key regulators of cell function in addition to the better understood pathways that are activated biochemically [11]. More work still need to be done to explore the roles and functions of the integrins' network involved in the detection and transmission of mechanical forces, and to understand how this will impact on cell functions. I will introduce here only the classical biochemical view of the signaling and transduction pathways under control of the integrins' network.

Following ligand binding, integrins mediate an "outside-in" signaling. As well, integrins can also mediate an "inside-out" signaling. This is strongly related to the property of integrins to switch between high- and low-affinity conformations that control their affinity with the ligands.

From a functional point of view, the "outside-in" signaling can provide information to the cells such as their location, local environment, adhesive state, and quality of the surrounding matrix [10]. "Inside-out" signaling will provide additional capabilities and flexibility to the cells to adapt to its local environment and eventually also to modify it.

From a structural point of view, the bases of the "bi-directional" signaling are described in Fig. 3. In the resting condition, the extracellular domains of integrins have no ligands binding

and exhibit a bent (inactive) conformation. Once they received activation signals from the cells, the extracellular domains will unfold and keep a stable, extended and active conformation. These conformational changes will expose their active binding sites to external ligands, allowing the transmission of signals from the outside. The detailed mechanisms that explain how the extracellular head domain changes to a high affinity status, and how these changes will impact on its affinity and specificity toward ligands still need to be further explored. To activate the “inside-out” signaling, a large number of cytoskeletal and signaling molecules are involved in the formation of the activation tail. In particular, two proteins, talin and kindlins, bind separately to distinct regions of beta integrin’s cytoplasmic tails, but cooperatively act to separate the cytoplasmic tails and to activate the integrins [12-14]

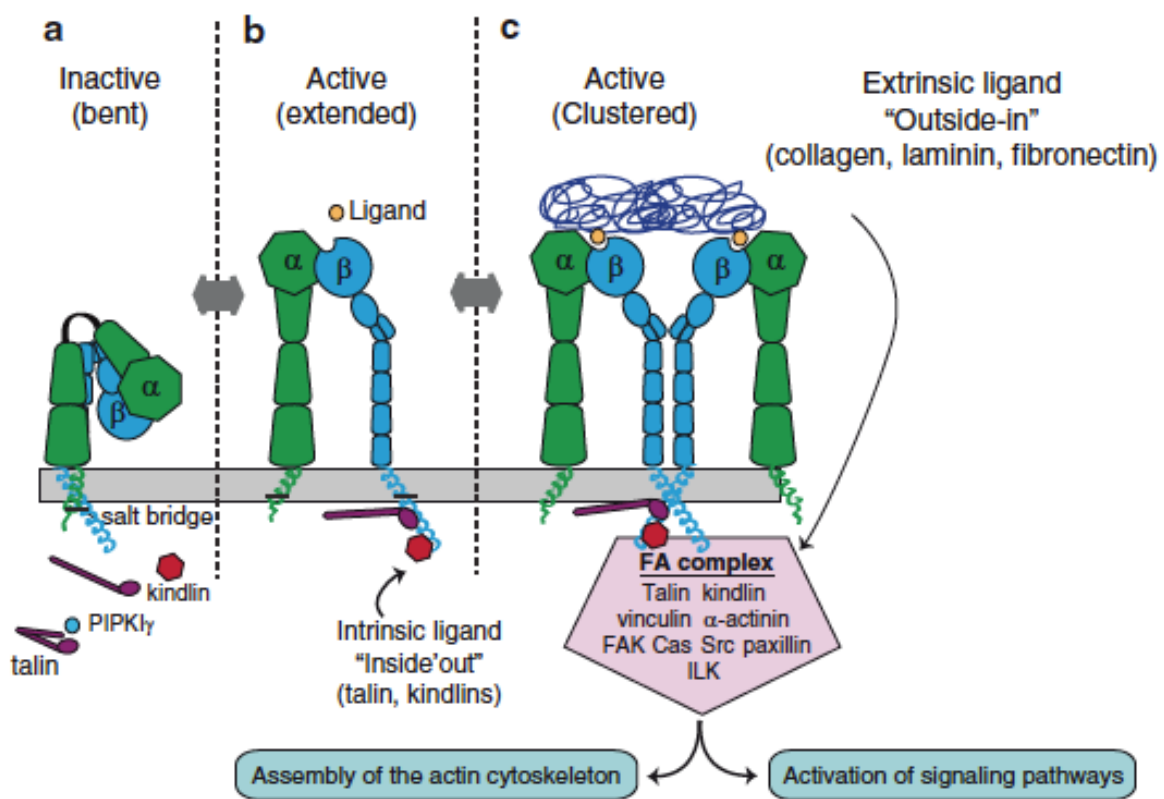


Fig. 3: Three different states indicating integrins conformational changes (R. Zent and A. Pozzi (eds.), Cell-Extracellular Matrix Interactions in Cancer).

Integrin-mediated “outside-in” signaling is very complex and affected by various crosstalks and network regulation that implies additional receptors such as RTK. Integrins do not have intrinsic enzymatic activity, but due to ligands’ binding, integrin clusters are formed, giving birth to focal adhesion (FA) complexes. This will activate downstream signaling pathways such as the Src-FAK, Ras-ERK/MAPK and PI3K/AKT cascades. Among the huge number of molecules contributing to this signaling, we can schematically isolate four different groups of signaling nodes (Table 2).

Signaling nodes	Main Function
<b>Focal adhesion kinase (FAK)</b>	<ul style="list-style-type: none"> <li>FAK acts as a phosphorylation-regulated signaling scaffold.</li> <li>Activated FAK forms a complex with SFK, this complex initiates multiple downstream signaling pathway.</li> </ul>
<b>Src-family kinase (SFK)</b>	<ul style="list-style-type: none"> <li>Recruited SFK activate downstream kinases and adaptors, and contribute to integrin-mediated cell adhesions.</li> <li>SFK can bind directly to beta integrin tails and control cell spreading.</li> </ul>
<b>Integrin-linked kinase (ILK)</b>	<ul style="list-style-type: none"> <li>ILK functions as a signaling scaffold at integrin adhesions.</li> <li>ILK directly phosphorylates downstream molecules such as GSK-3 <math>\beta</math>.</li> </ul>
<b>Non kinase proteins: Paxillin, Vinculin</b>	<ul style="list-style-type: none"> <li>Paxillin: a FAK- and ILK-binding protein, functions as a signaling scaffold and mediates binding of kinases, phosphatases, actin-binding proteins and Rho family members.</li> <li>Vinculin directly interacts with FA proteins including F-actin, talin, <math>\alpha</math>-actin etc.</li> </ul>

Table 2: Integrin signaling nodes and main functions.

Going back to integrin-mediated cell signaling during angiogenesis, Guido, *et al* presented an excellent review that emphasized that angiogenesis is characterized by the existence of opposed autocrine and paracrine loops implying several growth factors and semaphorins. These factors mediate the activation of integrins on the endothelial plasma membrane through a RTK and neuropilin/ plexin system [15]. More detailed information about these loops will be presented in the following chapters.

### 2.2.3 Integrin $\alpha_v\beta_3$ as a target for cancer therapies

Integrins function as very important regulators of cells' migration and invasion. The expression of integrins  $\alpha_v\beta_3$ ,  $\alpha_v\beta_5$ ,  $\alpha_v\beta_6$ ,  $\alpha_4\beta_1$ ,  $\alpha_5\beta_1$  and  $\alpha_6\beta_4$  correlates well with tumor progression [16]. As already seen,  $\alpha_v\beta_3$  is overexpressed in endothelial cells during angiogenesis, while it is not detected in quiescent endothelial cells of established blood vessels [17]. In several types of cancers such as lung, breast, brain and skin cancers,  $\alpha_v\beta_3$  is also highly expressed by the tumor cells [18], as shown in Fig. 4 [19]. A more detailed analysis confirmed that  $\alpha_v\beta_3$  expression is elevated in the active (central) part of the tumor (zone B).

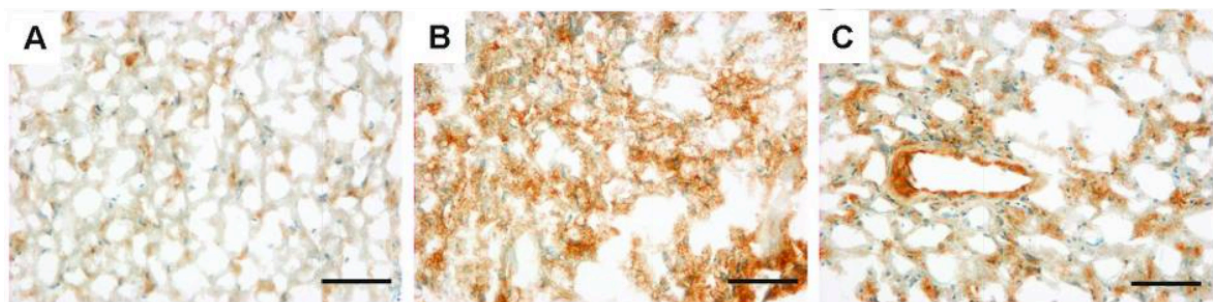


Fig. 4: IH studies of  $\alpha_v\beta_3$  (A-C) within the different parts of a tumor: center of the tumor next to a necrotic area (zone A), the vital central part of the tumor (zone B), and the infiltrating zone (next to the normal brain tissue, zone C) [19]. Scale bar is 100 $\mu$ m.

Because of its pattern of expression,  $\alpha_v\beta_3$  is one of the hot receptors for cancer targeted therapies as can be seen after a PubMed literature search (Fig. 5). In the past 10 years, 1210 publications are coming out when searching for the keywords “integrin alphavBeta3 AND

cancer”, while 8697 are obtained with “ integrin AND cancer”. Thus, ±14% of the publications on “integrin and cancer” are concerning  $\alpha_v\beta_3$ .

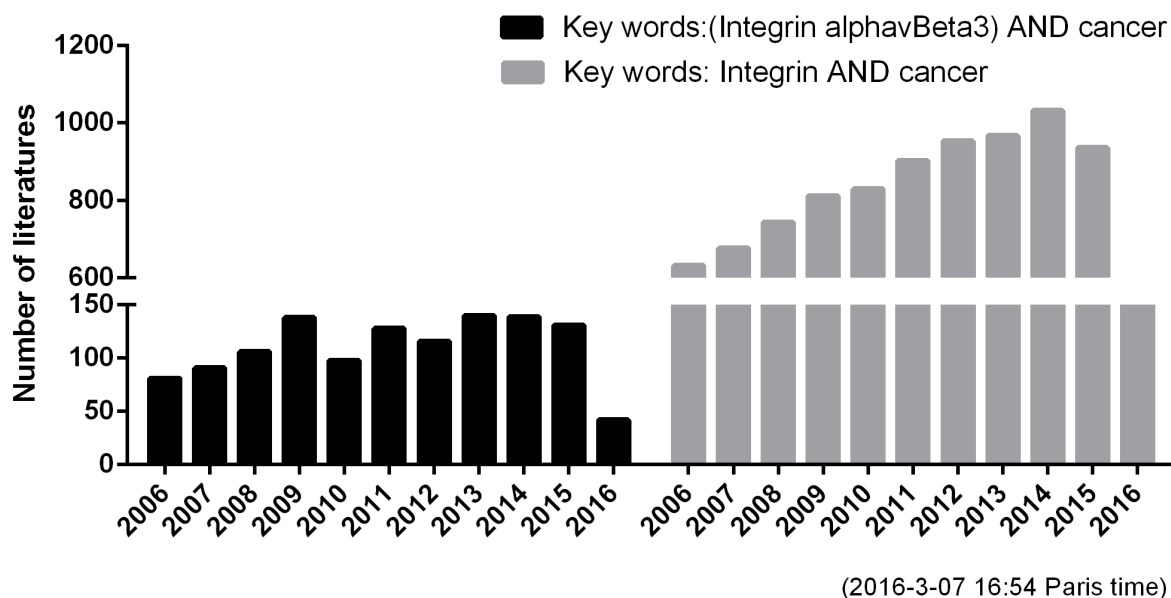


Fig. 5 Number of publications in PubMed

The crystal structures of the extracellular segment of  $\alpha_v\beta_3$  allowed a good characterization of its ligand-binding domain that reacts with the tri-peptide sequence RGD (Arg-Gly-Asp) [20, 21]. A very large series of peptides and peptidomimetics containing this sequence have been developed and used for cancer diagnosis and therapy. Of particular interest for anti-angiogenic therapies, cyclic RGD peptide was shown to selectively target tumor vasculature but also to impair angiogenesis and solid tumors’ growth and metastasis [22-24]. In our team, we developed an innovative molecule called RAFT-RGD, that presented a great potential for cancer targeted imaging and therapy [25, 26]. In addition to its role as an excellent delivery vector, cyclic RGD was reported to affect integrin  $\alpha_v\beta_3$  endocytosis by different pathways [27, 28] and thus to be a promising therapeutic candidate alone or in combination with other drugs to prevent tumor growth and metastasis. Recently, additional work proves that integrin trafficking contributes to cancer-related processes such as resistance to anoikis, anchorage independence and metastasis [29, 30]. Multivalent RGD scaffolds were found to present augmented cancer targeting and curing efficiencies as compared to the monomeric

peptide. I will give a detailed discussion about this point in the chapter “multifunctional targeting”.

## 2.3 VEGFRs, Neuropilins and cancer

### 2.3.1 Presentation of VEGFRs

Vascular endothelial growth factor (VEGF) was firstly identified as a mitogen promoting physiological and pathological angiogenesis. The family includes five members: VEGF A (known as VEGF), VEGF B, VEGF C and placenta growth factor (PlGF). Their classical receptors, VEGFR1, VEGFR2 and VEGFR3 [31] are listed in Table 4, and the correspondence between VEGFs and VEGFRs is summarized in Fig. 6.

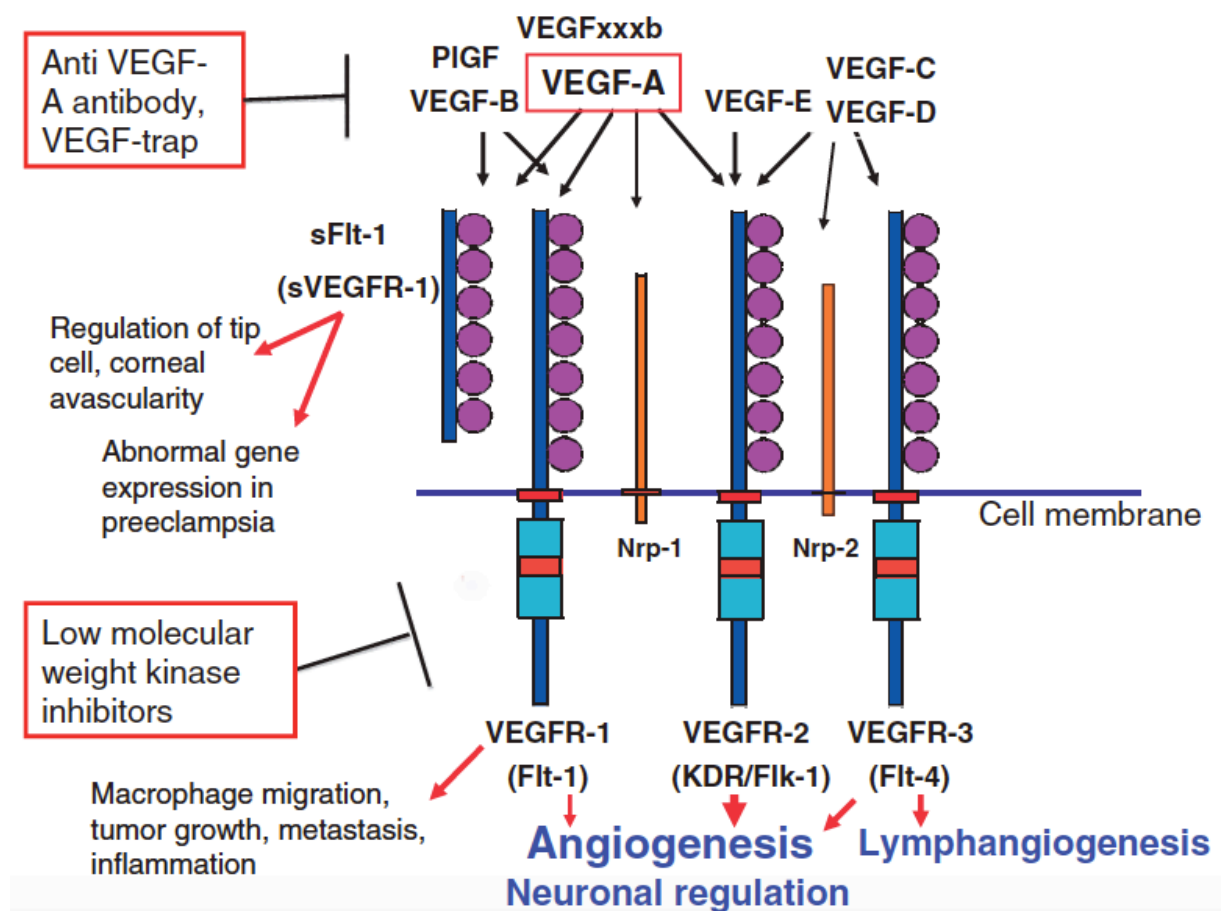


Fig. 6 Presentation of the VEGF-VEGFR system and their functions in physiological and pathological processes [22]

VEGF-A pre-mRNA alternative splicing generates at least 9 VEGFxxx variants with pro-angiogenic functions (VEGF<sub>111</sub>, VEGF<sub>121</sub>, VEGF<sub>145</sub>, VEGF<sub>148</sub>, VEGF<sub>162</sub>, VEGF<sub>165</sub>, VEGF<sub>183</sub>, VEGF<sub>189</sub> and VEGF<sub>206</sub>). But anti-angiogenic (VEGFxxx<sub>b</sub>) isoforms also exist that differ only from their VEGFxxx counterparts at the level of six amino acids in the C-terminal part of the protein owing to the selection of a distal splice site in the last exon 8. Several studies reported the differential pattern of expression of VEGF<sub>165b</sub> in cellular [32] and tumor models (Boudria et al. submitted).

With the exception of VEGF<sub>111</sub>/ VEGF<sub>111b</sub>, all VEGFxxx/ VEGFxxx<sub>b</sub> contain exons 1-5 and differ by the inclusion/ skipping of exon 6a, 6b, 7, 8a or 8b. Importantly, exons 6a and 7 confer affinity for heparin-containing proteoglycans and they will stick to the ECM. Schematically, short VEGF-A isoforms (C-terminal part) are diffusible, while larger are not. Fifty to seventy percent of VEGF<sub>165</sub> molecules are presented to the cell surface via the ECM. Importantly, at the molecular level, it has been shown that matrix-bound VEGF<sub>165</sub> induces different signaling patterns than soluble VEGF<sub>165</sub>. Therefore, the activity of VEGF-A splice variants will change if they are presented as freely diffusible ligands that can be internalized or as membrane-bound factors that will not be easily internalized. Furthermore, VEGF-A splice variants also present distinct affinities for various target receptors and co-receptors. To date, the signaling networks that differentially control the expression of various VEGF-A splice variants in tumors remains largely unknown.

VEGF<sub>165</sub> main biological activity is due to its predominant binding to VEGFR2 and its co-receptor, neuropilin-1 (NRP1) [33]. Unlike VEGFR2, VEGFR1 has a ten time higher affinity for VEGF<sub>165</sub>, but its kinase activity is much lower [34]. As we will see in the results part, 20ng/ml VEGF<sub>165a</sub> can induce a very strong, rapid and long lasting phosphorylation of VEGFR2 and of its downstream effectors FAK and AKT within as little as 7min, while no activation of VEGFR1 could be detected in these conditions. On the contrary, in several tumor cell lines, treatments with up to 200 ng/ml VEGF<sub>165a</sub> did not generate a detectable response in the

VEGFR2-AKT pathway. This strongly suggests that the activity of VEGF on endothelial versus tumor cells will have variable impacts on the tumorigenesis process. Indeed, its activity will differ widely whether we consider tumor angiogenesis, cancer stem cells' function, tumor metabolism, etc. Two very important reviews are describing the distinctive roles of VEGF in the tumor microenvironment [35, 36].

### 2.3.2 Presentation of Neuropilins

The NRP families are multifunction non-tyrosine kinase cell surface receptors involved in several fundamental signaling cascades. NRP1 and NRP2 are two conserved NRP family members in vertebrates. The structure of NRPs is containing briefly (Fig. 7): a N-terminal signaling peptide, two calcium-binding C1r/C1s/Uegf/Bmp1 (CUB) domains (a1a2), two coagulation factor V/VIII-like discoidin domains (b1b2), a Meprin/A5-antigen/ptp-Mu (MAM) domain (c), a single transmembrane helix, and a short intracellular domain [37]. Post-translational modifications are also critical for NRP functions. NRP1 and NRP2 can be modified both by N- and O-linked glycans [37] and their glycosaminoglycan (GAG) modification improves VEGF binding to NRP in vascular smooth muscle cells (vSMCs) and endothelial cells (ECs). Interestingly, GAG modifications decrease VEGFR2 expression in vSMCs only [38]. Recently, Usman and colleagues proposed an experimental model in which glycosylated-NRP1 is physically supporting the communication between myofibroblasts and soluble fibronectin. This could impact on the stiffness of the tumor matrix and participate to the formation of a favorable tumor microenvironment [39].

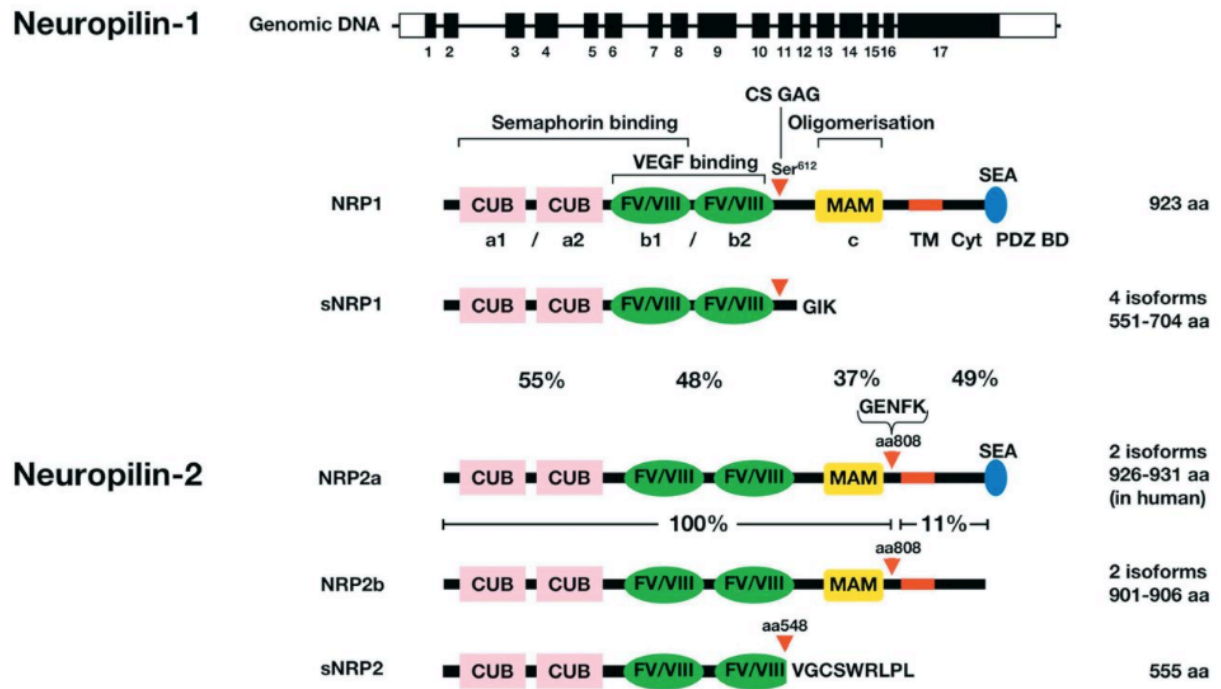


Fig. 7 Neuropilin gene organization and protein structure [40]

The different domains of NRP present diverse signaling and adhesive functions (Table 3). NRP was initially discovered as the semaphorin receptor involved in the axon guidance of neurons. Recently, more and more work emphasized NRP's pleiotropic roles, not only in VEGF-dependent angiogenesis but also in several VEGF-independent activities such as its critical positive capacity to regulate the hedgehog (Hh) signaling pathway [41, 42].

Ligand	NRP1 domain	Effect
SEMA3A	CUB (a1/a2) extracellular domain	Promotes prolonged T cell–DC interaction and T cell activation and IL-10 secretion
SEMA4A	CUB (a1/a2) extracellular domain	Promotes contact-independent Treg function (via IL-10 & IL-35) and maintains Treg stability in vivo
TGF- $\beta$ & TGF- $\beta$ RI/II/III	b1/b2 extracellular domain	Activates latent LAP–TGF- $\beta$ enhancing TGF- $\beta$ immune suppression and TGF- $\beta$ mediated Treg generation. TGF- $\beta$ RI–NRP1 complex formation also enhances TGF- $\beta$ activity
VEGF <sub>165/145</sub>	b1/b2 extracellular domain	VEGF <sub>165</sub> enhances VEGFR2–NRP1 complex formation by acting as a ‘bridging molecule’—this enhances pro-angiogenic effects of VEGF <sub>165</sub>
VEGFR1/2	b1/b2 extracellular domain	VEGFR2–NRP1 complex formation enhances VEGF <sub>165</sub> binding and pro-angiogenic effects
EGFR	NRP1 extracellular domain, possibly b1/b2 domain	NRP1 binds the oncogene EGFR enhancing its downstream signalling activity via AKT phosphorylation—this promotes tumour cell differentiation and proliferation
HGF	b1/b2 extracellular domain	NRP1–HGF binding enhances c-Met signalling promoting endothelial cell proliferation and angiogenesis
HGFR (or c-Met)	CUB (a1/a2) extracellular domain	NRP1–HGFR complex is internalised in a HGF-dependent mechanism resulting in increased cancer cell invasiveness (observed in a model of human PDAC)
PDGF	Unconfirmed physical interaction with NRP1; possibly b1/b2 domain	PDGF upregulates NRP1 expression promoting VSMC mobilisation and angiogenesis
PDGFR- $\alpha$	b1/b2 extracellular domain	NRP1 binding enhances PDGFR- $\alpha$ affinity for PDGF, promoting MSC and VSMC mobilisation, tissue remodelling and angiogenesis
FGF2	Unconfirmed physical interaction with NRP1; possibly b1/b2 domain	NRP1 binding of FGF2 enhances the FGF2 growth stimulatory functions and pro-angiogenic activity
PIGF	b1/b2 extracellular domain	PIGF signals through its receptor, NRP1, promoting angiogenesis and tumour growth

Table 3 Summary of NRP1 interactions with extracellular ligands (modified from [43]).

NRP’s expression in normal tissues and in cancer is summarized in Table 4. Due to alternative splicing, NRP also contains secreted isoforms that can function as autocrine (natural) inhibitors [44, 45] like soluble VEGFR. Soluble NRP and VEGFR are now reported as possible biomarkers for cancer staging and prognosis [46–49]. Whether soluble NRP1 could be harnessed for anti-angiogenesis and anti-tumors therapies is an interesting question, which is discussed in the chapter of "Anti-angiogenic therapies targeting NRP1".

Computational biology and modeling are now offering promising approaches to investigate the VEGF reactivity with VEGFR and NRP [50, 51], but the evaluation of the quantity of each receptor is still a major issue in particular to be able to evaluate the angiogenic signaling balance. The quantification of VEGF receptors were reported by several groups, but the results are not reliable because of the use of different type of cells (non-human, clonal and transfected cells) [52], culture conditions (with or without serum), donor origin (single or

pooled), and *in vitro* versus *ex vivo* analysis. The level of expression of these receptors is highly variable in particular in primary cells [53]. In our model, VEGF downregulates VEGFR2 expression within 15min. This demonstrates that VEGF receptors are very sensitive to external changes. This is an extremely important notion to keep in mind since this phenomenon has to be considered very carefully when we investigate these pathways.

<b>VEGF receptors</b>	<b>Normal condition</b>
<b>VEGFR1</b>	monocytes, macrophages, human trophoblasts, renal mesangial cells, vascular smooth muscle cells and dendritic cells
<b>VEGFR2</b>	vascular endothelial cells and their embryonic precursor, pancreatic duct cells, retinal progenitor cells, megakaryocytes and haemopoietic cells
<b>VEGFR3</b>	primary vascular plexus, venous endothelial cells in cardinal vein, lymphatic endothelial cell, osteoblasts, neuronal progenitors and macrophages
<b>NRP1</b>	plasmacytoid dendritic cells, T regulatory cells, activated T cells (CD4+), vascular endothelial cells, vascular smooth muscle cells, pericyte, fibroblasts (occasionally)
<b>NRP2</b>	Lymphatic endothelial cells, venous endothelial cells, alveolar macrophages, fibroblasts (occasionally)
<b>VEGF receptors</b>	<b>Cancer</b>
<b>VEGFR1</b>	Bladder, brain, breast, colon, head and neck, lung, melanoma, mesothelioma, myeloid leukemia, mesothelioma, myeloid leukemia, esophageal, ovarian, pancreatic and prostate

---

<b>VEGFR2</b>	Bladder, brain, breast, cervical, colon, endometrial, gastric, head and neck, hepatocellular, lung, melanoma, mesothelioma, multiple myeloma, myeloid leukemia, esophageal, ovarian, pancreatic, prostate, renal cell carcinoma, squamous and thyroid
<b>VEGFR3</b>	Breast, cervical, colon, gastric, head and neck, lung, esophageal, prostate
<b>NRP1</b>	Brain, breast, colon, lung, melanoma, ovarian, pancreatic, prostate and tumor associated fibroblasts
<b>NRP2</b>	Bladder, breast, colon, lung, melanoma, ovarian, pancreatic, prostate, renal cell and tumor associated fibroblasts

---

Table 4 Expression of VEGF receptors in human normal tissues and cancer [31, 43, 54-56]

### 2.3.3 VEGFR2 signaling

VEGFR2 belongs to the family of monomeric RTKs (as the EGF and PDGF receptors). In general, bivalent VEGF interacts simultaneously with two VEGFR2 monomers and crosslinks them. These active transmembrane dimer forms are compatible with trans-autophosphorylation, stimulation of RTK activity and downstream signal transduction that include PI3K, Src, FAK, etc. The specificity of signaling nodes' recruitment is controlled by the choice of VEGFR2-tyrosine residues that will be phosphorylated. As an example, Y1175 present in the C-terminal tail of VEGFR2 is critical for the recruitment of SHB (an adaptor protein). Recruited SHB binds to FAK and regulates VEGF-induced formation of focal adhesions and cell migration [57]. Besides this Y1175 site, Y951 located in the kinase insert domain, Y1054 and Y1059 within the kinase domain, as well as Y1214 in the carboxy-terminal domain are also directly associated with VEGFR2 signaling [58]. In my hands, the amplitude and kinetics of phosphorylation of each different tyrosine sites are really different; for example, Y1175 site of VEGFR2 is more sensitive to the presence of 20ng/ml VEGF<sub>165a</sub> in HUVEC cells. The spatial and temporal changes in the phosphorylation of each residue

dynamically regulate the VEGF-mediated specific functions: EC-migration, EC-permeability, EC-proliferation. Clarifying the wide range of signal transduction mediators involved in VEGF-induced cell response is still a very challenging work, especially *in vivo*.

As already discussed, VEGF-mediated signal transduction via extracellular Ig-like domains 2 and 3 of VEGFR2 results in a wide biological response of ECs. This will affect their proliferation, migration, survival and permeability. A signal is transmitted via a complex network involving PI3K/AKT, Ras/ MAPK, PLC, p38 and FAK (Fig. 8) [58].

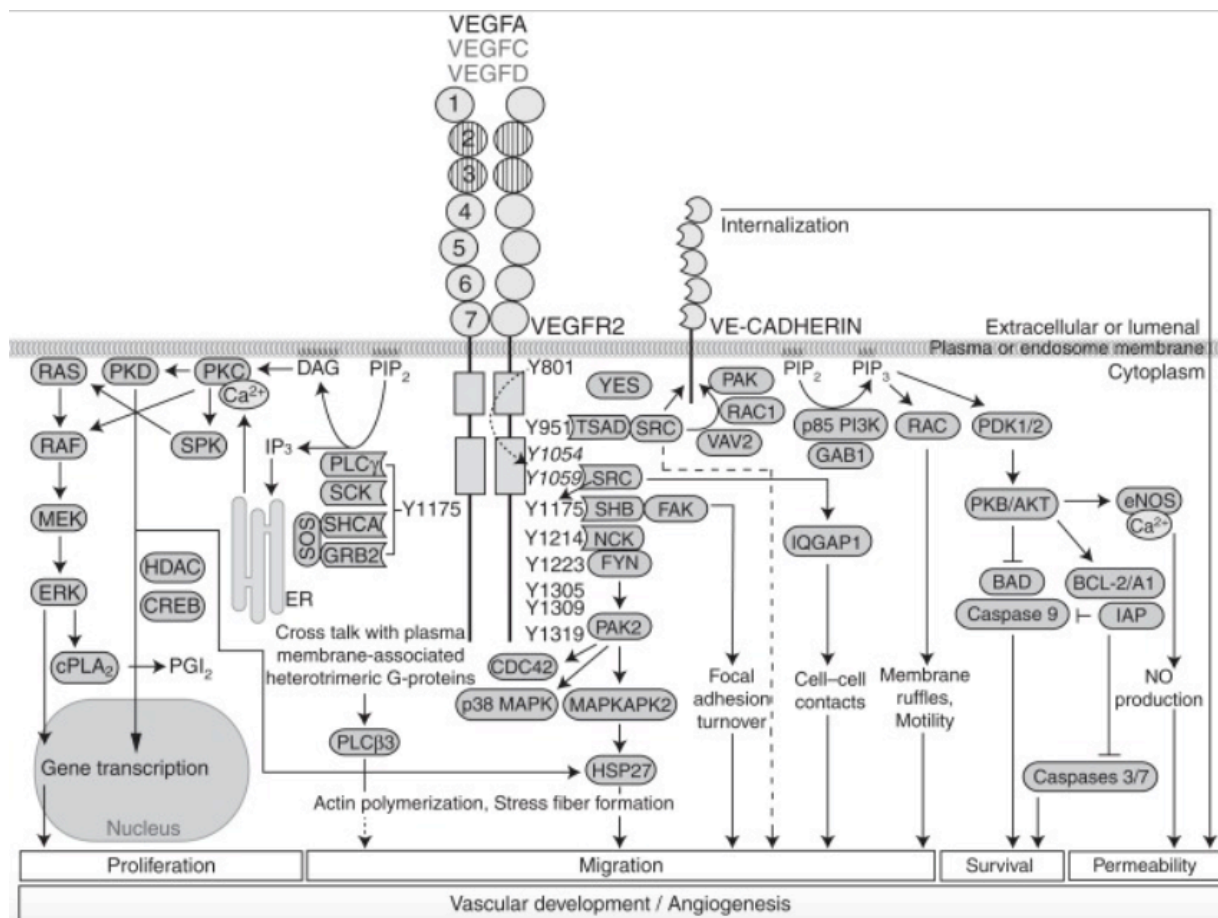


Fig. 8 VEGFR2-mediated signal transduction in response to VEGF on endothelial cells [58]

Although we understand quite well the mechanisms of initiation of VEGF-VEGFR2 signaling, very little is known on the following cascades that actually control the final cell response. VEGF generates an immediate clathrin-dependent endocytosis of VEGFR2. This is involving Cbl ubiquitination [59-61] and is considered as the “intrinsic feed-back” mechanism that will stop VEGFR2-mediated signaling. However, an increasing number of studies emphasize that

the intracellular vesicles formed after internalization of activated RTKs, including VEGFR2, can continue to recruit and to activate intracellular signaling [62-66]. Recently, Gareth and coworkers reported that different VEGF-A isoforms induce distinct patterns of VEGFR2 endocytosis [62]. This will in turn generate specific and variable cell responses to VEGF-A isoforms via a unique VEGFR2 receptor controlled by its differential trafficking (Fig. 9).

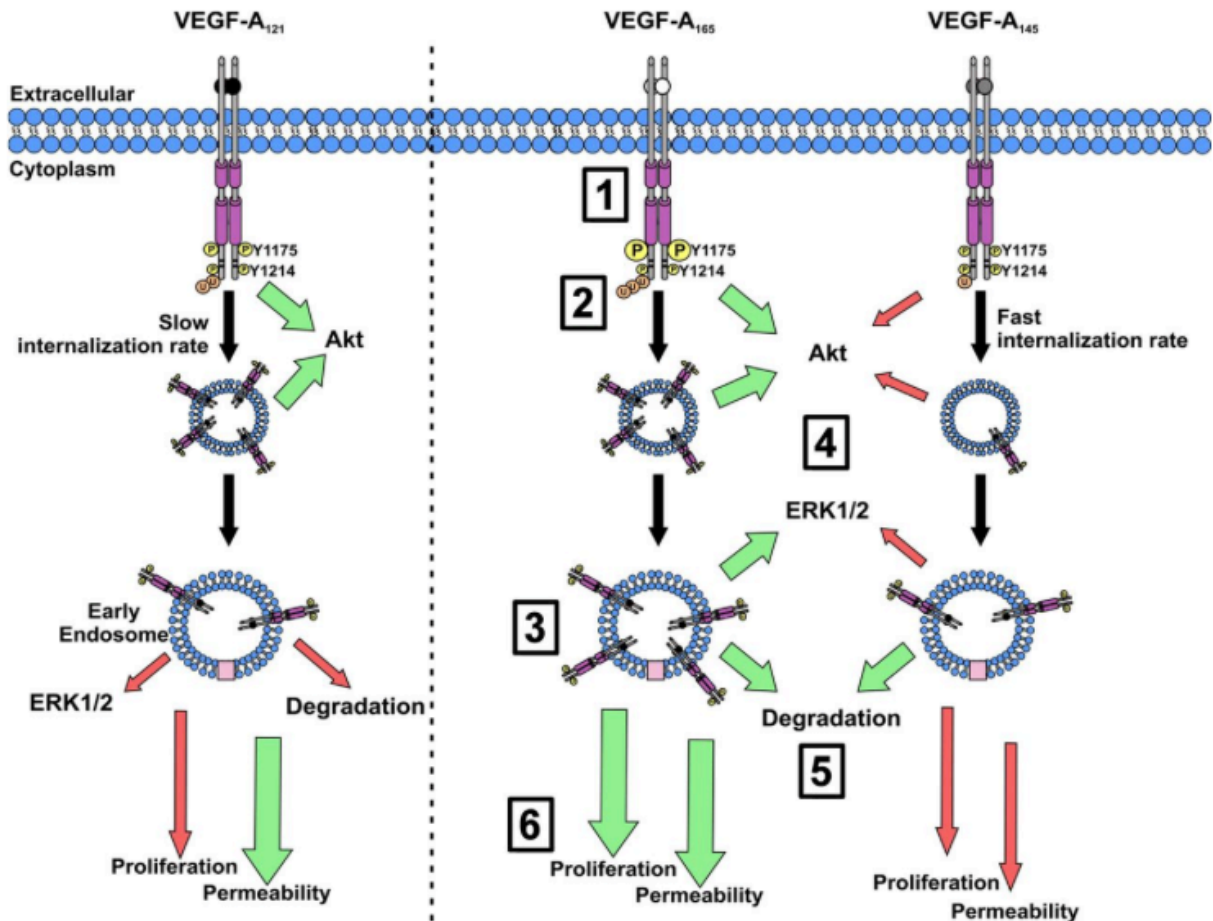


Fig.9 VEGF-A isoform-specific VEGFR2 trafficking and downstream signaling. Upon ligand binding (1) VEGFR2 undergoes dimerization and either differential (Y1175) or comparable (Y1214) trans-autophosphorylation of specific tyrosine sites, depending on the VEGF-A isoforms used. (2) This results in distinct levels of receptor ubiquitylation (3) and internalization into EEA1-positive early endosomes. (4) Differential levels of VEGF-A isoforms-induced VEGFR2 internalization impact on AKT and ERK1/2 activation in combination with VEGFR2-Y1175 phosphorylation. (5) From early endosomes VEGFR2 is send to late-endosomes where it undergoes VEGF-A isoform-specific proteolysis prior to lysosome degradation. (6) VEGF-A isoform-specific VEGFR2 activation and receptor

trafficking, mediate their individual capacities to regulate ECs permeability, proliferation and blood vessel formation. Size and magnitude of arrows reflect the magnitude of response; red, reduced; green, increased [62].

RTK (VEGFR2) endocytosis and signaling are closely related. But the mechanisms involved are poorly understood. It is admitted that the set of signaling molecules associated with an activated receptor can be significantly different whether it is in the cell membrane, in an endosome or in other compartments such as exosomes. The fine description of the spatiotemporal regulation of RTK signaling during endocytosis and trafficking, will undoubtedly give quantitative clues on the mechanisms of VEGFR2 signaling initiation, progression and termination.

#### 2.4 Crosstalks among VEGFR2 and NRP1 as well as integrin $\alpha_v\beta_3$

The crucial role of ECM and its communication with RTKs during the development of physiological and pathological vasculature is well established. In 1999, S. Raffaele and coworkers presented the first experimental evidences and proved the direct physical interaction between integrin  $\alpha_v\beta_3$  and VEGFR2 in the presence of VEGF<sub>165a</sub> [67]. They emphasized the fact that the full function of integrin  $\alpha_v\beta_3$  contributes to the full activation of VEGFR2 triggered by VEGF, but they did not explore the participation of VEGFR2 in the bi-directional signaling of integrins. One year later, T.V. Byzova and coworkers provided the first experimental proof that VEGF signaling regulates integrin activation in tumor and endothelial cells [68]. Thus, the positive feedback-signaling loop between VEGFR2 and integrin  $\alpha_v\beta_3$  looks well defined through the signaling node PI3K/AKT (Fig. 10). During step 1, VEGF binds to the recognition domains of VEGFR2 and NRP1 and triggers the polymerization of the receptors. In step 2, autophosphorylation of VEGFR2 recruits PI3K and activates AKT cascades; in step 3, PI3K/AKT activates integrin-linked kinases (ILKs) and change the spatial conformation of integrin  $\alpha_v\beta_3$ , thus enhancing integrin activity by inside-out signaling. Finally, step 4, activation of integrin function provides a second, outside-in, signal to AKT and, in parallel, the activated immobilized integrin  $\alpha_v\beta_3$  in the cell membrane may contribute to sustain the phosphorylation of VEGFR2 by inhibiting VEGFR2 trafficking. This provides a third

sustained activation signal to AKT.

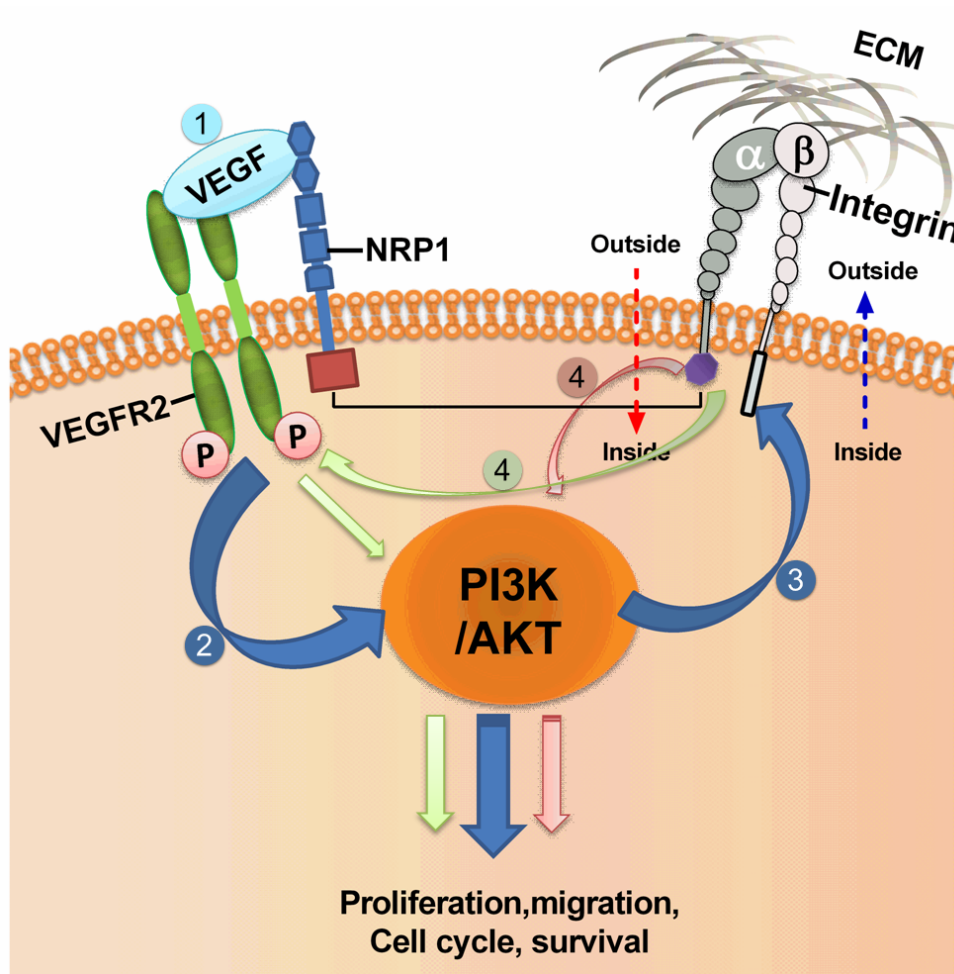


Fig. 10 VEGF induces positive signaling loops between VEGFR2 and integrin  $\alpha_v\beta_3$  to promote cell proliferation, migration and survival.

Besides the crosstalk between VEGFR2 and integrin  $\alpha_v\beta_3$ , more work highlighted that NRPs may play a central role in VEGF signaling since they regulate the function of VEGFR2 and of integrin  $\alpha_v\beta_3$  [54]. Because they regulate VEGFR2 internalization, NRPs potentiate the signaling function of VEGFR2; NRPs could interact with specific integrins and activate their affinity to ECM, thus potentiating integrin-mediated signaling via FAK; NRPs could also regulate integrin function by promoting their endocytic recycling. Since NRPs have a PDZ-binding domain, they can directly and independently transmit a signal, but they can also form macromolecular complexes that integrate additional components and generate additional signals. Interestingly, F. M. Gabhann and coworkers emphasized the vital role of NRP1 in VEGF signaling using a systematic biological view [51]. They used the first molecular

detailed computational model of VEGF and performed simulation studies of *in vivo* VEGF binding and transport. This model predicts that blockade of NRP-VEGFR coupling would be more efficient than other approaches in decreasing VEGF-VEGFR2 signaling.

Clinically,  $\alpha_v\beta_3$ -integrin, VEGFR2 and NRP1 are all key anti-angiogenic targets because of their role in ECs' function. But in both preclinical and clinical settings, patients always benefit modestly from monotherapies that target only one of these receptors. This has been demonstrated using cRGD for  $\alpha_v\beta_3$  and bevacizumab for VEGFR2 blockades. After transient responses at the beginning of the treatments, innate and acquired resistances rapidly occur, which could be explained by the complex networks and crosstalks among VEGFR2 and NRP1 as well as integrin  $\alpha_v\beta_3$ . A.R. Reynolds and coworkers presented that low concentrations (nanomolar) of RGD-mimetic  $\alpha_v\beta_3$  and  $\alpha_v\beta_5$  inhibitors can paradoxically accelerate tumor growth and angiogenesis by alteration of  $\alpha_v\beta_3$  and VEGFR2 trafficking [69]. This alternative pathway provides another route to survival during anti integrin  $\alpha_v\beta_3$  treatments.

Multi-target attacks look more promising to disturb tumor angiogenesis and to inhibit tumor progression. Recently, S. D. Robinson presented exciting proof-of-concept that dual-inhibition of  $\alpha_v\beta_3$  and NRP1 can inhibit solid tumor growth and angiogenesis [70]. Before, they had proved that  $\beta_3$  integrin could regulate negatively VEGFR2 expression and VEGF-mediated angiogenesis by limiting the interaction between NRP1 and VEGFR2 [71]. Meanwhile, simultaneous targeting of VEGFR2 and integrin  $\alpha_v\beta_3$  is also more efficient to block tumor migration, proliferation and angiogenesis, than individual single treatments [72-75]. As well, the combined use of antibodies targeting NRP1 and VEGFR2 to inhibit tumor growth has been proved 10 years ago [51].

### 3 Angiogenesis and cancer targeted therapies

As Folkman and coworkers proposed 40 years ago [76], angiogenesis is a very important target in cancer. In particular the VEGF-VEGFR system has been intensively targeted and several pro-drugs and mAbs blocking their functions have successfully entered clinical phases in patients with various solid tumors including breast, lung, glioblastoma and colorectal cancers. Bevacizumab, a humanized neutralizing antibody targeting VEGF approved by FDA, was initially shown to extend survival of patients with advanced colorectal cancer [77]. It was then extended to the treatment of other type of solid tumors including non-small cell lung, breast and metastatic renal cell carcinoma. Despite its great success at the preclinical level, and with the exception of patients with renal cell carcinoma [78], the curing efficiency of bevacizumab was observed only in patients under combination therapies (chemotherapy and/or radiotherapy). Combined chemotherapy or radiotherapy with anti-angiogenic therapies are promising for patients with solid tumors, yielding better overall survival (OS) than mono-therapies. Indeed, monotherapies could rather be assimilated to adjuvant therapies. This led to the recent development of agents targeting multiple pro-angiogenic factors in order to augment the anti-angiogenic efficacy and to overcome adaptive or intrinsic drug resistances. Successful cases of blocking pro-angiogenic factors' functions simultaneously are also discussed in the chapter of "crosstalk among VEGFR2 and NRP1 as well as integrin  $\alpha_v\beta_3$ " and the chapter of "multifunctional targeting of tumors".

In the following chapters, I will firstly introduce current clinical trials of anti-angiogenic therapies targeting integrin  $\alpha_v\beta_3$ , VEGF-VEGFR and NRP1 respectively, followed by a discussion about the advantages and disadvantages of anti-angiogenic therapies.

#### 3.1 Anti-angiogenic therapies targeting integrin $\alpha_v\beta_3$

Brooks et al firstly reported that the expression of integrin  $\alpha_v\beta_3$  correlates with tumor angiogenesis and that antagonists of integrin  $\alpha_v\beta_3$  can induce tumor regression [79, 80]. Later, preclinical studies established that antagonists of integrin  $\alpha_v\beta_3$  can suppress tumor angiogenesis and growth either alone or in combination with other therapeutics [16]. But

until now, only few anti-integrin  $\alpha_v\beta_3$ -based drugs have been tested as anti-angiogenic cancer therapies in clinical trials. Only MEDI-522 (a humanized antibody anti  $\alpha_v\beta_3$ ), CNTO95 (a humanized antibody anti  $\alpha_v\beta_3 / \alpha_v\beta_5$ ) and Cilengitide (an anti  $\alpha_v\beta_3 / \alpha_v\beta_5$  peptide) were tested. Since they all target the extracellular domains of integrin  $\alpha_v\beta_3 / \alpha_v\beta_5$ , they are interesting tools for integrin-targeted imaging and treatments [81].

MEDI-522 (etaracizumab) was the first antagonist of integrin  $\alpha_v\beta_3$  approved for clinical trials. According to the database of clinical trials (*A service of the US. National institutes of Health*, <https://clinicaltrials.gov/ct2/search/index>), there are 10 phase 1 or 2 studies of MEDI-522 alone or combination with anti-VEGF therapies (Bevacizumab) or chemotherapeutic drug (Dacarbazine an alkylating agent) in patients with melanoma, refractory solid tumors, renal cancer, prostate cancer, colorectal cancer or Lymphoma. A Phase II study proved the efficiency of MEDI-522 in the treatment of metastatic melanoma [82].

CNTO 95 (intetumumab) was also evaluated in combination with anti-VEGF therapies (Bevacizumab) or with Dacarbazine in patients with melanoma, refractory solid tumors (<https://clinicaltrials.gov/ct2/search/index>). There are 3 phase 1 or 2 studies of CNTO 95 alone or with Avastin or Dacarbazine in patients with solid tumors, stage 4 melanoma or metastatic hormone refractory prostate cancer. A recent phase I in patients with advanced solid tumors proved that bevacizumab plus intetumumab can be administrated safely, and the combinational treatment resulted in changes in the plasma levels of several extracellular matrix interacting proteins and angiogenic factors, which is a promising signal to move to next phase studies [83].

As repeated in the former chapter, Cilengitide is also an inhibitor of both integrin  $\alpha_v\beta_3$  and  $\alpha_v\beta_5$ . It has been tested in dozens of clinical trials (phase 2 or 3) in America or Europe. 30 studies of *US. National institutes of Health* (<https://clinicaltrials.gov/ct2/search/index>) and 8 studies of *EU Clinical Trials Register* (<https://www.clinicaltrialsregister.eu>) have been performed using Cilengitide alone, or in combination with chemotherapies (Temozolomide, platinum) or RTK inhibitors (Cetuximab) with concomitant radiation therapy in patients with brain, head and neck, glioblastoma, leukemia, melanoma, prostate, advanced non small cell

lung cancer and sarcoma. Cilengitide exhibited significant promises in treating patients with glioblastoma by extending OS (overall survival) with minimal side effects [16]. However, a recent phase III in glioblastoma using Cilengitide failed because of a lack of anti-angiogenic activity [84]. We are thus back to the preclinical level, to better understand the role of integrins, and especially beta3, as reviewed by S.D Robinson *et al* who emphasized the need we have to be more careful on the dosage of  $\alpha_v\beta_3$  antagonists and that we need to pay more attention to the type of target cells as well as on the quality of their microenvironment [85].

### 3.2 Anti-angiogenic therapies targeting VEGF-VEGFR

There are several approaches to inhibit VEGF signaling, including antibodies neutralizing the ligands or corresponding receptors, inhibitors blocking VEGFR activation and signaling. List of anti-VEGF agents and targets, which have entered clinical phase trials, is presented in Fig. 11. Two excellent reviews concerning the current anti-angiogenic strategies are also presented [86, 87].

Anti-VEGF therapy affects numerous cell types in the tumor microenvironment, including endothelial cells, tumor cells and dendritic cells. It also affects vascular function (flow and permeability) in addition to blocking tumor angiogenesis.

Considering the therapeutic outcomes of anti-VEGF therapy for various solid tumors, Lee M. Ellis and coworkers emphasized that it is efficient as a single agent in renal cell carcinoma and hepatocellular carcinoma, whereas it must be combined with chemotherapy in patients with metastatic colorectal, lung or breast cancer [36].

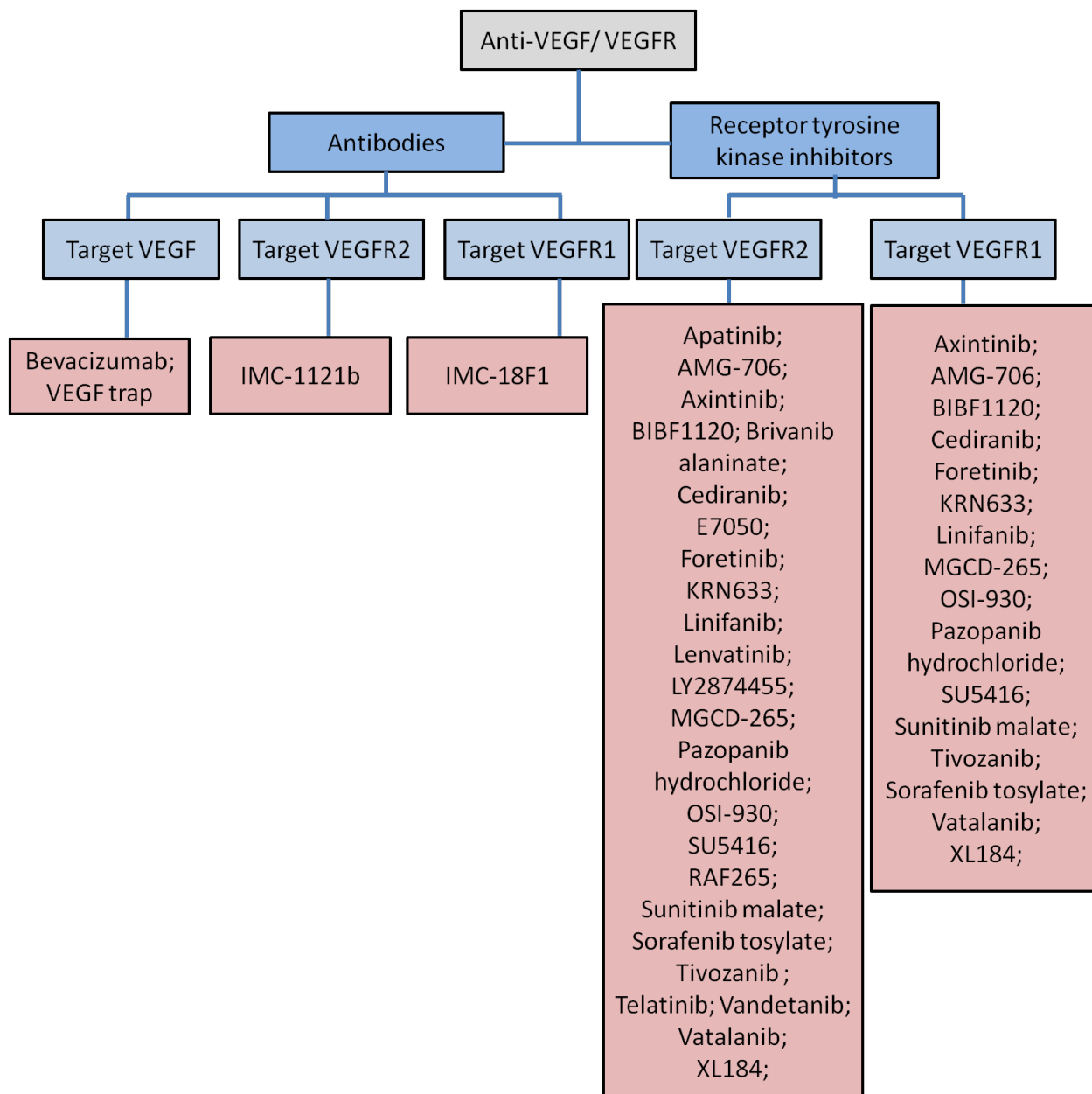


Fig. 11 List of anti-angiogenic agents targeting VEGF-VEGFR currently in clinical phase trials

[86] ([http://www.selleckchem.com/pathways\\_VEGFR-PDGFR.html](http://www.selleckchem.com/pathways_VEGFR-PDGFR.html)).

### 3.3 Anti-angiogenic therapies targeting NRP1

As discussed previously, NRP1 plays a central role in VEGF signaling because it regulates both the RTKs' and integrins' function. And it is becoming a very promising cancer target, especially in solid tumors. In patients with non-small cell lung cancer (NSCLC), the expression level of NRP1 is an independent predictor of cancer relapse and of poor survival. Its inhibition by small interfering RNA (siRNA), soluble NRP1 (sNRP1) or peptides could significantly suppress tumorigenesis, cancer invasion and angiogenesis [88].

An anti-NRP1 mAb, MNRP1685A, was developed to target the b1/b2 domain of NRP1 [89, 90]. Three phase I clinical trials proved its therapeutic efficacy [91-93]. MNRP1685A alone was well tolerated in patients [92]. But although it was especially effective when combined with bevacizumab (an anti-VEGF mAb) in patients with advanced solid tumors [91], MNRP1685A combination with bevacizumab was found to induce toxic grade 3 proteinuria [93].

Gagnon *et al* firstly reported that soluble NRP1 exists and appears to function as a VEGF antagonist [94]. NRP1 can be detected in the circulation (cNRP1) in mice, rats, monkeys, and humans in 2 forms: soluble NRP1 (sNRP1) that contains a1a2 and b1b2 extracellular domains and the complete NRP1 ECD shed from the membrane-bound NRP1. Circulating sNRP-1 is abundantly found in plasma of healthy donors (mean level of 200 ng/mL). It augments to 330 pg/mL in breast cancer and to 400 ng/mL in colorectal or non-small cell lung cancer [91]. An augmentation of sNRP1 was also established for cervical cancer and cervical intraepithelial neoplasia [46].

Administration of anti-NRP1 antibody increases the circulation levels of both soluble and full NRP1 proteins that could potentially sequester VEGF and augment the anti-tumor effects of anti-NRP1 antibody [95]. Interestingly, the biodistribution of MNRP1685A is different in humans than in monkeys and in monkeys the increase of total cNRP1 seems to be driven by the accumulation of drug-cNRP1 complexes [96]. In humans, MNRP1685A treatment is associated with a 90% saturation of both NRP1 isoforms by the antibody.

Other anti-NRP1 therapies currently in preclinical studies are using peptides, small inhibitors, siRNA and sNRP1 (Fig. 12). Concerning peptides, iRGD is a very intriguing one. It presents a C-terminal consensus R/KXXR/K sequence (CendR) that interacts with the b1/b2 domain of NRP1, and induces NRP1-dependent cell internalization [97]. The CendR motif is masked within the iRGD tumor-homing peptide but it could be activated by protease(s) within the tumor microenvironment [98] that will expose the arginine residue of CendR. Besides its strong tumor tissue-penetrating capacity, iRGD inhibits tumor metastasis [74] and can serve for drug delivery [99].

Another peptide that presents also a Cterm arginine residue, ATWLPPR (A7R), was discovered by a phage epitope library screening based on its affinity for VEGFR2 and its capacity to compete with an anti-VEGF neutralizing monoclonal antibody [100]. Because it can inhibit VEGF<sub>165</sub> interaction with NRP1 but not with VEGFR2 [101], it blocks tumor angiogenesis and induces apoptosis in NRP1-expressing tumor cells [102, 103]. Similar anti-tumor effects were also reported in another three type of peptides, V3 (ATWLPPRAANLLMAAS) [104], DG1 and DG2 [88]. DG1 treatment nearly abrogated tumorigenicity in mice with CL1-5 lung tumor xenografts. Recently, Kamarulzaman *et al* presented that four pentapeptides (DKPPR, DKPRR, TKPPR and TKPRR) and one hexapeptide CDKPRR exhibit an excellent inhibitory activity against NRP-1 *in vitro* [105]. Coupling of DKPPR to a photosensitizer may provide potential anti-angiogenic and anti-tumor targeted peptides [106].

Small molecule inhibitors of NRP1 (EG00229), small interfering RNA (siRNA) targeting NRP1 and secreted sNRP1 were also developed to reduce tumor growth in mouse models where they significantly impaired tumor vascularization [88, 107-110].

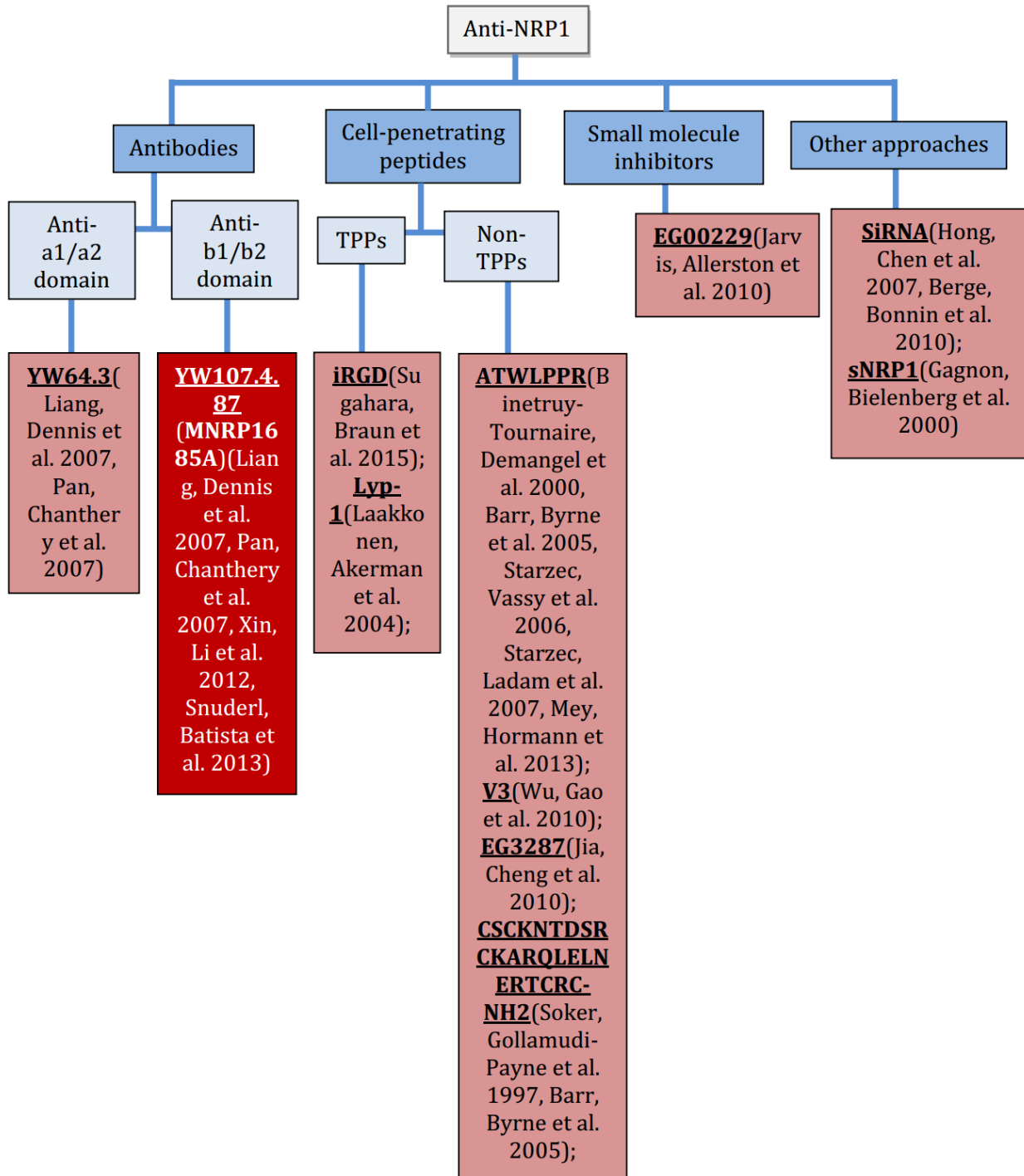


Fig. 12 Current anti-tumor therapies targeting NRP1 in preclinical and clinical studies. Red box indicates that MNRP1685A has moved to phase I clinical trial.

Barr, M. P., A. M. Byrne, A. M. Duffy, C. M. Condrón, M. Devocelle, P. Harriott, D. J. Bouchier-Hayes and J. H. Harmey (2005). "A peptide corresponding to the neuropilin-1-binding site on VEGF(165) induces apoptosis of neuropilin-1-expressing breast tumour cells." *Br J Cancer* 92(2): 328-333.

- Berge, M., P. Bonnin, E. Sulpice, J. Vilar, D. Allanic, J. S. Silvestre, B. I. Levy, G. C. Tucker, G. Tobelem and T. Merkulova-Rainon (2010). "Small interfering RNAs induce target-independent inhibition of tumor growth and vasculature remodeling in a mouse model of hepatocellular carcinoma." *Am J Pathol* **177**(6): 3192-3201.
- Binetruy-Tournaire, R., C. Demangel, B. Malavaud, R. Vassy, S. Rouyre, M. Kraemer, J. Plouet, C. Derbin, G. Perret and J. C. Mazie (2000). "Identification of a peptide blocking vascular endothelial growth factor (VEGF)-mediated angiogenesis." *EMBO J* **19**(7): 1525-1533.
- Gagnon, M. L., D. R. Bielenberg, Z. Gechtman, H. Q. Miao, S. Takashima, S. Soker and M. Klagsbrun (2000). "Identification of a natural soluble neuropilin-1 that binds vascular endothelial growth factor: In vivo expression and antitumor activity." *Proc Natl Acad Sci U S A* **97**(6): 2573-2578.
- Hong, T. M., Y. L. Chen, Y. Y. Wu, A. Yuan, Y. C. Chao, Y. C. Chung, M. H. Wu, S. C. Yang, S. H. Pan, J. Y. Shih, W. K. Chan and P. C. Yang (2007). "Targeting neuropilin 1 as an antitumor strategy in lung cancer." *Clin Cancer Res* **13**(16): 4759-4768.
- Jarvis, A., C. K. Allerston, H. Jia, B. Herzog, A. Garza-Garcia, N. Winfield, K. Ellard, R. Aqil, R. Lynch, C. Chapman, B. Hartzoulakis, J. Nally, M. Stewart, L. Cheng, M. Menon, M. Tickner, S. Djordjevic, P. C. Driscoll, I. Zachary and D. L. Selwood (2010). "Small molecule inhibitors of the neuropilin-1 vascular endothelial growth factor A (VEGF-A) interaction." *J Med Chem* **53**(5): 2215-2226.
- Jia, H., L. Cheng, M. Tickner, A. Bagherzadeh, D. Selwood and I. Zachary (2010). "Neuropilin-1 antagonism in human carcinoma cells inhibits migration and enhances chemosensitivity." *Br J Cancer* **102**(3): 541-552.
- Laakkonen, P., M. E. Akerman, H. Biliran, M. Yang, F. Ferrer, T. Karpanen, R. M. Hoffman and E. Ruoslahti (2004). "Antitumor activity of a homing peptide that targets tumor lymphatics and tumor cells." *Proc Natl Acad Sci U S A* **101**(25): 9381-9386.
- Liang, W. C., M. S. Dennis, S. Stawicki, Y. Chanthery, Q. Pan, Y. Chen, C. Eigenbrot, J. Yin, A. W. Koch, X. Wu, N. Ferrara, A. Bagri, M. Tessier-Lavigne, R. J. Watts and Y. Wu (2007). "Function blocking antibodies to neuropilin-1 generated from a designed human synthetic antibody phage library." *J Mol Biol* **366**(3): 815-829.
- Mey, L., M. Hormann, N. Schleicher, P. Reuter, S. Donges, R. Kinscherf, M. Gassmann, T. Gerriets and N. Al-Fakhri (2013). "Neuropilin-1 modulates vascular endothelial growth factor-induced poly(ADP-ribose)-polymerase leading to reduced cerebrovascular apoptosis." *Neurobiol Dis* **59**: 111-125.
- Pan, Q., Y. Chanthery, W. C. Liang, S. Stawicki, J. Mak, N. Rathore, R. K. Tong, J. Kowalski, S. F. Yee, G. Pacheco, S. Ross, Z. Cheng, J. Le Couter, G. Plowman, F. Peale, A. W. Koch, Y. Wu, A. Bagri, M. Tessier-Lavigne and R. J. Watts (2007). "Blocking neuropilin-1 function has an additive effect with anti-VEGF to inhibit tumor growth." *Cancer Cell* **11**(1): 53-67.
- Snuderl, M., A. Batista, N. D. Kirkpatrick, C. Ruiz de Almodovar, L. Riedemann, E. C. Walsh, R. Anolik, Y. Huang, J. D. Martin, W. Kamoun, E. Knevels, T. Schmidt, C. T. Farrar, B. J. Vakoc, N. Mohan, E. Chung, S. Roberge, T. Peterson, C. Bais, B. H. Zhelyazkova, S. Yip, M. Hasselblatt, C. Rossig, E. Niemeyer, N. Ferrara, M. Klagsbrun, D. G. Duda, D. Fukumura, L. Xu, P. Carmeliet and R. K. Jain (2013). "Targeting placental growth factor/neuropilin 1 pathway inhibits growth and spread of medulloblastoma." *Cell* **152**(5): 1065-1076.
- Soker, S., S. Gollamudi-Payne, H. Fidder, H. Charmahelli and M. Klagsbrun (1997). "Inhibition of vascular endothelial growth factor (VEGF)-induced endothelial cell proliferation by a peptide corresponding to the exon 7-encoded domain of VEGF165." *J Biol Chem* **272**(50): 31582-31588.
- Starzec, A., P. Ladam, R. Vassy, S. Badache, N. Bouchemal, A. Navaza, C. H. du Penhoat and G. Y. Perret (2007). "Structure-function analysis of the antiangiogenic ATWLPPR peptide inhibiting VEGF(165) binding to neuropilin-1 and molecular dynamics simulations of the ATWLPPR/neuropilin-1 complex." *Peptides* **28**(12): 2397-2402.
- Starzec, A., R. Vassy, A. Martin, M. Lecouvey, M. Di Benedetto, M. Crepin and G. Y. Perret (2006). "Antiangiogenic and antitumor activities of peptide inhibiting the vascular endothelial growth factor binding to neuropilin-1." *Life Sci* **79**(25): 2370-2381.
- Sugahara, K. N., G. B. Braun, T. H. de Mendoza, V. R. Kotamraju, R. P. French, A. M. Lowy, T. Teesalu and E. Ruoslahti (2015). "Tumor-penetrating iRGD peptide inhibits metastasis." *Mol Cancer Ther* **14**(1): 120-128.
- Wu, D., Y. Gao, L. Chen, Y. Qi, Q. Kang, H. Wang, L. Zhu, Y. Ye and M. Zhai (2010). "Anti-tumor effects of a novel chimeric peptide on S180 and H22 xenografts bearing nude mice." *Peptides* **31**(5): 850-864.
- Xin, Y., J. Li, J. Wu, R. Kinard, C. D. Weekes, A. Patnaik, P. Lorusso, R. Brachmann, R. K. Tong, Y. Yan, R. Watts, S. Bai and P. S. Hegde (2012). "Pharmacokinetic and pharmacodynamic analysis of circulating biomarkers of anti-NRP1, a novel antiangiogenesis agent, in two phase I trials in patients with advanced solid tumors." *Clin Cancer Res* **18**(21): 6040-6048.

### 3.4 Pros and cons of anti-angiogenesis therapies

In this chapter, I will list some of the interests and in particular the limits of current anti-angiogenic treatments in a perspective that will bring to the development of more effective and personalized therapies.

The initial objective of Folkman's theory was to starve tumors by inhibiting tumor vessels formation. Nowadays, we mainly try to stabilize the disease and keep tumorigenesis under control and to develop anti-angiogenic therapies that look more like pro-angiogenic and leading to remodeling of tumor blood vessels, which lead to transient increased of blood flow within the tumor and improved delivery of chemotherapeutic agents [86]. This could explain in particular why combination of chemotherapy or radiotherapy with bevacizumab is usually performing better [111, 112]. Recent reviews on the results obtained with VEGF-targeted cancer therapies clearly suggest the urge to develop combinations of rational combinations of anti-angiogenic agents [113, 114] in agreement with the previous interrogation of P. Carmeliet and coworkers: *should tumor vessels be destroyed to starve primary tumors from oxygen and to induce tumor shrinkage, or should they be normalized to reduce metastatic dissemination from oxygen-enriched tumors and to improve responses to conventional anticancer therapies? Alternatively, should we attempt to take advantage of both approaches combined?* [3]. This seems to be successful for VEGF based treatments but also for RGD-based ones and lead to the idea that « *vascular promotion therapy is a means to improve cancer treatment* » as claimed by Wong et al. [115]. Another way to understand the limitation of VEGF-mediated anti-angiogenic is represented in Fig. 13.

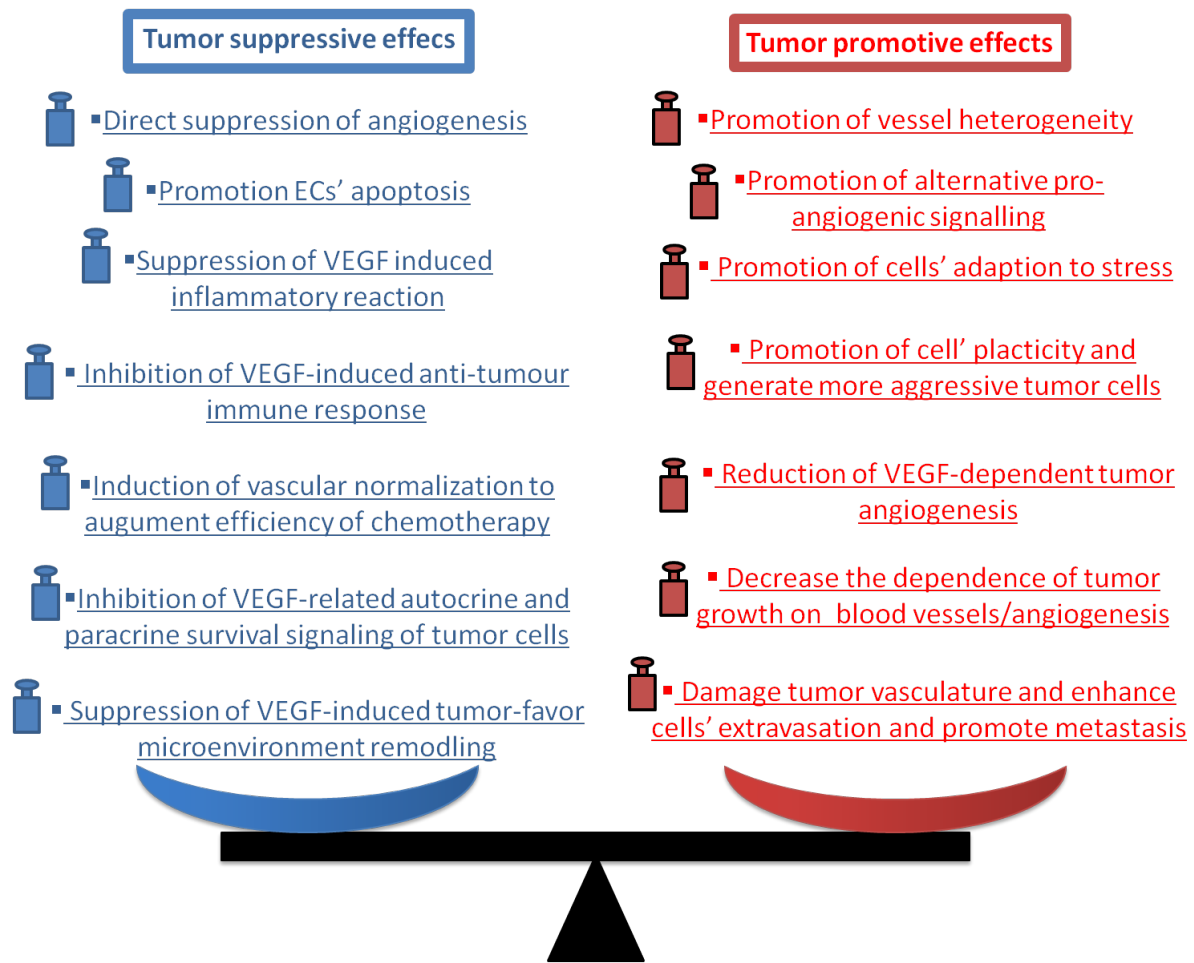


Fig.13 A summary of mechanisms contributing to the tumor suppressive or promoter effects of therapies targeting the VEGF system

Clinical studies clearly proved that targeting angiogenesis is a valid therapeutic approach. But at the same time they as clearly showed the emergence of resistance affecting the overall survival rate of patients. Resistance is a consequence of both the adaptive and intrinsic (pre-existing) non-responsive resistances of the tumors and if we want to improve the benefit for patients we will need to:

- Better understand the intracellular signaling crosstalks and intercellular networks in the tumor micro-environment
- Better understand the vascular biology of different tumors to explore their intrinsic differences
- Better understand the principles and mechanisms of tumor vessel normalization

- Develop appropriate predictive biomarkers and select the appropriate strategy for each type of patient

- Generate agents targeting multiple pro-angiogenic molecules but also precisely adjust their pharmacokinetic and pharmacodynamics parameters in order determine the optimal duration and scheduling of such agents.

This is actually why I started my PhD work. And in particular we wanted to take advantage of the large size of nanoparticles to generate such multifunctional drugs.

## 4 Nanoparticles and cancer therapy

### 4.1 Passive targeting of nanoparticles to cancer

Nanoparticles (NPs) are routinely defined as objects with sizes between 1 and 100 nm, which exhibit specific chemical and physical properties like unexpected optical properties, high surface area to volume ratio and so on. Anti-cancer nanotherapeutics are rapidly progressing since they could overcome many limitations of conventional drug such as: nonspecific biodistribution and targeting, lack of water solubility, poor oral bioavailability and low therapeutic indexes [116].

Nanotherapeutics have intrinsic properties that allow them to target heterogeneous and complex tumor microenvironments. This targeting can be passive via the so-called EPR (enhanced permeability and retention) effect or active when the NP is covered of ligands. Ligands can be small molecules, peptides, proteins, sugars, nucleic acid or antibodies directed against selected tumor targets.

For passive targeting, stealth macromolecules with a MW >40 kDa (>5 nm) accumulate preferentially in the neoplastic tissues as a result of EPR phenomenon, which was firstly described by Yasuhiro Matsumura and Hiroshi Maeda in 1986 [117, 118]. The EPR effect could be over-simplified and explained by the presence of a fenestrated endothelium (permeability) and of the inefficient lymphatic drainage within tumors, which generates the retention effect [119]. But it is actually a complex phenomenon linked to several biological process including: angiogenesis, vascular permeability, hemodynamic regulation, heterogeneities of the genetic profiles of tumors, heterogeneities in the tumor microenvironment and lymphangiogenesis [120], in addition to the NPs' intrinsic properties, such as size, shape, rigidity, hydrophobicity and surface charge (Fig. 14) [119].

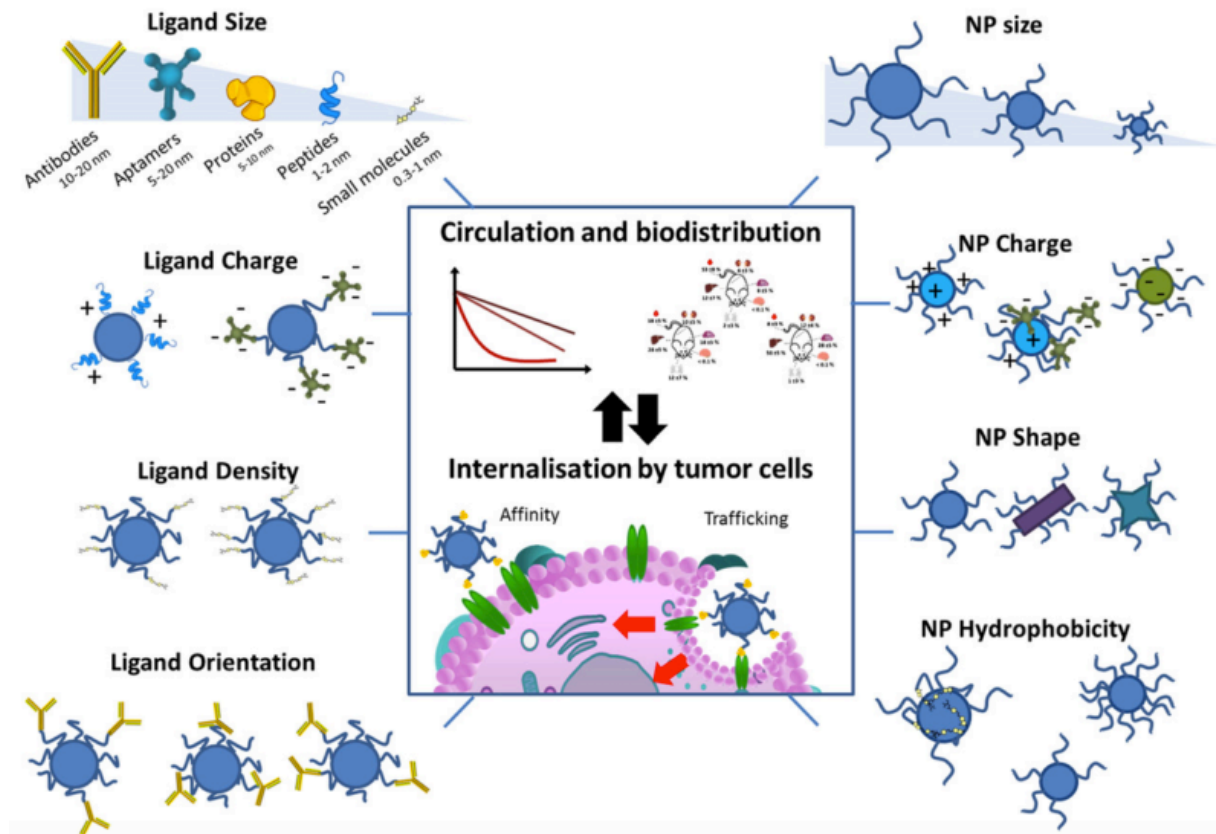


Fig. 14 Physicochemical properties of the ligand and the NP affect their blood circulation profiles, their biodistribution and their ability to be internalized by cancer cells [120].

In our team, we recently used DCE-MRI and VSI-MRI to quantify the parameters of tumor microenvironment in addition to that of tumor-specific vascularization in preclinical cancer models. Three types of fluorescent NPs' EPR effects were studied by optical imaging in eight different subcutaneous and orthotopic tumor models [121]. Even if no direct correlation was detected between NPs' passive accumulations and the number and size of blood vessels, their permeability, quantity of blood or water diffusion coefficient, we established that the combination of "permeability" and "blood volume fraction" parameters would enable the prediction of whether the tested NPs will accumulate or not in the different preclinical tumors. And it further emphasized that NPs' PK values and tumor specific characteristics cooperatively decide their passive accumulation in tumor sites.

Concerning the NPs' size, we used larger NPs ranging from 25 to 100nm to test their impacts on passive tumor targeting efficiency. Although the smallest nanoemulsions (25nm) disappeared from the blood circulation faster than the larger ones (50 and 100nm) due to a

rapid elimination and wider tissue distribution, all the NPs' biodistribution were quite the same after 24 hours [122]. Similar phenomenon was also detected in another comparative study using polymeric micelles with diameters of 30, 50, 70 and 100nm tested in highly permeable tumors, but smallest NPs exhibit better penetration in poorly permeable tumors [123]. Recently, Skykes *et al* studied the impact of NPs' size on active and passive tumor targeting efficiency [124]. They used spherical gold NPs with different sizes (15, 30, 60 and 100nm) to discern the effect of particle diameter on passive (poly (ethylene glycol)-coated) and active (transferrin-coated) targeting in MDA-MB-435 orthotopic tumor xenografts. Interestingly, the difference of NPs' PK value between passive and active NPs was only detected in the size of 30 or 60nm, especially within the 60nm diameter range. Targeted NPs exhibited 5 times faster and approximately 2-fold higher tumor accumulation as compared to their passive counterparts (Fig. 15). This work is of great interest for us since we are using 40nm large silica NPs as a base for peptides' modification to generate multifunctional NPs [125].

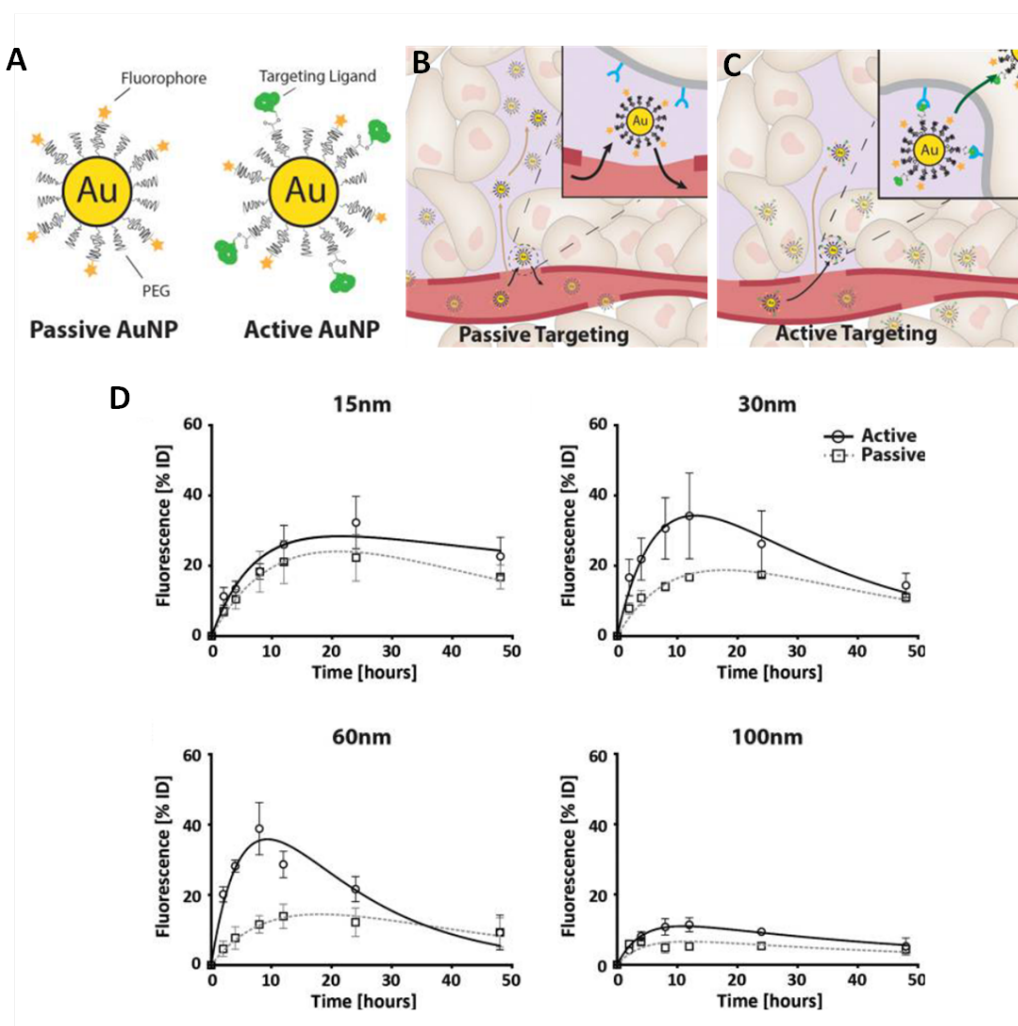


Fig. 15 Illustration of the proposed mechanism for passive and active gold NPs tumor targeting, and the comparative PK studies of NPs with different diameters (15, 30, 60 and 100nm). (A) Schematic representation of passive NPs with poly (ethylene glycol) is presented on the left, the right figure shows the active NPs with transferrin. Systemically circulating NPs enter the tumor space through leaky blood vessels and may sequester in cancer cells (beige) or in vascular pools (purple) of the interstitial matrix. Insets demonstrate that passive particles (B) do not directly associate with cancer cells, while active particles (C) are capable of endocytosis through surface-bound targeting ligands (green). (D) Kinetic profiles depict the relative tumor fluorescence for mice injected with passive (dotted) and active (solid) AuNPs over 48 HPI. Tumor fluorescence (% ID) indicates the relative difference in tumor signal to opposing mouse flank expressed as a percentage of tumor fluorescence immediately after injection (Modified from [124]).

## 4.2 Active targeting of nanoparticles

Active targeting is utilizing high or low affinity-ligands on the surface of NPs for specific retention and uptake by targeted disease cells [120]. Ligands are selected to bind cell surface proteins overexpressed in the damaged organs, tissues, cells or subcellular domains, and are introduced on the surface of NPs. But the design of actively-targeted NPs is very complex, since a lot of factors will affect their avidity, including NPs' architecture, ligand conjugation chemistry, ligand density, or the choice of targeting ligand (Fig. 14) [119].

Concerning the choice of receptors and ligands used for active targeting, an excellent summary was made by Xu *et al* (Table 5) [126]. Since my PhD work is focused on two peptides, ATWLPPR and RGD targeting NRP1 and integrin  $\alpha_v\beta_3$  /  $\alpha_v\beta_5$  respectively, I will only present nanotherapeutics that were already described using these two ligands.

Receptor Category	Receptor Subtype	Targeting molecule	Carrier/Vehicle	Cargo	Target Cells/Tissues
Receptor tyrosine kinase	EGFR	EGF	gelatin nanoparticle	cisplatin	A549 human lung adenocarcinoma tumor
	EGFRvIII	Antibody	iron oxide magnetic nanoparticles		glioblastoma multiforme (GBM) tumor
	VEGFR	Antibody	nanostructured lipid carriers	docetaxel	B16 mouse melanoma tumor
GPCR	Y1-receptor	Agonist/ Antagonist	quantum dots		MCF-7 breast cancer cell line
Folate receptor		Folate	polymer nanoparticle	DNA	Calu-3 cell line, KB cell line
		Folate	polymer nanoparticle	<sup>90</sup> Y, paclitaxel	SKOV-3 cell line, SKOV-3 tumor
		Folate	PEGylated liposome	doxorubicin	KB cell line, SKOV-3, KB and KBV tumors
		Folate	polymer nanoparticle	<sup>123</sup> I	HeLa tumor
		Folate		siRNA complex	KB tumor
	FR-β	Folate	liposome	doxorubicin	MV4-11 and K562 human leukemia cell line, AML patient cells
Integrins	α <sub>v</sub> β <sub>3</sub>	Antibody	human serum albumin nanoparticles	doxorubicin	M21 melanoma cell line
		RGD sequence	PEGylated-copolymer-coated iron oxide nanoparticles		U87MG glioblastoma tumor
			chitosan nanoparticles	siRNA	SKOV3ip1, HeyA8, and A2780 tumors
			Adenovirus	DNA	Recurrent gynecologic solid tumor in Phase I clinical trial patients
TfR		Transferrin (Tf)	PEGylated gold nanoparticles		Neuro2A neuroblastoma tumor
			PEGylated non-ionic surfactant-based liposome (niosome)	hydroxycamptothecin	sarcoma-180 tumor
			stealth liposome	doxorubicin	HepG2 human hepatocellular carcinoma tumor
			liposome	oxaliplatin	Adenocarcinoma in Phase Ib/IIa clinical trial patients
			polymer nanoparticle	siRNA	metastatic melanoma solid tumor in Phase I clinical trial patients
	TfRscFv	liposome	DNA	Solid tumors in Phase Ib clinical trial patients	
LDLR		LDL	LDL nanoparticle	siRNA	HepG2 cell line
			LDL nanoparticle	near-infrared dyes	HepG2 human hepatocellular carcinoma tumor

Table 5 Examples of cellular targeting strategies in cancer therapeutics [126].

#### 4.2.1 Interest of ATWLPPR for cancer targeted therapies

The ATWLPPR peptide was used in different systems (table 6). Coupling ATWLPPR to the surface of NPs can significantly and selectively improves their binding on cells that express elevated levels of NRP1 (HUVEC or MDA-MB-231), especially *in vitro*. But their low affinity and poor penetration within the tissues added to a fast wash-out, are still limiting their use *in vivo*.

<b>Particles</b>	<b>Linker</b>	<b>Target cells/ Tissues</b>
[ <sup>99m</sup> Tc]Tc-ATWLPPR (Perret, Starzec et al. 2004)	-	MDA-MB-231
Liposomes (DiD)-ATWLPPR (Janssen 2003)	PEG	HUVEC
TPC-ATWLPPR (Thomas, Tirand et al. 2008)	6-aminohexanoic acid	U87
Verteporfin-ATWLPPR (Renno, Terada et al. 2004)	polyvinyl alcohol (PVA) polymer (verteporfin PVA)	Rat laser-injury model of CNV
Lipopeptide C16-ATWLPPR (Slimani, Guenin et al. 2006)	-	MDA-MB-231
TPC-ATWLPPR (Tirand, Frochot et al. 2006)	6-aminohexanoic acid	HUVEC, U87

Table 6 Use of ATWLPPR for targeted delivery

Janssen, A. (2003). "Peptide-targeted PEG-liposomes in anti-angiogenic therapy." International Journal of Pharmaceutics **254**(1): 55-58.

Perret, G. Y., A. Starzec, N. Hauet, J. Vergote, M. Le Pecheur, R. Vassy, G. Léger, K. A. Verbeke, G. Bormans, P. Nicolas, A. M. Verbruggen and J.-L. Moretti (2004). "In vitro evaluation and biodistribution of a <sup>99m</sup>Tc-labeled anti-VEGF peptide targeting neuropilin-1." Nuclear Medicine and Biology **31**(5): 575-581.

Renno, R. Z., Y. Terada, M. J. Haddadin, N. A. Michaud, E. S. Gragoudas and J. W. Miller (2004). "Selective photodynamic therapy by targeted verteporfin delivery to experimental choroidal neovascularization mediated by a homing peptide to vascular endothelial growth factor receptor-2." Arch Ophthalmol **122**(7): 1002-1011.

Slimani, H., E. Guenin, D. Briane, R. Coudert, N. Charnaux, A. Starzec, R. Vassy, M. Lecouvey, Y. G. Perret and A. Cao (2006). "Lipopeptide-based liposomes for DNA delivery into cells expressing neuropilin-1." Journal of Drug Targeting **14**(10): 694-706.

Thomas, N., L. Tirand, E. Chatelut, F. Plénat, C. Frochot, M. Dodeller, F. Guillemin and M. Barberi-Heyob (2008). "Tissue distribution and pharmacokinetics of an ATWLPPR-conjugated chlorin-type photosensitizer targeting neuropilin-1 in glioma-bearing nude mice." Photochemical & Photobiological Sciences **7**(4): 433.

Tirand, L., C. Frochot, R. Vanderesse, N. Thomas, E. Trinquet, S. Pinel, M.-L. Viriot, F. Guillemin and M. Barberi-Heyob (2006). "A peptide competing with VEGF165 binding on neuropilin-1 mediates targeting of a chlorin-type photosensitizer and potentiates its photodynamic activity in human endothelial cells." Journal of Controlled Release **111**(1-2): 153-164.

#### 4.2.2 Interest of RGD for cancer targeted therapies

The RGD peptide is probably the more widely investigated peptide ligand. RGD-based targeting is successful in the delivery of drugs, imaging agents, virus, and NPs to tumor vasculature [98], but its low ability to cross the vascular bed and to penetrate deeply into tumor lesions are main drawbacks.

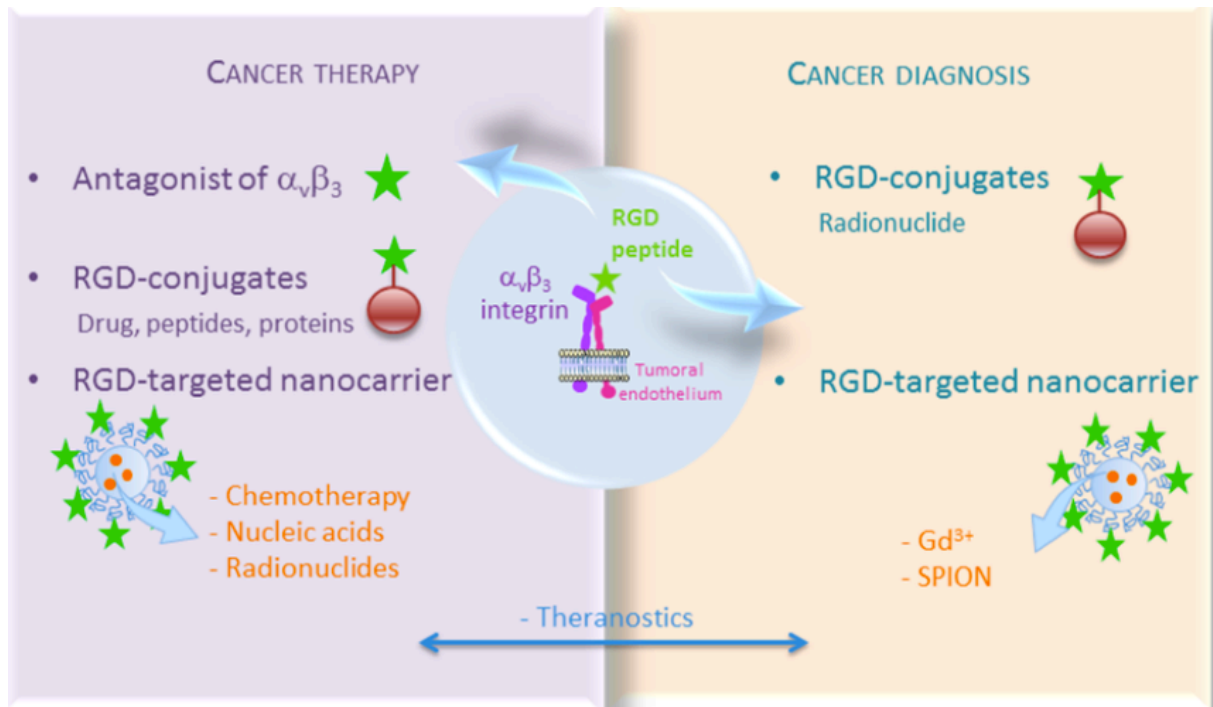


Fig. 16 RGD-targeted cancer theranostics [127].

As shown in Fig. 16, RGD-based targeting strategies are quite popular in both cancer therapy and diagnosis. Numerous publications report the synthesis and use of RGD-targeted NPs [128], in particular, a silica-based small NP (<7 nm) was used as a multimodal NIR-optical imaging and PET imaging contrast agent (labeled with <sup>124</sup>I) in the presence of an RGD-targeting ligand [129]. In preclinical models, these targeted NPs provided a  $\pm 2$ -fold increase in the targeting of a melanoma subcutaneous tumor, with an overall modest 1.5% ID/g at 4 hours due to the presence of RGD. This study was further extended to a phase I clinical trial in humans [130], which essentially confirmed the pharmacodynamics data obtained in mice but provided very modest tumor detection, with short retention times in a melanoma metastasis present in the liver. These preclinical data are in agreement with our own, which also indicated a  $\pm 2$ -fold increase in RGD-mediated targeting of U87MG glioblastoma

subcutaneous tumors using gadolinium-based Small Rigid Platforms [131]. Similarly, we also obtained a tumor versus skin fluorescence ratio of  $1.53 \pm 0.07$  at 24 hours after intravenous administration of large 35 nm lipid NPs in mice bearing subcutaneous tumors that overexpress very high levels of integrin  $\alpha_v\beta_3$ . However, using larger NPs ( $\pm 120$  nm), the presence of RGD peptides did not augment active targeting *in vivo*, as evidenced using  $^{19}\text{F}$  MRI [132]. This disappointing phenomenon was also found in another active targeting system using transferrin-coated NPs in MDA-MB-435 orthotopic tumor xenografts [124]. As we discussed in the chapter of "Passive targeting of nanoparticles to cancer", the superiority of active targeting system to passive targeting counterpart may only occur with NPs' sizes of  $\pm 50\text{nm}$ . It also emphasized the importance and difficulties of rational using of EPR and ligand-dependent targeting systems.

At the same time, the above results also raise questions concerning the added value of the presence of RGD in terms of gain in the efficacy of accumulation of the NP in the tumors. Importantly, this targeting may be more helpful for the delivery of therapeutic agents, as demonstrated for siRNA [133]. That is exactly the interest of combinational treatments of RGD with other type of therapeutics tested in preclinical trials, because the major advantage of RGD-targeting NPs is precisely double targeting on tumor associated endothelial cells and cancer cells (which also express the integrin  $\alpha_v\beta_3$ ). While this double targeting of both ECs and tumor cells is not yet exploited nor discussed in literatures, only few were reported [127, 134, 135]. More work need to explore the synergistic, additive or potentiation effects of RGD with other kind therapies and their molecular mechanisms. In addition, the potential blood normalization caused by RGD-based anti-angiogenic properties need also to be further studied, as discussed in the chapter of "Pros and Cons of anti-angiogenesis therapies".

## 4.3 Multifunctional targeting of tumors

### 4.3.1 Multivalent targeting for drug delivery

Multivalency refers to the interaction of multiple ligands with several receptors. According to the ligands' variety, multivalent drug carriers can be divided into two groups, one group is homomultimers with multiple copies of the same recognition element, and another group is heteromultimers with combinations of different ligands [126]. The interest of heteromultivalent targeting as compared to a homomultivalent counterpart seems intuitive because it will recognize and bind different types of cell membrane receptors, thus potentially improving the targeting of heterogeneous tumors. Furthermore, the phenotypic and functional heterogeneity of the tumor microenvironment is not limited to the tumor cells themselves, but also to the cancer-associated fibroblasts, endothelial cells, macrophages and other tumor-associated stromal cells. Recently, Dr. Rihe Hu and his colleagues generated a tetra-specific targeting ligand that recognizes four different cancer biomarkers and grafted them on gold NPs. These “smart” nanomaterials have greatly broadened tumor targeting ranges and efficiency [136]. The AuNPs is presented in Fig.17.

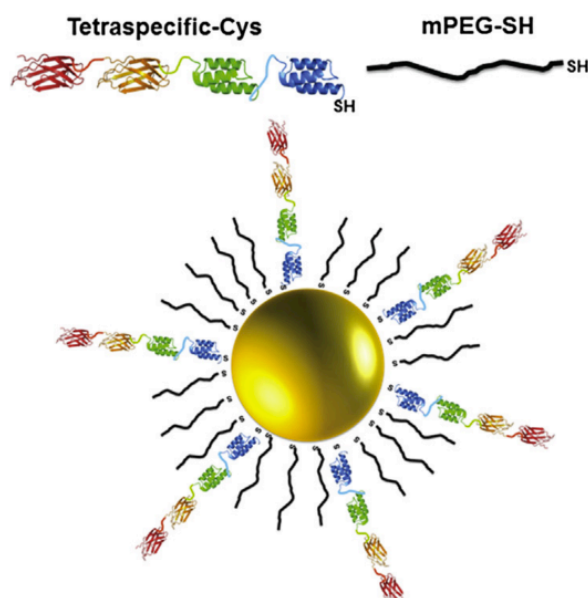


Fig.17 Schematic representation and design of the tetraspecific ligand and AuNPs

The stronger binding efficiency of a multivalent NP can be explained by sequential contacts and binding interactions that will proceed without additional penalties in their entropy after the first receptor-ligand contact [137]. However, it is difficult to find a quantitative, accurate and systematic study that describes the binding equilibrium between homo- or hetero-multivalent NPs and their receptors. It may be unnecessary to calculate the binding constant between hetero-multivalent NPs and its receptors, because the preference of what kind of specific ligand is binding and the induction of endocytosis need also to be considered. Notably, the dissociation ( $k_d$ ) and association constants ( $k_a$ ) may not exhibit a linear relationship as the ratio of the different ligands changes. As presented by the work of Kibria, G and coauthors on dual-ligand targeting liposomes (LPs) [138], R8 (Stearylated octaarginine) /PEG-LPs was taken up by R8 dependent clathrin-mediated endocytosis pathway, while RGD-PEG-LPs was taken up mainly by caveolae-mediated endocytosis triggered by cRGD. However, the internalization of mixed R8/ RGD-PEG-LPs was predominantly governed by clathrin-mediated endocytosis pathway, which allows it to be efficiently internalized by HUVEC cells in dependence on R8. Nevertheless, recent work concerning the binding of dendrimer-based folate NPs to surface-immobilized folate binding protein (FBP) gave direct experimental clues to understand the nature of such interactions and unravel the key factors contribution to the binding avidity of multivalent targeting NPs [139]. They proved that the dissociation constants ( $K_D$ ) between NPs and FBP are significantly improved in function of the number of ligands grafted on the NPs, which are not related with enhanced rate of endocytosis by the cell-based assays. Further, SPR (surface plasmon resonance) analysis revealed a linear increase in the  $k_a$  with the number of targeting agents. This strongly indicates that ligand-receptor association is not cooperative, whereas the off-rate,  $k_d$ , decreases exponentially with the number of targeting agents. This is show in Fig. 18.

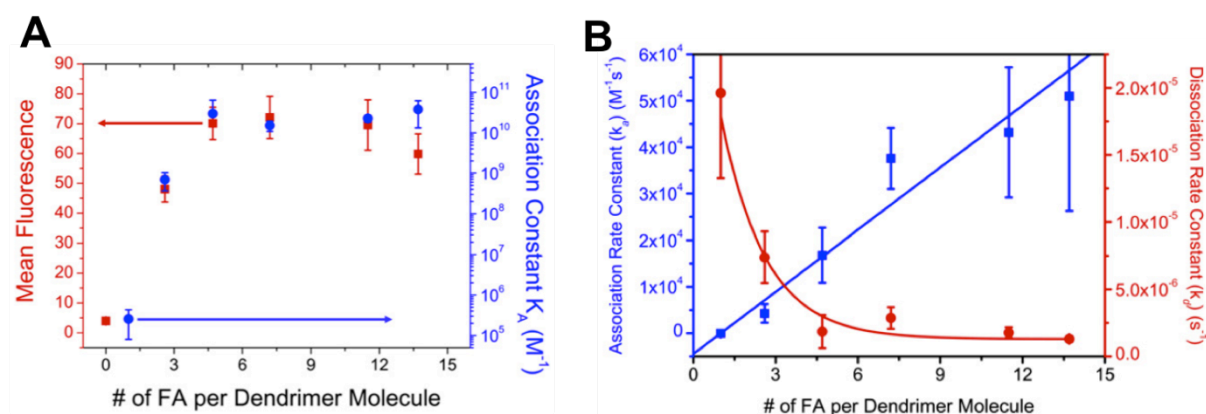


Fig. 18 Binding avidity studies of a NP-based multivalent targeted drug delivery platform. (A) Comparison of the model study using SPR and the *in vitro* study using FACS of the effect of the number of FA (vitamin folic acid, a ligand for FAR) per dendrimer upon binding constant. (B) Association and dissociation rate constants of dendrimers with varying numbers of folic acid as measured by SPR.

S. Hong and coworkers' analysis demonstrated that the nonlinear augmentation of  $K_D$  with the increase of ligands' number comes from the impact of multivalency on the dissociation ( $k_d$ ) and not on the association ( $k_a$ ). But how a multivalent NP presenting two or more different ligands will react is still an opened question.

In addition, the techniques to characterize the effectiveness of NPs with different valencies do not exist currently [140], and the selection of shape, flexibility, size, valency and orientation of individual recognition ligands must still be done empirically. Considering the huge amount of parameters involved, the generation of such NPs cannot be envisioned without the development of simple and quantitative chemical methodologies.

#### 4.3.2 Pro and cons of heteromultivalent targeting

As explained already, multivalent targeting and especially heteromultivalency, seems preferable to address the diversity and variability of receptors expression in cancer. Most importantly, the heteromultivalent targeting could improve therapeutic efficiencies by the simultaneous suppression of multiple essential signaling pathways and thus by-passing drug

resistance issues. Numerous examples of multivalent targeting have been reported. However, the use of heteromultivalent targeting has also its dark-sides because it could generate dangerous cell signaling events caused by receptors clustering and communication, as well as it could also affect the *in vivo* PK parameters.

Several heteromultivalent targeted systems for *in vitro* delivery with improved specific and binding efficiencies have already been reported, such as heteromultimers of AS1411-Nucleolin with RGD-integrin plus TTA1-Tenascin C [141], RGD-integrin plus NGR-aminopeptidase N (CD13) [142], Anginex-galectin 1 plus RGD-integrin [143]. But, compared to these convincing results *in vitro*, the *in vivo* studies are not satisfying. For example, multivalent targeting using transferrin, RGD or both indeed increased NPs' retinal delivery when compared to naked NPs, but no "synergistic" effects are obtained as compared to single-ligand, homomultivalent targeting (Fig. 19A) [144]. As well, dual-targeting of  $\alpha_v\beta_3$  and galectin-1 indeed improved the specificity of NPs to tumor endothelium *in vivo* as expected from their synergistic effect *in vitro*, but the blood clearance kinetics of dual- NPs (Anx/RGD-NPs) was three-fold more rapid than single RGD-NPs in melanoma-bearing mice [145]. Notably, due to their long circulation time, RGD-NPs were targeting tumor endothelium more efficiently than the mixed Anx/RGD-NPs (Fig. 19B).

We must thus be very cautious when selecting the ligands, but also the *in vitro* and *in vivo* models and we should pay a particular attention to the trade-off that exists between the pharmacokinetic properties and the receptors' targeting efficiencies.

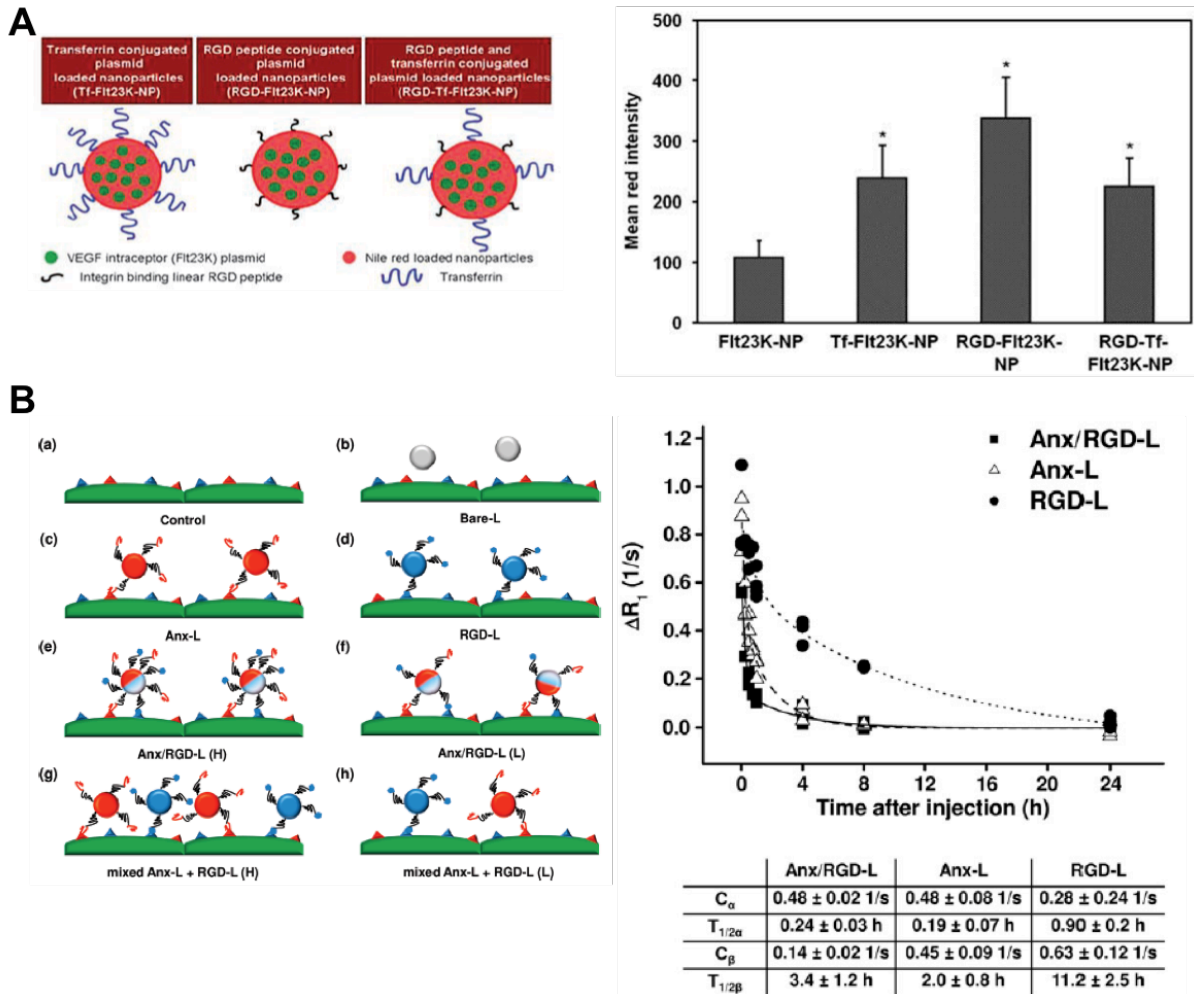


Fig. 19 *In vivo* studies of dual-targeting NPs. (A) Schematic representation of functionalized NPs is presented on the left. The right figure shows NPs' accumulation into the retina after intravenous administration. (B) Schematic representation of functionalized NPs is presented on the left, blood clearance kinetics of NPs is presented by changes in the longitudinal relaxation rate ( $\Delta R_1$ ) compared to the baseline over time (modified from [143-145]).

In terms of biological therapeutic effects, heteromultivalency is also attractive to design inhibitors of tumor survival dependent receptors because of their intrinsic multivalency-induced high affinity and steric stabilization [126]. Dong and co-workers reported bispecific antibodies (BsAbs) targeting EGFR and IGF-1R with enhanced anti-tumor activity [146]. Similar strategy was used to develop BsAbs against HER2 and VEGF. The affinity-improved BsAbs could inhibit both receptors-regulated cell proliferation *in vitro* and tumor progression in multiple tumor mouse models [147]. Notably, Chiu et al. used multivalent antibodies

(trastuzumab and rituximab) to generate dual-targeted liposomes, with improved cytotoxicity in breast cancer cell lines through clustering of the target/antibody complex [148]. In LCC6<sup>HER2</sup> breast tumor bearing mouse, intravenously injected trastuzumab grafted liposome (1.0 mg/kg) exhibited long-term inhibition of tumor growth with 4/6 complete tumor regressions. These striking data strongly proved the potential of multivalent NPs to fight cancer.

As shown in Fig. 20, Xu and coworkers suggested that the interaction of a multivalent carrier with the extracellular domain of receptors may inexplicably activate cell signaling cascades and modify the expected activity [126]. For example, cell membrane receptor clustering could provide cell survival signaling by RGD-based NPs in PC12 cells [149]. As well, immobilized BMP-2 on gold nanostructures could induce sustained p-Smad and trigger the Smad-transcriptional pathway, which is essential for osteogenic differentiation of bone precursor cells [150].

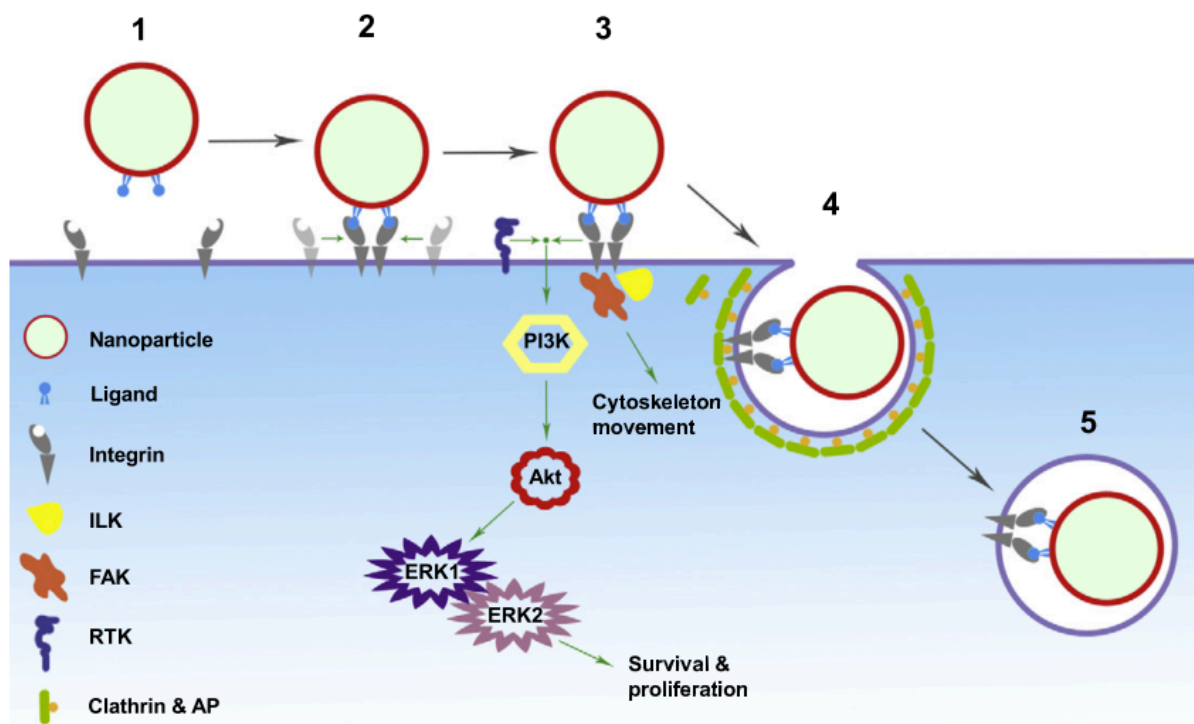


Fig. 20 Multivalent targeting of integrin receptors activates signaling. Phase 1, the cargo bearing ligands approaches the plasma membrane bearing receptors; Phase 2, the ligands bind the recognition domain of the receptors and triggers their polymerization; Phase 3, the spatially segregated intracellular domains of the receptors initiate downstream signaling;

Phase 4, the cargo falls into the invagination formed by the plasma membrane; Phase 5, the cargo is internalized for subsequent intracellular trafficking/signaling. Binding of NPs to integrins can activate signaling pathways and subsequently affect cell proliferation, differentiation or migration. Integrins synergize with other cell surface receptors, such as receptor protein tyrosine kinases, to activate signaling via ERK1/2 cascade [126]

Receptor clustering due to multivalent binding is contributing to a wide range of biological processes, involving cell communication, differentiation, survival, migration and so on. And their clustering acts more like a “double-edged” sword in deciding cell fate, which implies that different cell membrane receptors may direct the cells into opposite destinies. So when we feel more powerful using this sword to kill cancer, careful consideration of receptors’ structure, receptor to receptor communication and the network of receptors’ intracellular signaling must really be considered in order to generate smart multivalency for cancer targeted therapies.

## 5 Results Part 1

### 5.1 Design of NPs

#### 5.1.1 Design of the NPs A, B, C and D

The group of Prof. Gilles Subra developed a method for obtaining well-defined tunable multi-functional fluorescent particles in a single step, that present several ligands covalently linked on their surface. Using this innovative chemistry, four different kinds of silica NPs were generated in Montpellier (Fig. 21). The detailed protocol, peptides and NPs' quantification information are attached in the appendices of paper I. The four NPs were covalently labeled with FITC, and named A-NP, B-NP, C-NP and D-NP, and the overall estimated peptide loading is approximately 0.25, 2.5, 25 and 250  $\mu\text{mol/g}$  respectively, which corresponds to 10, 100, 1000, 10,000 peptides per NP. The schematic presentation of all nanoparticles can be found in Fig. 21 and 22. The calculations are presented in the attached paper published in journal of Chemistry of Materials (CM). NPs, introduced with fluorine atoms in the peptides, were named NP<sub>F</sub>.

- A-NP are naked silica NP grafted with cRGD and ATWLPPR respectively with a short linker of four Alanines between the peptides and the silica.
- B-NP are identical to A plus PEG2000 also added on the surface.
- For C-NP, the naked NP are grafted with PEG2000 but this time the peptides are separated from the silica by a spacer made of PEG3000.
- D-NP are like C-NP but without the PEG2000.

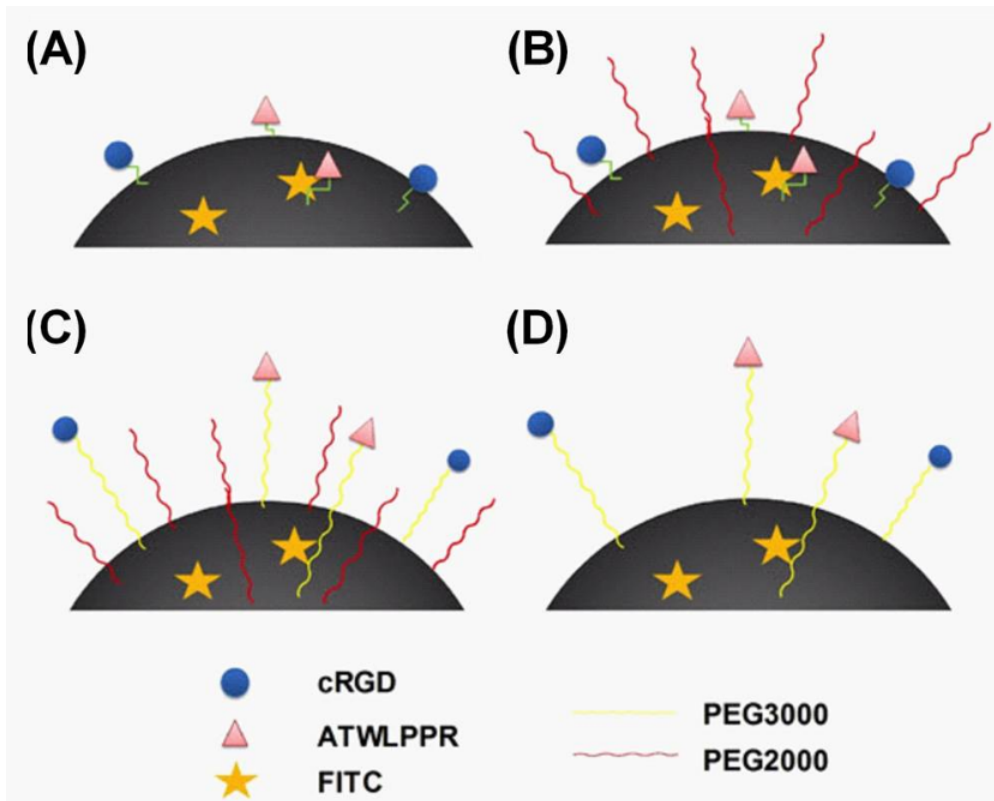


Fig. 21 Schematic presentation of four different series of silica NPs

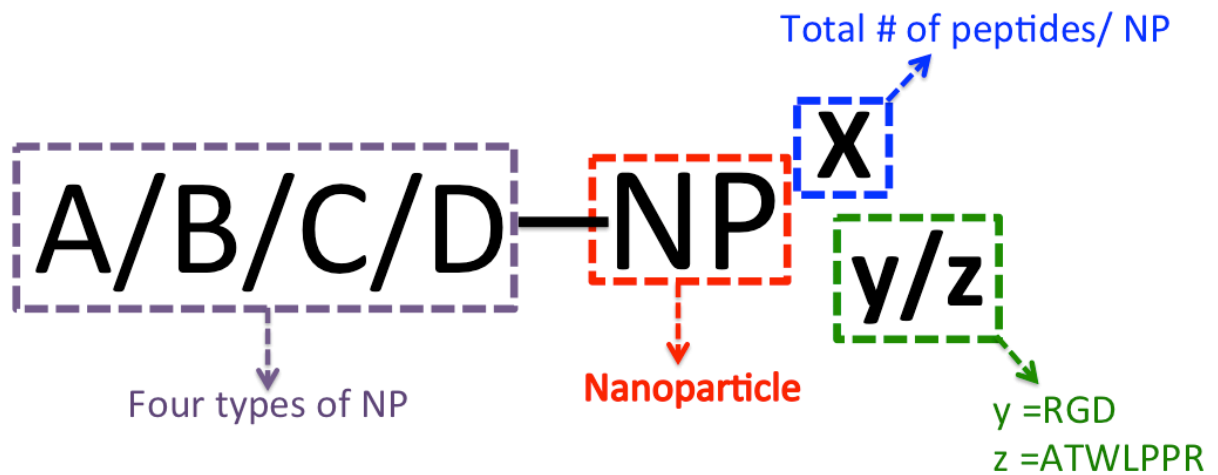


Fig. 22 Schematic presentation of the terminology A/B/C/D, NP, X and y/z

### 5.1.2 Different chemical synthesis (FITC, Fluorine)

FITC was used to label all NPs. In order to accurately quantify the peptides' number and ratio on the surface of NP, fluorine atoms were introduced in the spacers. The original fluorine nuclear magnetic resonance method is also presented in the following chapter.

### 5.1.3 Characterization of receptor expression in the selected cell lines

#### *5.1.3.1 Flow cytometry analysis of the integrin $\alpha_v\beta_3$ and NRP1 expression in 9 cell lines*

Expression of integrin  $\alpha_v\beta_3$  and NRP1 was tested by FACS analysis using chosen antibodies that recognized their extracellular domains only (Fig. 23). The results are reported as mean fluorescence intensities (MFI) histogram counts while pa-MFI (table 7) indicates the Percentage of Augmentation of the MFI as compared to the auto-fluorescence levels. Pa-MFI is thus providing a semi-quantitative evaluation of the relative level of expression of the receptors in the selected cells.

Endothelial cells express high levels of  $\alpha_v\beta_3$  and NRP1, whereas 3T3 fibroblasts are negative and will serve as negative controls. M21, MDA-MB-231 and PANC-1 cells also express high levels of  $\alpha_v\beta_3$ . In particular, the Pa-MFI of  $\alpha_v\beta_3$  in M21 is the highest one among the tumor cell lines while, as expected, the mutant M21L cell line derivative of M21 was confirmed to be negative for  $\alpha_v\beta_3$ . Concerning the expression level of NRP1 in tumor cells, MDA-MB231, PANC-1 and H358 are strongly positive while both clones of M21 are very weakly positive if not negative.

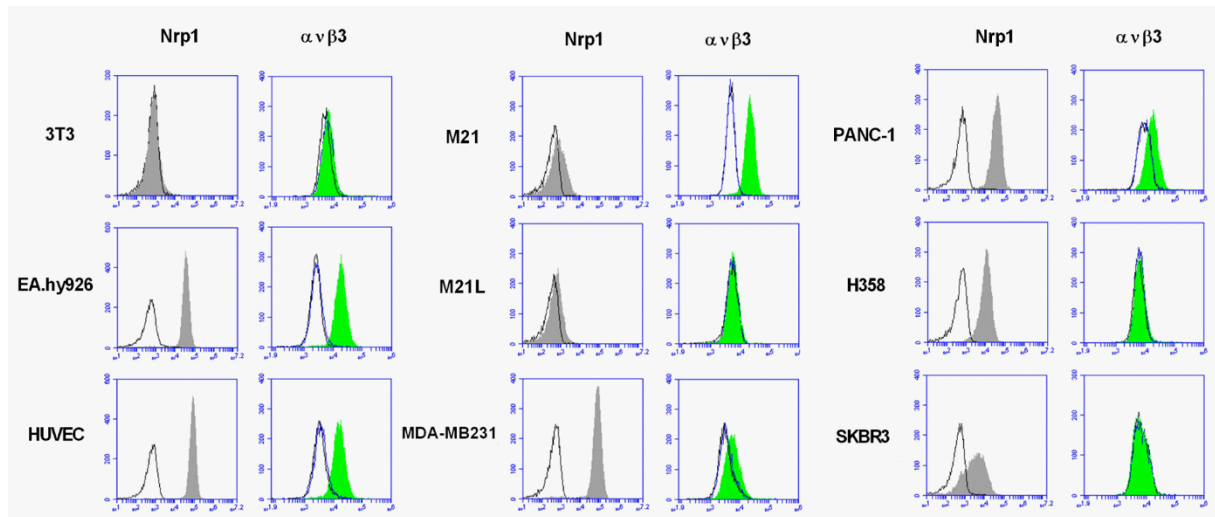


Fig. 23:  $\alpha v \beta 3$  (green) and NRP1 (gray) expression levels in the different cell lines.

	3T3	EA.hy 926	HUVEC	SKBR3	H358	PANC-1	M21L	M21	MDA-MB 231
<b><math>\alpha v \beta 3</math></b>	1,1	6,9	4,5	1,0	1,0	1,8	0,9	4,75	1,9
<b>NRP1</b>	1,2	70,4	139,2	11,6	23,2	67,0	1,9	2,6	176,7

Table 7 Pa-MFI values of integrin  $\alpha v \beta 3$  and NRP1 in 9 cell lines

#### 5.1.3.2 WB analysis of VEGFR1/2 and NRP1/2 expression in 5 tumor cell lines

WB was used to measure the total level of VEGF receptors in 5 tumor cell lines (Fig. 24). We then compiled our results with those of the literature to generate Table 8.

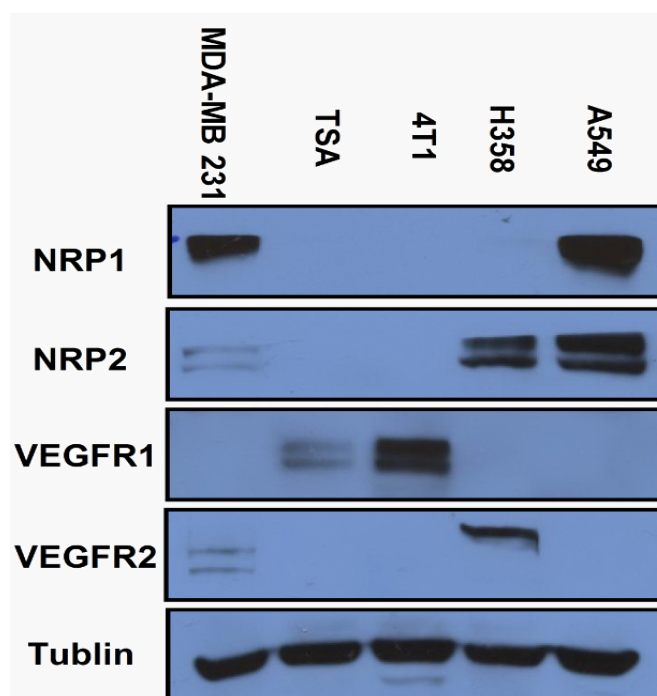


Fig. 24 WB analyses of VEGF receptors expression in five tumor cell lines

	Nrp	VEGFR	
MDA-MB231	R1+++	R1++[1]	1. Lee, T.H., et al., <i>Vascular endothelial growth factor mediates intracrine survival in human breast carcinoma cells through internally expressed VEGFR1/FLT1</i> . PLoS Med, 2007. <b>4</b> (6): p. e186. 2. Guo, S., et al., <i>Vascular endothelial growth factor receptor-2 in breast cancer</i> . Biochim Biophys Acta, 2010. <b>1806</b> (1): p. 108-21. 3. Roland, C.L., et al., <i>Cytokine levels correlate with immune cell infiltration after anti-VEGF therapy in preclinical mouse models of breast cancer</i> . PLoS One, 2009. <b>4</b> (11): p. e7669. 4. Wu, W., et al., <i>Targeted therapy of orthotopic human lung cancer by combined vascular endothelial growth factor and epidermal growth factor receptor signaling blockade</i> . Mol Cancer Ther, 2007. <b>6</b> (2): p. 471-83. 5. Sini, P., et al., <i>Inhibition of multiple vascular endothelial growth factor receptors (VEGFR) blocks lymph node metastases but inhibition of VEGFR-2 is sufficient to sensitize tumor cells to platinum-based chemotherapeutics</i> . Cancer Res, 2008. <b>68</b> (5): p. 1581-92.
	R2++	R2+++[2]	
4T1	R1++	R1+++[3]	
	R2+	R2 — [3]	
TSA	R1+	R1++	
	R2+	R2 —	
H358	R1+	R1 ?	
	R2+++	R2 —[4]	
A549	R1+++	R1+[5]	
	R2+++	R2 —(R2++[5])	

Table 8 VEGF receptor levels in 5 tumor cell lines

#### 5.1.4 Binding efficiency of naked-NP on endothelial and tumor cells

According to their receptors' profile, we selected endothelial cells HUVEC and tumor cells MDA-MB-231, 4T1, H358 and A549 and tested their interaction with naked-NP *in vitro*. No matter how many receptors are present, naked-NP positively binds non-specifically to all cells (Fig. 25).

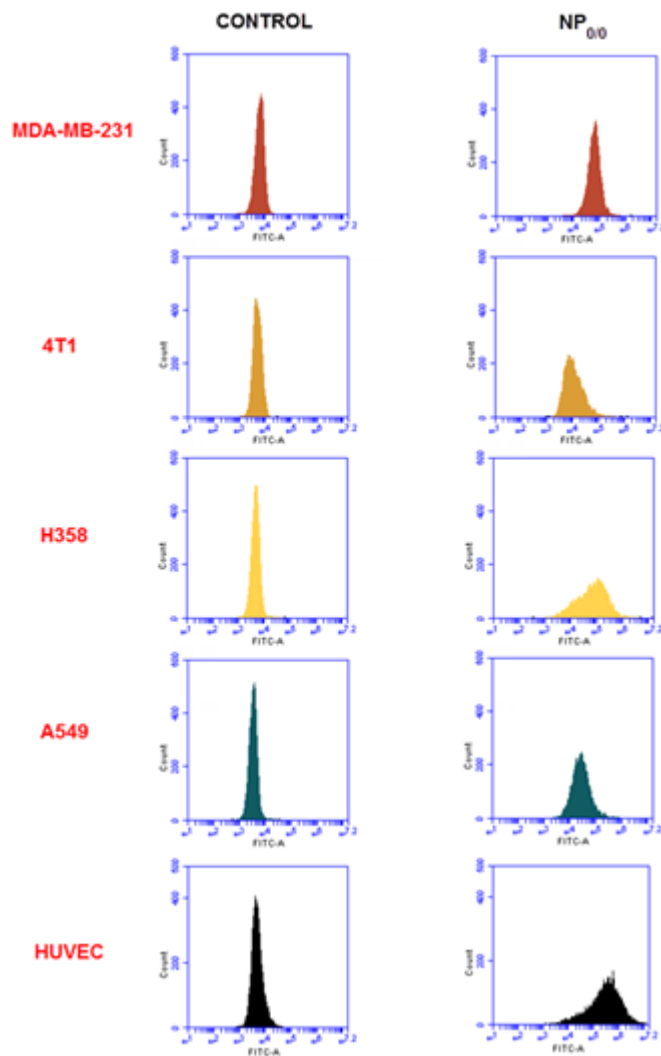


Fig. 25 Binding efficiencies of naked-NP on MDA-MB-231, 4T1, H358, A549 and HUVEC cells after an incubation of 30 min at 37°C.

The non specific binding of naked NP in all cells was not expected initially since the different NPs are presenting a negative zeta potential of -28mV that should avoid non specific electrostatic interactions with the negatively charged cell membranes.

## 5.2 Binding of type A NP on endothelial and tumor cells

### 5.2.1 Binding of type A NP with increasing amount of peptides/NP

A total of 10 to 10,000 cRGD and ATWLPPR peptides were grafted with a ratio of 50/50 on the naked NP and their binding efficiencies tested in three cell lines (Fig. 26 and 27) in comparison to the naked NPs. As described before, naked NP non-specifically binds to all cells. The presence of 10 or 100 peptides on their surface significantly reduced the non-specific binding, as indicated by the reduced value of the Pa-MFIs and by the percentage of positively stained cells, in particular for H358 and MDA-MB-231 cells. Thus the grafting of a small concentration of peptides seemed to prevent the non-specific binding rather than to provide an active ligand-mediated interaction. The positive action of the ligands was then visible as soon as 1000 peptides were grafted.

HUVEC reacted more sensitively and showed a very good specific interaction with the NPs. While the percentage of stained cells was slightly augmented with only 10 peptides on the NPs, the pa-MFI was strongly reduced. This suggested that a “threshold level” of highly reactive receptors exist in HUVEC but not in the 2 tumor cell lines. This may be solely related to the higher amount of both receptors on HUVEC, but may also reflect a better reactivity of the receptors in these normal primary endothelial cells as opposed to the two tumor cell lines.

Despite their different basal sensibilities at low peptide-concentration, each cell type was then reacting proportionally to the number of peptides grafted on the NPs.

As we expected in regard to the level of expression of both receptors, the functional NPs were binding more efficiently on HUVEC cells than on the 2 others. H358 cells showed the lowest binding with the NPs. The 2 tumor cell lines have similar levels of integrin  $\alpha_v\beta_3$ , but there is a seven times lower level of NRP1 in H358 than in MDA-MB-231 (Table 7). However the pa-MFI were quite similar. This may indicate that the binding of the peptides presenting-NPs was depending more on the cRGD interaction rather than on ATWLPPR's. This was

confirmed when compared to HUVECs. The signal intensities of each NP in HUVEC cells was 10 times as much as that of MDA-MB-231, although the level of NRP1 in HUVEC cells is lower than in MDA-MB-231. However, the integrin level is twice as much as that of MDA-MB-231. This strongly supports the notion that the integrin  $\alpha_v\beta_3$  is the “driver” of the interaction with the NPs, while NRP1 seems to be of minor importance.

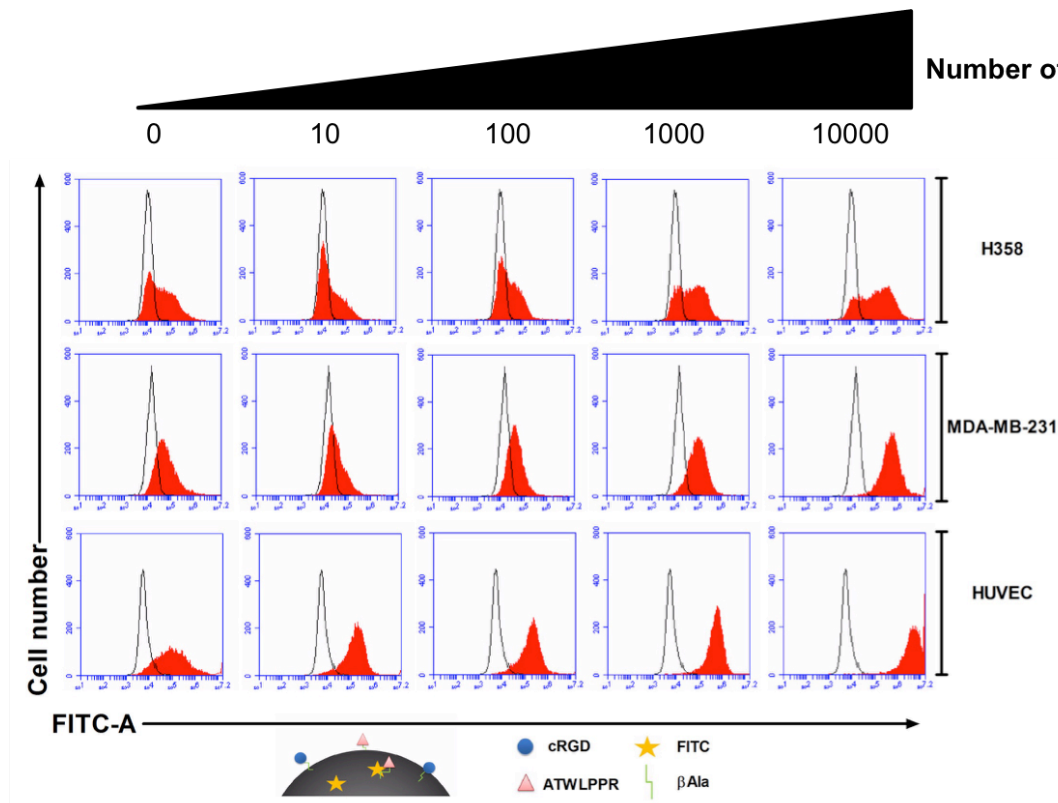


Fig. 26 . Influence of the ligands’ amount on binding efficiencies of type A NP<sub>50/50</sub> in HUVEC, MDA-MB-231 and H358 cells. Flow cytometry analysis of H358, MDA-MB-231 and HUVEC cells incubated with the different NPs for 30 min at 37°C in 5% CO<sub>2</sub>.

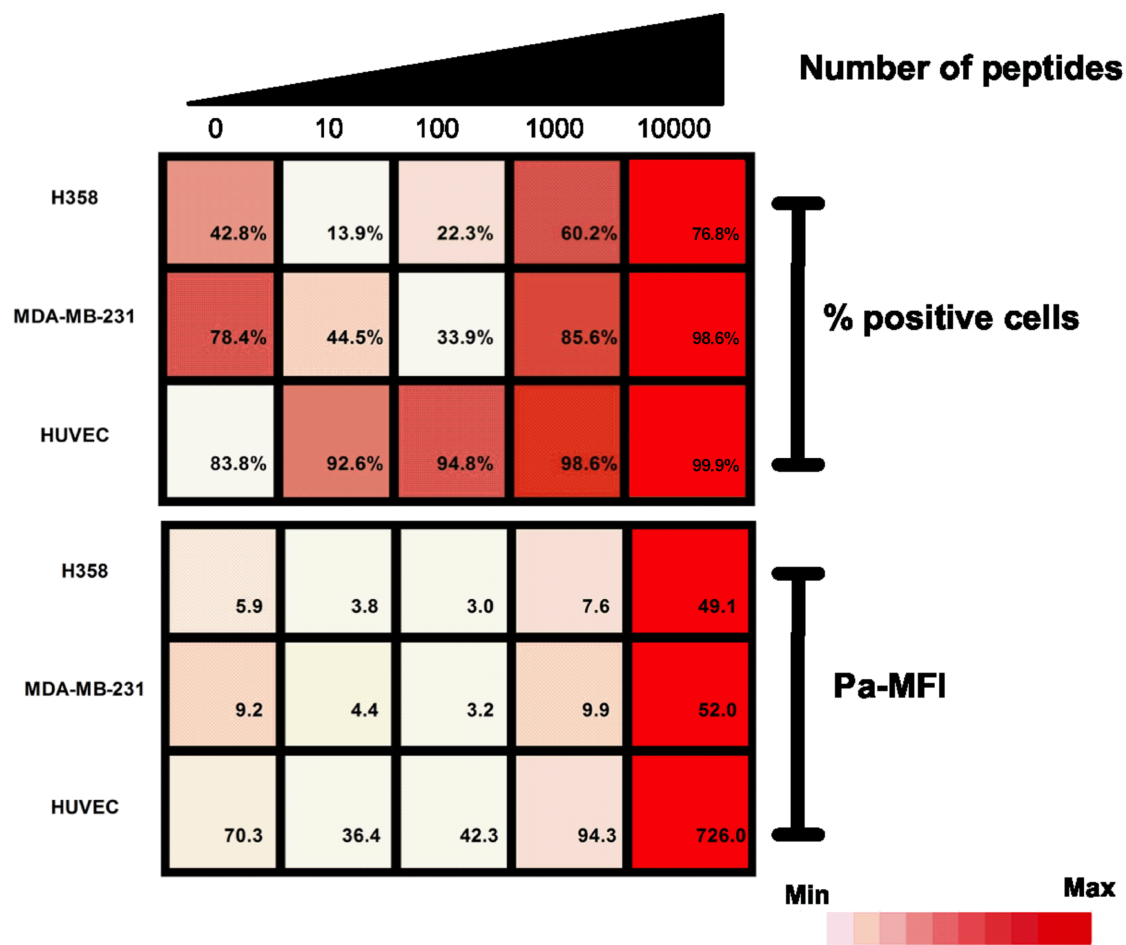


Fig. 27 Row normalized sorting of the values of Pa-MFI and the percentage of positive cell populations. Influence of the ligands' amount on the binding efficiency of type A NP<sub>50/50</sub> in HUVEC, MDA-MB-231 and H358 cells.

### 5.2.2 Binding of type A NP on tumor cells as a function of peptide ratios and concentrations

We generated 15 batches of bifunctional [anti integrin] / [anti NRP1] silica-NPs, with different ratio of peptides (100/0, 25/75, 50/50, 75/25 or 0/100 % cRGD/ATWLPPR respectively) and increasing concentrations of total amount of peptides/ NP (10, 100 and 1000).

We then tested their binding efficiency on H358 and MDA-MB-231 by FACS (Fig. 28, 29, 30, 32, 33 and 34). Confocal microscopy was also used to visualize their possible internalization (Fig. 31 and 35).

All the NPs exhibited high binding efficiencies and internalization in both MDA-MB-231 and H358 cells. The binding intensities were quite similar among NPs with different ratio of peptides except when they were grafted with ATWLPPR only (0/100). In this case the binding was not as good, in agreement with our previous hypothesis on the poor efficiency of ATWLPPR. Also consistent with the previous data, we confirmed that more peptides on the surface of NP will bring better binding signal to both tumor cells.

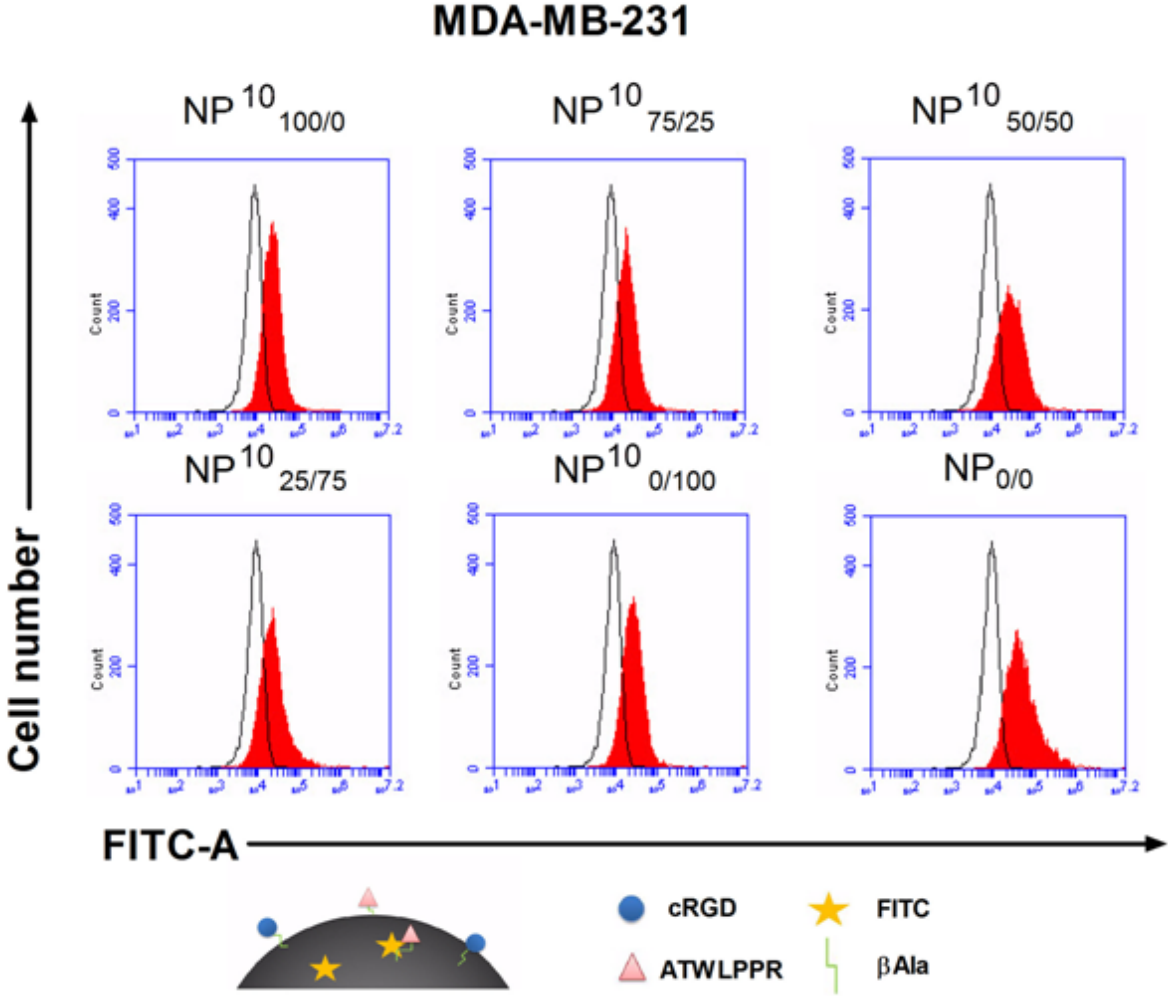


Fig. 28 Binding of type A  $NP^x_{y/z}$  on MDA-MB-231 cells. X indicates the loading amount of peptides on each NP, and y/z indicates the ratio of ligands. Flow cytometry analysis of MDA-MB-231 cells incubated with the different NPs for 30 min at 37°C in 5% CO<sub>2</sub>. Influence of the ratio y/z.

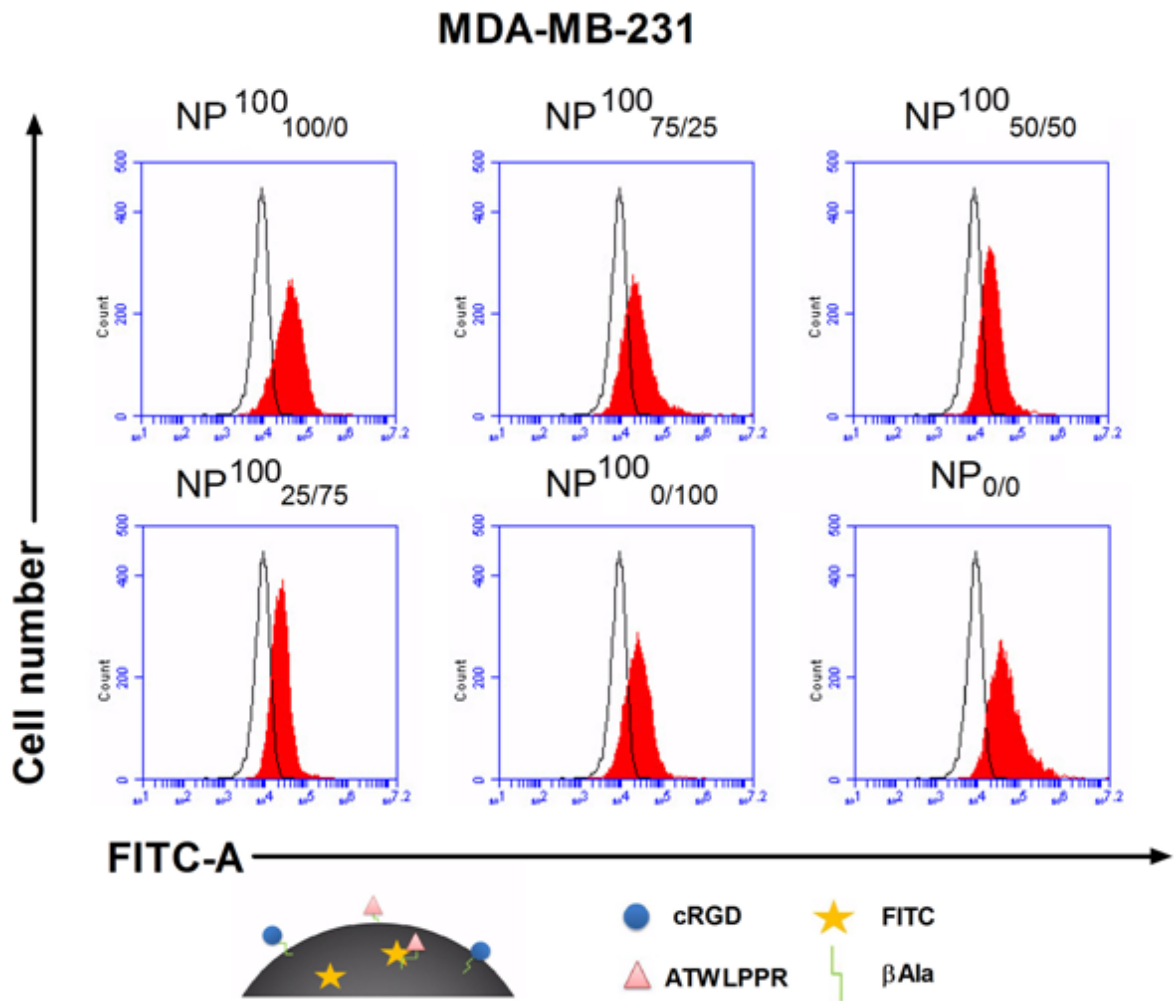


Fig. 29 Binding of type A NP<sup>x</sup><sub>y/z</sub> on MDA-MB-231 cells. X indicates the loading amount of peptides on each NP, and y/z indicates the ratio of ligands. Flow cytometry analysis of MDA-MB-231 cells incubated with the different NPs for 30 min at 37°C in 5% CO<sub>2</sub>. Influence of the ratio y/z.

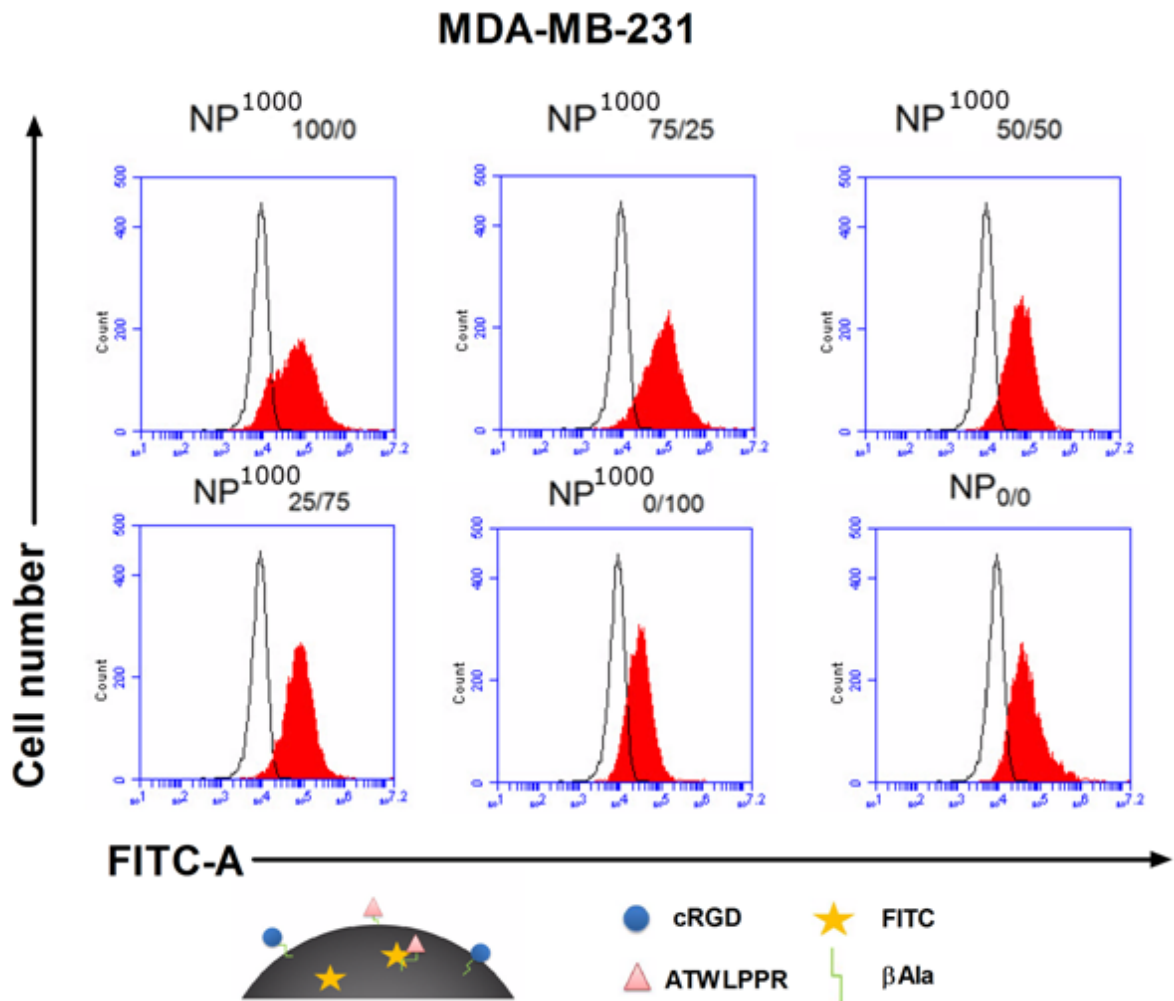


Fig. 30 Binding efficiency studies of type A NP<sup>x</sup><sub>y/z</sub> on MDA-MB-231 cells. X indicates the loading amount of peptides on each NP, and y/z indicates the ratio of ligands. Flow cytometry analysis of MDA-MB-231 cells incubated with the different NPs for 30 min at 37°C in 5% CO<sub>2</sub>. Influence of the ratio y/z.

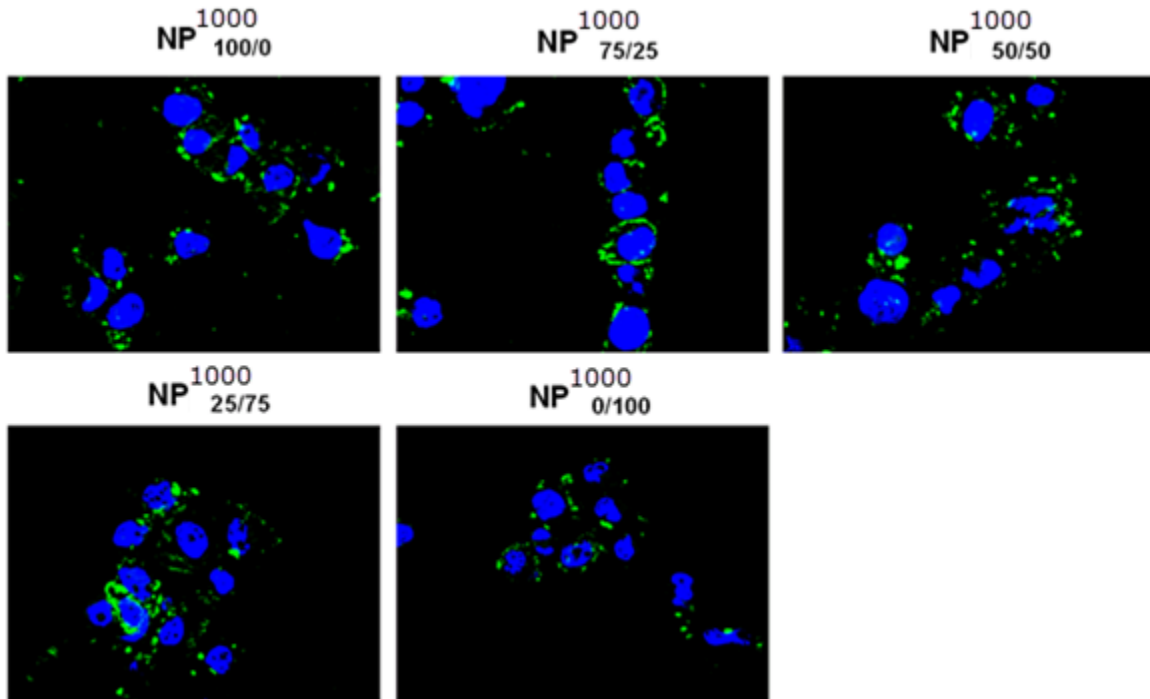


Fig. 31 Confocal microscopy studies of MDA-MB-231 cells incubated with the different type A  $NP_{y/z}^x$  for 60 min at 37°C in 5%  $CO_2$ . X indicates the loading amount of peptides on each NP, and y/z indicates the ratio of ligands. Green means FITC staining of NP, blue means the staining of cell nuclei. Influence of the ratio y/z.

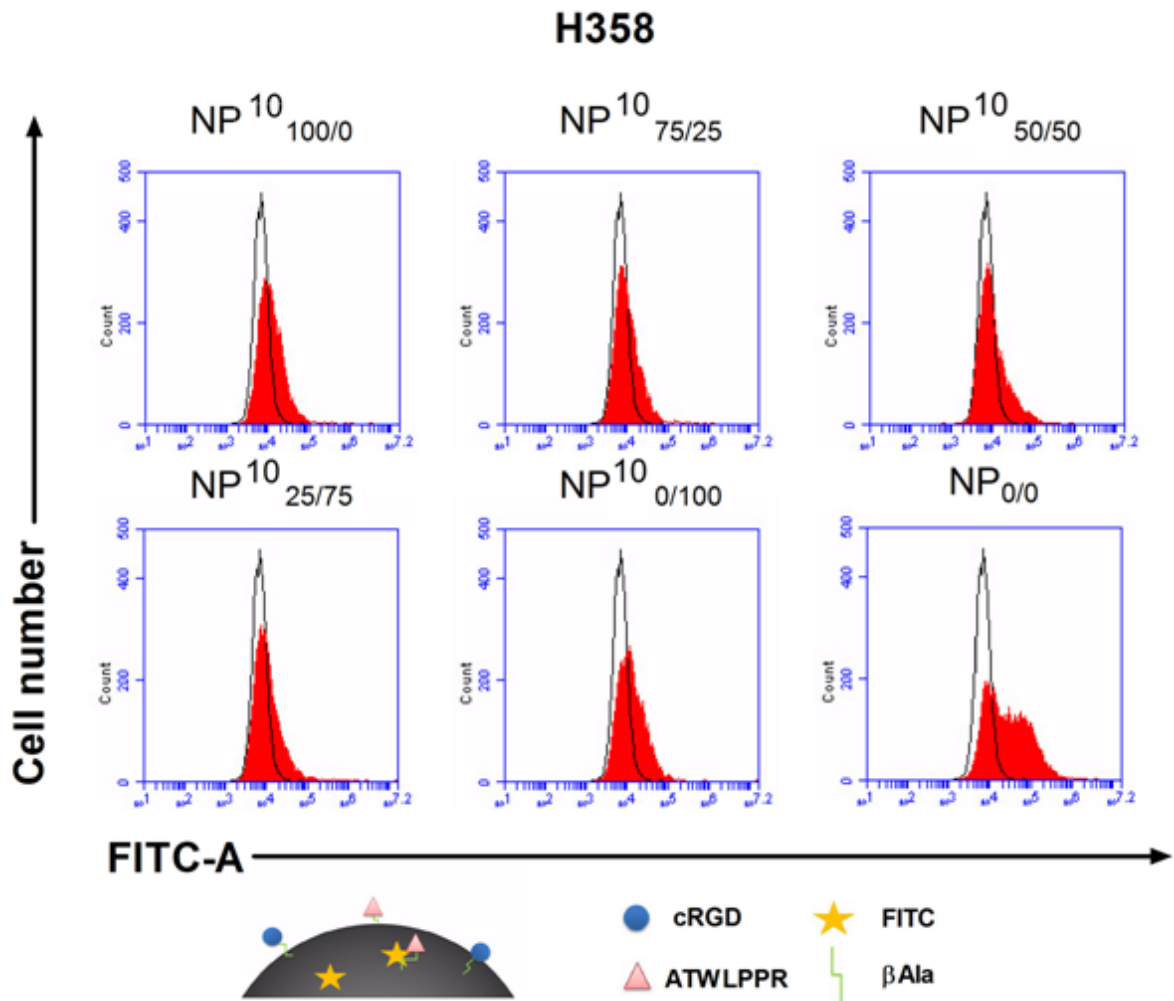


Fig. 32 Binding efficiency studies of type A NP<sup>x</sup><sub>y/z</sub> on H358 cells. X indicates the loading amount of peptides on each NP, and y/z indicates the ratio of ligands. Flow cytometry analysis of H358 cells incubated with the different NPs for 30 min at 37°C in 5% CO<sub>2</sub>. Influence of the ratio y/z.

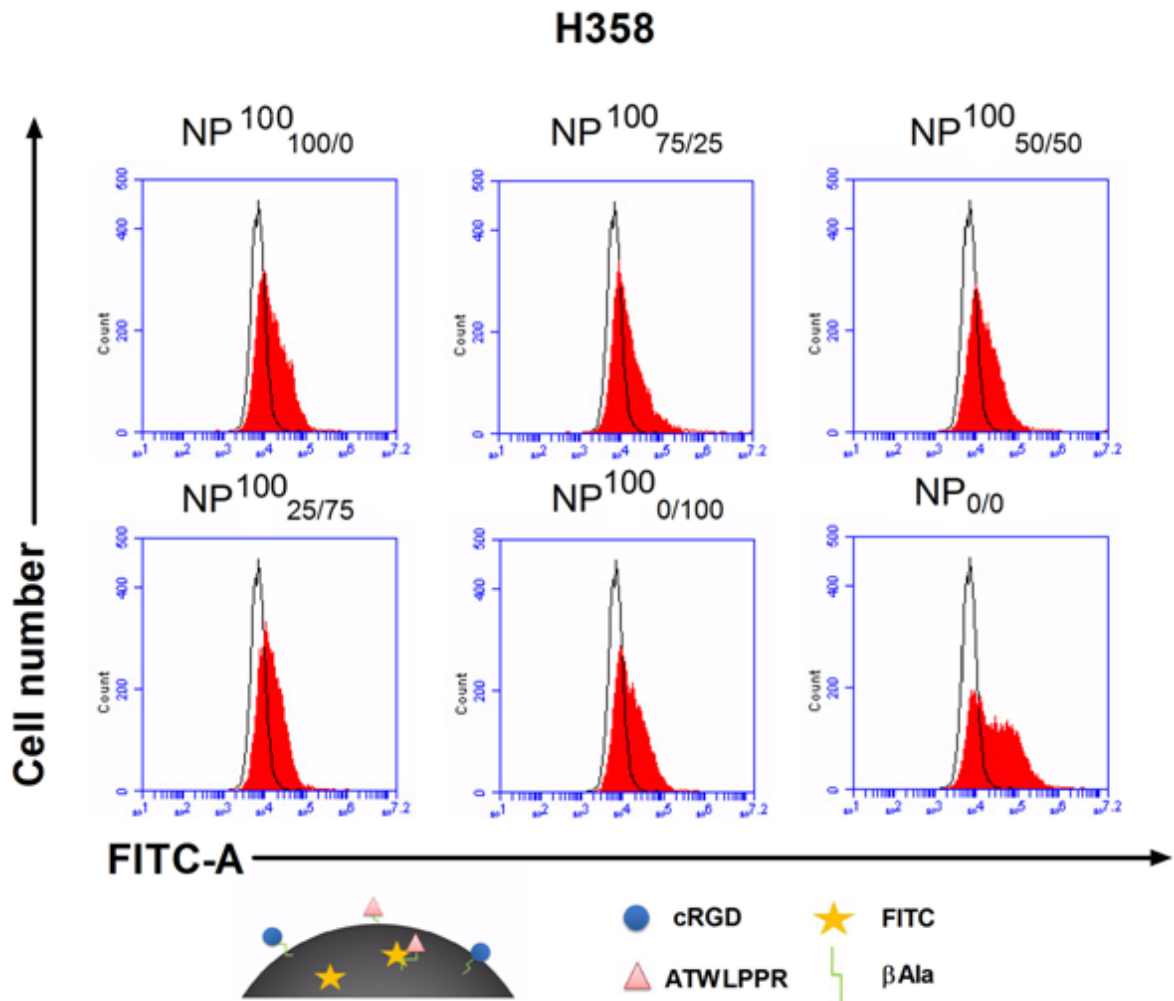


Fig. 33 Binding efficiency studies of type A NP<sup>x</sup><sub>y/z</sub> on H358 cells. X indicates the loading amount of peptides on each NP, and y/z indicates the ratio of ligands. Flow cytometry analysis of H358 cells incubated with the different NPs for 30 min at 37°C in 5% CO<sub>2</sub>. Influence of the ratio y/z.

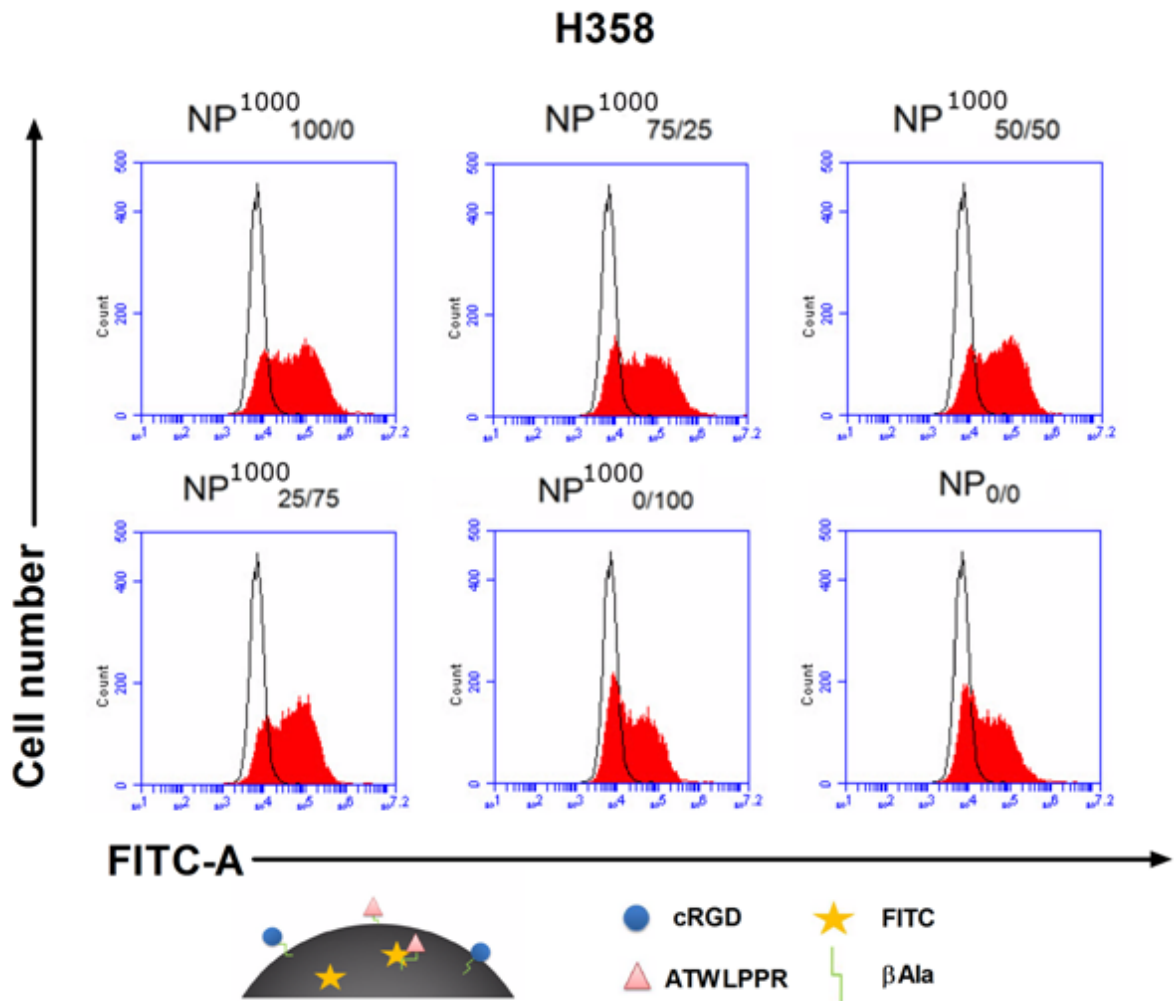


Fig. 34 Binding efficiency studies of type A  $NP^x_{y/z}$  on H358 cells. X indicates the loading amount of peptides on each NP, and y/z indicates the ratio of ligands. Flow cytometry analysis of H358 cells incubated with the different NPs for 30 min at 37°C in 5% CO<sub>2</sub>. Influence of the ratio y/z.

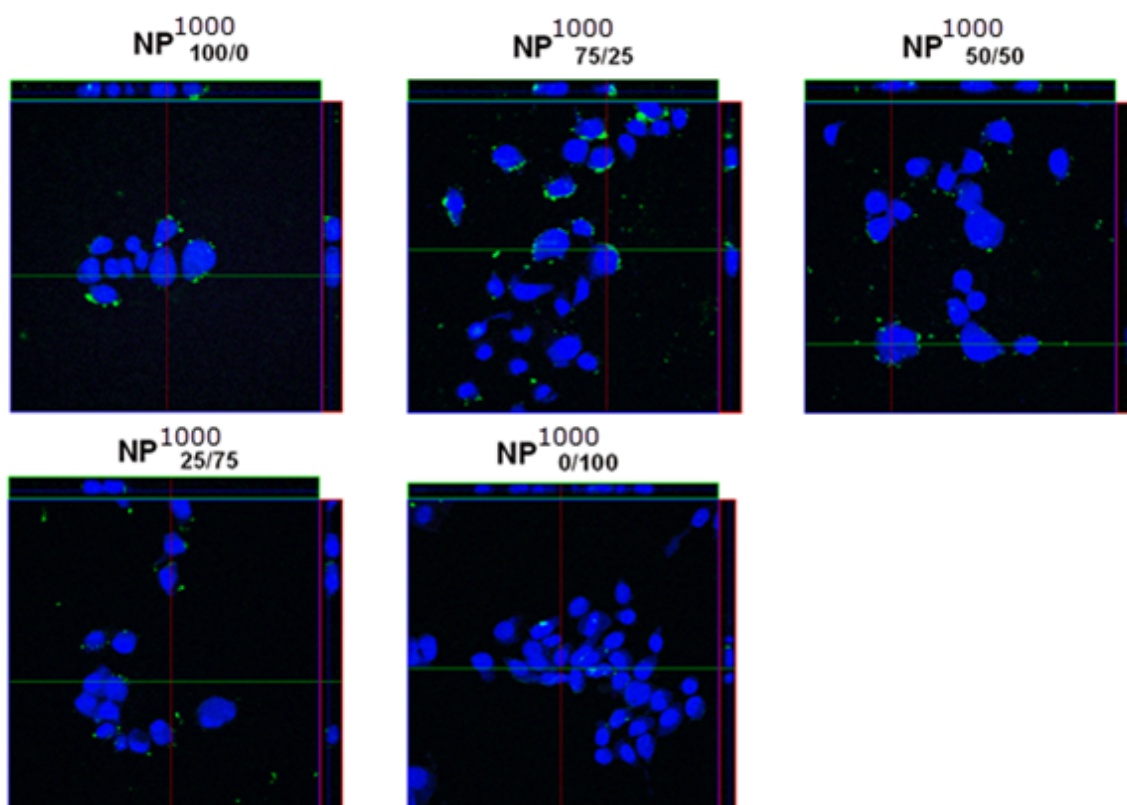


Fig. 35 Confocal microscopy studies of H358 cells incubated with the different type A  $NP_{y/z}^x$  for 60 min at 37°C in 5%  $CO_2$ . X indicates the loading amount of peptides on each NP, and y/z indicates the ratio of ligands. Green means FITC staining of NP, blue means the staining of cell nuclei. Influence of the ratio y/z.

### 5.3 Binding of type A Fluorinated-NP on HUVEC and tumor cells

#### 5.3.1 Interest of the presence of Fluorine

Pr. G Subra and coworkers used an innovative method to tune the ratio of two types of ligands on the surface of silica NPs by adjusting the relative concentrations of hybrid species in the starting solution. It is quite urgent and necessary to check the exact loading efficiency of each peptide on each NP. As I discussed in the introduction, the development of simple and quantitative methods would undoubtedly accelerate the translational process of nanomedicine from empirical research to controllable, “smart” and “personalized” therapeutics.

An original fluorine nuclear magnetic resonance (NMR) method was developed and applied to the quantitative measurement of loading of peptides. As presented in the attached paper, this relative and quantitative integration of  $^{19}\text{F}$  NMR signals allow a perfect characterization of the multifunctional nanoparticles.

## 5.3.2 Results published in CM

sml00 | ACSJCA | JCA10.0.1465/W Unicode | research.3f (R3.6.i11:4432 | 2.0 alpha 39) 2015/07/15 14:30:00 | PROD-JCA1 | rq\_4554034 | 1/07/2016 15:18:09 | S | JCA-DEFAULT

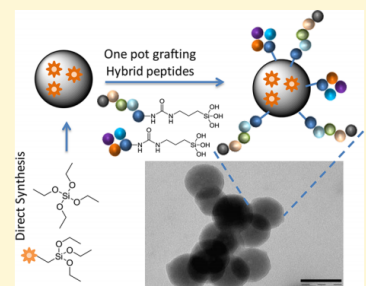
# Unambiguous and Controlled One-Pot Synthesis of Multifunctional Silica Nanoparticles

Jeremie Ciccione,<sup>†,‡</sup> Tao Jia,<sup>§</sup> Jean-Luc Coll,<sup>§</sup> Karine Parra,<sup>†</sup> Muriel Amblard,<sup>†</sup> Said Jebors,<sup>†,‡</sup> Jean Martinez,<sup>†</sup> Gilles Subra,<sup>\*,†</sup> and Ahmad Mehdi<sup>\*,‡</sup>

<sup>†</sup>Institut des Biomolécules Max Mousseron (IBMM), UMR5247 CNRS, ENSCM, Université de Montpellier, Montpellier, France  
<sup>‡</sup>Institut Charles Gerhardt-UMR5253, Equipe Chimie Moléculaire et Organisation du Solide, Université de Montpellier, Place Eugène Bataillon, F-34095 Montpellier Cedex 05, France  
<sup>§</sup>Institut Albert Bonniot IAB INSERM/UJF U823, Université Joseph Fourier, La Tronche, France

Supporting Information

**ABSTRACT:** Existing strategies for the synthesis of functional silica nanoparticles (SiNPs) rely on surface modifications followed by grafting of the organic moiety via chemoselective chemistry. Under these conditions, the introduction of several elements (e.g., ligands, drugs, fluorophores, vectors, etc.) on the same particle in a desired ratio and density is particularly difficult to achieve. We developed a method for obtaining in a single step well-defined tunable multifunctional fluorescent particles, presenting at their surface multiple ligands, covalently linked to their surface. Our strategy relies on the synthesis of hybrid bioorganic–inorganic peptide ligands, greatly simplifying the design of multifunctional nanoparticles. We demonstrated that it was possible to tune the ratio of two grafted ligands on the surface of the SiNPs simply by adjusting the relative concentration of hybrid species in the starting solution. An original fluorine nuclear magnetic resonance method was applied to the dissolved SiNPs to demonstrate our hypothesis.



## INTRODUCTION

To improve diagnosis and cancer treatment, conjugation of targeting elements to a drug and/or a detection probe is one of the most investigated approaches.<sup>1–3</sup> In this field, design of multifunctional particles on a nanometric scale can be seen as a promising therapeutic, diagnostic, or theranostic tool.<sup>4</sup> However, the orientation of molecules and their grafting density on the surface of the particle have a huge influence on the targeting efficiency.<sup>5,6</sup> These parameters are particularly difficult to control using classical surface chemistry, and their quantification remains a challenge. This is a crucial impairment when synergistic effects of two or more ligands on the same particle have to be investigated. Silica nanoparticles<sup>7</sup> (SiNPs) constitute a quite fascinating family of materials, attracting numerous research groups because of their ease of synthesis by the sol–gel process,<sup>8</sup> their size control, their biocompatibility,<sup>9</sup> and their ability to encapsulate different types of cargo molecules.<sup>10–13</sup> In this context, we developed a method for obtaining well-defined tunable multifunctional fluorescent SiNPs, presenting at their surface multiple ligands, covalently linked to their surface. Fluorine nuclear magnetic resonance (NMR) was used to accurately quantify their ratio. We previously reported the use of hybrid trialkoxysilyl peptides<sup>11</sup> for the synthesis of bioorganic–inorganic hybrid materials either by grafting<sup>14</sup> or by direct synthesis,<sup>15</sup> i.e., condensation of a hybrid block with tetraethoxysilane.

In this study, we first describe a straightforward and controlled synthesis of multifunctional fluorescent SiNPs involving hybrid triethoxysilylated peptides (2–5) and hybrid fluorescein 1 by combining grafting and direct synthesis (Figure 1). It is noteworthy that, in contrast to existing methods that require orthogonal protecting strategies, click or ligation methods, and surface modification, this functionalization

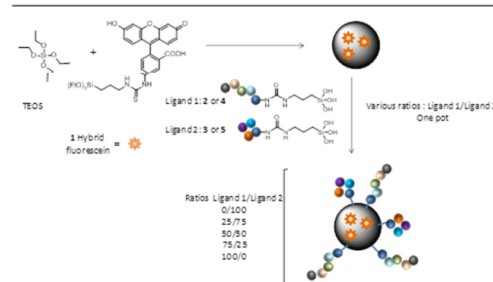


Figure 1. Synthesis of multifunctional fluorescent SiNPs.

Received: November 13, 2015

Revised: December 30, 2015

57 proceeds in a single step and does not require any additional  
58 chemical reagent.

## 59 ■ EXPERIMENTAL SECTION

60 Abbreviations: ACN, acetonitrile; Ac<sub>2</sub>O, acetic anhydride; DIEA,  
61 diisopropylethylamine; DMF, *N,N'*-dimethylformamide; NMM, 4-  
62 methylmorpholine; TFA, trifluoroacetic acid; TFE, 2,2,2-trifluoroetha-  
63 nol; TIS, triisopropylsilane; TNBS, trinitrobenzenesulfonic acid; PS,  
64 polystyrene; rt, room temperature; SPPS, solid phase peptide  
65 synthesis; BOP, *O*-(1*H*-benzotriazol-1-yl)-1,1,3,3-tetramethylphospho-  
66 nium hexafluorophosphate; Boc, *tert*-butyloxycarbonyl; Fmoc, fluo-  
67 renylmethoxycarbonyl; Z, benzyloxycarbonyl.

68 **Synthesis of Hybrid Triethoxysilyl Fluorescein 1.** Twenty-five  
69 milligrams of fluorescein isothiocyanate was stirred with 500  $\mu$ L of  
70 dimethyl sulfoxide (DMSO) and 3-aminopropyltriethoxysilane for 2 h  
71 in the dark at room temperature and used without further purification

72 **Synthesis of Fluorescent SiNPs.** Fluorescent nanoparticles were  
73 prepared by mixing 300 mL of cyclohexane and 80 mL of Triton X-  
74 100; 40 mL of an ammonia solution at 4.6 mol/L was added dropwise  
75 under vigorous stirring followed by 80 mL of 1-hexanol, 340  $\mu$ L of a  
76 fluorescein precursor solution, and 15 mL of tetraethylorthosilicate  
77 (TEOS). The reaction mixture was stirred at room temperature for 12  
78 h in the dark. The resultant product was precipitated by adding a large  
79 quantity of diethyl ether, filtered, washed by Soxhlet in ethanol as a  
80 solvent for 24 h, and desiccated to yield 3.80 g of fluorescent  
81 nanoparticles.

82 **Grafting of Hybrid Peptides 3 and 5 on Fluorescent SiNPs**  
83 **Was Detailed for a 50/50 (3/5) Ratio.** First, 1.59 mg of hybrid  
84 peptide 3 and 1.91 mg of hybrid peptide 5 were mixed with 100 mg of  
85 fluorescent SiNPs in 2 mL of a DMF/1% (v/v) AcOH mixture and  
86 stirred for 12 h at 65 °C. Ten milliliters of DMF was added, and the  
87 solution was centrifuged at 20000 rpm before the filtrate was removed.  
88 This procedure was repeated twice with DMF (10 mL) and twice with  
89 EtOH (10 mL). Grafted fluorescent nanoparticles were poured into 2  
90 mL of demineralized water and freeze-dried. An aliquot (60 mg) was  
91 dissolved in 650  $\mu$ L of NaOD in a D<sub>2</sub>O solution at a concentration of  
92 1.5 mol/L containing 10 mM TFA and analyzed by <sup>19</sup>F NMR for  
93 qualitative and quantitative determination. The five following spectra  
94 are given just for qualitative information. For quantification, peaks  
95 were isolated and integrated in a smaller window of 10 ppm.

96 **Synthesis of Pegylated Nanoparticles (NP-PEG) Used as**  
97 **Nonbinding NPs.** Twenty milligrams of commercially available  
98 triethoxysilyl polyethylene glycol (MW = 2000 g/mol) was mixed with  
99 100 mg of fluorescent SiNPs in 2 mL of a DMF/1% AcOH mixture  
100 and stirred 12 h at 65 °C. Ten milliliters of DMF was added, and the  
101 solution was centrifuged at 20000 rpm before the filtrate was removed.  
102 This procedure was repeated twice with DMF (10 mL) and twice with  
103 EtOH (10 mL). Grafted fluorescent nanoparticles were poured into 2  
104 mL of demineralized water and freeze-dried.

## 105 ■ RESULTS AND DISCUSSION

106 First, triethoxysilylated fluorescein derivative 1 was prepared by  
107 reaction of fluorescein isothiocyanate with 3-aminopropyl  
108 triethoxysilane (see the Supporting Information). Fluorescent  
109 nanoparticles were synthesized by the water/oil microemulsion-  
110 mediated alkoxide hydrolysis method<sup>16,17</sup> but using co-  
111 condensation between tetraethylorthosilicate (TEOS) and  
112 compound 1 (0.064% molar). Particles were characterized by  
113 DLS and TEM (see the Supporting Information) showing a  
114 monodisperse distribution [Dh = 79 nm; pdi (0.124); and  
115 diameter = 40 nm]. It is noteworthy that these particles  
116 contained the fluorophore covalently bound (Si-C), and no  
117 leaching of fluorescein was observed even after 48 h in solution.  
118 Different sequences recognizing the overexpressed receptors in  
119 tumor cells were selected and displayed on the surface of  
120 SiNPs. The cyclic [RGDFK] sequence, which binds to integrin  
121  $\alpha_v\beta_3$  receptor,<sup>18,19</sup> will be co-presented by the particles along

with a different peptide that can bind to specific receptors co-  
expressed with this integrin receptor. For that purpose, we  
chose the antiangiogenic peptide ATWLPPR-OH, a neuropilin-  
1 receptor (NRP1) antagonist involved in the spread of  
cancer.<sup>20</sup>

The synthesis of the different hybrid peptides was started by  
Fmoc SPPS<sup>21</sup> on trityl resin, followed by several steps in  
solution (see the protocols in the Supporting Information). A  
spacer was introduced to increase the distance between the  
bioactive sequence and the surface of the SiNPs.<sup>22</sup>

Peptides were purified by RP-HPLC. Finally, the free amino  
group of the  $\beta$ -Ala spacer of the peptide sequence was reacted  
with 3-isocyanatopropyltriethoxysilane (ICTPES). After pre-  
cipitation by addition of diethyl ether, hybrid peptides 2–4  
(Table 1) were recovered and used immediately.

**Table 1.** Hybrid Triethoxysilylated Ligands 2–5

Id	MW RSi(OEt) <sub>3</sub> RSi(OH) <sub>3</sub>	m/z <sup>[a]</sup> found	spacer	peptide sequence
2	1205.6 1121.3	1122.6	(EtO) <sub>3</sub> Si-CH <sub>2</sub> -CH <sub>2</sub> -CH <sub>2</sub> -NH-	cyclic(LysArgGlyAsp(D)Phe) <sub>4</sub>
3	1273.6 1189.5	1190.6	(EtO) <sub>3</sub> Si-CH <sub>2</sub> -CH <sub>2</sub> -CH <sub>2</sub> -NH-	cyclic(LysArgGlyAsp(D)Phe) <sub>2</sub>
4	1370.7 1286.6	1287.4	(EtO) <sub>3</sub> Si-CH <sub>2</sub> -CH <sub>2</sub> -CH <sub>2</sub> -NH-	AlaThrTrpLeuProPr oArg-OH
5	1535.8 1452.7	1453.6	(EtO) <sub>3</sub> Si-CH <sub>2</sub> -CH <sub>2</sub> -CH <sub>2</sub> -NH-	AlaThrTrpLeuProPr oArg-OH

According to our experience related to hydrolysis and  
polycondensation of different organosilanes to obtain multi-  
functional hybrid thin films<sup>23</sup> or powder,<sup>24</sup> we hypothesized  
that the efficiency of grafting hybrid trialkoxysilyl peptides on  
the silica surface will be not significantly influenced by the  
peptide sequence. In other words, we thought that one can  
control the final ratio of grafted peptides on the silica  
nanoparticles by simply blending the hybrid peptides in the  
desired ratio in the grafting solution (Figure 1).

To validate our hypothesis, hybrid peptides 3 and 5 were  
prepared. The linker contained an (*R,S*)-3,3,3-trifluoroalanine  
or an (*R*)-2-fluorophenylalanine, these residues being used as  
probes for <sup>19</sup>F NMR quantification.

All multifunctionalization of SiNPs was performed in one  
step. Interestingly, in contrast with grafting methods relying on  
chemical activation like *N*-hydroxysuccinimide esters, unpro-  
tected peptide sequences were used during surface functionali-  
zation. Moreover, unlike other ligations or click methodologies,  
no chemical reagent or catalyst was required to achieve covalent  
bonding. Briefly, 100 mg of fluorescent SiNPs was poured into  
2 mL of a DMF/AcOH [99/1 (v/v)] solution containing  
hybrid peptides 3 and 5, whose spacer arm contained fluorine  
atoms, at five different molar ratios (100/0, 75/25, 50/50, 25/  
75, and 0/100) noted NP<sub>F</sub><sup>x</sup><sub>y/z</sub> with *x* is the loading and *y/z* is  
the 3('c[RGDFK]')/5('ATWLPPR') ratio. The total concentra-  
tion of hybrid peptide ([compound 3] + [compound 5])  
was set to 1.25 mM. The suspension was stirred for 12 h at 60  
°C. After being washed with DMF and EtOH and dried, the  
NPs were recovered. SiNPs are noted NP<sub>F</sub><sup>x</sup><sub>y/z</sub> where *x* is the  
loading and *y/z* is the 3('c[RGDFK]')/5('ATWLPPR') ratio.

B

DOI: 10.1021/acs.chemmater.5b04398  
Chem. Mater. XXXX, XXX, XXX–XXX

167 NP<sub>F</sub> were analyzed by TEM and DLS (see the Supporting  
168 Information). They maintained their size and monodisperse  
169 distribution.

170 Then, aliquots of SiNPs were completely dissolved in a 1.5 M  
171 NaOD/D<sub>2</sub>O solution and analyzed by <sup>19</sup>F NMR. As an  
172 example, the spectrum of SiNPs prepared with a 50/50 [3]/[5]  
173 ratio noted NP<sub>F</sub><sup>10</sup><sub>50/50</sub> is presented in Figure 2.

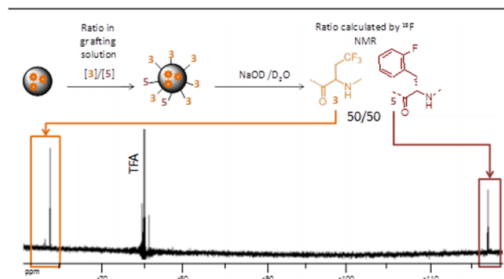


Figure 2. <sup>19</sup>F NMR spectrum of dissolved NP<sub>F</sub><sup>10</sup><sub>50/50</sub> (−64.0 ppm, CF<sub>3</sub> of 3; −117.0 ppm, PhF of 5; −75.5 ppm, TFA).

174 Each peptide presented fluorine atoms in a particular  
175 environment, yielding two distinct signals at −64.0 ppm for  
176 the three atoms of compound 3 and at −117.0 ppm for the  
177 single fluorine in the ortho position of the aromatic ring of 5.  
178 The relative and quantitative integration of <sup>19</sup>F NMR signals  
179 allowed a perfect characterization of the multifunctional  
180 nanoparticles. As expected, the five batches of SiNPs shared  
181 approximately the same overall peptide loading (≈10 μmol/g)  
182 that corresponded to 460 peptides per NP and 0.094 peptide/  
183 nm<sup>2</sup> (Table 2 and the Supporting Information for calculations).

Table 2. Relative and Quantitative Integration of <sup>19</sup>F NMR Signals of NP<sub>F</sub><sup>10</sup><sub>y/z</sub> Grafted with Peptides 3 and 5

NP <sub>F</sub> <sup>10</sup> <sub>y/z</sub>	theoretical [3]/[5] ratio	NMR [3]/[5] ratio	overall NMR peptide loading (μmol/g)
NP <sub>F</sub> <sup>10</sup> <sub>100/0</sub>	100/0	100/0	8.6
NP <sub>F</sub> <sup>10</sup> <sub>75/25</sub>	75/25	65/35	11.4
NP <sub>F</sub> <sup>10</sup> <sub>50/50</sub>	50/50	42/58	10.0
NP <sub>F</sub> <sup>10</sup> <sub>25/75</sub>	25/75	25/75	9.9
NP <sub>F</sub> <sup>10</sup> <sub>0/100</sub>	0/100	0/100	8.9

184 The <sup>19</sup>F NMR signal integrations, divided by a factor of 3 for  
185 compound 3, was proportional to the amount of each species  
186 found on the surface of the SiNPs. This validated our  
187 hypothesis: the estimated ratio by NMR signal integration of  
188 dissolved particles was very close to the [3]/[5] ratio used in  
189 the grafting solution.

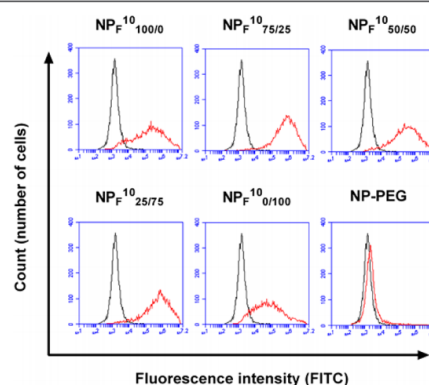
190 It demonstrated that it is possible to tune the ratio of grafted  
191 ligands on the surface of the SiNPs simply by adjusting the  
192 relative concentration of hybrid species in the starting solution.

193 Having proven the efficiency of our grafting method, we  
194 prepared a library of 15 multifunctional fluorescent SiNPs with  
195 hybrid peptides 2 and 4. Five different ratios (0/100, 25/75,  
196 50/50, 75/25, and 100/0) and three different loadings (10, 1,  
197 and 0.1 μmol/g) were used. SiNPs are noted NP<sup>x</sup><sub>y/z</sub>, where x is  
198 the loading and y/z is the 2(c[RGDFK])/4(ATWLPPR)  
199 ratio.

200 TEM images (see the Supporting Information) and DLS  
201 analyses (see the Supporting Information) showed our grafting

202 procedure neither altered the SiNPs nor modified their size. 202  
203 TGA and elemental analyses of NP<sup>10</sup> series, based on nitrogen  
204 and carbon atom content, indicated the successful immobiliza-  
205 tion of peptides (see the Supporting Information).

206 To investigate the tumor targeting ability, the NP<sub>F</sub> were  
207 assayed against three different human cell types. The human  
208 endothelial primary cells (HUVEC) express elevated levels of  
209 α<sub>v</sub>β<sub>3</sub> integrin and neuropilin-1 (NRP1). The human non-small  
210 cell lung cancer H358 cells present barely detectable amounts  
211 of the α<sub>v</sub>β<sub>3</sub> integrin and a medium amount of NRP1. The  
212 human breast cancer MDA-MB231 cells express modest levels  
213 of integrin and elevated levels of NRP1. We first established  
214 that NP<sup>10</sup> performed better than NP<sup>1</sup>, itself binding more  
215 strongly than NP<sup>0.1</sup> (see the Supporting Information). This  
216 indicated that the presence of 443 peptides/NP on the surface  
217 of these 40 nm large NP (density of 0.088 peptide/nm<sup>2</sup>) was  
218 the most relevant concentration under our conditions. This was  
219 established on HUVEC cells and confirmed on the both tumor  
220 cell lines (data not shown). We thus used the NP<sub>F</sub><sup>10</sup> with an  
221 adjusted ratio of peptides on HUVEC cells (Figure 3).



	% positive cells	Mean FL	CV FL
NP <sub>F</sub> <sup>10</sup> <sub>100/0</sub>	81%	780 634	198%
NP <sub>F</sub> <sup>10</sup> <sub>75/25</sub>	96%	1 396 234	127%
NP <sub>F</sub> <sup>10</sup> <sub>50/50</sub>	91%	928 553	168%
NP <sub>F</sub> <sup>10</sup> <sub>25/75</sub>	93%	1 347 248	141%
NP <sub>F</sub> <sup>10</sup> <sub>0/100</sub>	68%	407 930	283%
NP-PEG	6%	22 309	340%

Figure 3. Flow cytometry analysis of HUVEC cells incubated with the different NP<sub>F</sub><sup>10</sup><sub>y/z</sub> for 30 min at 37 °C in 5% CO<sub>2</sub>. Data for untreated control cells are presented as a black line. Influence of the y/z ratio. Mean FL indicates the mean fluorescent level, and CV FL corresponds to the coefficient of variation of the fluorescence level.

222 SiNPs pegylated with triethoxysilyl-PEG<sub>2000</sub> (NP-PEG) were  
223 used as nonbinding NPs for reference. The “pure” c[RGDF] 223  
224 100/0 grafted SiNPs were found to be better binders than the  
225 “ATWLPPR” NP<sub>F</sub><sup>10</sup><sub>0/100</sub> (Figure 3; the inset table shows the  
226 quantification of the fluorescent data). However, the best  
227 results were obtained when using the mixed NP<sub>F</sub><sup>10</sup><sub>25/75</sub> and  
228 NP<sub>F</sub><sup>10</sup><sub>75/25</sub>, suggesting that both peptides could cooperate to  
229 increase the binding efficiency if a 1/3 ratio of peptides is used.  
230 NP<sub>F</sub><sup>10</sup><sub>50/50</sub> was a better binder than the pure NP<sub>F</sub> also, but less

C

DOI: 10.1021/acs.chemmater.5b04398  
Chem. Mater. XXXX, XXX, XXX–XXX

231 efficient than NP<sub>F</sub><sup>10</sup><sub>75/25</sub> or NP<sub>F</sub><sup>10</sup><sub>25/75</sub>. These flow cytometry  
 232 results were confirmed on the two tumor cell lines (see the  
 233 Supporting Information), and similar results were obtained.  
 234 However, the binding efficiency was usually less important than  
 235 on HUVEC cells, in agreement with the modest expression of  
 236 both receptors on the tumor cell lines.

237 Interestingly, the presence of the two peptides compensated  
 238 well for the poor binding obtained with pure c[RGDf] 100/0 or  
 239 ATWLLPR 0/100. Fluorescence microscopy additionally  
 240 indicated that NPs were internalized after binding to their  
 241 receptors (Figure 4).

64

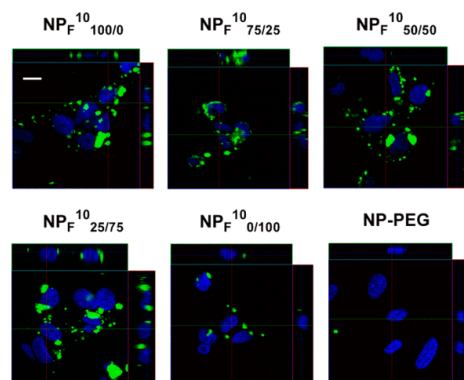


Figure 4. Confocal microscopy analysis of HUVEC cells incubated with the different NP<sub>F</sub><sup>10</sup> for 60 min at 37 °C in 5% CO<sub>2</sub>. Influence of the y/z ratio. The scale bar is 10 μm.

242 While pure NPs were mostly visible as patches attached to  
 243 the cell surface and as large aggregates of internalized vesicles,  
 244 mixed NPs presented a more discrete pattern of smaller  
 245 endocytosed vesicles with an augmented level of internalization  
 246 particularly visible with NP<sub>F</sub><sup>10</sup><sub>75/25</sub>. It is worth noting that the  
 247 nanoparticles remain stable in PBS even after a few hours. In  
 248 fact, the DLS measurements at 0, 40, 90, and 180 min show no  
 249 evolution for the hydrodynamic diameter (see the Supporting  
 250 Information). The presence of both ligands may thus affect the  
 251 internalization process. As expected, PEGylated NPs were not  
 252 binding to the cells.

## 253 ■ CONCLUSION

254 The use of hybrid triethoxysilylated peptides greatly simplifies  
 255 and rationalizes the design of multifunctional nanoparticles. For  
 256 the first time, an accurate control of the composition of the  
 257 surface grafting is achieved. This bottom-up approach is  
 258 virtually applicable to any kind of functional block (probes,  
 259 vectors, recognition elements, bioactive sequences, other  
 260 biomolecules, or biopolymers, etc.) as no orthogonal protection  
 261 strategy is required. Beyond the synthesis of multifunctional  
 262 NPs, the use of hybrid building blocks can have a real impact of  
 263 other fields of research, opening the way to numerous hybrid  
 264 bioorganic–inorganic materials in a manner much more  
 265 controlled than the postgrafting chemical strategies.

## ■ ASSOCIATED CONTENT

### Supporting Information

The Supporting Information is available free of charge on the ACS Publications website at DOI: 10.1021/acs.chemmater.5b04398.

Details of the polymer synthesis, experimental procedures, and complementary spectroscopic data (PDF)

## ■ AUTHOR INFORMATION

### Corresponding Authors

\*E-mail: gilles.subra@umontpellier.fr.

\*E-mail: ahmad.mehdi@umontpellier.fr.

### Author Contributions

J.C. and T.J. contributed equally to this work.

### Notes

The authors declare no competing financial interest.

## ■ ACKNOWLEDGMENTS

J.C. is supported by Institut Carnot Chimie Balard and LabEx ChemiSyst. T.J. is supported by the China Scholarship Council. Cyclic peptide synthesis optimization was performed using the facilities of the SynBio3 IBISA platform supported by ITMO cancer.

## ■ REFERENCES

- (1) Wang, L.; Zhao, W.; Tan, W. Bioconjugated Silica Nanoparticles: Development and Applications. *Nano Res.* **2008**, *1*, 99–115.
- (2) Coll, J.-L. Cancer Optical Imaging Using Fluorescent Nanoparticles. *Nanomedicine* **2011**, *6*, 7–10.
- (3) Dufort, S.; Sancey, L.; Coll, J.-L. Physico-Chemical Parameters That Govern Nanoparticles Fate Also Dictate Rules for Their Molecular Evolution. *Adv. Drug Delivery Rev.* **2012**, *64*, 179–189.
- (4) Li, Z.; Barnes, J. C.; Bosoy, A.; Stoddart, J. F.; Zink, J. I. Mesoporous Silica Nanoparticles in Biomedical Applications. *Chem. Soc. Rev.* **2012**, *41*, 2590–2605.
- (5) Hak, S.; Helgesen, E.; Hektoen, H. H.; Huuse, E. M.; Jarzyna, P. A.; Mulder, W. J. M.; Haraldseth, O.; Davies, C. d. L. The Effect of Nanoparticle Polyethylene Glycol Surface Density on Ligand-Directed Tumor Targeting Studied in Vivo by Dual Modality Imaging. *ACS Nano* **2012**, *6*, 5648–5658.
- (6) Stefanick, J. F.; Ashley, J. D.; Kiziltepe, T.; Bilgicer, B. A. Systematic Analysis of Peptide Linker Length and Liposomal Polyethylene Glycol Coating on Cellular Uptake of Peptide-Targeted Liposomes. *ACS Nano* **2013**, *7*, 2935–2947.
- (7) Claire Goldmann, C. Charge Transfer at Hybrid Interfaces: Plasmonics of Aromatic Thiol-Capped Gold Nanoparticles. *ACS Nano* **2015**, *9*, 7572.
- (8) Zha, J.; Roggendorf, H. In *Sol–gel Science, the Physics and Chemistry of Sol–gel Processing*; Brinker, C. J., Scherer, G. W., Eds.; Academic Press: Boston, 1990; xiv, pp 908. *Adv. Mater.* **1991**, *3*, S22.
- (9) Asefa, T.; Tao, Z. Biocompatibility of Mesoporous Silica Nanoparticles. *Chem. Res. Toxicol.* **2012**, *25*, 2265–2284.
- (10) Ambrogio, M. W.; Pecorelli, T. A.; Patel, K.; Khashab, N. M.; Trabolsi, A.; Khatib, H. A.; Botros, Y. Y.; Zink, J. I.; Stoddart, J. F. Snap-Top Nanocarriers. *Org. Lett.* **2010**, *12*, 3304–3307.
- (11) de la Torre, C.; Agostini, A.; Mondragón, L.; Orzáez, M.; Sancenón, F.; Martínez-Mañez, R.; Marcos, M. D.; Amorós, P.; Pérez-Payá, E. Temperature-Controlled Release by Changes in the Secondary Structure of Peptides Anchored onto Mesoporous Silica Supports. *Chem. Commun.* **2014**, *50*, 3184–3186.
- (12) Wang, Y.; Price, A. D.; Caruso, F. Nanoporous Colloids: Building Blocks for a New Generation of Structured Materials. *J. Mater. Chem.* **2009**, *19*, 6451.

D

DOI: 10.1021/acs.chemmater.5b04398  
Chem. Mater. XXXX, XXX, XXX–XXX

- 326 (13) Wang, Y.; Caruso, F. Mesoporous Silica Spheres as Supports for  
327 Enzyme Immobilization and Encapsulation. *Chem. Mater.* **2005**, *17*,  
328 953–961.
- 329 (14) Jebors, S.; Enjalbal, C.; Amblard, M.; Mehdi, A.; Subra, G.;  
330 Martinez, J. Bioorganic Hybrid OMS by Straightforward Grafting of  
331 Trialkoxysilyl Peptides. *J. Mater. Chem. B* **2013**, *1*, 2921–2925.
- 332 (15) Jebors, S.; Cecillon, S.; Faye, C.; Enjalbal, C.; Amblard, M.;  
333 Mehdi, A.; Subra, G.; Martinez, J. From Protected Trialkoxysilyl-  
334 Peptide Building Blocks to Bioorganic-Silica Hybrid Materials. *J.*  
335 *Mater. Chem. B* **2013**, *1*, 6510–6515.
- 336 (16) Iovino, G.; Malvindi, M. A.; Agnello, S.; Buscarino, G.; Alessi,  
337 A.; Pompa, P. P.; Gelardi, F. M. Optical and Morphological Properties  
338 of Infrared Emitting Functionalized Silica Nanoparticles. *Mater. Chem.*  
339 *Phys.* **2013**, *142*, 763–769.
- 340 (17) Arriagada, F. J.; Osseo-Asare, K. Synthesis of Nanosize Silica in a  
341 Nonionic Water-in-Oil Microemulsion: Effects of the Water/  
342 Surfactant Molar Ratio and Ammonia Concentration. *J. Colloid*  
343 *Interface Sci.* **1999**, *211*, 210–220.
- 344 (18) Haubner, R.; Finsinger, D.; Kessler, H. Stereoisomeric Peptide  
345 Libraries and Peptidomimetics for Designing Selective Inhibitors of  
346 the  $\alpha\beta3$  Integrin for a New Cancer Therapy. *Angew. Chem., Int. Ed.*  
347 *Engl.* **1997**, *36*, 1374–1389.
- 348 (19) Kanteleiner, M.; Schaffner, P.; Finsinger, D.; Meyer, J.; Jonczyk,  
349 A.; Diefenbach, B.; Nies, B.; Hölzemann, G.; Goodman, S. L.; Kessler,  
350 H. Surface Coating with Cyclic RGD Peptides Stimulates Osteoblast  
351 Adhesion and Proliferation as Well as Bone Formation. *ChemBioChem*  
352 **2000**, *1*, 107–114.
- 353 (20) Thomas, N.; Tirand, L.; Chatelut, E.; Plénat, F.; Frochet, C.;  
354 Dodeller, M.; Guillemain, F.; Barberi-Heyob, M. Tissue Distribution  
355 and Pharmacokinetics of an ATWLPPR-Conjugated Chlorin-Type  
356 Photosensitizer Targeting Neuropilin-1 in Glioma-Bearing Nude Mice.  
357 *Photochem. Photobiol. Sci. Off. J. Eur. Photochem. Assoc. Eur. Soc.*  
358 *Photobiol.* **2008**, *7*, 433–441.
- 359 (21) Amblard, M.; Fehrentz, J. A.; Martinez, J.; Subra, G. Methods  
360 and Protocols of Modern Solid Phase Peptide Synthesis. *Mol.*  
361 *Biotechnol.* **2006**, *33*, 239–254.
- 362 (22) Boturyn, D.; Coll, J.-L.; Garanger, E.; Favrot, M.-C.; Dumy, P.  
363 Template Assembled Cyclopeptides as Multimeric System for Integrin  
364 Targeting and Endocytosis. *J. Am. Chem. Soc.* **2004**, *126*, 5730–5739.
- 365 (23) Mehdi, A.; Dourdain, S.; Bardeau, J.-F.; Reyé, C.; Corriu, R. J.  
366 P.; Gibaud, A. First Direct Synthesis of Highly Ordered Bifunction-  
367 alized Mesoporous Silica Thin Films. *J. Nanosci. Nanotechnol.* **2006**, *6*,  
368 377–381.
- 369 (24) Mouawia, R.; Mehdi, A.; Reyé, C.; Corriu, R. J. P. From Simple  
370 Molecules to Highly Functionalised Lamellar Materials. *J. Mater.*  
371 *Chem.* **2008**, *18*, 2028–2035.

### 5.3.3 Supplementary data attached to the CM publication

- ❖ I compared the binding efficiency of different NPs (no Fluorine) with different amount and composition of peptides on HUVEC cells.

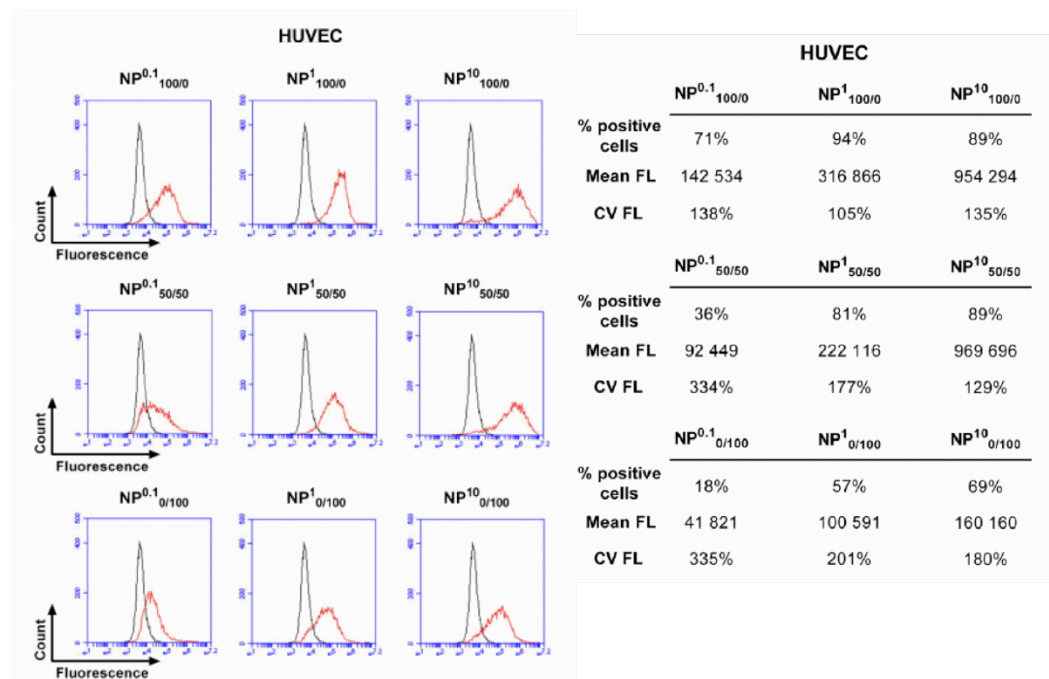


Fig. 36 Binding efficiency of type A NP<sup>x</sup><sub>y/z</sub> on HUVEC cells by FACS. X indicates three different loadings of peptides (0.1, 1 and 10 μmol/g) on NP, and y/z indicates the ratio of ligands. Flow cytometry analysis of HUVEC cells incubated with the different NPs for 30min at 37°C in 5% CO<sub>2</sub>. There is peptide dose effect on the binding efficiency. NP<sup>10</sup> bind more efficiently in HUVEC cells than NP<sup>1</sup> and NP<sup>0.1</sup>. The table shows the fluorescence data. Mean FL indicate the mean fluorescent level and CV FL corresponds to the coefficient of variation of the fluorescence level.

- ❖ I checked the binding efficiency of different type A Fluorine-NP in tumor cells MDA-MB-231 and H358.

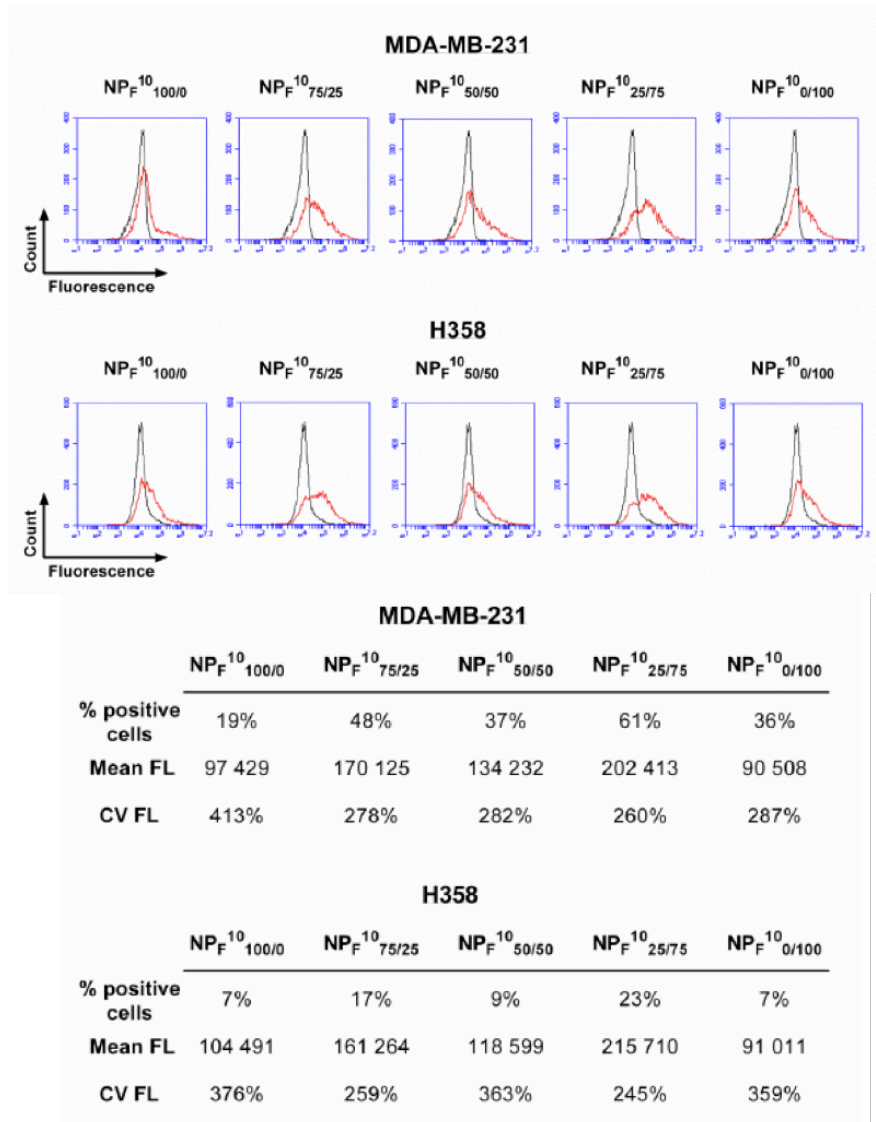


Fig. 37 Binding efficiency of type A Fluorine-NP<sup>10</sup><sub>y/z</sub> on MDA-MB-231 and H358 cells by FACS. Influence of the ratio y/z. Flow cytometry analysis of MDA-MB-231 and H358 cells incubated with the different NP<sub>F</sub> for 30 min at 37°C in 5% CO<sub>2</sub>. The Table shows the fluorescence data. Mean FL indicates the mean fluorescent level and CV FL corresponds to the coefficient of variation of the fluorescence level.

- ❖ The calculation of peptides on each NP:
  - The NP's diameter is around 40 nm;
  - The NP's surface is:  $S=5.02 \times 10^3 \text{ nm}^2$ ;

- The NP's volume is:  $v=3.35 \times 10^4 \text{ nm}^3$ ;
  - The density of NP is:  $\rho=2.2 \text{ g/cm}^3$ ;
  - The number of NP per gram is:  $1/(v \times \rho) \approx 1.36 \times 10^{16} \text{ NP/g}$ ;
  - A loading of 0.01 mmol/g represents 10  $\mu\text{mol}$  of peptide for  $1.36 \times 10^{16} \text{ NP}$ ;
  - The number of peptides per particle is:  $(1.0 \times 10^{-5} \times \text{NA}) / 1.36 \times 10^{16} \approx 443 \text{ peptides/NP}$ ;
- The number of peptides per square nanometer is:  $443/S \approx 0.09 \text{ peptides/nm}^2$ .

#### 5.4 Conclusion:

As compared with single-ligand grafted NPs, bifunctional NPs targeting integrin  $\alpha_v\beta_3$  and NRP1 simultaneously exhibit a better binding efficiency, especially for NP<sub>75/25</sub>. This indicates that the two peptides cooperate to increase NPs' binding. And this "cooperative" superiority is more pronounced on HUVEC cells than on tumor cells, in agreement with the modest expression of both receptors in the tumor cells. Tables of summary of the receptors' level and the binding efficiencies of different NPs are presented.

- Receptors level

	HUVEC	H358	MDA-MB-231
integrin $\alpha_v\beta_3$	+++++	+	++
NRP1	+++++	+	+++++

- Binding efficiency levels (**Obtained with type A NPs without fluorine**)

	HUVEC	H358	MDA-MB-231
NP <sup>1000</sup> <sub>100/0</sub>	+++++++	++	++
NP <sup>1000</sup> <sub>75/25</sub>	++++++++(best)	++(best)	+++ (best)
NP <sup>1000</sup> <sub>50/50</sub>	+++++++	+	++
NP <sup>1000</sup> <sub>25/75</sub>	+++++++	+	++
NP <sup>1000</sup> <sub>0/100</sub>	+++ (lowest)	+(lowest)	+(lowest)

Our *in vitro* results also demonstrate that NPs with the highest number of ligands present the strongest binding efficiency on all cells. This is mainly depending on the integrin  $\alpha_v\beta_3$  than on NRP1 expression. Finally, the binding rapidly leads to the internalization of all NPs.

## 6 Results Part 2: Type A NPs on primary ECs

### 6.1 NPs' binding efficiency

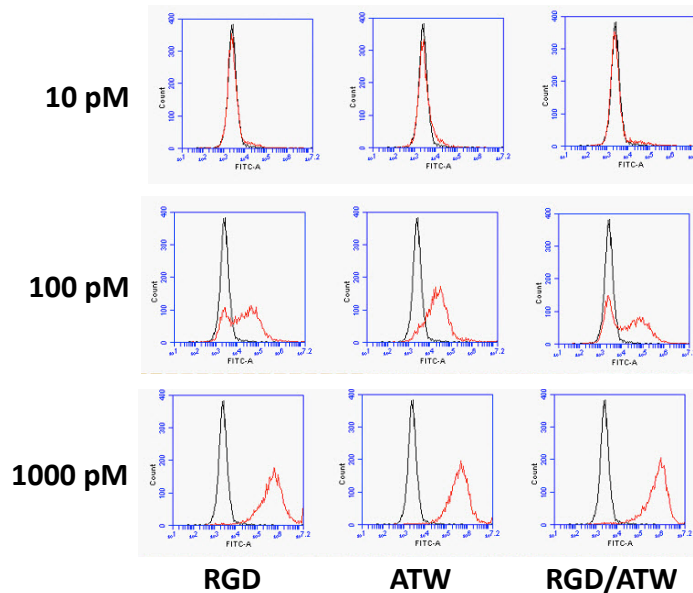


Fig. 38A Flow cytometry analysis of HUVEC incubated with the RGD-, ATW- or RGD/ATW-NPs at 10 pM, 100 pM or 1000 pM for 15min at 37°C in 5% CO<sub>2</sub> in serum free medium.

We firstly compared the binding efficiency of RGD-NP, RGD/ATW-NP (50/50) and ATW-NP on HUVEC cells at 10 pM, 100 pM or 1 nM. None of the NPs was significantly binding at 10 pM, but a dose-dependent augmentation of the fluorescent signal was detected at 100 pM and more pronounced at 1 nM (Fig. 38A).

Mixed RGD/ATW-NP generated the highest signal, and ATW-NP the lowest, thus confirming our previous results and confocal microscopy experiments [125].

We then focused on the 100 and 1000 pM concentrations and compared the binding efficiency versus the scrambled ones in the presence of serum (Fig. 38B).

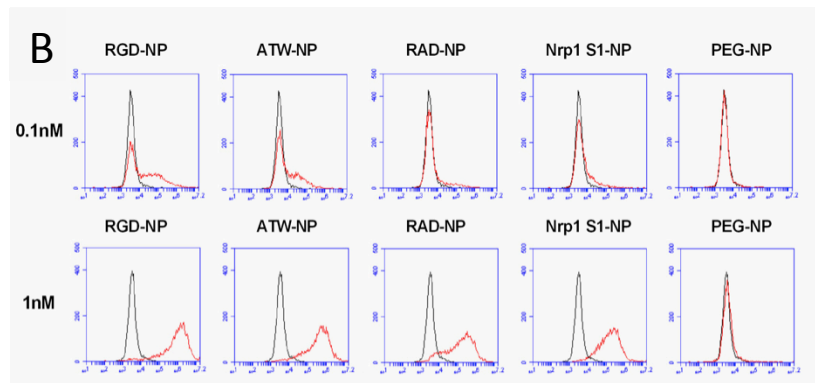


Fig. 38B RGD- or ATW-NPs were compared to their negative controls RAD- or Nrp1 S1-NPs on HUVEC after a 30 min incubation in serum containing medium at 0.1 nM concentration or 1 nM. Negative controls NPs coated with PEG are also presented.

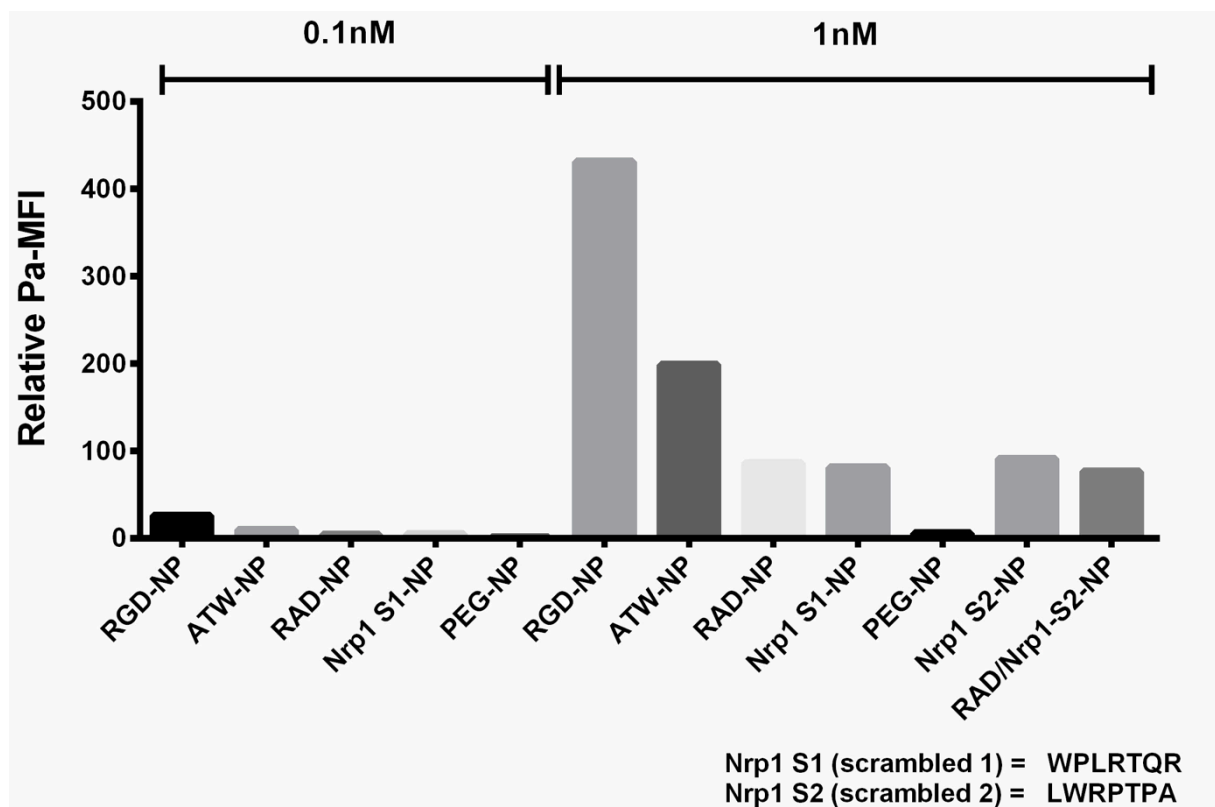


Fig. 38C Quantification of the NPs' binding efficiency of Fig. 38B. Pa-MFI indicates the percentage of augmentation of the Mean Fluorescence Intensities (MFI) as compared to the auto-fluorescence levels.

As shown in Fig. 38B and C, at 0.1 nM, none of the different negative controls (RAD-, Scrambled ATW- or PEG-NP) were binding to the cells. When the concentration reached 1 nM, all NPs, except PEG-NP, were presenting a strong positive binding. RGD-NP were still

generating a 5 times higher Pa-MFI than the RAD-NP. In parallel, the Pa-MFI of ATW-NP was almost 2.5 times as high as that of its negative control presenting NRP1 scrambled peptides. Notably, no differences were detected among the RAD and NRP1 scrambled peptides.

These results confirmed that bifunctional [anti integrin  $\alpha v \beta 3$ ] / [anti NRP1] NPs were binding more efficiently than monoligand-grafted NPs. However, a significant non-specific binding started to be observed when the doses reached 1 nM, except when these silica-based NP were coated with PEG.

## 6.2 VEGFR2 blocking activity and NRP1 internalization

We then tested the capacity of the NPs to prevent VEGF-induced-phosphorylation of VEGFR2 or integrins activation and their impact on the signaling cascades.

In the absence of NPs, a 10 min treatment of HUVEC cells with 1nM VEGF induced a strong phosphorylation of VEGFR2 on its tyrosine residues at positions 1175, 1054/59 and 1214 (Fig 39A). This was associated with an apparent decrease of the total amount of VEGFR2 suggesting a rapid degradation of the phosphorylated receptor. The VEGF treatment also induced p-AKT (Ser473) and P-FAK (Y397).

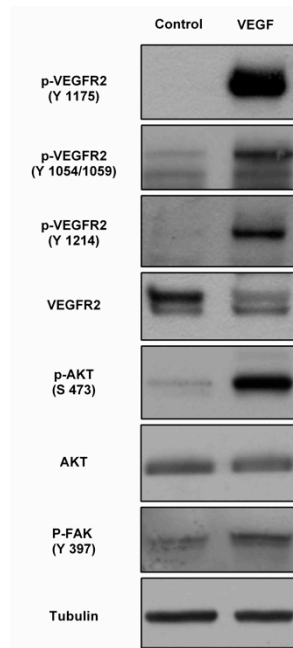


Fig. 39A HUVEC were incubated in the absence of serum during 20 hrs before treatment with 20ng/ml VEGF and their protein contents were analyzed using western blotting. Activation of VEGFR2-FAK/AKT pathway was induced in the presence of VEGF for 10min.

As expected from previous binding results, none of the NPs was blocking VEGF-effect when used at 10 pM (Fig. 39B).

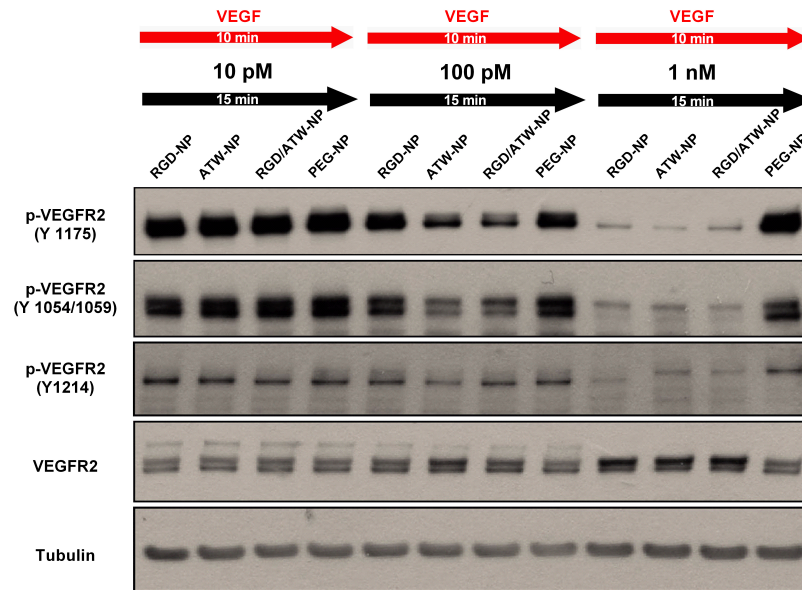


Fig. 39B NPs' impact on VEGF-VEGFR2. The inhibition of the VEGF-induced phosphorylation of VEGFR2 can be blocked by a preincubation with 0.1 nM and 1 nM NPs but not with 0.01 nM. The different NPs were added 5 min before VEGF. At a concentration of 0.1 nM, ATW containing NPs (ATW- and RGD/ATW-) specifically inhibit the phosphorylation of VEGFR2. This ATW specificity was not observed anymore when the NPs were used at 1 nM because in this case RGD-NPs also blocked VEGFR2.

In the presence of as little as 100 pM of NPs, we observed a significant ATW-specific inhibition of the phosphorylation of VEGFR2 on the 4 tyrosine residues. This inhibition was slightly stronger with the mixed RGD/ATW-NP than with ATW-NP on Tyr-1175, which was confirmed in fig. 40A. The Tyr-1054/1059 and 1214 residues were blocked efficiently by ATW-NP and this was associated with a stabilization of VEGFR2 (Fig. 39B and 40A).

At 1 nM, all the peptide-loaded NPs including RGD-only-NP, nearly abrogated VEGF-mediated phosphorylation of VEGFR2 on the four tyrosine residues (Fig. 39B).

Since ATWLPPR specifically binds to NRP-1, we examined its level of expression on the HUVEC's surface (Fig. 39C).

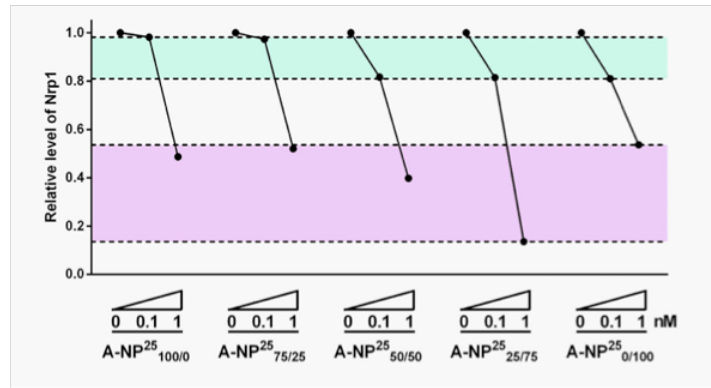


Fig. 39C NRP1 presence on the cell membrane was analyzed by FACS after contact with NPs at 0.1 nM (green) or 1 nM (purple).

As soon as the NPs are presenting 50% or more ATWLPPR, they induced a very significant reduction of NRP-1 present on the cell surface. This was observed with 0.1 nM of RGD/ATW mixed NPs (with ratios of 50/50 and 25/75 % respectively) as well as with ATW-only NP. When 1 nM was used, all the tested NPs were reducing the level of NRP-1 down to  $\pm$  50% of its normal value. This was dramatically more pronounced when the 25/75 ratio of the mixed NPs were used, and a reduction of  $\pm$ 90% of the level of NRP-1 was measured.

Thus the presence of ATWLPPR, in particular when it is associated to 25% cRGD on the surface of NPs, increased the binding affinity of the NPs but also induced a very efficient and rapid internalization of NRP-1.

In parallel, western blot analysis showed that ATW-NP induced a more rapid decrease of NRP-1 after at least 60min, as compared to RGD-NP and RGD/ATW-NP treatments (Fig. 39D).

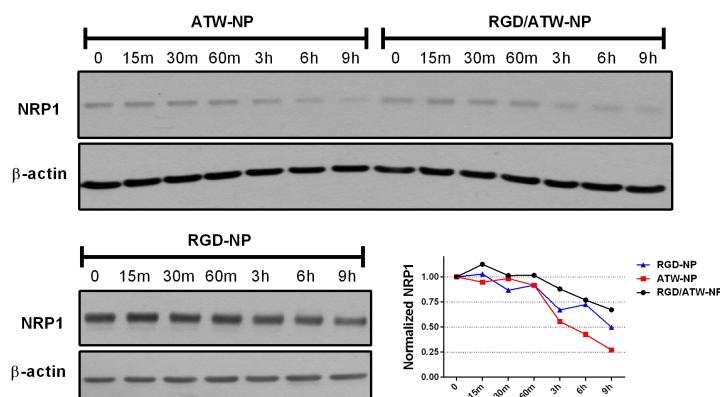


Fig. 39D ATW-NPs induced a more rapid decrease of NRP1 on whole cell extracts. HUVEC were incubated with 0.1 nM NPs for indicated times. Graph shows the quantification of total NRP1 levels after normalization of the values with the respective control group.

VEGFR2 expression was not affected by the presence of all the different NPs (data not shown), except after a 12h incubation with RGD-NP that was associated with a moderate decrease of its presence.

In summary, 100 pM NPs grafted with ATWLPPR (50 to 100%) specifically inhibit VEGF-induced phosphorylation of VEGFR2. This is associated with a very active internalization of NRP1. At 1000 pM, all NPs coated with peptides nonspecifically prevented VEGFR2 phosphorylation and induced an active internalization of NRP1 that was maximal with the 25/75 ratio of RGD/ATW.

### 6.3 AKT signaling

We investigated the capacity of the different NPs to block VEGFR2 and the associated AKT signaling cascades. As partly seen already, after a 10 min treatment, VEGF is inducing a strong phosphorylation of VEGFR2 on its tyrosine residues 1175 and 1054/59. This is followed by the activation of downstream cascades including AKT (Ser473), GSK $\beta$ 3 (Ser9) and eNOS (Ser1177) (Fig. 40A).

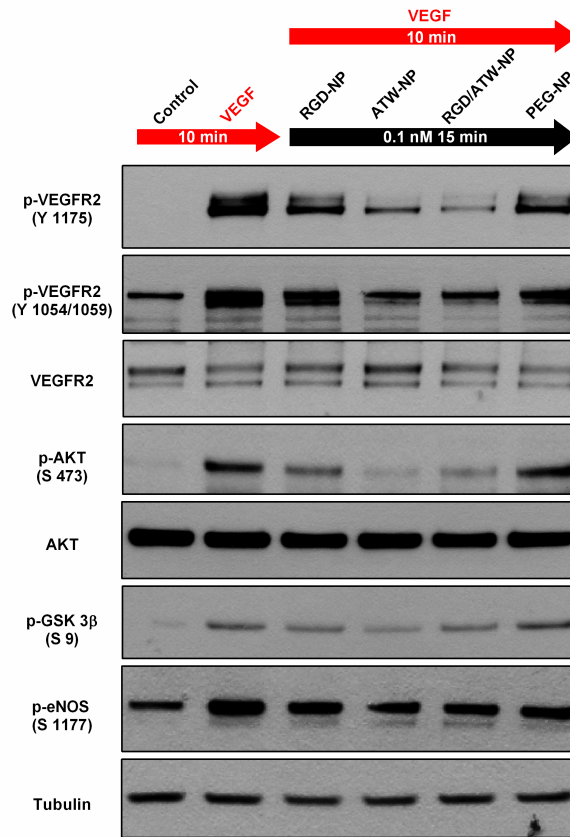


Fig. 40A ATW containing NPs (ATW- and RGD/ATW-NP) significantly inhibited the VEGF activity on VEGFR2-AKT-GSK3 $\beta$  signaling. HUVEC were serum starved for 20 hours, followed by the treatment with the different NPs at 0.1 nM for 5 min prior to the treatment with VEGF (20 ng/ml) for another 10 min.

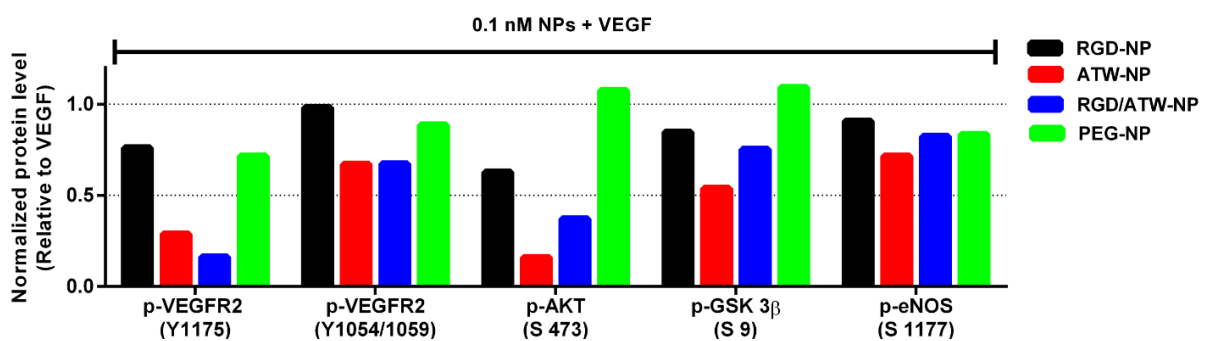


Fig. 40B Semi-quantification of the results presented in Fig. 40A. The inhibition of the phosphorylation of the different proteins in HUVEC cells treated by different NPs was normalized versus that of only VEGF-treated cells.

In the presence of 100 pM of RGD- or PEG-NP, VEGF activity on the phosphorylation of residues 1175 and 1054/59 of VEGFR2 is weakly affected (Fig 40A and B). However, the presence of RGD-NP is reducing the phosphorylation of AKT and of GSK 3 $\beta$  while PEG-NP has no effect. RGD/ATW-NP and ATW-NP strongly inhibited the whole cascade of phosphorylation, starting from VEGFR2 and down to GSK 3 $\beta$ .

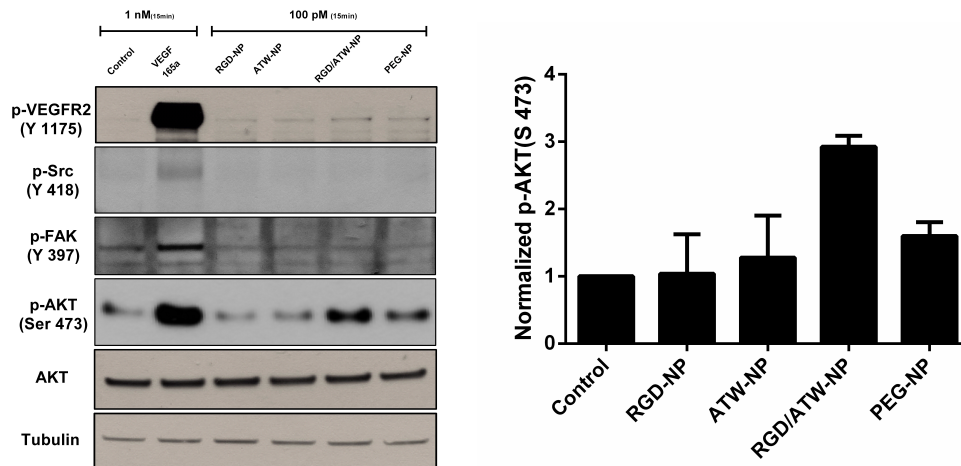


Fig. 40C&D RGD/ATW-NPs activates AKT, with no effects on VEGFR2, Src and FAK activation at 0.1 nM. Histogram indicates the semi-quantification of p-AKT levels versus the values of the control group (n=2).

As shown in fig. 40C and D, 100 pM of the mixed RGD/ATW-NP were stimulating p-AKT (Ser473) but without detectable activation of p-VEGFR2 (Tyr1175), p-Src (Tyr 418) or FAK (Tyr 397) in the absence of VEGF. None of the other targeted NPs was activating Src or FAK in these conditions. The absence of stimulation of the FAK/Src pathway is surprising and not explained yet. However, it should be noticed that it may take longer than 15 min to see a clear impact on FAK or Src, as previously described by the group of Benezra M. et al who saw a very small change in their phosphorylation after 2h incubation of integrin  $\alpha_v\beta_3$  positive melanoma cells M21 with cRGD-coated ultrasmall NP [151].

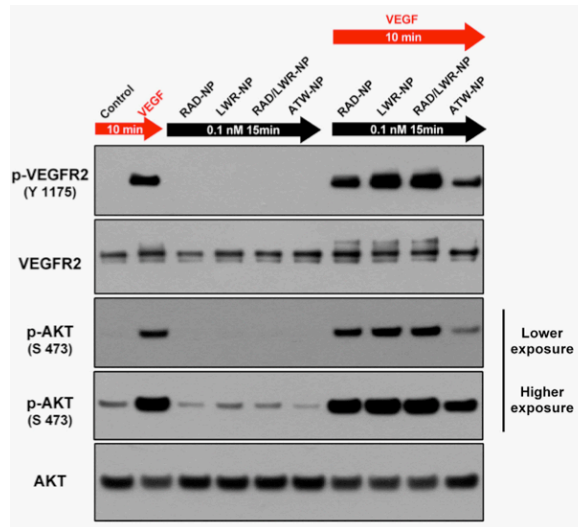


Fig. 40E Scrambled NPs show neither activation of AKT nor inhibition of VEGF induced VEGFR2 and AKT phosphorylation at 0.1 nM. ATW-NPs were used as positive control of specific antagonist of VEGF.

As well, none of the negative control NPs were interfering with VEGFR2 or AKT nor blocking VEGF-activity (Fig. 40E).

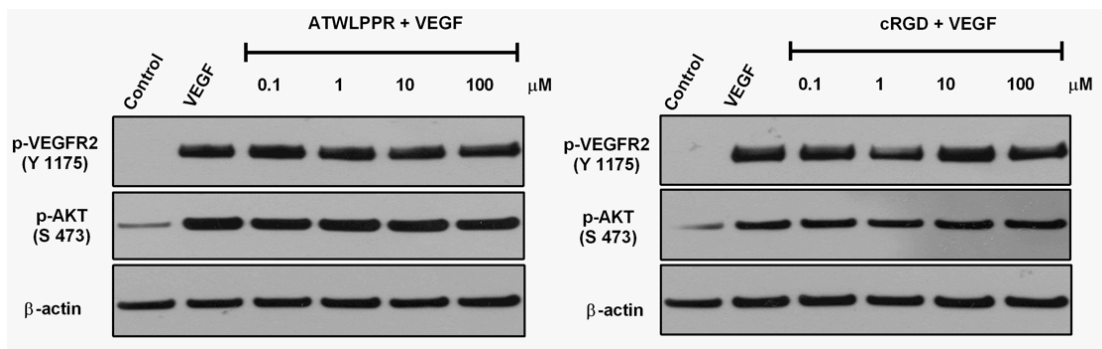


Fig. 40F Free monomeric ATW and cRGD (0.1  $\mu$ M, 1  $\mu$ M, 10  $\mu$ M and 100  $\mu$ M) showed no blocking effects on VEGF/VEGFR2/AKT signaling.

As well, concentrations of up to 100  $\mu$ M of the free ATWLPPR or cRGD peptides in solution were not blocking the VEGF-VEGFR2/AKT signaling (Fig. 40F). Thus as compared to free peptides at 100 nM, ATWLPPR presented by the NPs has a much potent and specific antagonist activity.

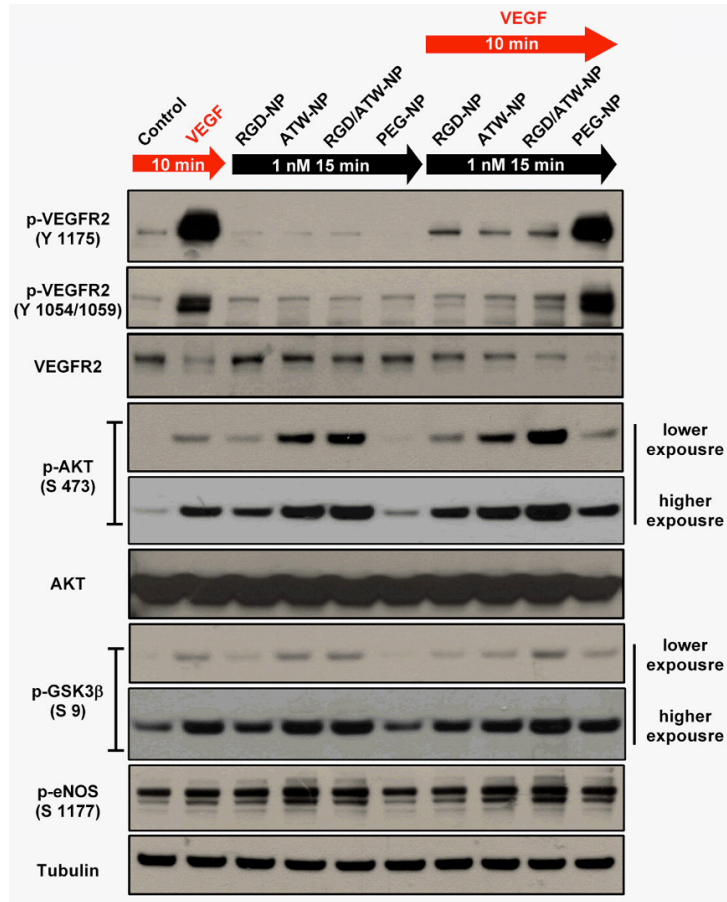


Fig. 41A 1nM of functional NPs (RGD-, ATW-, RGD/ATW-) augment AKT, GSK3 $\beta$  and eNOS phosphorylation despite their strong inhibition of VEGF-VEGFR2 and independently of the presence of VEGF. HUVEC were incubated with 1 nM NPs for 15 min in the absence of VEGF or in the presence of VEGF added 5 min before.

The situation changes when the NP's concentration augments. At 1nM, each NP coated with peptides (RGD-, ATW, RGD/ATW-) was blocking VEGF-mediated phosphorylation of VEGFR2 (Fig. 41A).

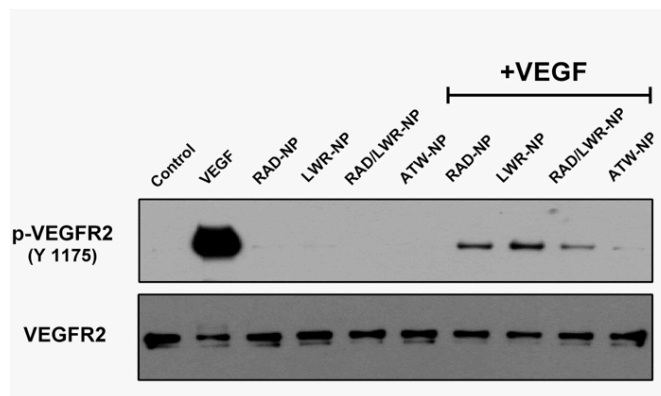


Fig. 41B 1nM of scrambled NPs (RAD-, LWR-, RAD/LWR-) show strong inhibition of VEGF-VEGFR2. HUVEC were incubated with 1nM NPs for 15 min in the absence of VEGF or in the presence of VEGF added 5 min before. ATW-NPs were used as positive control of specific antagonist of VEGF.

Furthermore, this also occurred when NPs coated with negative control peptides were used (RAD-, LWR- or RAD/LWR-) (Fig. 41B).

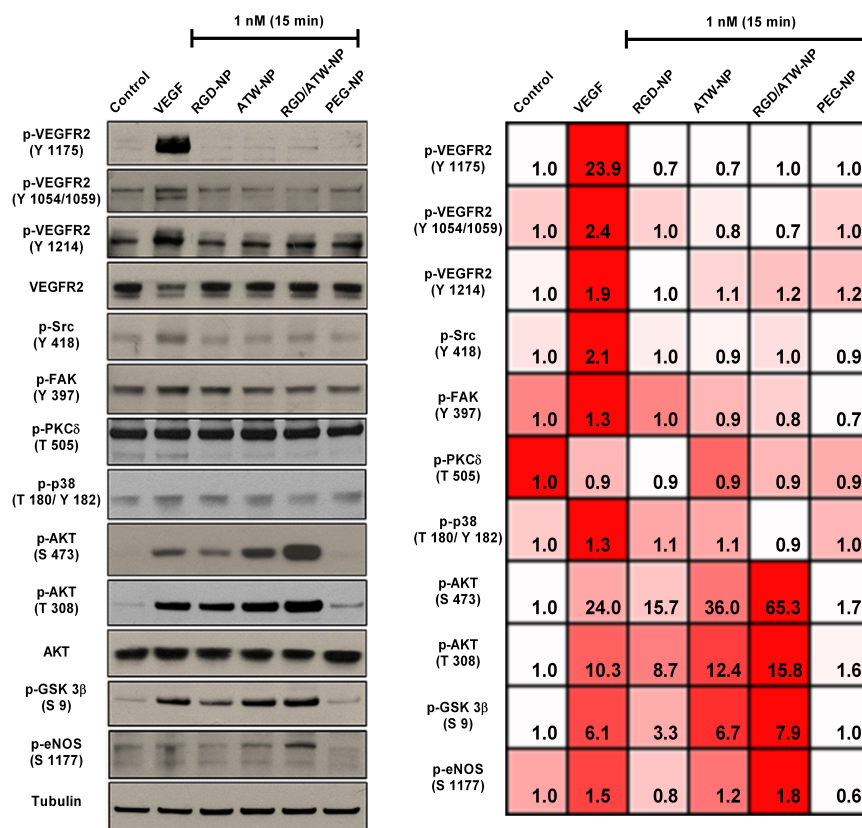


Fig. 41C At 1 nM, peptide-coated NPs induce the AKT signaling, with no effect on VEGFR2 and integrin activation. The cells were treated with 1 nM NPs for 15 min. VEGF was used as a positive control for the activation of VEGFR2 and integrin signaling. The levels of each protein phosphorylation was quantified and displayed as heat map of row-normalized sorting. Number indicates the fold changes of phosphorylated levels after normalizing its grey value versus their respective controls.

Even more surprisingly, all these NPs induced a phosphorylation of AKT despite their blockage of VEGFR2 and independently of the presence of VEGF (Fig. 41C and D).

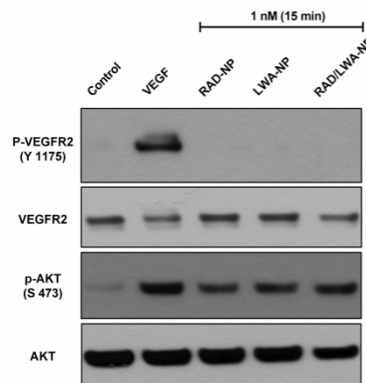


Fig. 41D 1nM scrambled NPs non-differentially activated AKT. The cells were treated with 1 nM NPs for 15 min. VEGF was used as a positive control for VEGFR2-AKT activation.

Interestingly, the different NPs were presenting variable impacts on the AKT/GSK/eNOS signaling axis as can be seen on the heat map raw normalized presentation (Fig. 41C). Mixed RGD/ATW-NP activated AKT at both vital sites 473 (Ser) and 308 (Tyr), as well as GSK  $\beta$ 3 and eNOS. ATW-NP were less efficient to stimulate the phosphorylation of AKT and GSK  $\beta$ 3. Finally, RGD-NP was even less active than ATW-NP. This resulted in a weaker phosphorylation of eNOS on its residue Ser 1177, which is strongly phosphorylated by mixed RGD/ATW-NP. In particular, 1nM RGD/ATW-NP were more active than 1nM VEGF on the downstream AKT, GSK  $\beta$ 3 and eNOS activation without passing through the activation of VEGFR2.

None of the tested NPs influenced the integrin-mediated phosphorylation cascade including p-FAK (Tyr 397), p-Src (Tyr 418), p-PKC (Thr 505) or p-P38 (Thr 180/Tyr 182). They did not affect either the phosphorylation of VEGFR2 (Tyr 1175, 1214 and 1054/59).

Finally, it should be noted that PEG-NP were mostly inactive on these different events.

#### 6.4 MAPK/ERK signaling

Next, we investigated NPs' effects on MAPK/ERK signaling in HUVEC cells. At 100pM and without VEGF, no direct activity on ERK phosphorylation was noticed with all the tested NPs including PEG and scrambled ones. In the presence of 20ng/ml VEGF for 10min, a very modest inhibition of p-ERK was detected in the presence of ATW-NP only (Fig. 42A).

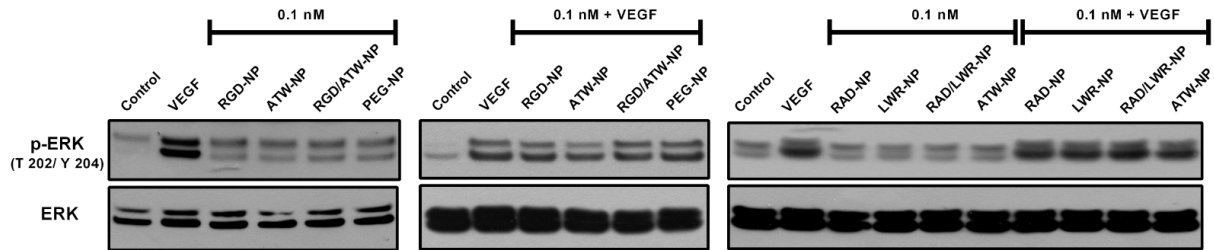


Fig. 42A All NPs at 0.1nM did not impact on the phosphorylation of ERK, nor did they prevent its phosphorylation under VEGF treatment. Cells were treated either with 0.1 nM NPs for 15 min or with 0.1 nM NPs 5 min prior to the treatment with VEGF (20 ng/ml) for another 10 min.

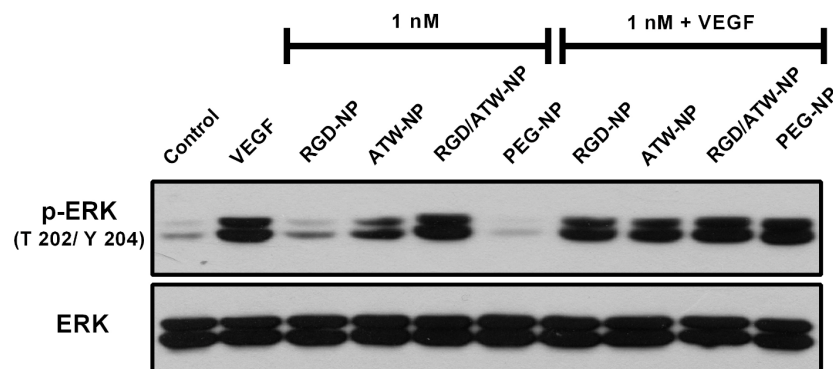


Fig. 42B When the concentration of NPs reached 1 nM, ATW containing NPs (especially the dual RGD/ATW-NP) directly induced a significant augmentation of p-ERK, but none of them prevented the VEGF-activity. Note that RGD-NPs, like PEG-NPs, did not activate ERK in these conditions.

When augmenting NPs' concentration to 1nM, ATW- and RGD/ATW-NP, but not RGD- or PEG-NP, are strongly and directly stimulating the phosphorylation of ERK but are not blocking the effect of VEGF. The VEGF-mediated phosphorylation of ERK was identical with every NP.

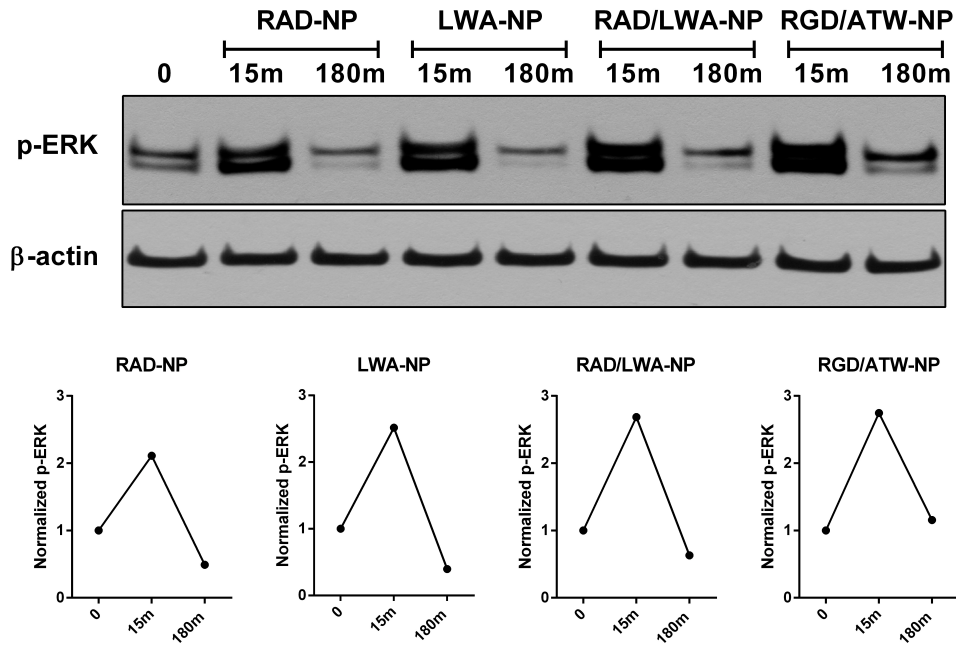


Fig. 42C The negative controls NPs coated with RAD or LWR-peptides also stimulated a strong and transient ERK phosphorylation at 1 nM, similar to that obtained with 1nM RGD/ATW-NP. This effect was very strong at 15min and not detectable after 3h.

Surprisingly, in the presence of negative control NPs such as RAD-NP, LWA-NP or mixed RAD/LWA-NP, a very strong phosphorylation of ERK is also observed, as strong as the one generated by the positive RGD/ATW-NP (Fig. 42C). This effect is transient and is not present after 3 hours.

Actually ERK stimulation is observed with all the NPs that specifically or non-specifically bind to HUVEC but not with RGD-NP. Pegylated NP that do not bind to these cells do not activate ERK either. As seen earlier, RAD-, LWA- or mixed RAD/LWA-NP are binding non-specifically to HUVEC at 1nM. This may come from the presence of one Arginine residue in these peptides. Because Arginine is presenting a positive electric charge it may interfere with the negative charges of the cell membrane such as GAGs and/or phosphatidylserine that may be exposed on our serum starved HUVEC cells.

RGD-NP is a strong binder. In this case, its binding to the integrins is dominant as compared to the low-non specific interaction of other peptides containing NPs. As already observed for the FAK, src, or P38 proteins, the RGD-NP is not activating ERK either.

ATW-NP binds to NRP1 and activates AKT and ERK. RGD/ATW-NP strongly binds integrin and NRP1 and strongly activates AKT and ERK in addition to others.

At 1 nM RAD-, LWA- or mixed RAD/LWA-NP binds via electrostatic interactions that leads to the transient activation of ERK.

This pattern was already observed with AKT, but ERK seems to be more sensitive and appears to work on an “on/off” mode as soon as a small stimulation is happening on these stressed HUVEC cells. AKT seems to have a broader spectrum of reactivity and may need a stronger input to be fully activated. This can be represented in Fig. 43:

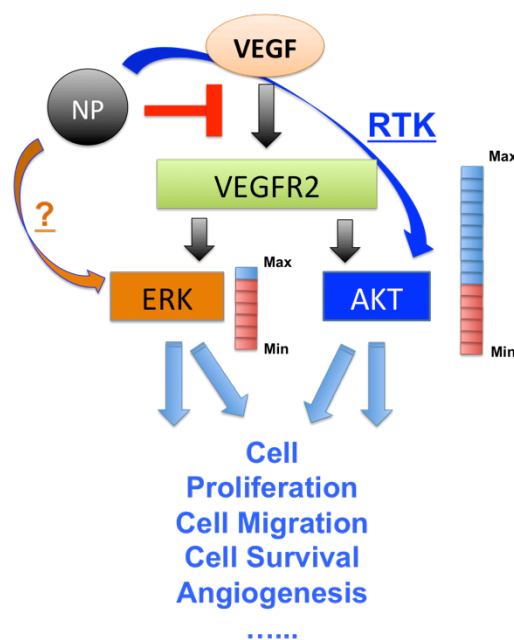


Fig. 43 AKT and ERK show different capacity in response to NPs' treatments on HUVEC. At higher concentration 1nM, all peptides-grafted NPs show non-differential blocking effects on activation of VEGFR2 with non-differential activation of ERK in the presence of VEGF. While, all NPs induce AKT activation but in a distinctive manner. ATW containing NPs (especially RGD/ATW-NP) induce high RTK-AKT activation either in the presence of VEGF or not. NPs'

effects on RTK are studied in the following chapter. As compared to the ERK signaling on HUVEC, AKT shows a much higher up-threshold to arrive signal saturation.

## 6.5 RGD/ATW-NP protects HUVEC from cell death

In order to better understand the impact of AKT/ERK activation, we extended our study from 15 min to 9 hours of incubation with high concentrations of NPs (1nM). This was performed on HUVEC cultured at 37°C in the absence of serum (starvation of 10 hours).

### 6.5.1 RGD/ATW-NP prevents caspase-3 activation

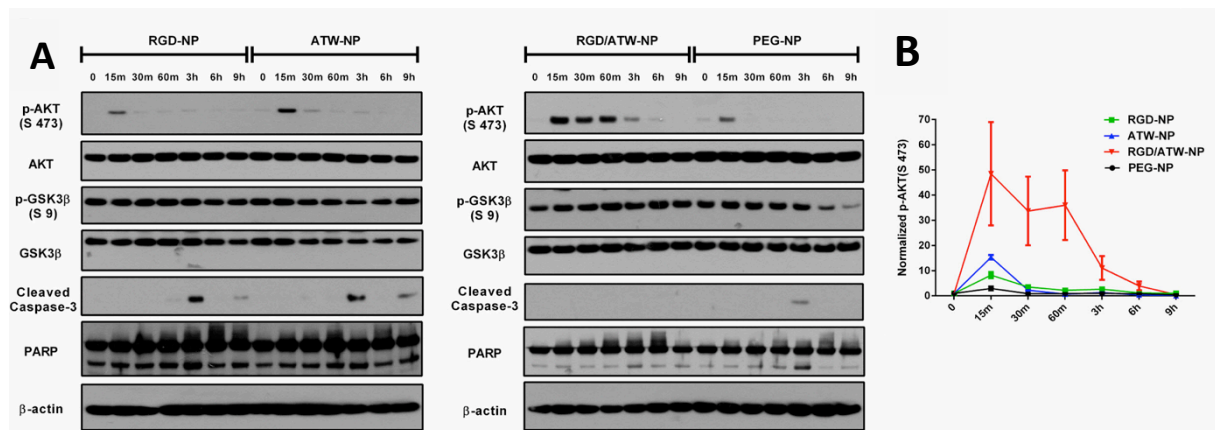


Fig. 44A&B RGD/ATW-NPs induces a long lasting powerful activation of AKT and suppress caspase-3 activation caused by serum deprivation. HUVEC were serum starved for 10 hrs before 1 nM NPs were added. Protein extracts were obtained at different times from 15 min to 9 hrs. (A, B) in comparison with RGD- or ATW- or PEG-NPs, the dual RGD/ATW-NPs induces a sustained activation of AKT and do not activate caspase-3. The graph shows the semi-quantification of AKT phosphorylation (Ser-473) after normalization with the first sample at T0 (n=3).

While RGD-, ATW- or PEG-NP were still inducing the expected phosphorylation of AKT (Ser 473) at 15 min (Fig. 41A and C), this phenomenon was extremely transient and not detectable at later time points (Fig. 44A&B). Because of the serum starvation, these cells

were then entering in active cell death that was detected by the activation of caspase-3 and a more modest degradation of PARP after three to nine hours (Fig. 44A&B).

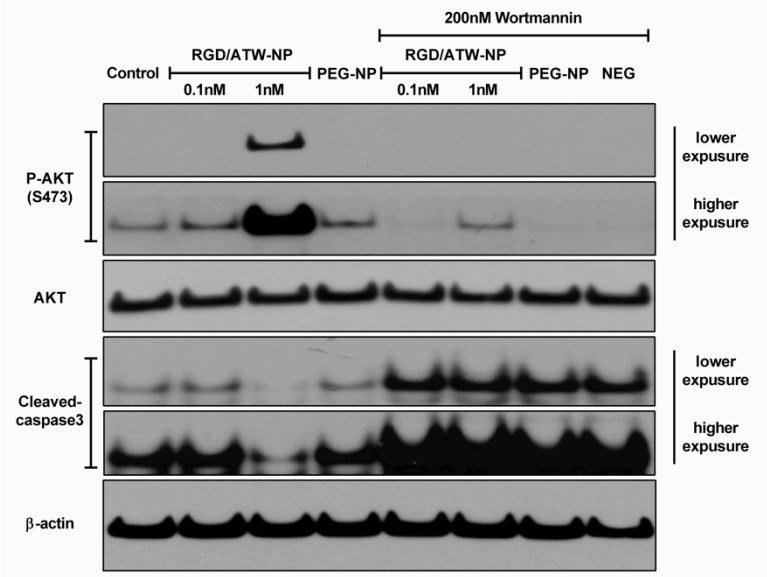


Fig. 44C RGD/ATW-NPs at 1 nM but not 0.1 nM is activating AKT and prevents caspase-3 activation due to the deprivation of serum, which is reversed by PI3K inhibitor Wortmannin. PEG-NPs at 1 nM do not affect AKT or caspase 3. HUVEC were cultured without serum during 20 hrs prior to the addition of the NPs during 60 min. NEG indicates the treatment of only Wortmannin.

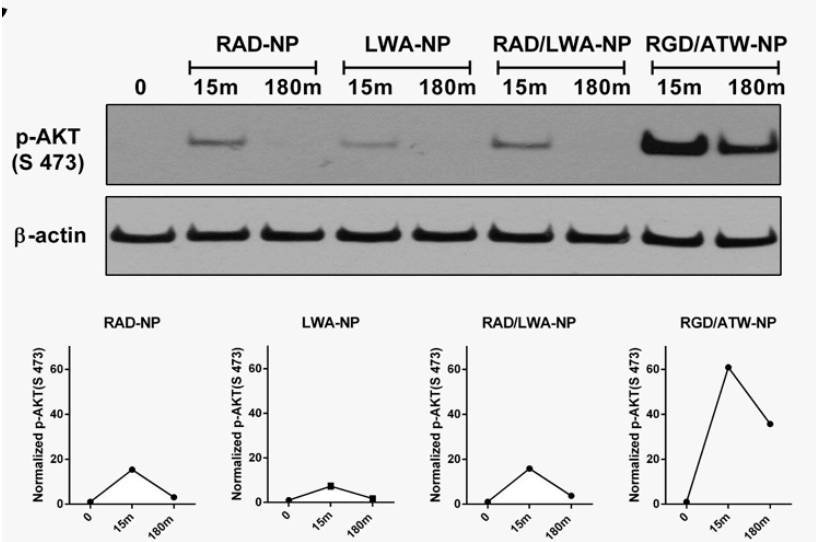


Fig. 44D All the negative NPs at 1 nM are inducing a transient phosphorylation of AKT but its level of induction and duration are not in the same range than those obtained with

RGD/ATW-NP. The graph indicates the semi-quantification of AKT phosphorylation (Ser-473) (n=2).

Very interestingly, the mixed RGD/ATW-NP was capable of inducing a long lasting level of p-AKT up to 3-6 hours, which resulted in the absence of caspase-3 activation. Blocking AKT activity using PI3K inhibitor (wortmannin) reversed RGD/ATW-NP's protective effect (Fig. 44C). As well, we verified that this sustained phosphorylation of AKT and the concomitant caspase-3 inhibition were not detected in the presence of 100 pM of mixed RGD/ATW-NP (Fig. 44C) or with 1 nM of each negative control-NP after one hour of incubation (Fig. 44D).

### 6.5.2 RGD/ATW-NP prevents HUVEC cell death

Cell viability tests were then performed at these two concentrations (100 pM and 1 nM) on HUVEC for 1 day in the presence or absence of VEGF (20ng/ml) or of FBS (1%).

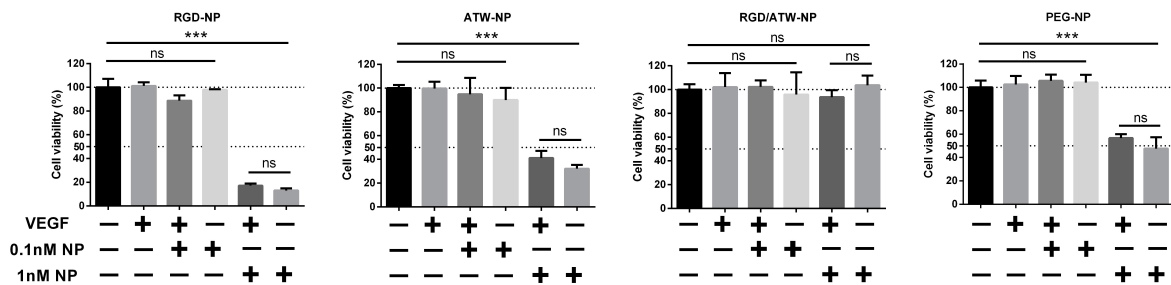


Fig. 45A no FBS  $\pm$  VEGF: Cells were treated with 0.1 nM or 1 nM NPs in serum free medium for 15 min prior to the addition of VEGF (20 ng/ml) and incubated for 1 day. One-way ANOVA was studied, followed by Student's t test. Data are presented as mean  $\pm$  SD (n $\geq$ 3), \*P< 0.05, \*\*P< 0.01, \*\*\*P< 0.001.

Without serum, HUVEC lose  $\pm$  10% cell viability after 24 hours. 20ng/ml VEGF<sub>165a</sub> (VEGF) did not show protective effects in our serum-deprived conditions. Cell viability was not affected by the addition of 100 pM of the different NPs (Fig. 45A).

In contrast, 1nM of RGD-, ATW- or PEG-NP were highly toxic even in the presence of VEGF. This was expected since these 3 NPs are activating caspase-3 in these conditions. Very interestingly, this toxicity was completely abrogated when the NPs were presenting the mixed RGD/ATW peptides certainly because of the sustained phosphorylation of AKT and inhibition of caspase-3.

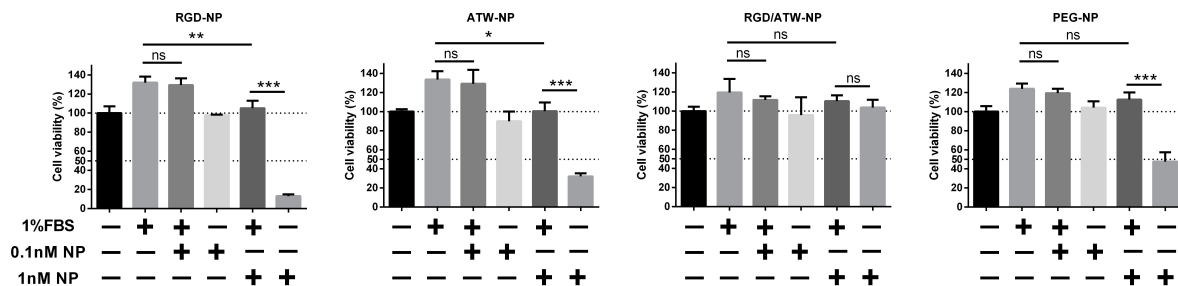


Fig. 45B 1% FBS: Cells were treated with 0.1 nM or 1 nM NPs in serum free medium for 15 min prior to the addition of 1% FBS and incubated for 1 day. One-way ANOVA was studied, followed by Student's t test. Data are presented as mean  $\pm$  SD ( $n \geq 3$ ), \* $P < 0.05$ , \*\* $P < 0.01$ , \*\*\* $P < 0.001$ .

The toxicity of 1 nM RGD-, ATW- or PEG-NP was less pronounced in the presence of 1% FBS (Fig 45B) since cells viability was equal to that of the control group without FBS. Thus in the first 24h, the presence of 1nM NPs was just abrogating the increase in cell viability induced by 1% FBS.

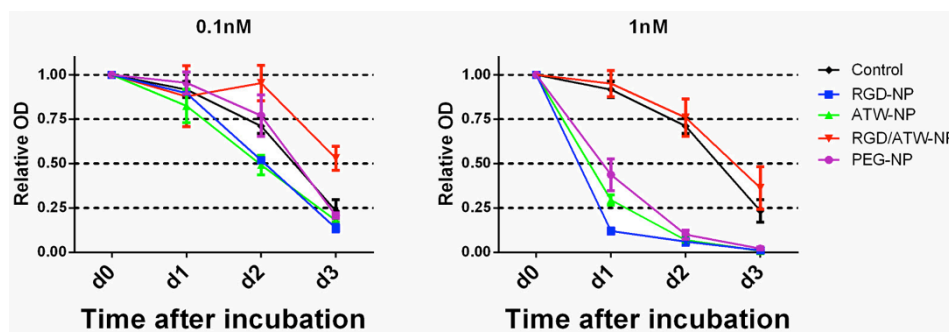


Fig. 45C no VEGF and no FBS: Cell viability assay in serum free medium during 3 days in the presence of NPs 0.1 nM or 1 nM of NPs. Data are represented as mean  $\pm$  SD ( $n \geq 3$ ).

When this assay was prolonged for 3 days without VEGF or FBS (Fig. 45C), we observed that 0.1 nM of RGD/ATW-NP was helping HUVEC cells resisting the starvation-induced cell death.

PEG-NP showed no effects. Importantly, RGD- and ATW-NP exaggerated serum starvation-caused cytotoxicity, significantly in 2 days (Fig. 45C). As well, we confirmed that the presence of both peptides on the surface of the NP was also preventing the NP's toxicity at 1 nM.

Taken together, our results suggest that the RGD peptide is driving the binding strength onto the cells via the integrin  $\alpha_v\beta_3$ , but it is not activating the FAK/Src/MAPK pathway(s) and has no protective effect on serum deprivation-induced cell death or cell proliferation. The ATWLPPR peptide is a weak binder but a strong inhibitor of VEGFR2 via NRP1. But despite its blocking activity on VEGFR2 it is activating a transient AKT/GSK3 $\beta$ /eNOS and ERK phosphorylation. This transient activity does not produce any detectable anti-apoptotic activity or any effect on cell proliferation.

The mixed RGD/ATW share the advantages of RGD in terms of binding and of ATWLPPR in terms of inhibitor of VEGFR2 signaling. But its action is stronger, as observed on the internalization of NRP1, and level of activation of AKT/GSK3 $\beta$ /eNOS phosphorylation. In particular, this action if prolonged on AKT and this is clearly protecting the cells from dying in the absence of serum.

Our data emphasize the importance of NPs' concentration in deciding their function as an antagonist or agonist, or non-effector. In our system, at 100pM, ATW-NP presents the better VEGFR2 antagonist activity with a strong inhibition of VEGF-AKT signaling; RGD/ATW-NP functions as an agonist of AKT. At 1nM, all NPs (including PEG-NP) function as AKT agonist, and RGD/ATW-NP is the strongest. At the same time, all of them, except PEG-NP, also function as non-specific VEGFR2 antagonists.

To be emphasized, NPs-mediated signaling integration process are quite complex not solely depending on the particular input of signal transmitted from single antagonist or agonist. As presented in Fig. 43, more work is required to clarify the NPs' effects on different signaling nodes and additional functional studies also need to be conducted such as cell migration, angiogenesis, 3-D culture, etc. A systematic analysis and understanding of the relationship that exist between different signaling nodes and their corresponding functional (phenotypic)

changes would undoubtedly accelerate the understanding of NPs' effects in complex biological micro-environments.

## 6.6 *In vivo* evaluation

Two of these NPs were preliminary investigated *in vivo* using a subcutaneous model of glioblastoma (U87MG). This model was selected for preliminary tests because we know that it is EPR positive and also integrin  $\alpha_v\beta_3$  positive [121].

Five million U87MG cells, suspended in 100 $\mu$ L PBS, were injected subcutaneously into female NMRI nude mice (6 weeks old). After 5 weeks, the animals were randomized into 2 groups (n=4 per group). The first group was continuously administered for 2 days: PEG-NPs (n=2; 8mg/ml; 200 $\mu$ l i.v; daily) and RGD/ATW-NPs (n=2; 8mg/ml; 200 $\mu$ l i.v; daily). The second group was continuously administered for 4 days with the same treatment. After 1 hour of the final i.v injection of NPs, mice were sacrificed. It is presented in Fig. 46.

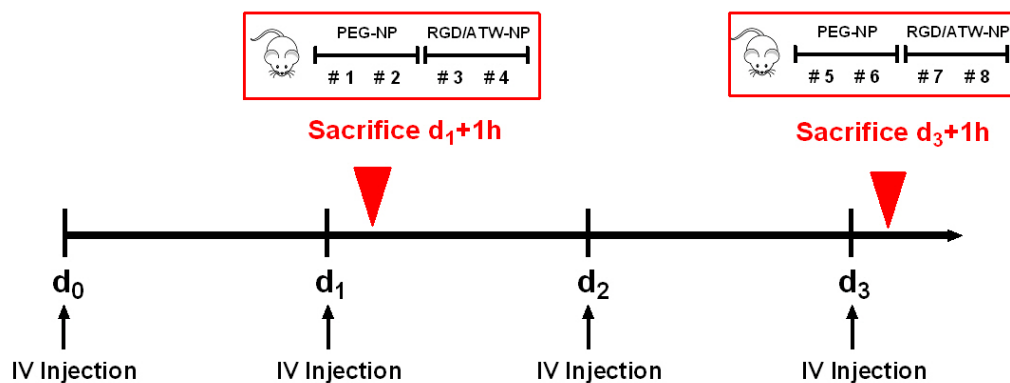


Fig. 46 Procedures of i.v injection of NPs in U87MG subcutaneous mice model. Detailed information is depicted in main text.

As can be seen in the figure ( $d_1$ ), cell proliferation (Ki67 immunostaining) and p-AKT are strongly induced one day after an injection of mixed NP but not with PEGylated NP.

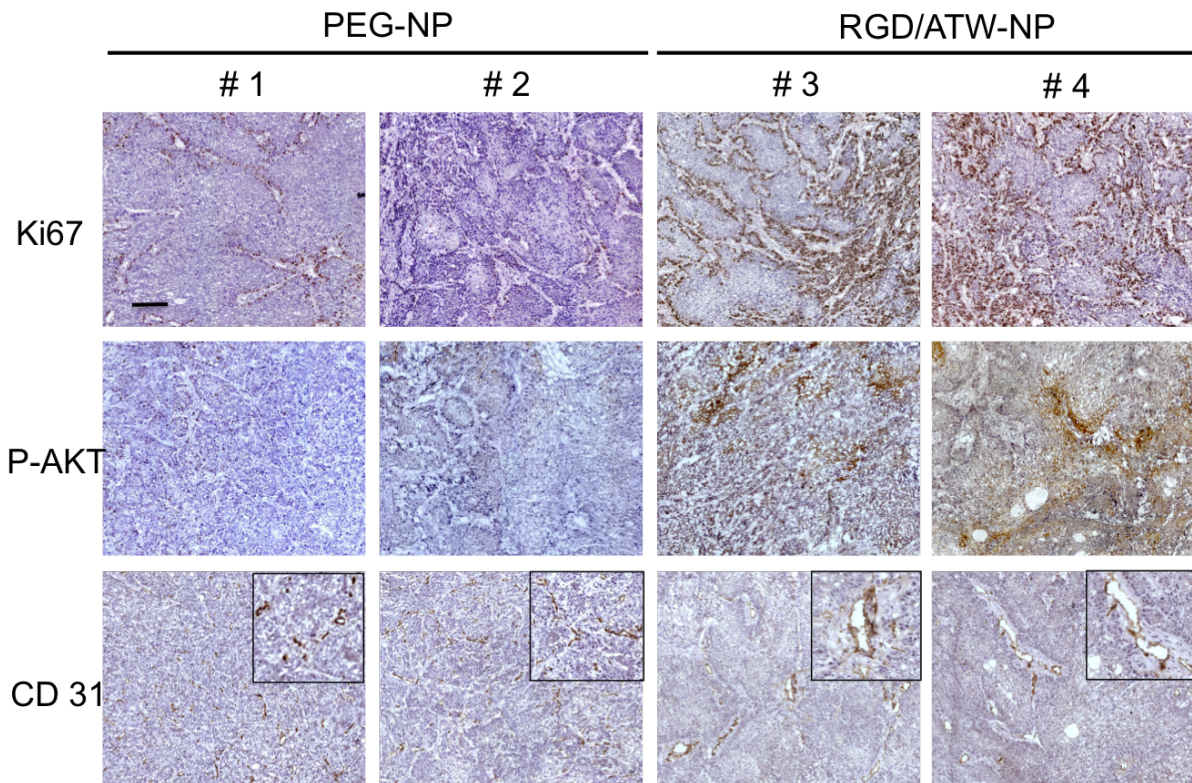


Fig. 47 One day after two times of intravenous administration of the 2 different NPs a very strong staining of Ki67 (dark brown) and p-AKT (dark brown) is observed in RGD/ATW-NP treated U87MG subcutaneous tumors as compared to the PEG-treated ones. The immunostaining of CD31 (dark brown), also known as Platelet Endothelial Cell Adhesion Molecule (PECAM-1) provides a visualization of the blood vessels. An augmented surface of the lumen of the vessels was detected in RGD/ATW-NP treated U87MG samples. Scale bar: 200  $\mu$ m.

This is more obvious in the first layers of tumor cells in contact with the peri-nodular stroma. The inner layers of tumor cells are not activated as can be seen at a higher magnification (Fig. 48):

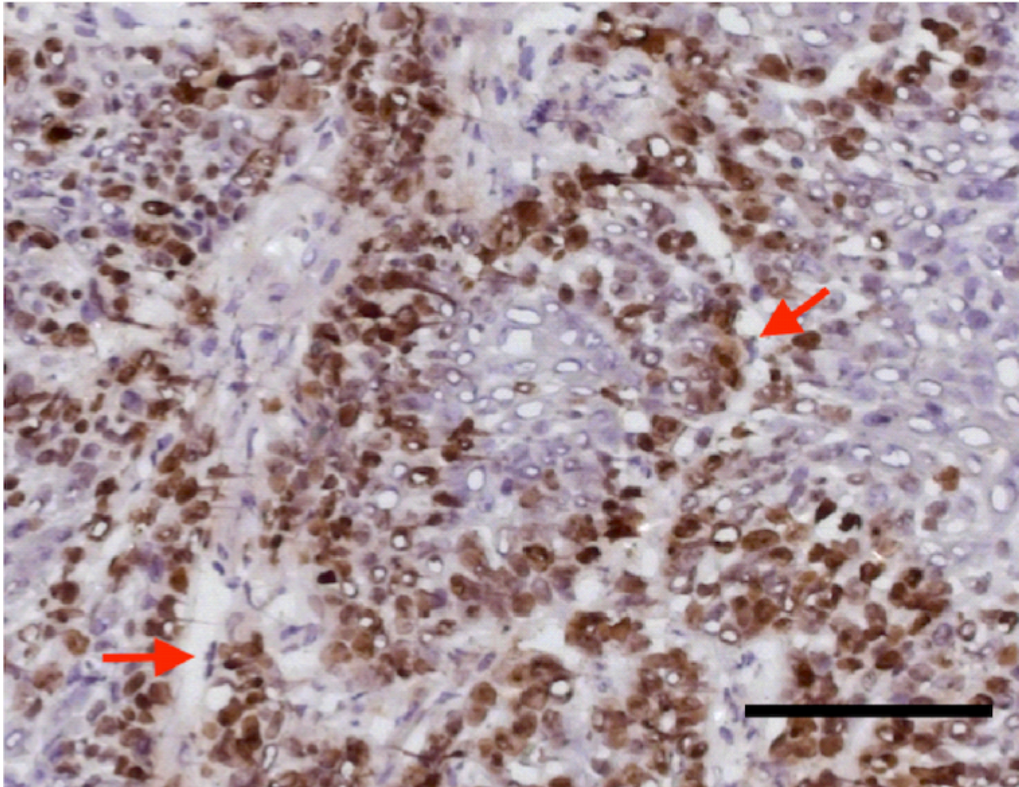


Fig.48 The impact of RGD/ATW-NPs on the Ki67 staining is mainly observed in the first layers of tumor cells that are in contact with the peri-nodular stroma. The red arrows indicate tumor endothelial cells. The red arrows illustrate the fact that endothelial nuclei are Ki67 negative while the tumor cells at the periphery of each nodule are mostly positive. Scale bar: 200  $\mu$ m.

In parallel, the CD31 staining shows larger blood vessels in the treated tumors. We did not established a direct correlation, but it may be important to understand whether this vasodilatation effect can be connected to the capacity of these RGD/ATW-NP to induce eNOS.

Two days later, the staining look very similar, but PEGylated NPs are also inducing Ki67 and p-AKT although to a lower extend than found in the mixed NPs treated tumors (Fig. 49).

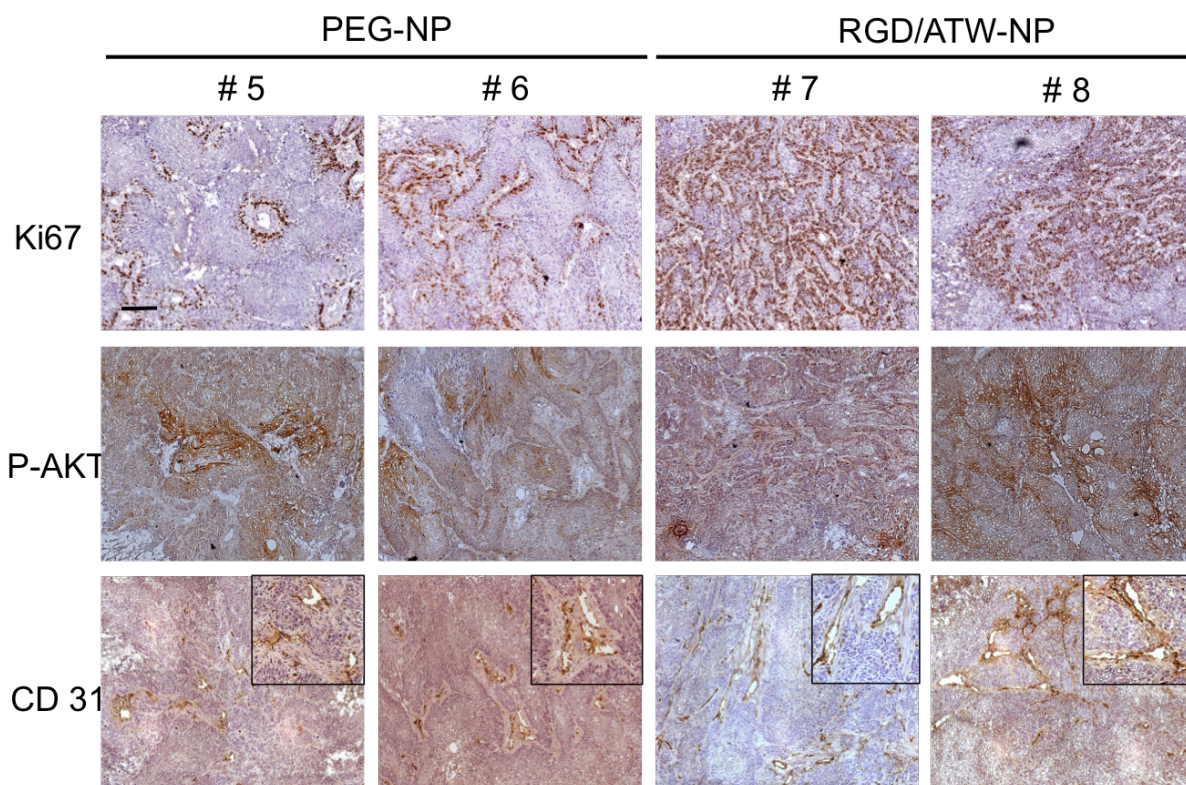


Fig. 49 Three days after four times of intravenous administration of the 2 different NPs a strong staining of Ki67 (dark brown) and p-AKT (dark brown) is observed in both PEG- and RGD/ATW-NP treated U87MG subcutaneous tumors, while Ki67 staining show much stronger in RGD/ATW-NP treated group. An augmented surface of the vessel lumen was detected in all U87MG samples treated with 3 days of NPs, as compared to 1 day i.v injection of PEG-NP. Scale bar: 200  $\mu$ m.

The immunostaining of CD31 (dark brown), also known as Platelet Endothelial Cell Adhesion Molecule (PECAM-1) provides a visualization of the blood vessels. An augmented surface of the lumen of the vessels was detected in both PEG- and RGD/ATW-NP treated U87MG samples. Scale bar: 200  $\mu$ m.

This is confirmed after counting the number of Ki67 positive cells and a clear augmentation of the proliferation index is visible one or three days after Mixed-NP injection as compared to the PEG-NP treated group (Fig. 50).

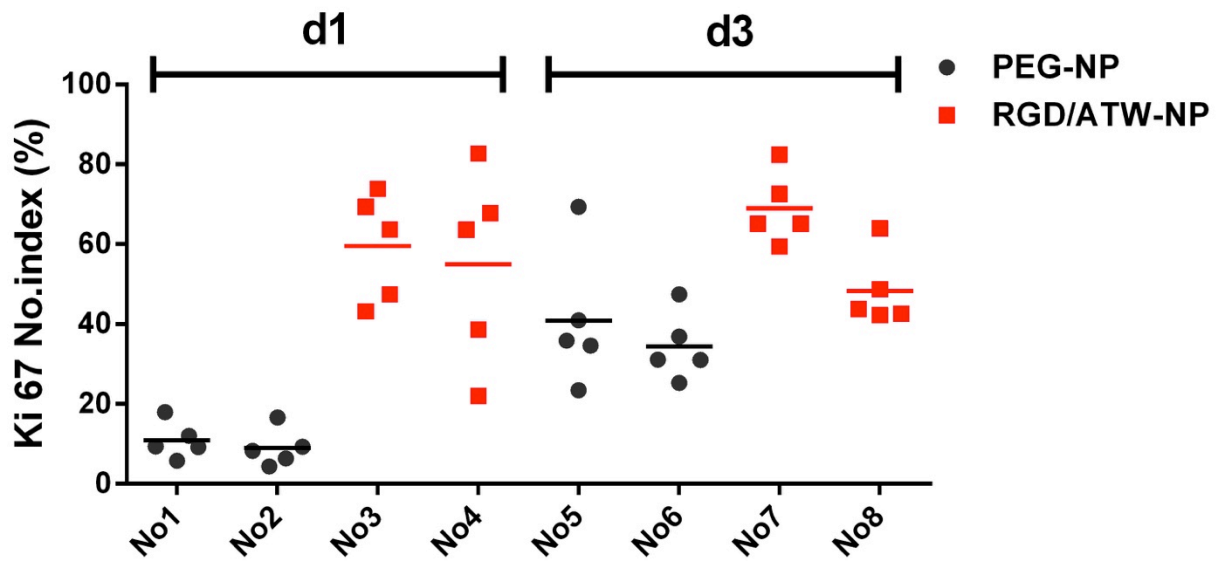


Fig. 50 The Ki67 index was calculated as the ratio of number stained cells reported to total number of cells for each tumor section, excluding necrotic areas. Five sections per animal were analyzed.

CD31 immunostaining shows that the number of endothelial cells is not affected by the treatment (Fig. 51):

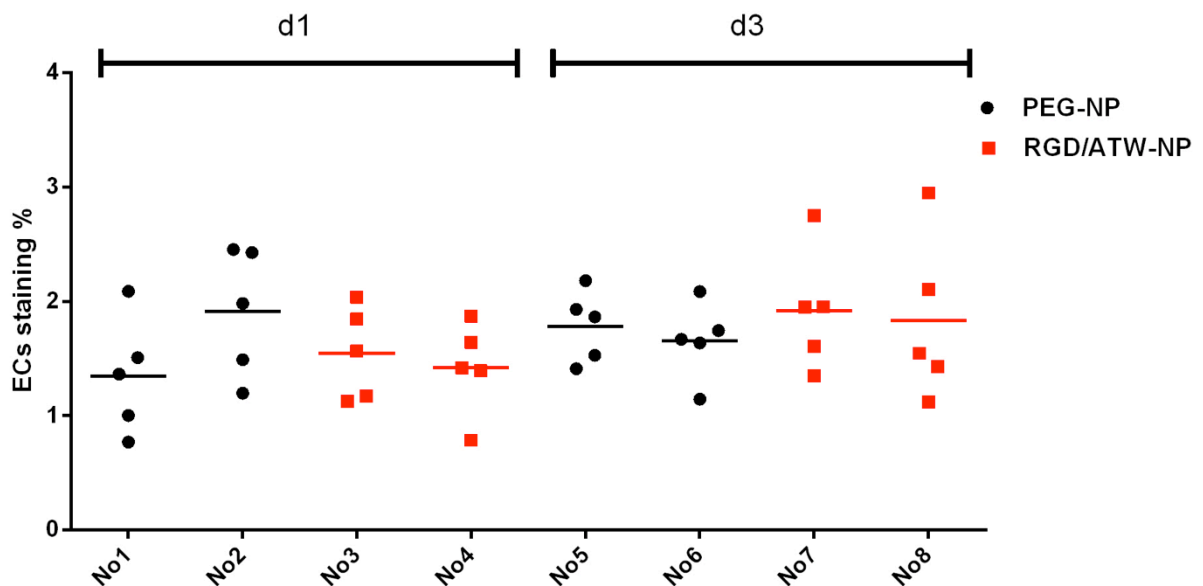


Fig. 51 The ECs staining percentage was calculated as the ratio of CD31 staining surface to total cells' surface, excluding necrotic areas. Five sections per animal were analyzed.

However, although the number of blood vessels remains identical, their size is largely augmented in the presence of mixed-NP in particular after one day (Fig.52).

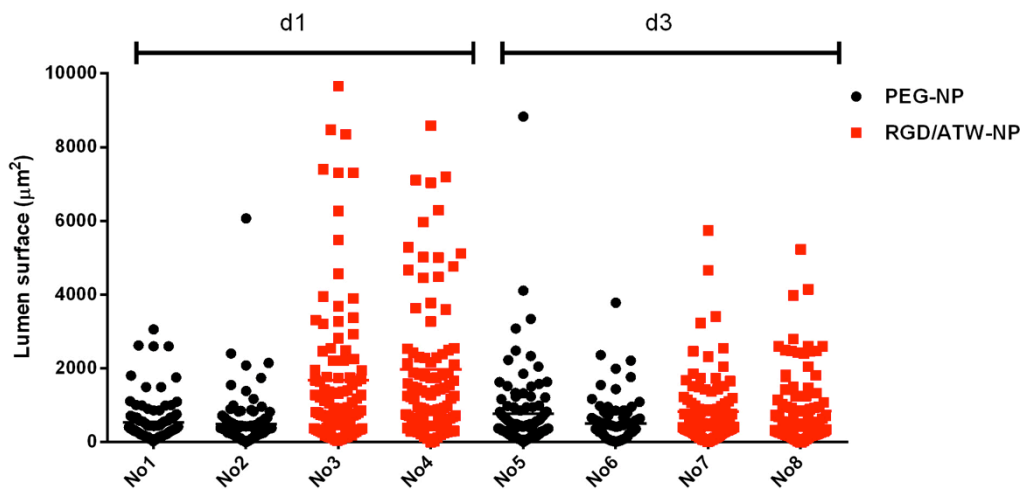


Fig. 52 The Lumen surface per microvessel was calculated by random selection (vessels' number is  $\geq 100$ )

At day 3 the difference in shape and certainly on functionality of blood vessels is identical in all animals. This may explain also the standardization of the number of proliferating cells.

Protein extracts obtained from the same tumors confirmed the strong and rapid induction of p-AKT and p-ERK in the mixed treated tumors at day 1 (Fig. 53). No particular impact was detected with an anti active caspase-3 antibody staining.

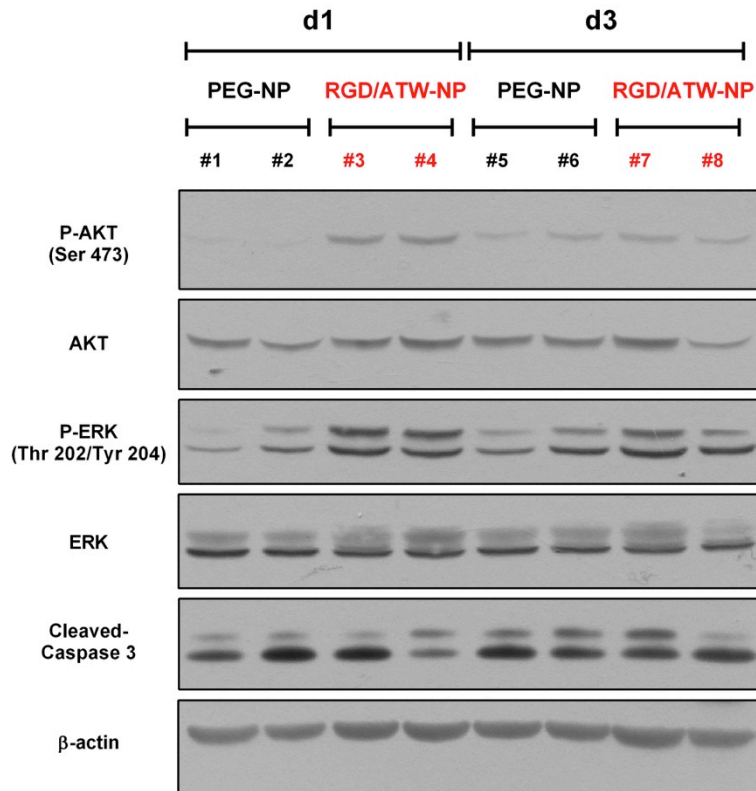


Fig.53 In d1 group, an elevated phosphorylation of AKT and ERK was observed in the RGD/ATW-NP treated tumors. In d3 group, all tumor samples show non-differential augmentation of AKT and ERK phosphorylation, as compared to 1 day of PEG-NP treated U87MG subcutaneous tumors.

Although these *in vivo* results are still incomplete and preliminary, they sustain those obtained *in vitro* concerning the induction of p-AKT and p-ERK. In addition it is suggesting that mixed NP are inducing a vasodilatation which, combined or not with a direct effect of the mixed-NP on the activation of tumor cell proliferation and eNOS, leads to a stimulation of tumor cells proliferation.

However, because we are still missing the appropriated non-treated controls, we cannot rule out the opposite hypothesis, i.e. that PEGylated NP may induce a vasoconstriction and thus an inhibition of tumor cell proliferation at day 1.

In order to understand how mixed NP can induce p-AKT and p-ERK, we then looked for the phosphorylation levels of other transmembrane receptors.

## 6.7 RGD/ATW-NP activates EGFR, IGF1-R/Insulin R and Met in HUVEC

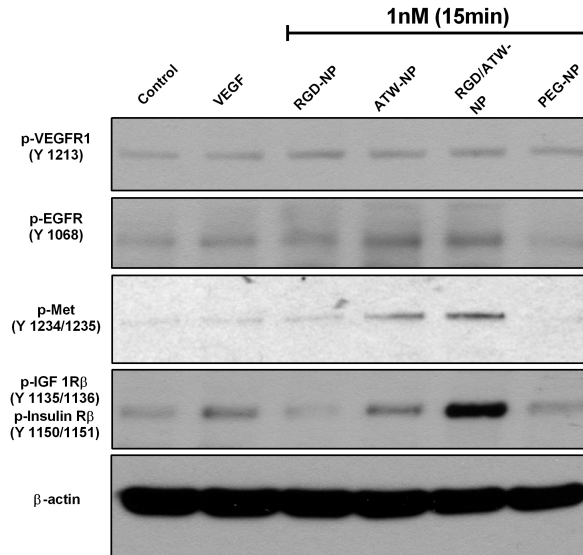


Fig. 54 1 nM ATW containing NPs (especially RGD/ATW-NP) significantly induced Met, EGFR and IGF 1R/IR phosphorylation, but not that of VEGFR1. HUVEC were serum starved for 20 hours, followed by 1nM NPs' treatment of 15min.

As can be seen in Fig. 54, 1 nM of the different NPs do not change significantly the phosphorylation of VEGFR1 in the first 15 min (like VEGF also). In contrast, the presence of ATWLPPR in particular when associated to RGD clearly induce the activation of EGFR, Met and IGF1R $\beta$ /IR. The later is clearly the most responsive one with an 8 folds augmentation of its phosphorylation level (Fig. 55):

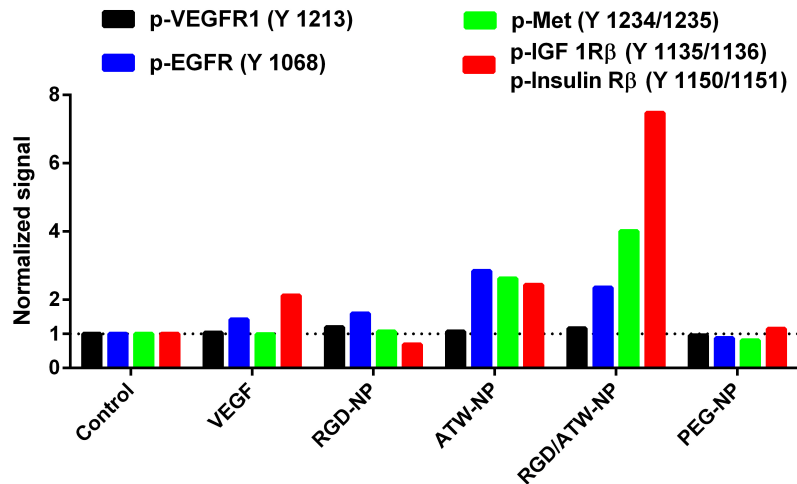


Fig. 55 Semi-quantification of phosphorylation level (Fig. 54) after normalization with the control group.

We thus started to investigate how inhibitors of IGF1R (R1507, Linsitinib) or of RTKs (Sorafenib) could interfere.

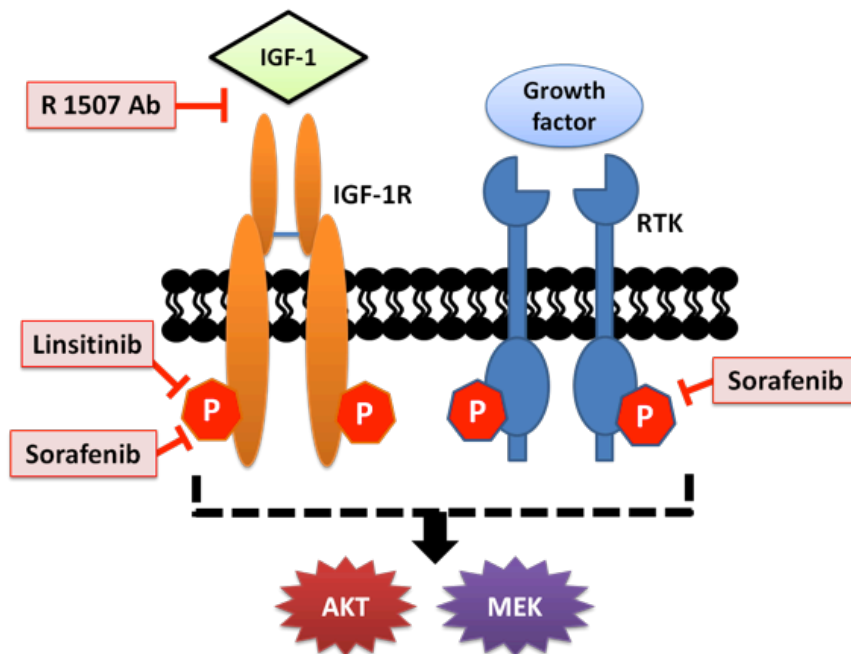


Fig. 56 Schematic representation of the action of the antibody antagonist and tyrosine kinase inhibitors of IGF 1R/IR and other RTKs. Detailed information is depicted in main text.

Importantly, R1507 is a monoclonal antibody that block the IGF1R from the outside, preventing its activation by exogenous ligands. Linsitinib is a small-molecule dual IGF-1R/insulin receptor (IR) kinase inhibitor and Sorafenib a small molecule multiple VEGFR, PDGFR and Raf kinase inhibitor (Fig. 56).

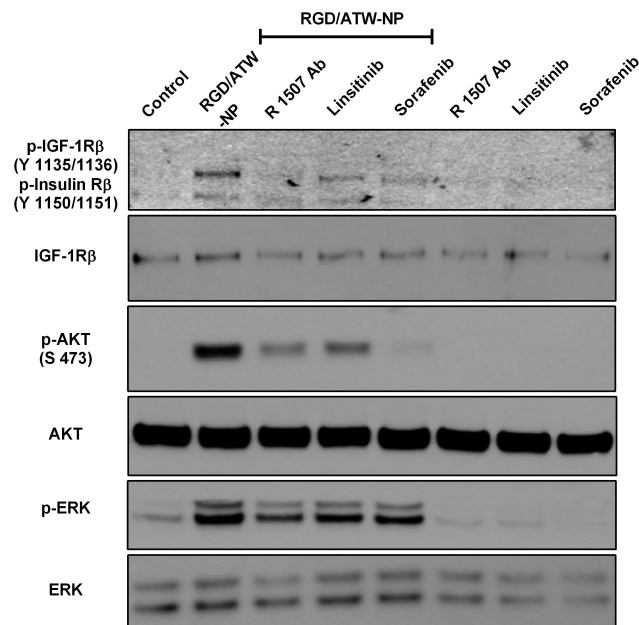


Fig. 57 IGF1R/IR specific and RTK nonspecific inhibitors prevent RGD/ATW-NPs induced IGF1R/IR-AKT activation, while being dramatically less efficient on ERK phosphorylation. HUVEC were treated with R 1507 Ab (100 nM), Linsitinib (1  $\mu$ M) or Sorafenib (1  $\mu$ M) during 15 min prior to the incubation with 1 nM NPs for another 15 min.

As shown in Fig. 57, although R1507 (100nM) is the stronger, the 3 tested inhibitors are partially blocking the RGD/ATW-mediated phosphorylation of the IGF1-R $\beta$ /IR. Sorafenib (1 $\mu$ M) is particularly capable of preventing the activation of AKT. However, the 3 treatments are much less efficient on p-ERK suggesting that the two different pathways triggered by the mixed NP are not always interdependent.

## 6.8 Proposed model of action

The different results lead us to propose the following scheme (Fig. 58). Under serum-starved condition, type A RGD/ATW-NP induces transient ERK activation by unknown mechanism, and it recruits RTKs like IGF 1R/IR, Met, EGFR .etc and induces strong and sustained AKT activation, which brings out protective effects to resist serum-starvation induced cell death.

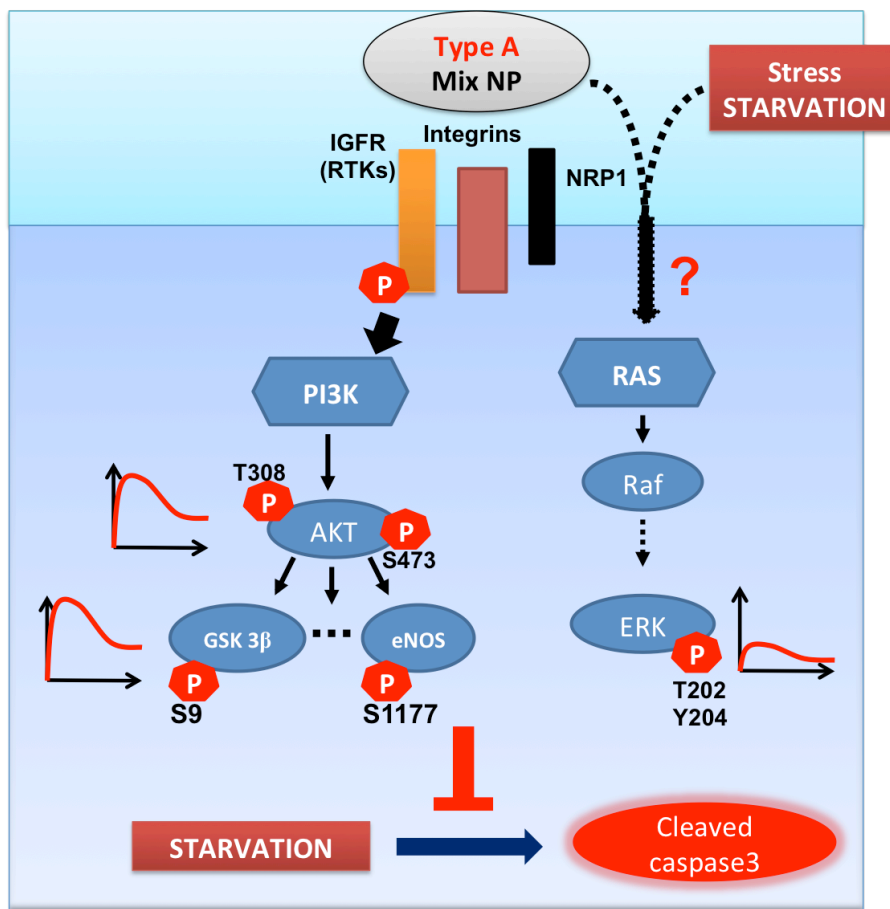


Fig. 58 Proposed model of RGD/ATW-NPs' reactivity on HUVEC under serum-deprived condition. Detailed information is depicted in main text.

## 6.9 Confirmation of these results on HDMEC

The activation of the pathways described in HUVEC were also tested in another primary endothelial cell type, HDMEC:

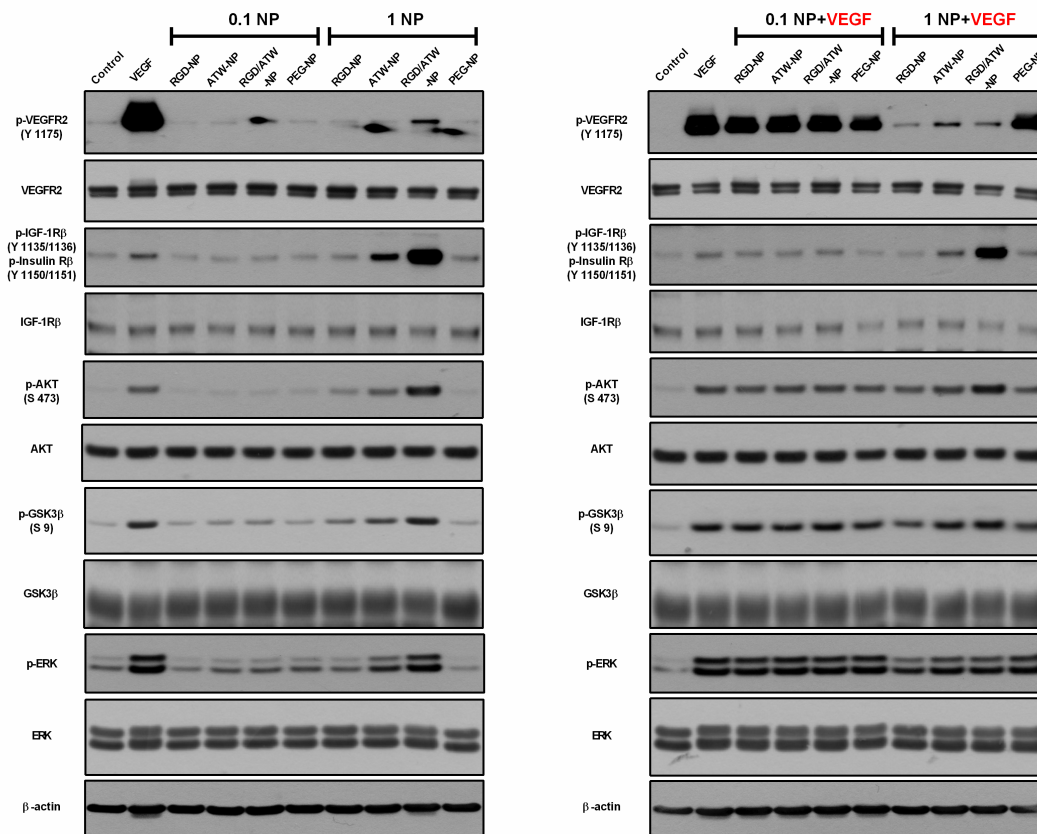


Fig. 59 Confirmation on HDMEC. HDMEC were treated with 0.1 nM or 1 nM of NPs for 5 min prior to the treatment with VEGF (20 ng/ml) for another 10 min. VEGF was used as a positive control of VEGFR2 associated signaling activation. Left panel: The ATW- and more importantly the RGD/ATW-NPs are activating VEGFR2 and IGF 1R/IR cell signaling in a dose-dependent manner. Right panel: in the presence of 20 ng/ml VEGF, the RGD-, ATW- and dual RGD/ATW-NPs are actively blocking VEGFR2 at 1 nM, but at this concentration the dual NPs is still inducing the phosphorylation of IGF 1R/IR, AKT, ERK and GSK-3 $\beta$ .

The blocking effect of ATWLPPR-containing NPs on the phosphorylation of VEGFR2 in the presence of VEGF is not detectable when 0.1 nM of NPs are used (top right panel). This is an important difference with HUVEC. However, 1nM of peptides containing NPs including RGD-NP, but not PEG-NP are blocking VEGF' activity on VEGFR2 as it was already observed in HUVEC.

Another difference can be seen also using 1 nM RGD/ATW-NP. In HDMEC, this NP can directly phosphorylate VEGFR2 in the absence of VEGF.

Despite these differences that may come from a higher expression/activity of VEGFR2 in HDMEC than in HUVEC or crosstalk (reciprocal phosphorylation) between IGF-1R/IR and VEGFR2 in HDMEC [152], the rest of the IGFR1R/IR, AKT, ERK, GSK3 $\beta$  is activated with similar patterns. This is summarized and semi-quantified in the graph below (Fig. 60):

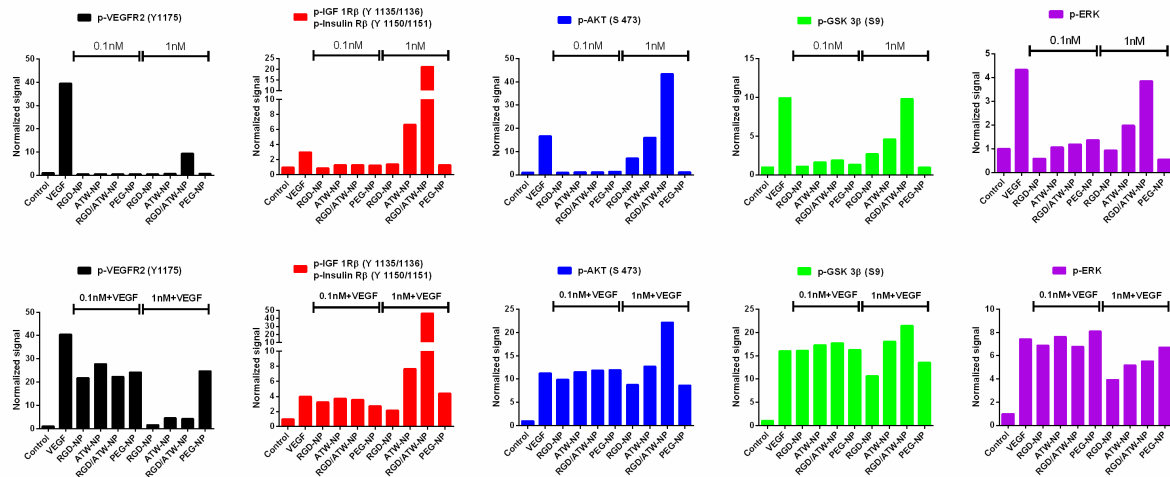


Fig. 60 Semi-quantification of phosphorylation level (Fig. 59) after normalization with the control group.

## 7 Results Part 3: Signaling on tumor cells

### 7.1 Study of VEGF response on the tumor cell lines

In order to test NPs' blocking effects on VEGF-VEGFR2 signaling in tumor cells, I firstly studied the reaction of VEGF in tumor cells at the concentration of 20ng/ml used with endothelial cells. Because I did not detect positive responses (Fig. 61), I augmented its concentration to 200ng/ml and tested the kinetics of VEGF's effects on VEGFR2-AKT/ERK signaling in PANC-1, M21 and MDA-MB-231 cells from 10min to 60min. VEGF increases weakly the phosphorylation VEGFR2 and AKT in all the three cell types while no activation of p-ERK was detected (Fig. 62).

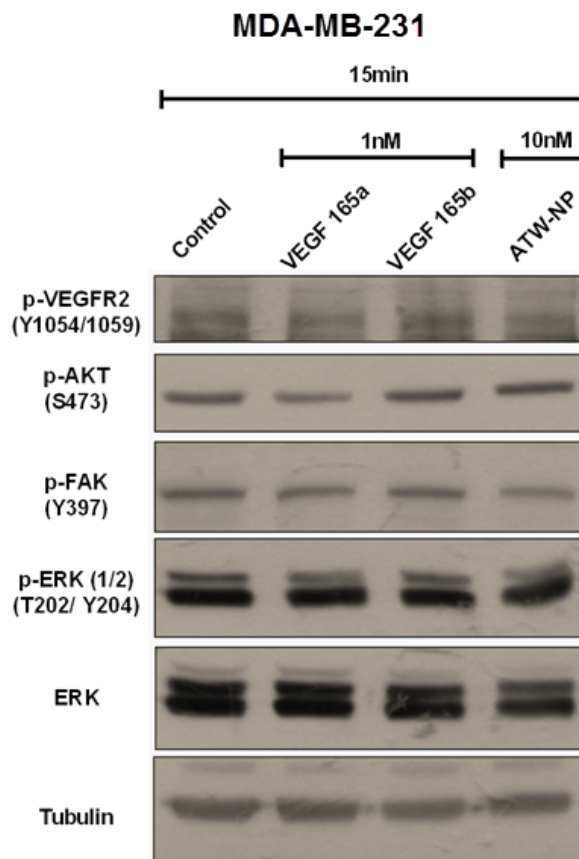
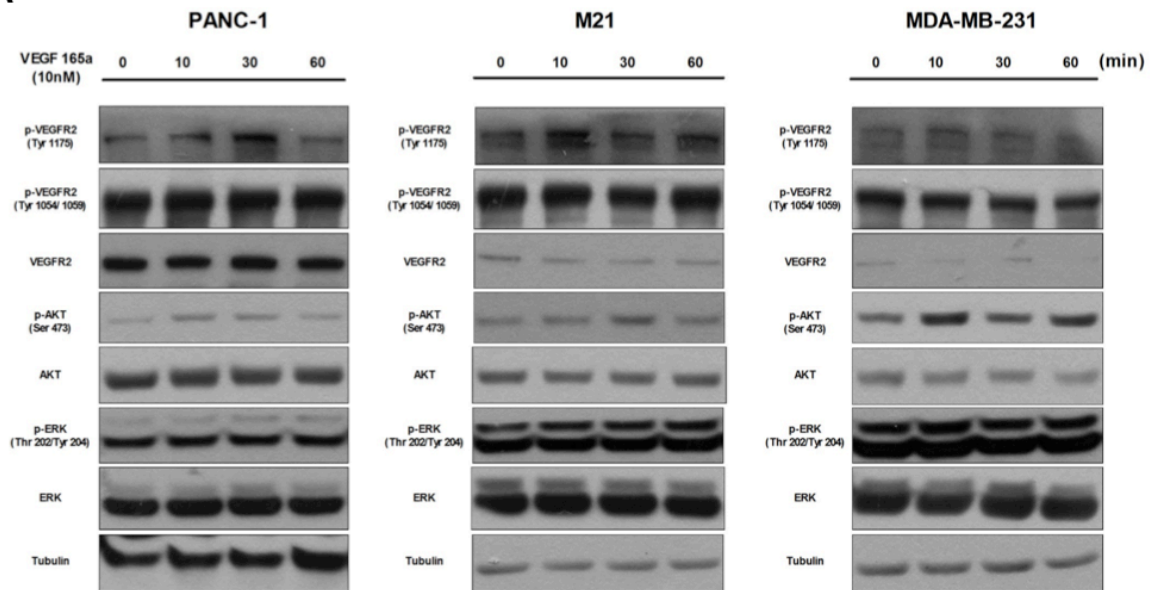


Fig. 61 VEGF does not mediate AKT activation in MDA-MB-231 cells. MDA-MB-231 cells were serum starved for 20 hours before the treatment of 1nM VEGF<sub>165a</sub> and VEGF<sub>165b</sub>, as well as 10nM ATW-NP for 15min.

**A**



**B**

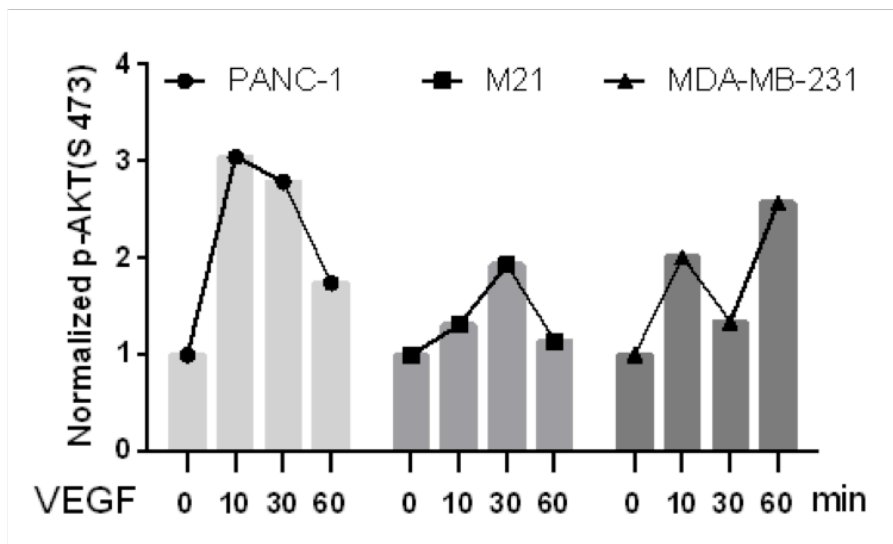


Fig. 62 VEGF mediates AKT phosphorylation in tumor cells. (A) Kinetic studies of 10nM (200 ng/ml) VEGF's effects on VEGFR2-AKT/ ERK signaling in PANC-1, M21 and MDA-MB-231 cells from 10min to 60min. All cells were serum starved for 20 hours before VEGF's treatment for the indicated time. (B) Quantitative analysis of p-AKT was performed by ImageJ. Graph shows the quantification of p-AKT levels after normalizing the values to their respective control group.

## 7.2 At 100pM, ATW-NP blocks VEGF and AKT on PANC-1 cells

Then we selected 200ng/ml of VEGF to test the blocking efficiency of different NPs on PANC-1 cells. Consistent with studies of NPs' effects on VEGF-VEGFR2 signaling in HUVEC cells, ATWLPPR only grafted NPs nearly abrogated VEGF-induced activation of AKT at the lower concentration of 100pM (Fig. 63), while no significant inhibition of AKT was detected in the presence of the other NPs.

### 7.3 At 1nM, RGD/ATW-NP activates AKT on PANC-1 cells

We next tested NPs "intrinsic" effects on AKT signaling at the higher concentration of 1nM. Only RGD/ATW-NP augments the phosphorylation of AKT at 15min on PANC-1 cells (Fig. 63).

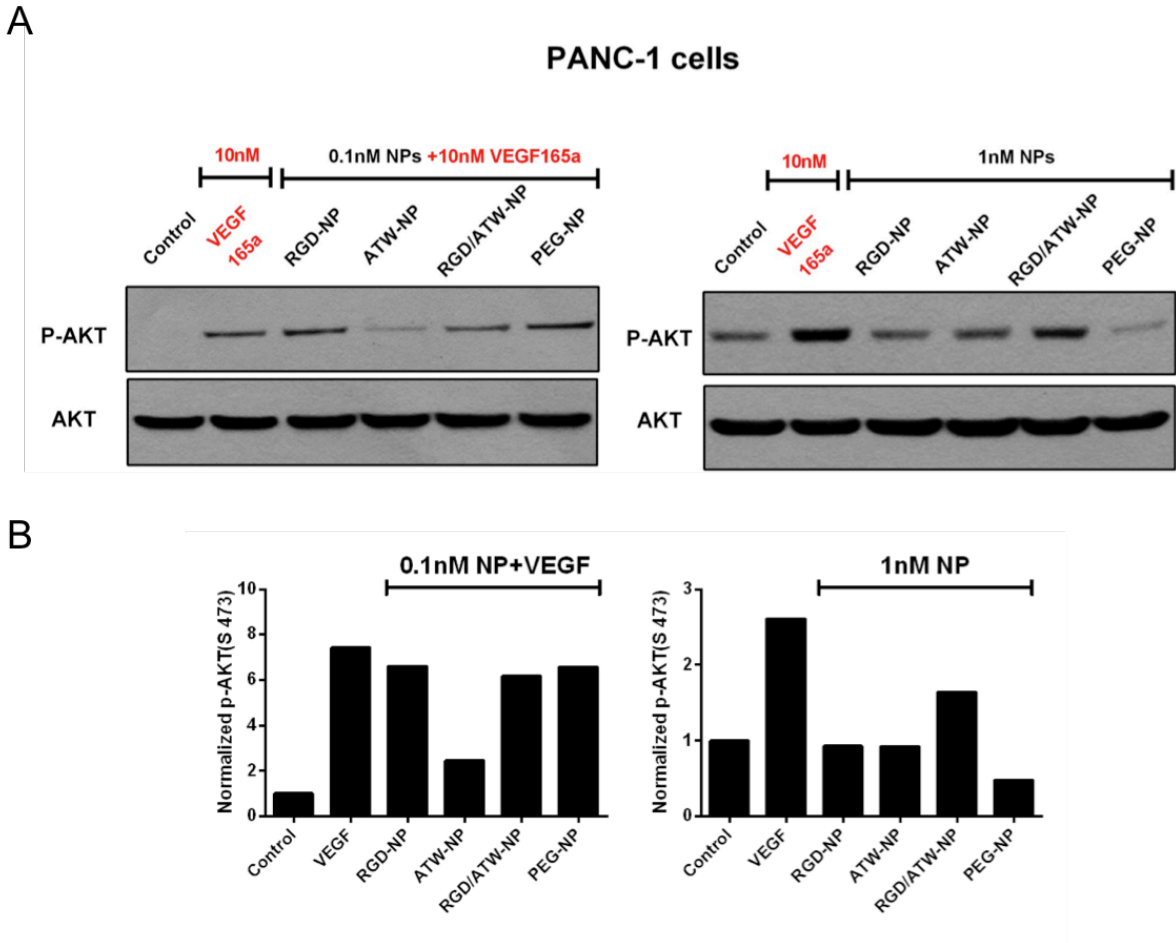


Fig. 63 NPs' effects on AKT signaling on PANC-1 cells. PANC-1 cells were serum starved for 20 hours before VEGF or NPs' treatments. (A) Left figure: PANC-1 cells were treated with 0.1nM NPs for 5min prior to treatment with VEGF (200ng/ml) for 30min. Right : PANC-1 cells were treated with 1nM NPs for 30min, VEGF was used as a positive control to indicate AKT

activation. (B) Quantitative analysis of p-AKT was performed by Image J. Graph shows the quantification of phospho-AKT level after normalizing the data to respective control group.

#### 7.4 PANC-1 cells proliferation is not affected

We studied the NPs' effects on the cell proliferation of PANC-1 at 0.1 and 1nM for 3 days using an MTS assay. In the absence of serum, PANC-1 cells still proliferate well (Fig. 64 and 68). None of the NPs affects PANC-1 cells proliferation at low (0.1nM) or high (1nM) concentrations (Fig. 64).

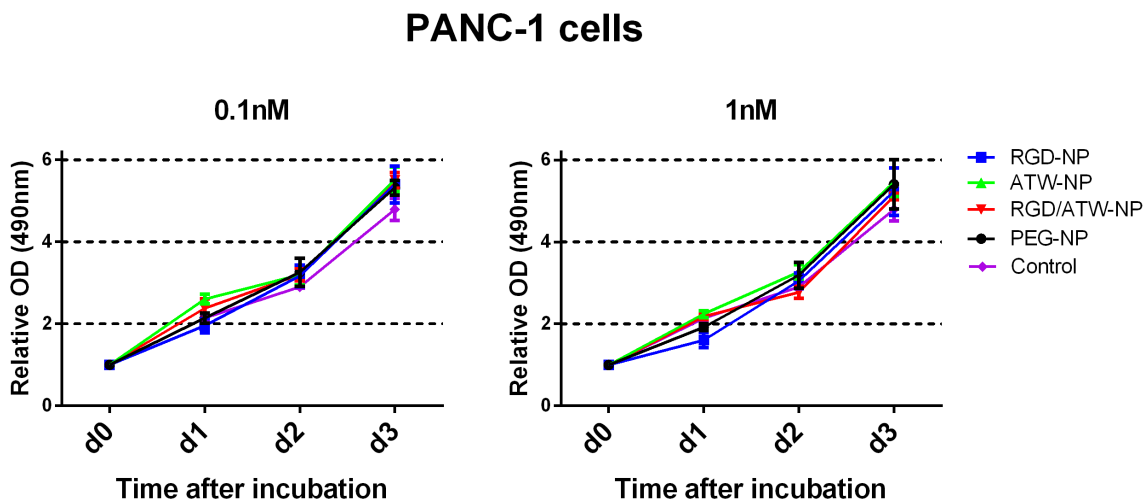


Fig. 64 PANC-1 cells proliferation in serum-free medium. Cells were treated with the indicated NPs (0.1 and 1nM) for 3 days. Data are representative of two different experiments conducted in quadruplicates and expressed as mean  $\pm$  SEM.

#### 7.5 Conclusion and Discussion:

In this chapter, we reported how different cell types (ECs and tumor cells) respond differently to VEGF. This can not be explained solely by the amount of receptors per cells but it may also comes from functional differences of receptors activities. This is obvious between tumor and normal primary cells that present important differences of reaction to VEGF, and to serum-deprivation. In tumor cells, their unstable metabolic reprogramming also confers

variability in response to VEGF. PANC-1 cells look more sensitive to the treatment of VEGF based on AKT phosphorylation. A summary of our results is listed in the following table 9.

Table. 9 VEGF-mediated activation of AKT phosphorylation in different cell types

VEGF	HUVEC	HDMEC	HMEC-1	MDA-MB-231	M21	PANC-1	U87
20ng/ml (1nM)	+++	+++	-	-	-	-	
100ng/ml (5nM)			-				
200ng/ml (10nM)				+	+	++	-

In the presence of 0.1 nM NPs, only ATWLPPR grafted-NPs inhibits VEGF-induced AKT phosphorylation in PANC-1 cells. When we augment the NPs' concentration to 1nM, AKT is only activated by RGD/ATW-NPs' treatment. Meanwhile, we did not detect any signal of activation of cell-proliferation at 1nM. More work need to be done to evaluate the phenotypic changes of these tumor cells, such as cell migration.

Collectively, these studies show how VEGF functions differently among primary ECs, and tumor cells. The impact of NPs treatment on tumor cells is more complex then that observed on primary ECs. In particular, preliminary data obtained *in vivo* suggest that in subcutaneous tumors, the proliferation of U87MG tumor cells is strongly stimulated by an IV injection of RGD/ATW-NP. This may come from a direct effect of this NP and/or a consequence of the vasodilatation activity of these mixed NP one day after injection.

## 7.6 Supplementary data:

- ❖ NPs' effects on AKT signaling were also tested in U87 cells. Even in U87 subcutaneous tumor-bearing mice injected with RGD/ATW-NPs, activation of AKT was detected as compared with that in mice injected by PEG-NPs. All NPs (1nM) exhibited no activation of AKT in U87 cells grown *in vitro* 2-D cell culture condition.

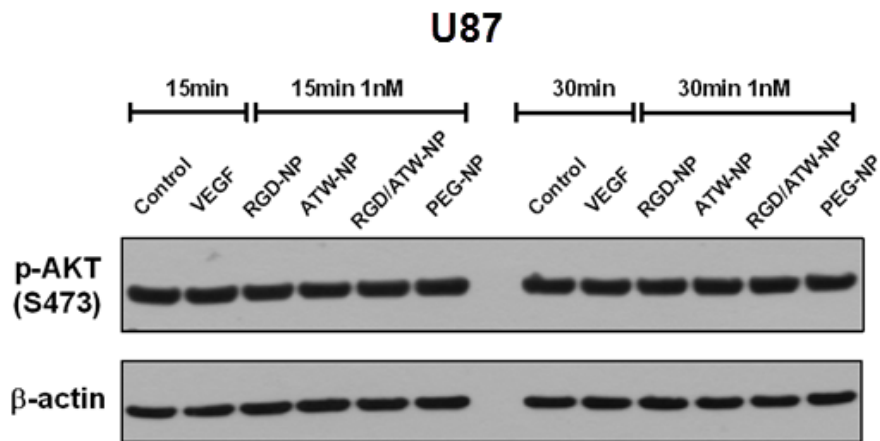


Fig. 65 NPs do not mediate AKT activation in U87 cells. U87 cells were serum starved for 20 hours before the treatment with 1nM NPs for 15 and 30min. Analysis of p-AKT changes was performed by western blotting. 10nM VEGF was used to check its effect on AKT signaling in U87 cells at 15 and 30min. Also shown is a blot for  $\beta$ -actin as a loading control.

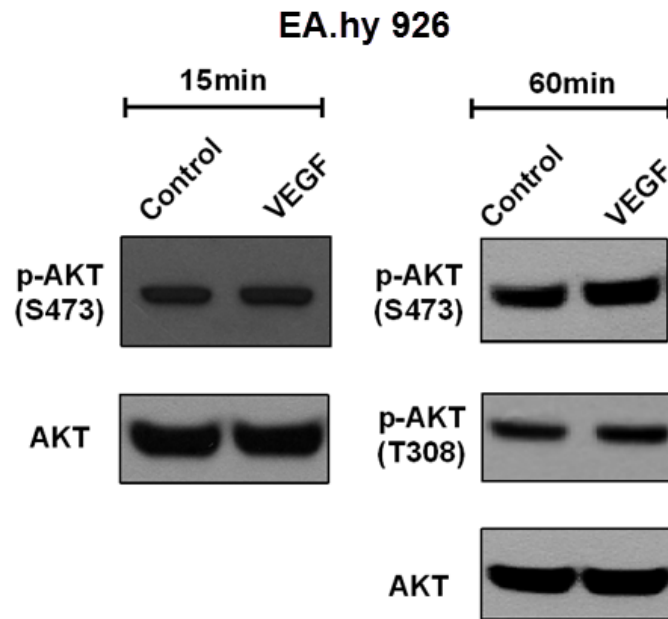


Fig. 66 VEGF does not mediate AKT activation in EA.hy 926 cells. EA.hy 926 cells were serum starved for 20 hours before 1nM VEGF's treatment for 15min and 60min. Analysis of p-AKT and AKT changes induced by VEGF was taken by western blotting.

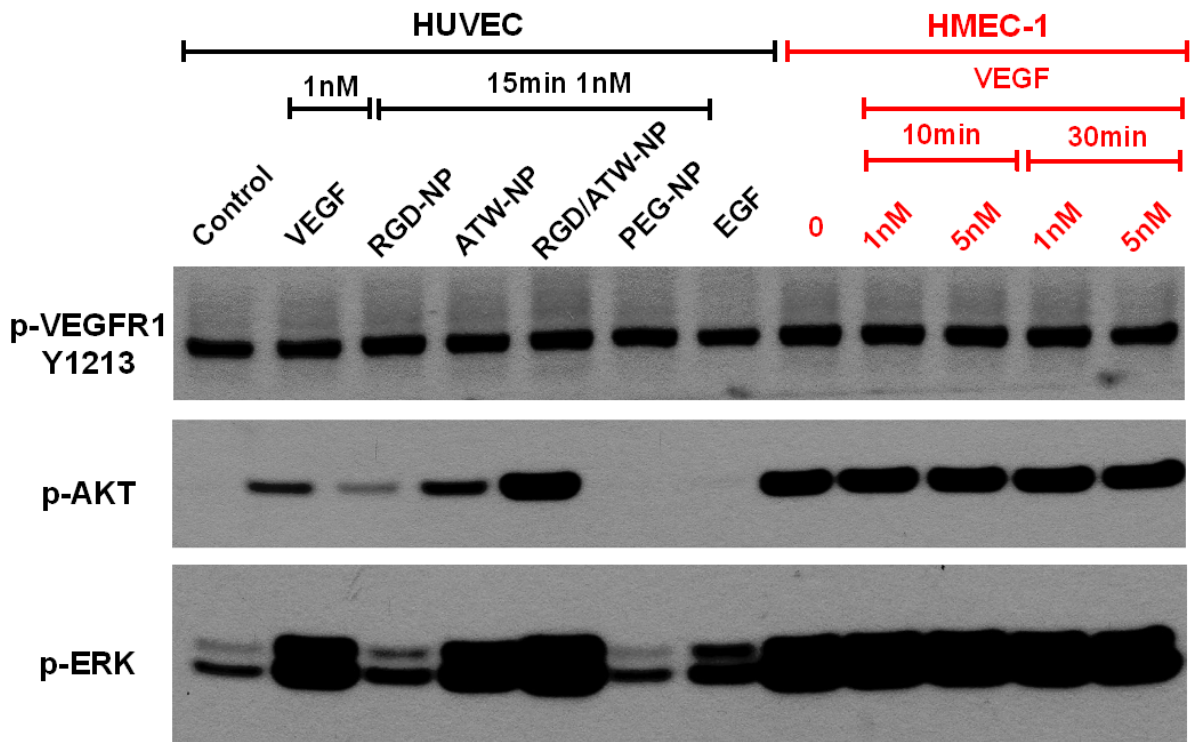


Fig. 67 VEGF mediates AKT phosphorylation in HUVEC, but not in HMEC-1 cells. HMEC-1 cells were serum starved for 20 hours before 1nM and 5nM VEGF's treatment for 10min and

30min. HUVEC cells were serum starved for 20 hours before the treatment of 1nM VEGF, EGF and 1nM NPs. Analysis of p-VEGFR1, p-AKT and p-ERK changes induced by VEGF, EGF and NPs was performed by western blotting. 15µg protein per lane were loaded.

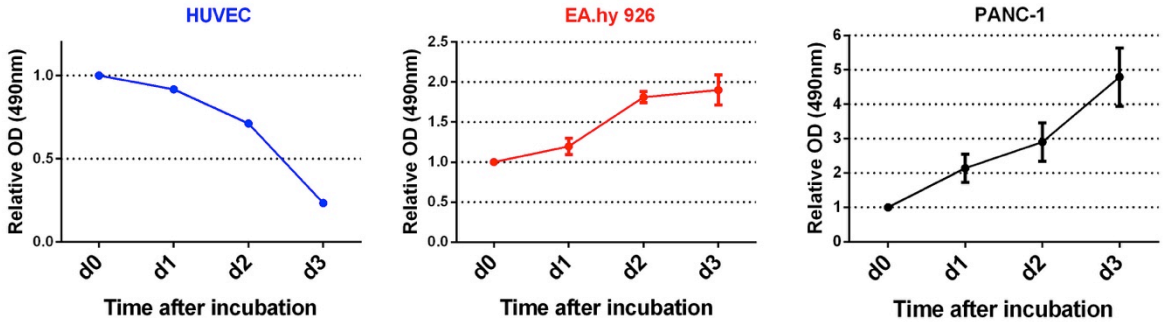


Fig. 68 Serum starvation effects on cell proliferation of HUVEC, EA.hy 926 and PANC-1. The cells were serum starved for 1, 2 and 3 days. The absorbance was determined as described in the text. Data are representative of three different experiments conducted in triplicates and expressed as mean  $\pm$  SD (n = 3).

## 8 Results Part 4: Comparative studies of type A, B and C NPs

### 8.1 Binding of A, B and C-NP on HUVEC

As shown below (Fig. 69 and quantification Fig. 70), type B NPs are the most efficient to bind to HUVEC cells, although type C performs really well also, followed by Type A:

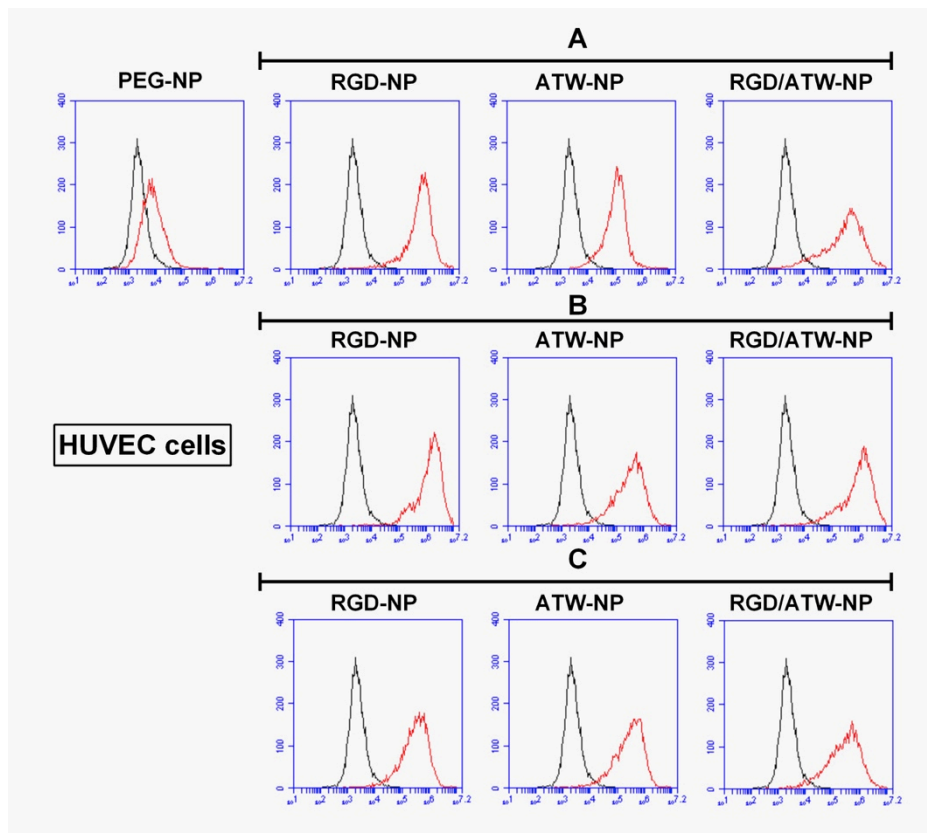


Fig. 69 NPs' binding efficiency on HUVEC cells by FACS. A, B, C indicate the type of NPs. The total amount of targeting peptides on each type of NPs is 1000. PEG-NP was used as a negative control. Flow cytometry analysis of HUVEC cells incubated with different NPs without serum for 60 min at 37°C in 5% CO<sub>2</sub>.

## 8.2 Phosphorylation of AKT

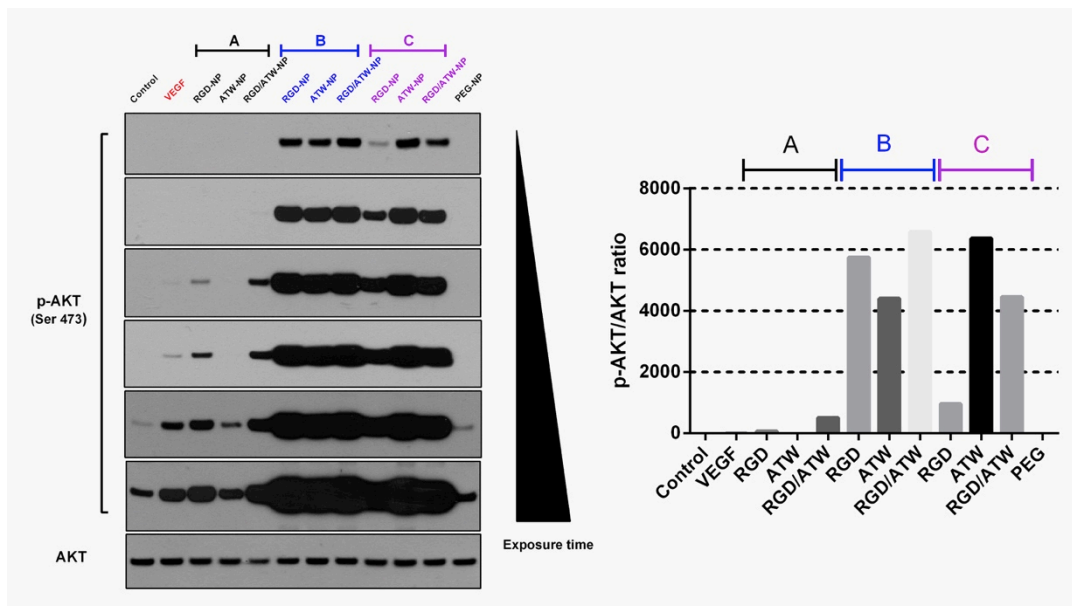
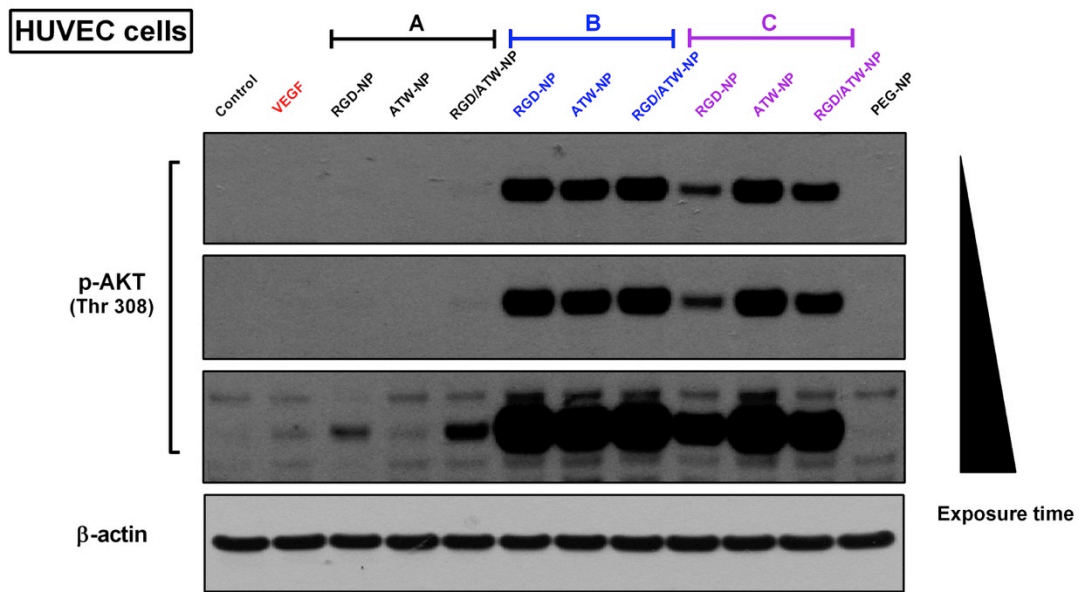


Fig. 70 p-AKT (Thr 308) and p-AKT (Ser 473) changes in HUVEC cells. A, B, C indicate the type of NPs. The amount of targeting peptides on each type of NPs is 1000. PEG-NP was used as a negative control. HUVEC cells were serum starved for 20hours before the treatment of 1nM NPs for 1hour. VEGF was used as a positive control of AKT in HUVEC cells.

In Fig. 71, the correspondence between binding intensities and AKT phosphorylation were examined:

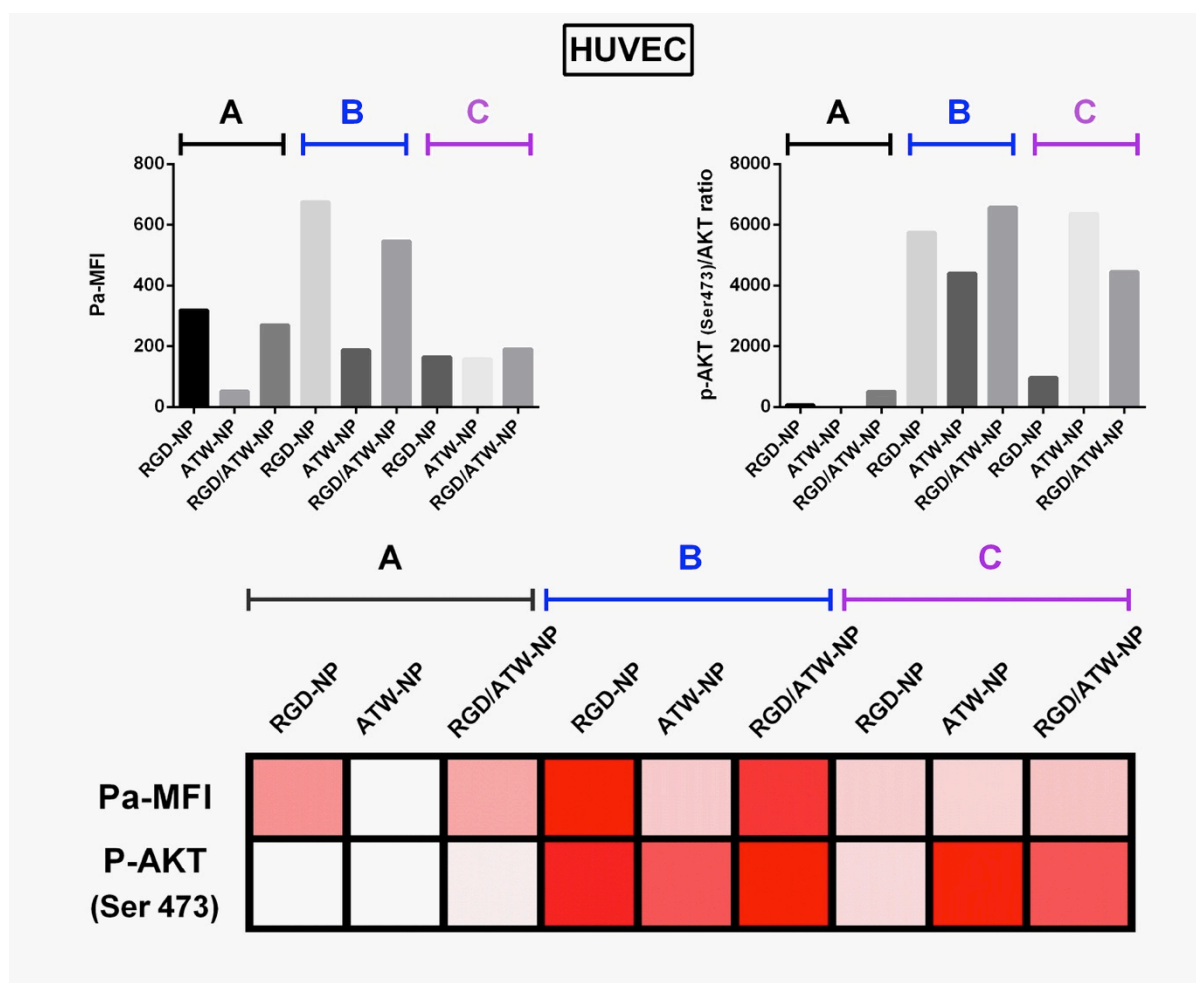


Fig. 71 Parallel comparative studies of NPs' binding efficiency and AKT activity in HUVEC cells. Top Left histogram summarizes the binding intensities (indicated as Pa-MFI) while the top right histogram represents a semi-quantitative analysis of the associated changes in the phosphorylation of AKT. Bottom: Row normalized sorting of the value of Pa-MFI and p-AKT.

Type A and B present the same pattern although type B is much more active. RGD is driving the binding efficiency and ATWLPPR is a good activator of AKT. When both RGD and ATWLPPR peptides are combined, they activate AKT synergistically.

The pattern obtained with type C is not similar. Type C NP is covered by PEG2000 and also by PEG3000-RGD and PEG3000-ATW. All 3 tested C-NPs present similar binding efficiencies. ATWLPPR-NP is the most potent activator of AKT. The dual C-NP does not show a synergistic action of the 2 peptides but a rather reduced activity as compared to the ATW-only C-NP.

A graphical scheme that highlights the effect of each peptide according to the type of NP is presented in Fig. 72:

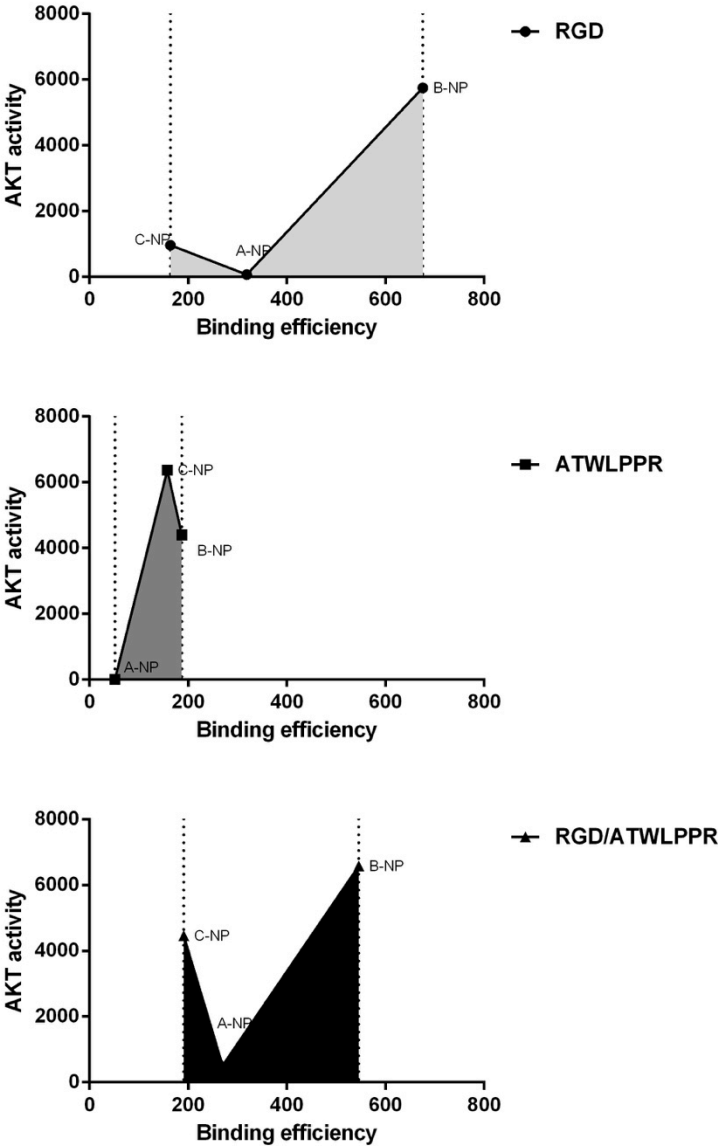


Fig. 72 Distribution of different NPs' binding efficiency and AKT activity in HUVEC cells. A, B, C indicate the type of NPs. The total amount of targeting peptides on each type of NPs is 1000. Circles: cRGD-NP. Squares: ATWLPPR-NP. Triangles cRGD/ATW-NP.

This confirms that the mixed presentation of both peptides is always the strongest combination in terms of binding and AKT activation and that the type B NP is the more active.

### 8.3 Signaling pathways activated by type A, B or C NPs

As presented in chapter 2, type A NPs activate RTK-AKT/ERK signaling axis in primary ECs (HUVEC and HDMEC). In particular, mixed RGD/ATW-NP (A-NP<sup>1000</sup><sub>50/50</sub>) induced a sustained activation of AKT that could protect ECs from serum-starved induced apoptosis. In this part, I compared all type of NPs' effects on the same signaling cascades tested in chapter 2.

Type B and C NPs were found to induce a very strong and non-specific AKT/ERK associated signaling, which correlates well with the NPs-induced activation of RTK (EGFR, IGF-1R/IR). Surprisingly, no protection of serum deprivation-induced caspase-3 activation was detected in the presence of neither type B nor C NPs in HUVEC cells. Consistent with the data of chapter 2, type A mixed NPs (A-NP<sup>1000</sup><sub>50/50</sub>) abrogated serum deprivation-induced activation of caspase-3.

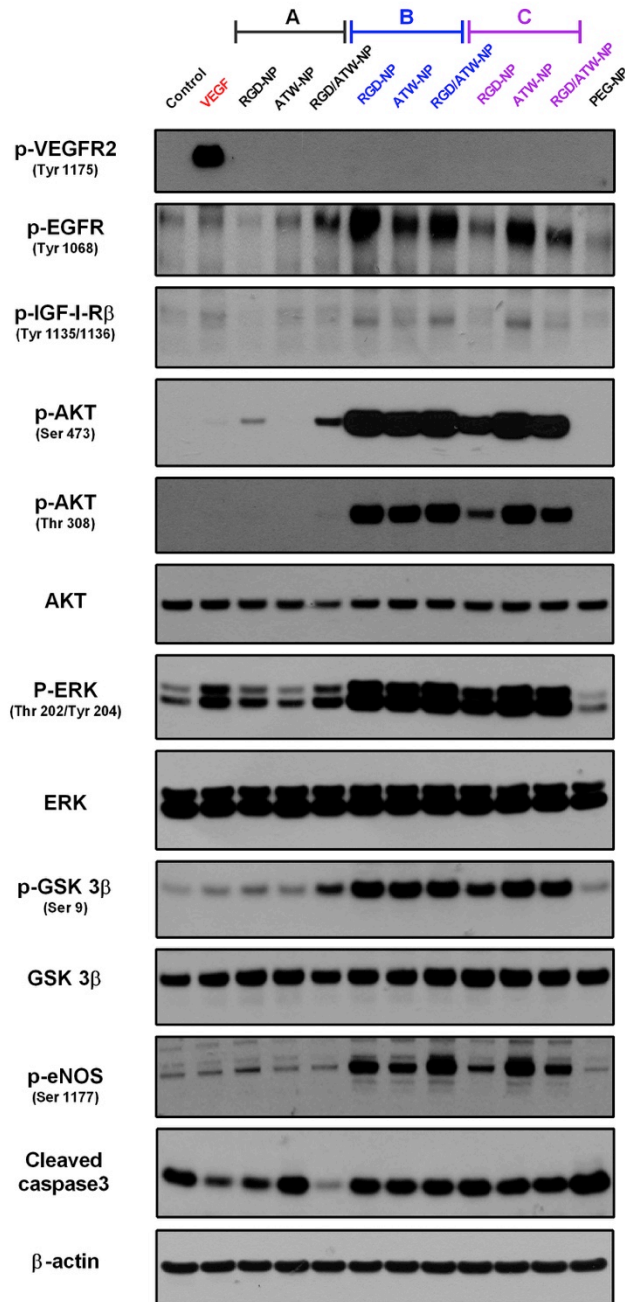


Fig. 73 Comparative studies of type A, B and C NPs' effects on RTK-AKT/ERK associated signaling in HUVEC cells. PEG-NP was used as negative control. HUVEC cells were serum starved for 20hours before the treatment of 1nM NPs for 1hour. VEGF was used as a positive control for VEGFR2/AKT activation.

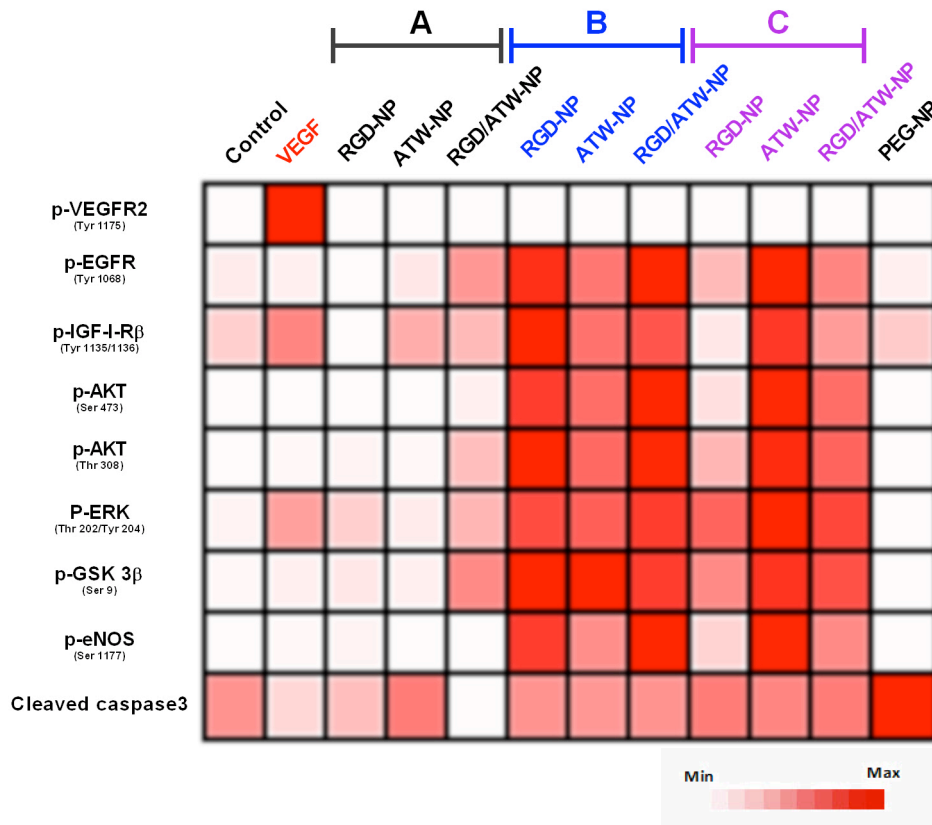


Fig. 74 Heat map studies of NPs' effects on RTK-AKT/ERK associated signaling in HUVEC cells.

In parallel to their action on AKT, type B and C NPs are all very strong activators of ERK, GSK3 $\beta$  and eNOS. Type B activates these cascades as type A does but 200 times more efficiently and mixed RGD/ATW is the more active. Type C is very powerful but a little bit less than B and the ATW-NP is the stronger inducer of AKT's response.

## 8.4 Binding of A, B and C-NP on tumor cell lines

### 8.4.1 Impact of the number of peptide/NP

We compared the binding efficiency of type A, B and C NPs on two tumor cells MDA-MB-231 and H358 that express different levels of integrin  $\alpha\beta_3$  and NRP1 (Fig. 75). We firstly re-evaluated the importance of total number of peptides grafted on each NP, and in a second time we looked for the impact of a fine-tuning of the ratio of each peptide.

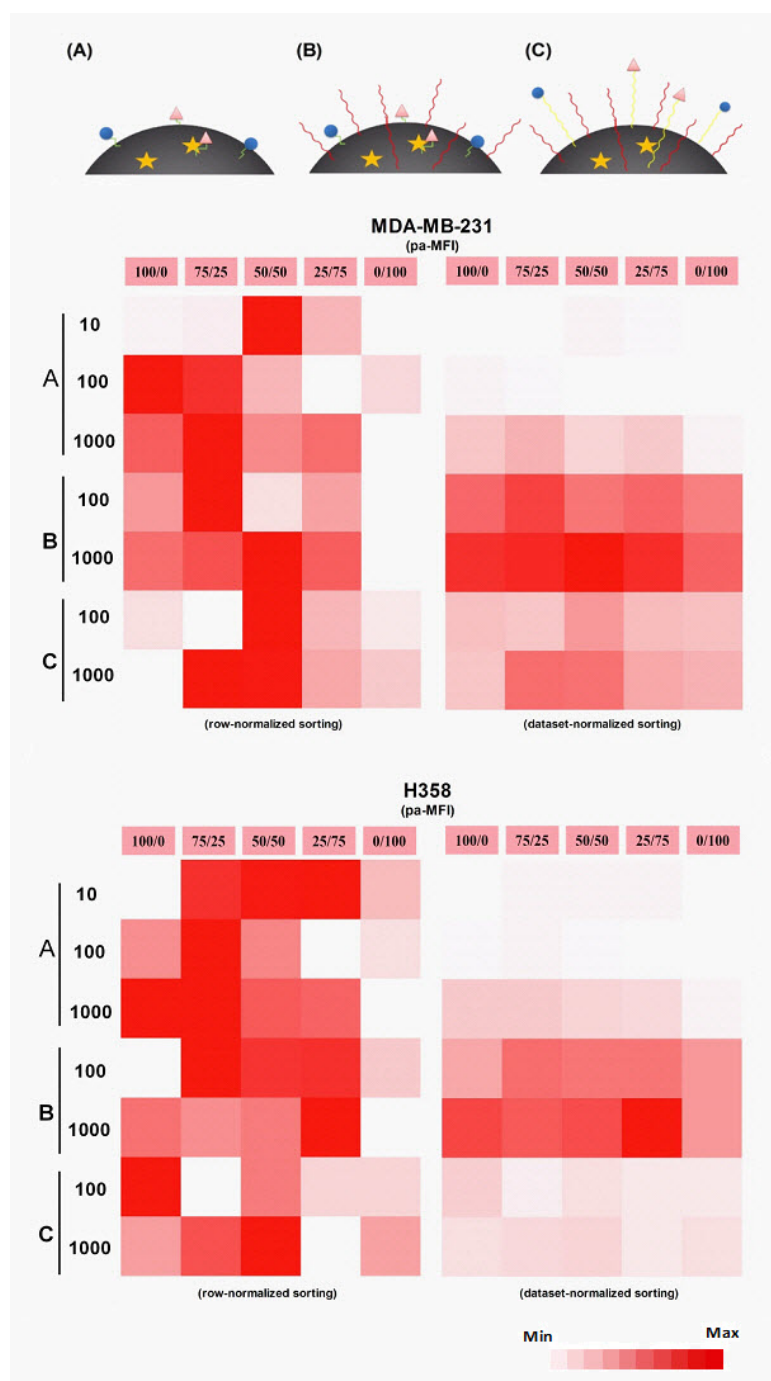


Fig. 75 Heat map studies of type A, B and C NPs' binding efficiency (Pa-MFI) on H358 and MDA-MB-231 cells. A, B, C indicate the type of NPs. 10, 100, 1000 indicate the amount of peptides grafted on NPs. X axis indicates the peptides' ratio of [anti integrin] and [anti NRP1] targeting ligands. Left figure indicates row normalized sorting of the value of Pa-MFI, right figure indicates dataset-normalized sorting of the values of Pa-MFI. Flow cytometry analysis of H358 and MDA-MB-231 cells incubated with different NPs for 30min at 37°C in 5%CO<sub>2</sub>. Data represents two independent experiments.

On MDA-MB-231 cells, RGD-NP ( $NP_{100/0}$ ) always binds more efficiently than ATW-NPs ( $NP_{0/100}$ ), except when RGD is presented by the C-type of  $NP^{1000}$ . On H358 cells, the superiority of  $NP_{100/0}$  on binding was not detected, as compared with  $NP_{0/100}$ , which might be explained by the lower expression level of integrin  $\alpha_v\beta_3$  on these cells. Notably, when compared with the binding of mono-ligands grafted NPs, dual-ligands grafted NPs did not always perform better. As an example,  $A-NP^{100}_{25/75}$  and  $C-NP^{100}_{75/25}$  present the lowest binding on both cells (Fig. 75). In summary  $A-NP^{10}_{50/50}$ ,  $A-NP^{1000}_{75/25}$ ,  $B-NP^{100}_{75/25}$  and  $C-NP^{1000}_{50/50}$  are the strongest ones on both cell lines.

By data-normalized sorting of the value of Pa-MFI (right panels) on H358 and MDA-MB-231 cells, B-NPs are binding more efficiently than C-NPs' and A-NPs' on both cell types and the  $B-NP^{1000}$  are the strongest ones, especially on MDA-MB-231 cells. This confirmed our previous results in HUVEC.

#### 8.4.2 Binding of B NPs on 9 different cell lines

We then characterized in more details the  $B-NP^{1000}$  and selected 9 cell lines to check their binding by FACS (Fig. 76). The cell lines were including 6 types of tumor cells (M21, M21L, MDA-MB-231, PANC-1, H358 and SKBR3), 2 types of ECs (HUVEC and EA.hy 926) and 1 fibroblast cell line (3T3). Expression levels of integrin  $\alpha_v\beta_3$  and NRP1 are presented in the left column of Fig. 76.

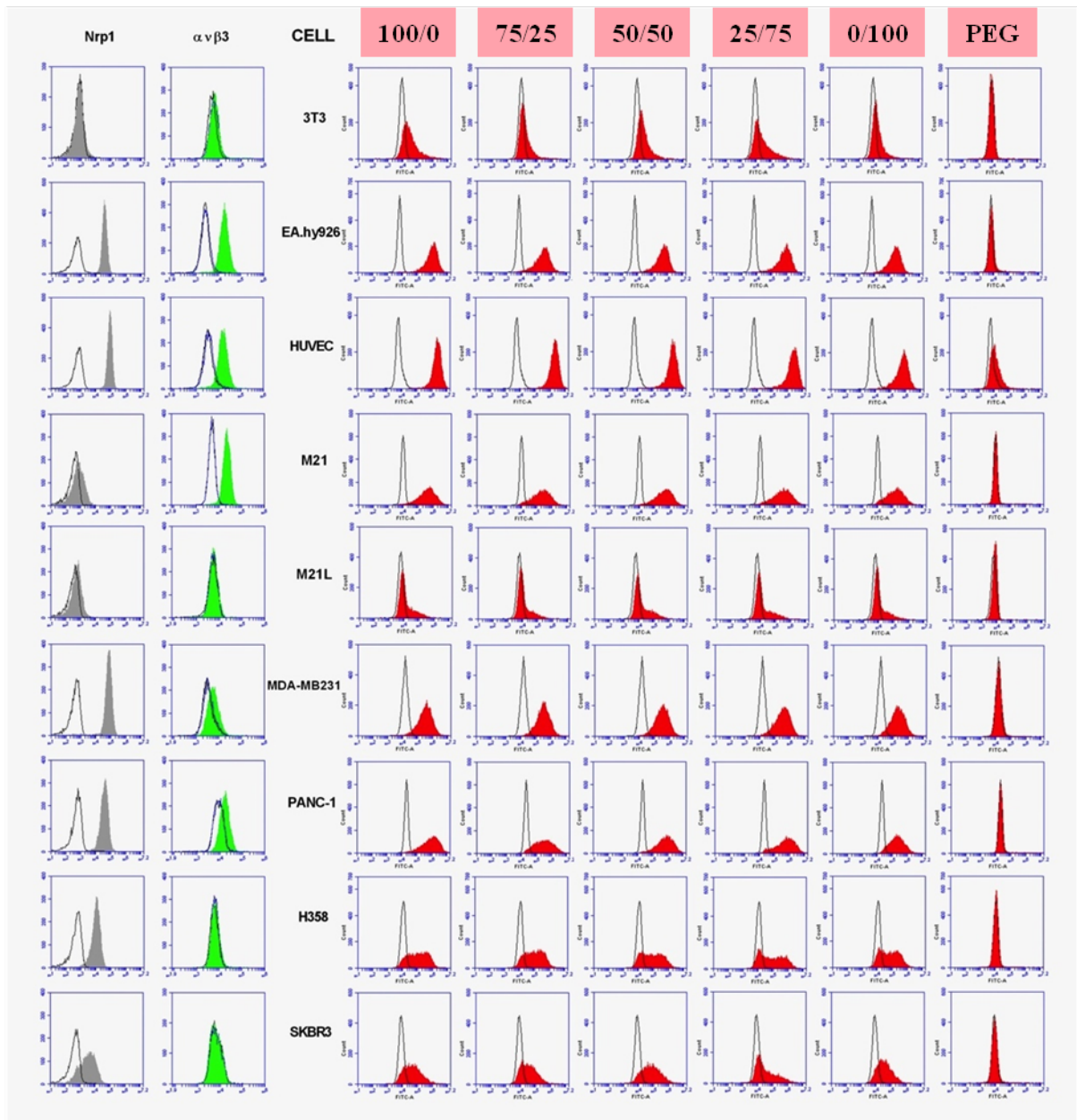


Fig. 76 Binding of  $B-NP^{1000}_{y/z}$  and  $PEG-NP_{0/0}$  on 9 cell lines. Left column indicates the expression level of the receptors. In gray: NRP1, and green: integrin  $\alpha_v\beta_3$ . The 9 cell lines were incubated with the different B NPs during 30min at 37°C in 5%CO<sub>2</sub>. The influence of the peptides ratio y/z is also presented.

As expected based on their level of receptors (Fig. 76), ECs are targets of choice while the negative fibroblast cells are not recognized. Importantly, knocking out of integrin  $\alpha_v$  subunit abrogates the binding the B-NP in M21 cells, which emphasizes the vital role of integrin  $\alpha_v\beta_3$  in determining the interaction of B-NP with M21 cells.  $B-NP^{1000}_{0/100}$  coated with ATWLPPR

only are very poorly binding the tested cells. Interestingly, a very weak but still positive binding of PEG-NP<sub>0/0</sub> was detected exclusively on a small percentage of HUVEC cells (Fig. 76).

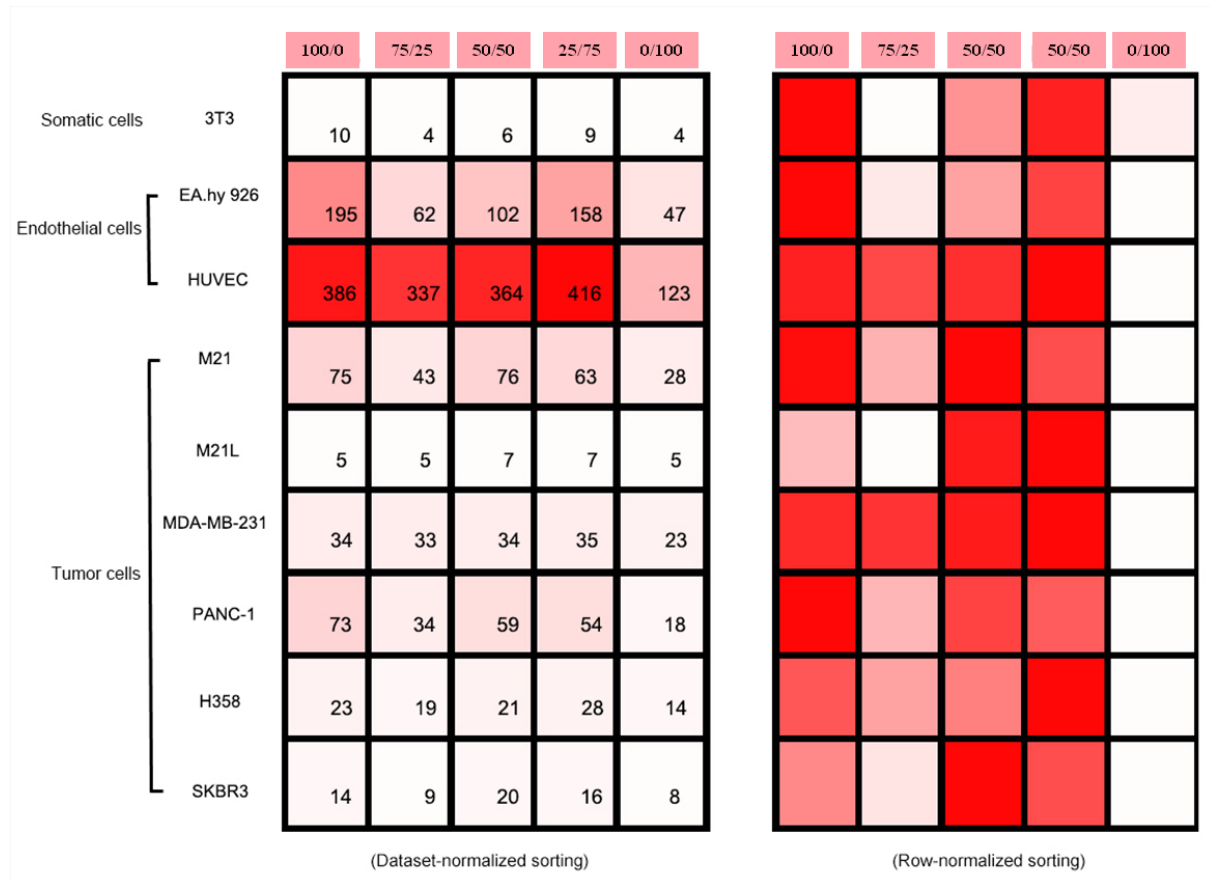


Fig. 77 Heat map studies of the binding of B-NP<sup>1000</sup><sub>y/z</sub>. X-axis indicates the peptides' ratio of [anti integrin] and [anti NRP1] targeting ligands. Y-axis indicates three types of cells: somatic cells, endothelial and tumor cells. Left heat map indicates dataset-normalized sorting of the values of Pa-MFI, right heat map indicates row normalized sorting of the values of Pa-MFI.

A Pearson correlation coefficient (PCC) study was performed to explore the relationship between the receptors' level and B-NPs' binding efficiency. When functional NPs are compared with PEG-only they present a better correlation with the level of receptors, integrin  $\alpha_v\beta_3$  and NRP1. B-NPs' binding is more correlated with the level of integrin  $\alpha_v\beta_3$  than with the level of NRP1. These data confirmed that the integrin  $\alpha_v\beta_3$  plays a dominant role in deciding the binding of the dual-ligands (RGD and ATWLPPR) or mono-ligand grafted NPs.

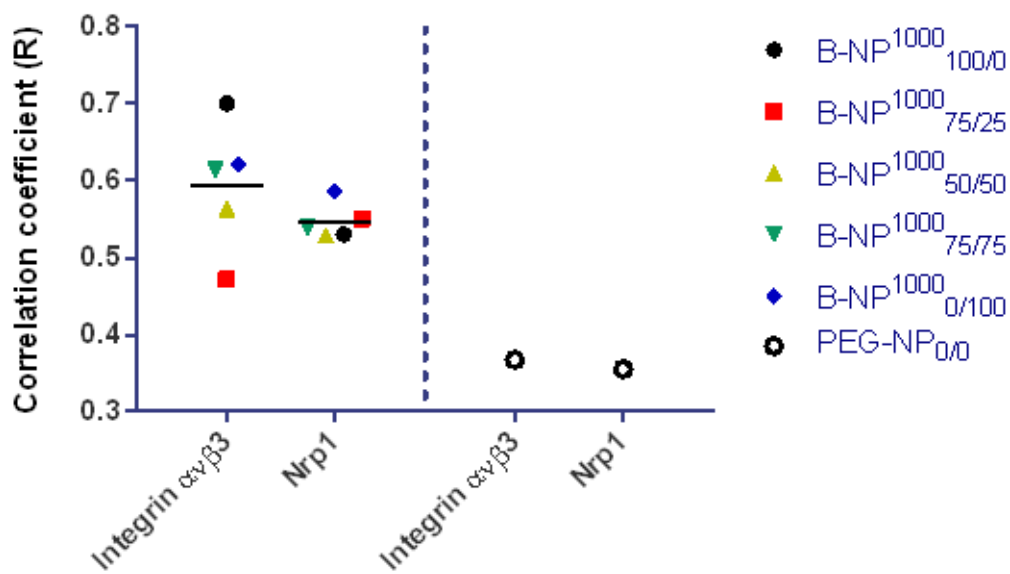
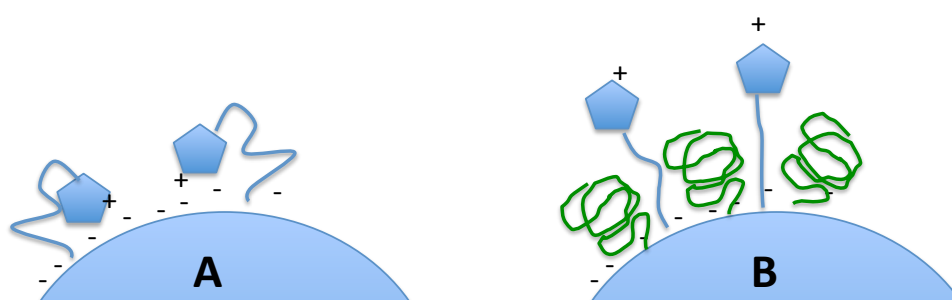


Fig. 78 Pearson correlation coefficient (PCC) study of B-NP<sup>1000</sup><sub>y/z</sub> and PEG-NP<sub>0/0</sub>'s binding efficiency with the level of integrin  $\alpha_v\beta_3$  and NRP1 receptors.

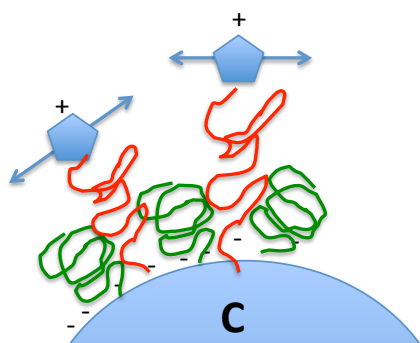
In addition, binding of ATWLPPR (anti-NRP1) grafted NP (B-NP<sup>1000</sup><sub>0/100</sub>) presents the highest correlation with the level of NRP1. The introduction of 25% ATWLPPR to RGD peptides significantly reduced the PCC of their binding with the expression level of the integrin. This implies that the relationship is not linear between the ligand's proportion and the corresponding receptor-dependent binding efficiency. The presence of 50% cRGD and 50% ATWLPPR correlates well with the level of integrin  $\alpha_v\beta_3$  but not with NRP1's.

## 8.5 Conclusion and discussion:

Our data indicate that the addition of PEG2000 on the surface of A NPs generates a more efficient binding efficiency on all the tested cell lines. Thus the presence of PEG polymers between the peptides may force them to be properly presented and accessible. We hypothesize that on type A NPs the peptides may stick to the negatively charged silica via their positive Arginine residues in particular. The presence of PEG may force them to remain exposed and accessible on the NP's surface.



In type C, we replaced the  $\beta$ Ala spacers below the RGD and ATWLPPR peptides by PEG3000. This PEG3000 spacer seems optimal for a correct presentation of ATWLPPR but not for RGD.



This may be related to a larger degree of liberty of the peptides at the extremity of this long spacer or also to an unexpected folding of RGD within the PEG that will mask it partially. Oppositely, the larger flexibility and/or interaction with PEG may be beneficial for ATWLPPR.

In terms of cell signaling, a strong hyperactivation of RTK-AKT-GSK3 $\beta$ /eNOS was detected in the presence of type B and C NPs in HUVEC cells. As already observed with type A mixed-NPs, AKT activation seems to be a consequence of the co-recruitment of other cell surface

receptors such as IGF1R and EGFR. This is also happening with type B and C NPs but in these cases, both peptides alone are also functioning well. This suggests that the co-recruitment is firstly depending on the avidity of the interaction between the NP and the cell membrane. If the avidity is elevated, many receptors are rapidly engulfed in multivalent complexes and these brutal lateral movements of proteins and lipids may directly activate a cell's response proportional to the avidity of the NP.

Interestingly, the hyperactivation of AKT/ERK caused by B/C-NP did not change the levels of cleaved caspase-3 as RGD/ATW-type-A-NP did. This may indicate that caspase activation and HUVEC cell survival is finely adjusted to the avidity of the NP, itself linked to the level and duration of the induction of the molecular cascades. A too weak or transient activation of AKT/ERK will not protect HUVEC cells from dying under serum deprivation. As well, if the activation is too strong it does not prevent the cells from dying and may actually participates to the toxicity of these NPs. This will need further investigations.

## 8.6 Supplementary data:

- ❖ In parallel, this study was also performed in EA.hy 926 cells (Fig. 79). Except for A-NP<sup>1000</sup><sub>0/100</sub>, B-NP<sup>1000</sup><sub>100/0</sub> and C-NP<sup>1000</sup><sub>50/50</sub>, all NPs potentiated non-differentially the phosphorylation of AKT on both vital sites serine 473 and threonine 308, but activation of AKT/GSK3 $\beta$  was not detected, as well as that of ERK. Since cleaved caspase3 can't be detected in EA.hy 926 cells, PARP was used and no differential level of PARP was detected among all the treatments. Thus the functional NPs could activate AKT in EA.hy 926 cells but the activation signal seems to end at the level of AKT. Another possibility is that the ERK and AKT downstream pathways are already ubiquitously activated in EA.hy 926 despite the serum starvation, and cannot be further activated. Notably, no activation of EGFR but activation of VEGFR2 was detected in the presence of all NPs, except PEG-NP.

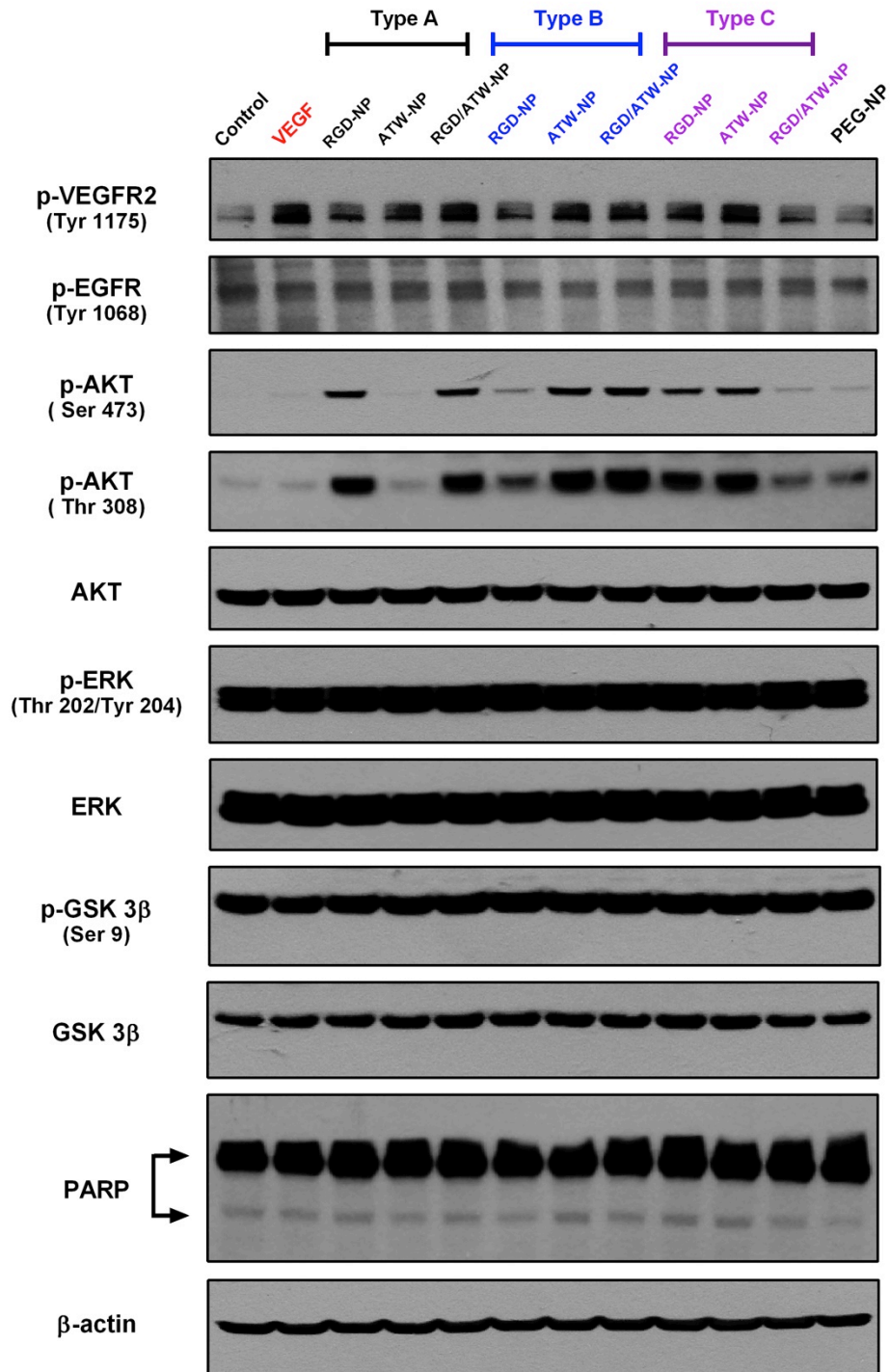


Fig. 79 Comparative studies of NPs' effects on RTK-AKT/ ERK associated signaling in EA.hy 926 cells. EA.hy 926 cells were serum starved for 20 hours before the treatment of 1nM NPs for 1hour.

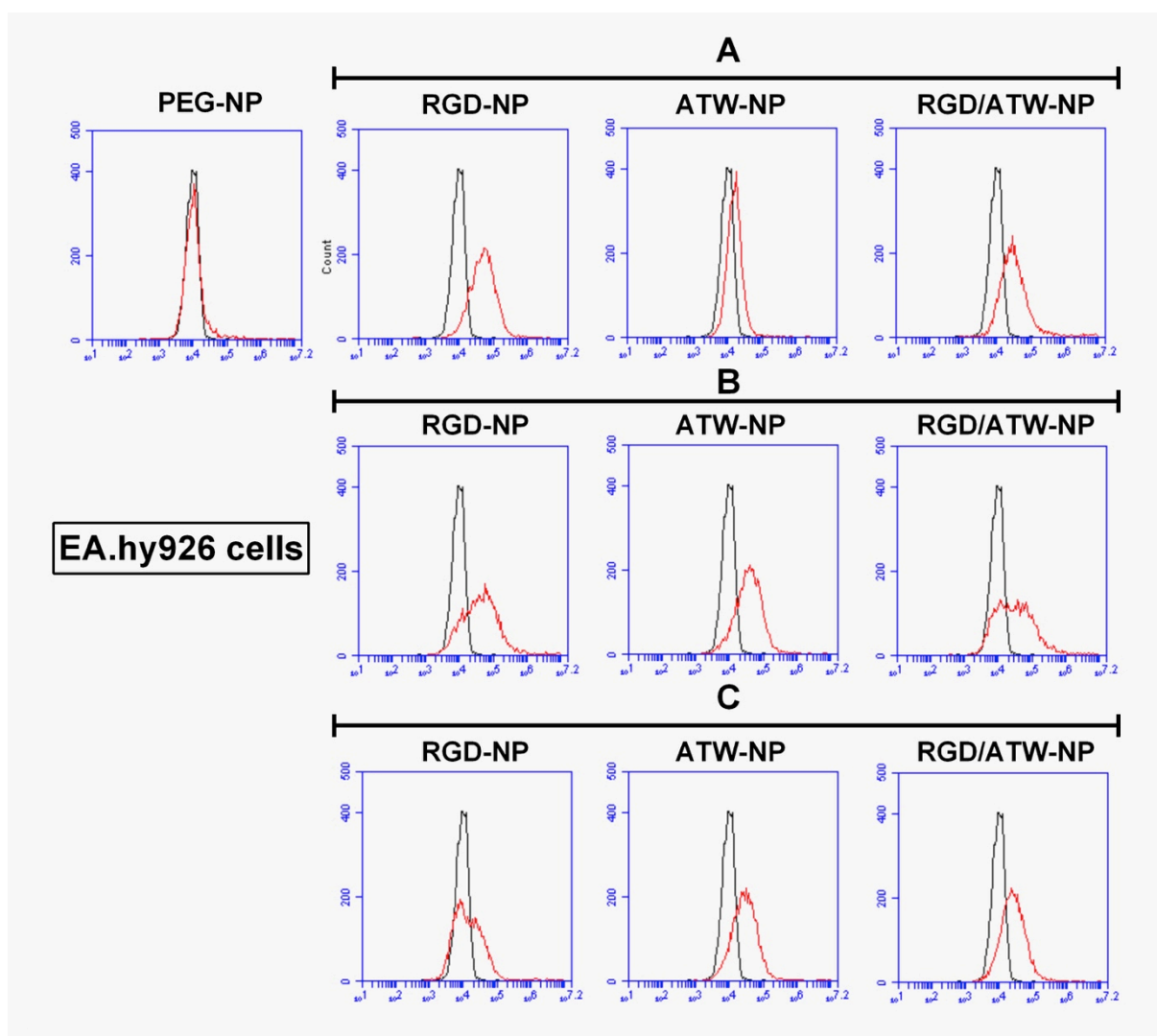


Fig. 80 Comparative studies of type A, B and C NPs' binding efficiency in EA.hy 926 cells by FACS. A, B, C indicate the type of NPs. The amount of targeting peptides on each type of NPs is 1000. PEG-NP was used to be a negative control. Flow cytometry analysis of EA.hy 926 cells incubated with different NPs without serum for 60 min at 37°C in 5% CO<sub>2</sub>.

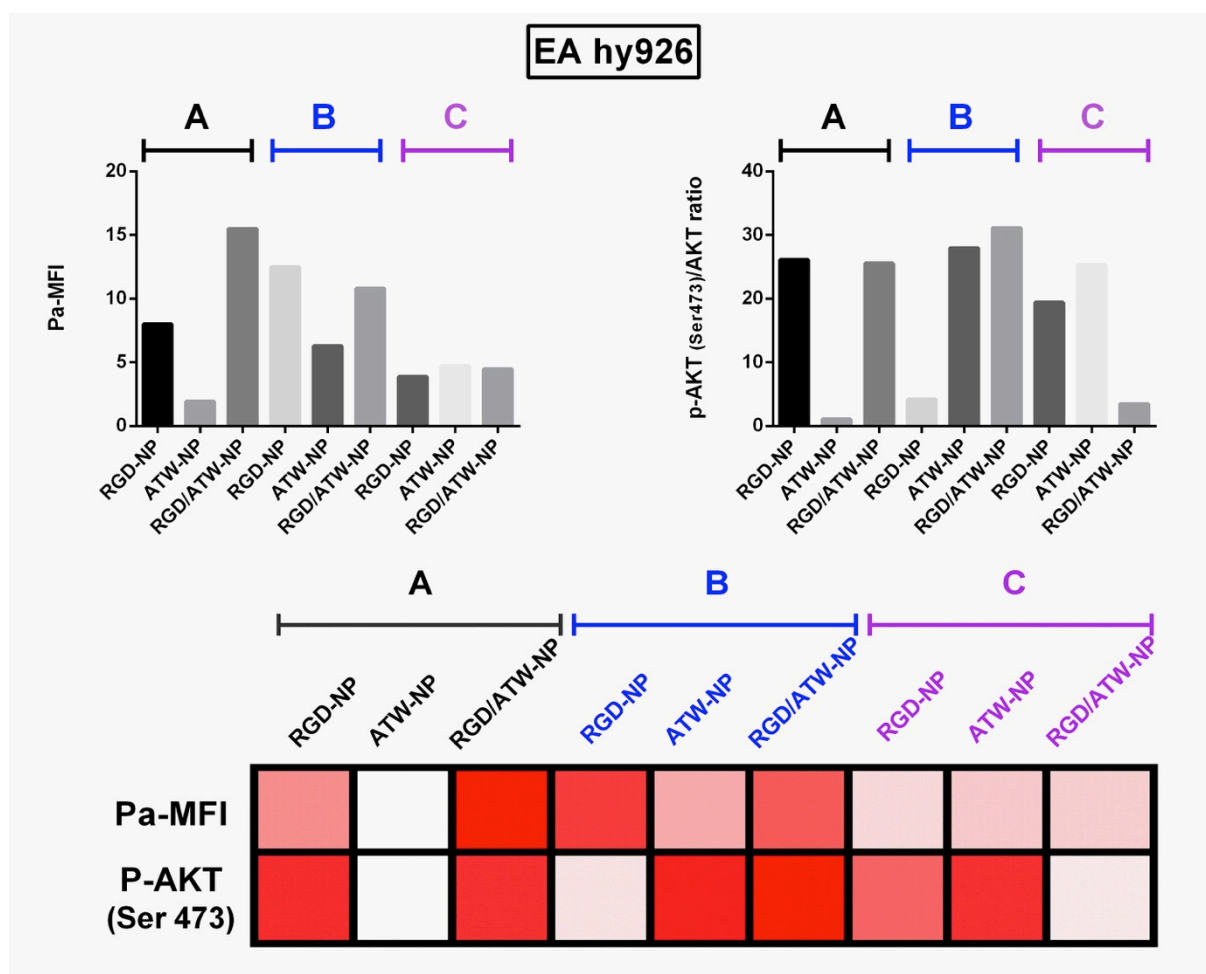


Fig. 81 Parallel comparative studies of NPs' binding efficiency and AKT activity in EA.hy 926 cells. A, B, C indicate the type of NPs. The amount of targeting peptides on each type of NPs is 1000. The binding efficiency signal was recorded and quantified by the value of Pa-MFI. Left histogram indicates the Pa-MFI of each NP in EA.hy 926 cells. Quantitative analysis of p-AKT changes in NPs' treatment was performed by Image J according to Fig. 79. Right histogram shows quantification of p-AKT level after normalizing the data to respective control group. Row normalized sorting of the value of Pa-MFI and p-AKT was performed to do parallel comparative study of NPs' binding efficiency with their biological activity in EA.hy 926 cells.

HUVEC

EA. hy 926

	PaMFI vs. p-AKT
Pearson r	
r	0.48
95% confidence interval	-0.27 to 0.87
R square	0.23
P value	
P (two-tailed)	0.1882
P value summary	ns
Significant? (alpha = 0.05)	No
Number of XY Pairs	9

	PaMFI vs. p-AKT
Pearson r	
r	0.32
95% confidence interval	-0.43 to 0.81
R square	0.11
P value	
P (two-tailed)	0.3938
P value summary	ns
Significant? (alpha = 0.05)	No
Number of XY Pairs	9

Table 10 Pearson correlation coefficient studies of NPs' binding efficiency (Pa-MFI) with their biological activity (p-AKT) on HUVEC and EA. hy 926 cells.

- ❖ Comparison of the binding of 4 types of NPs on H358 and MDA-MB-231 tumor cells. B-NP always exhibited the best binding and A-NP showed the lowest binding on both cells, except C-NP<sup>1000</sup><sub>100/0</sub> which presented the lowest binding on H358 cells.

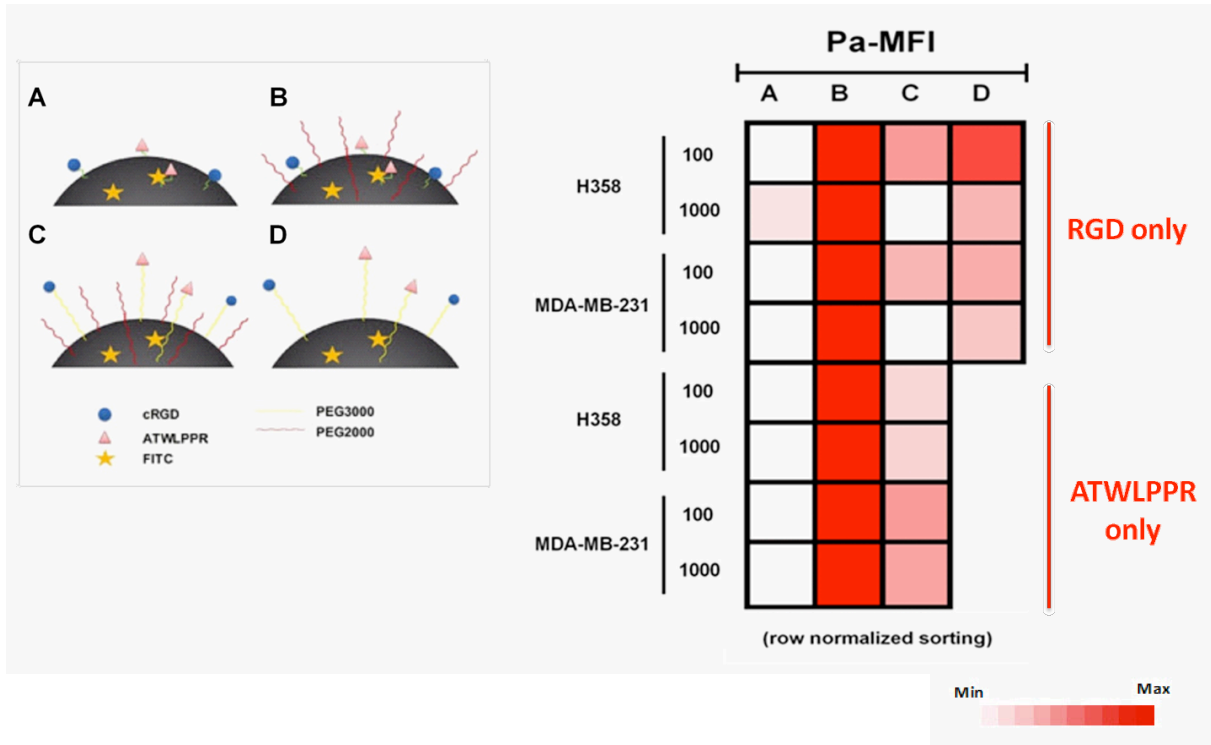


Fig. 82 Heat map study of four types of NPs' binding efficiency on H358 and MDA-MB-231 cells. Left panel indicates A, B, C, D four types of NPs, which are detailed in the main text of chapter 1. Right heat map is made by row normalized sorting of Pa-MFI value. 100, 1000 indicate the amount of peptides grafted on NPs. X axis indicates four types of NPs. Right Y axis indicates NPs are grafted by only RGD or ATWLPPR peptide. Flow cytometry analysis of H358 and MDA-MB-231 cells incubated with different NPs for 30min at 37°C in 5%CO<sub>2</sub>. Influence of NPs' type on their binding efficiency on H358 and MDA-MB-231 cells.

## 9 Final conclusion and perspective:

As I discussed in the introduction on integrin-mediated signaling, integrins do not have intrinsic enzymatic activity, but due to ligands' binding, integrin clusters are formed, giving birth to focal adhesion (FA) complexes. This will activate downstream signaling pathways such as the Src-FAK, Ras-ERK/MAPK and PI3K/AKT cascades.

Canonically, when integrin  $\alpha_v\beta_3$  is binding to (RGD) ligands in the ECM, it recruits and activates FAK via phosphorylation of its tyrosine residue 397 [153]. Active FAK then functions as phosphorylation-regulated signaling scaffold that forms a complex with the Src-family kinase (SFK) or other membrane-proximal signaling molecules such as PKC and p38. Remarkably, they are all depending on both integrin  $\alpha_v\beta_3$  and VEGFR2 signaling.

In HUVEC, all the functional NPs (RGD-, ATW- and RGD/ATW-) activate AKT at both vital sites of serine 473 and threonine 308. Nevertheless, we did not detect positive signals of FAK, Src, PKC and p-38. This indicates that our silica NPs targeting integrin  $\alpha_v\beta_3$ , NRP1 or both do not activate the canonical integrin and VEGFR2 mediated-signaling. Recently, M. Benezra reported that 7.0 nm core-shell silica NPs grafted with RGD can induce the AKT pathway in integrin positive M21 cells [151]. However, their data indicated an extremely weak augmentation of p-FAK and p-Src signals (1.2 and 1.4 times respectively), suggesting that RGD-NP induced AKT activation promoted M21 cell migration. Surprisingly, PF-228 (an inhibitor of FAK) was unable to prevent RGD-NP's activity. Similar effects on cell migration were also described in HUVEC but we did not find a description of the impact of RGD-coated NP on FAK-AKT signaling in HUVEC in the literature. Thus, more work still needs to be done in both ECs and tumor cells to understand the exact contribution of FAK/Src to RGD-NP mediated AKT signaling.

In our hands, the recruitment and activation of other RTK, especially IGF-1R/IR, seems to contribute greatly to NPs (ATW- and RGD/ATW-NP)-induced AKT activation in HUVEC and HDMEC. While a transient AKT activation was weakly but significantly detected with RGD-NP, neither FAK/Src nor RTKs activation was seen with these NPs. Since integrin receptors are

quite sensitive to mechanical stress [154], we propose that RGD-NPs-triggered mechanical signals are directly transduced through AKT and independently of FAK/Src or RTK activation.

Notably, the platelet endothelial cell adhesion molecule-1 (PECAM-1), has already been describe as capable of transducing mechanical forces directly to AKT/ERK via tyrosine phoshorylation [155, 156]. Other mechano-sensors like ions channels may also contribute to silica NPs-regulated AKT/ERK activation, since they are abundant in ECs and involved in the regulation of macromolecules trafficking by endocytosis and transcytosis [157].

Also already discussed in the chapter of "Pros and cons of heteromultivalent targeting", many signaling receptors are modular, with binding and signaling performed by distinct and spatially segregated domains. Direct or indirect clustering of receptors might activate cell signaling cascades via still unknown mechanisms. Twenty years ago, experimental proofs were reported by K. M.Yamada and coworkers [158] who reported that the simple aggregation alone can trigger integrin signaling. This was performed using beads coated with non-inhibitory mAbs (non-ligand aggregator) that function like RGD grafted beads in terms of accumulation of tensin, FAK and tyrosine phosphorylation. These results demonstrated that the receptor occupancy was not necessary for the initiation of a biochemical signaling. This might explain why RGD-NP, which induced receptor clustering, but also scramble NP that binds to HUVEC at 1nM without directly occupying integrins, may transiently aggregate several receptors and activate AKT.

Interestingly, K. M. Yamada also presented differences between non-ligand aggregator and targeted ligand aggregator. Indeed, combining receptors occupancy plus receptors clustering would induce the accumulation of seven cytoskeletal proteins. This was not detected with non-ligand aggregators which induced a receptor clustering only, without receptors occupancy. In our case, this might explain the different signal output we observed between RGD-NP and scrambled-NP in terms of ERK activation. We propose that the RGD-NP that occupes integrins would bypass the receptor clustering-induced effect on ERK but not on AKT. The activation of AKT alone might be related with receptor occupancy-induced accumulation of specific cytoskeletal proteins (Fig. 83).

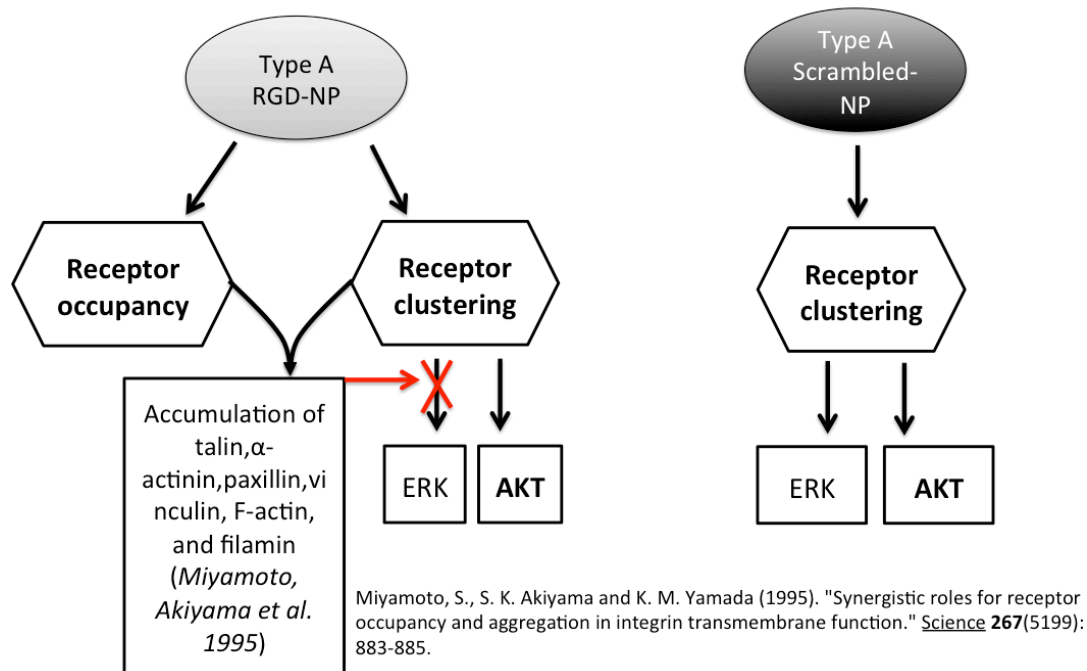


Fig. 83 Proposed model of the difference between type A RGD-NP and Scrambled-NP on their reactivity on HUVEC. Detailed information is depicted in main text.

In addition, since the endocytic trafficking is increasingly considered as the principal driver of cell signaling [159-161], nanoparticle's mediated phagocytosis (cell eating) and pinocytosis (cell drinking) might also generate signaling protein intermediates [161].

Because of Arginine, RGD and scrambled peptides all present positive charges on the NP's surface. Phosphatidylserine (PS) and Heparan sulfate proteoglycans (HSPGs) as well as Glycosaminoglycan (GAGs) are abundant negatively charged EC membrane receptors [162-164]. Meanwhile, they all take important roles in both intracellular and extracellular signaling transmission. So we believe that they also contribute to Si-NP mediated signaling by direct electrostatic interactions.

Collectively, we proposed several silica-NP-mediated **RTK-independent AKT/ERK activation mechanisms** in ECs, which are summarized in Fig. 84.

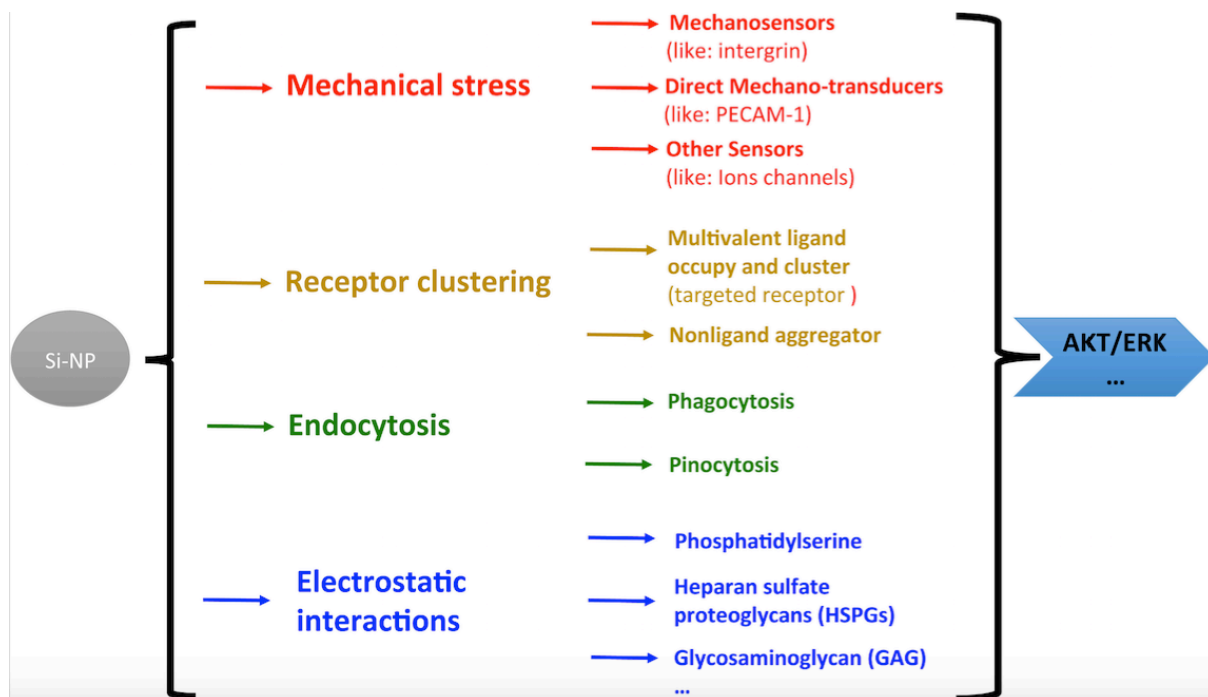


Fig. 84 Proposed mechanisms of silica-NP-mediated RTK-independent AKT/ERK activation in ECs. Detailed information is depicted in main text.

For mixed-NP, our data indicate that type A NPs grafted with both RGD and ATWLPPR peptides induced a sustained activation of IGF1R/IR (RTKs)-AKT-GSK3 $\beta$ /eNOS signaling with a slight and transient activation of ERK in primary ECs. This led to cells' resistance to serum deprivation-induced cell death. In contrast, for type B and C NPs, hyper-activation of the same signaling cascade was detected (Fig. 85), that did not show any protective effect in the same conditions of stress of these cells. It would thus be interesting to see whether B/C-NP induced hyper-activation of AKT/ERK could bring "protective effects" in 3-D or *in vivo* conditions.

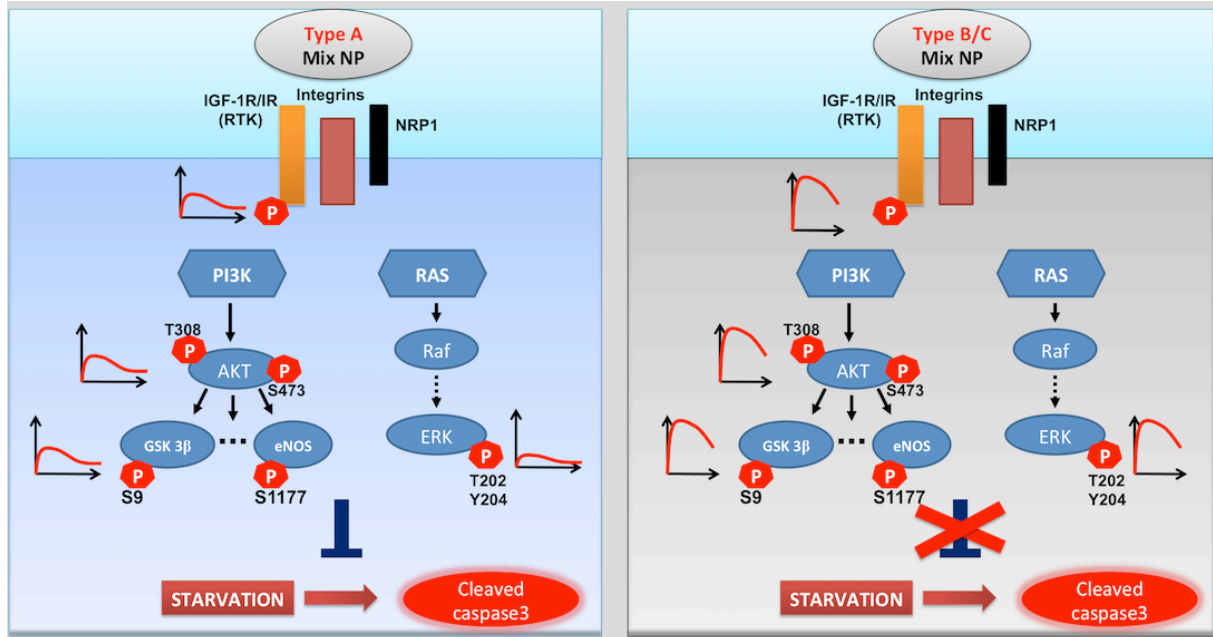


Fig. 85 Proposed model of the different action (Biochemistry) induced by different type of silica-NPs on HUVEC. Detailed information is depicted in main text.

A comparative study of A/B/C-NP on binding, signaling and cell viability was performed, especially in HUVEC cells. As shown in Fig. 86, ligands' type and their different pattern of presentation on silica NPs affect NPs' binding and AKT signaling. Type B NPs show the strongest activity. Our current hypothesis is that the accessibility and degrees of liberty of the exposed ligands on the surface of the NPs contribute positively on their binding avidity and thus to their biological activity.

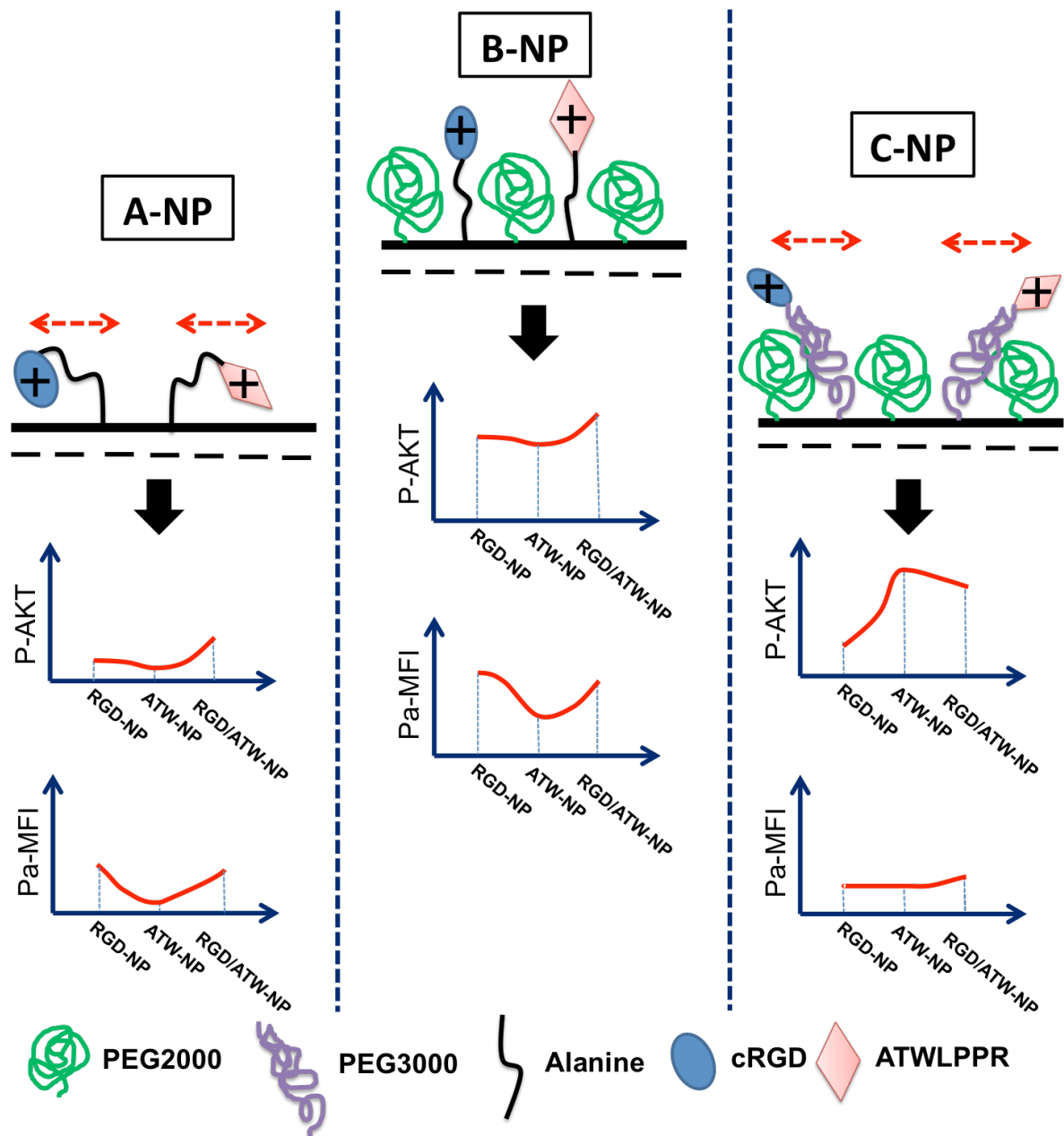


Fig. 86 Proposed model of the different action (Chemistry) induced by different type of silica-NPs on HUVEC. Detailed information is depicted in main text.

In order to better understand our results, and in particular the relationship between binding, signaling, and cell phenotypes, in Fig. 87, we propose that the silica NPs may be divided into three groups according to their binding efficiency (I, II and III). Group I NPs (like: type A ATW-NP) show the lower binding efficiency without strong AKT activation; group II NPs (like: type A RGD/ATW-NP) present moderate binding with sustained activation of AKT induced by the 2 specific peptides. This is providing a potent cell survival signal. In group III, the NPs (like: type B NPs) show the strongest binding with the hyperactivation of AKT, but this is not promoting cell survival.

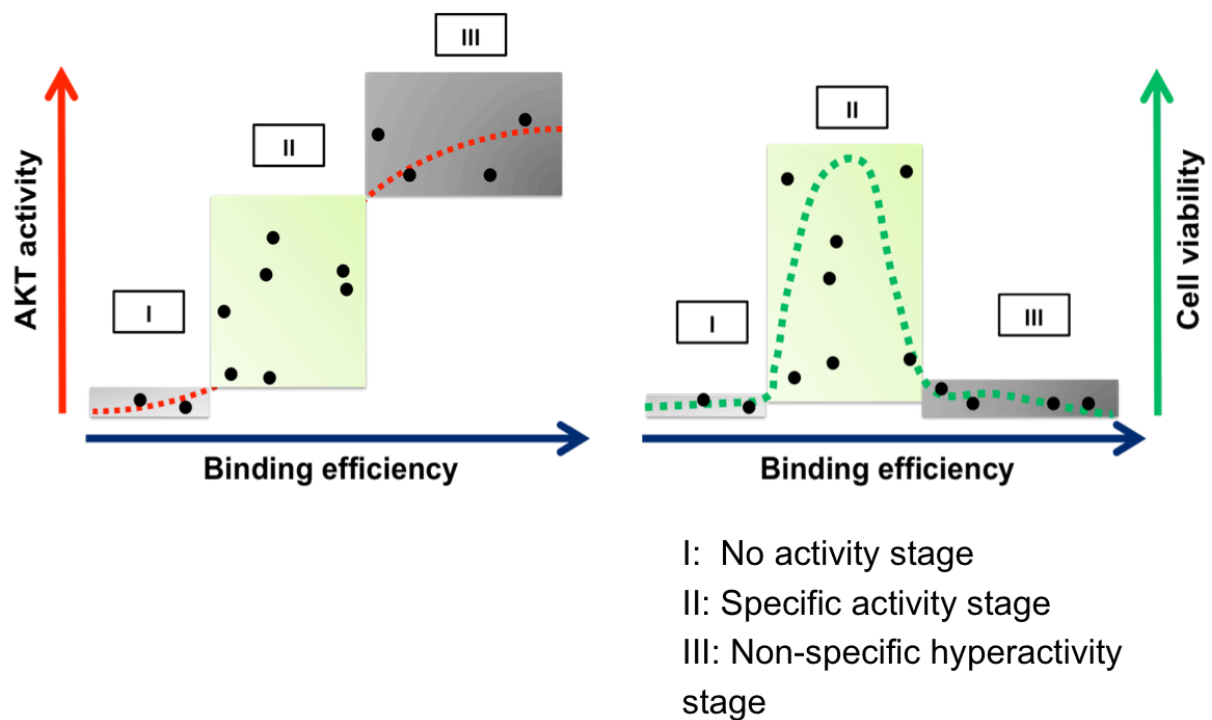


Fig. 87 Proposed model of the relationship among Binding efficiency, AKT activity and Cell viability on ECs in the presence of Silica-NPs. Detailed information is depicted in main text.

## Perspectives

My work is raising a lot of issues that still need to be investigated.

1. Concerning the NPs, we observed that the amount of ligands, ratio of the 2 peptides and more importantly the chemistry used to load them onto the silica NP are very strongly affecting their properties. It would be of the outmost importance to see whether our model applies to other type of NPs such as liposomes, dendrimers, block-copolymers, nanogold, etc... It would be also important to test this model with other ligands. Finally, we show that the silica backbone itself may generate an important toxicity on stressed endothelial cells *in vitro*. This should be further investigated since silica is a very commonly used nanomaterial.
2. We established that the reactivity of different cell types varies a lot, and it will be important to investigate this phenomenon on a larger set of cell lines in 2D cell cultures but also in 3D (mixed) spheroids containing the tumor cells and their stroma.
3. Our preliminary data obtained *in vivo* are very surprising and should be further investigated. In priority, we need to evaluate the biodistribution of the different NPs. Then, we need to verify the phenotypes we obtained on a larger series of animals and tumor models. Mechanical and biochemical studies need to be performed in order to understand the impact on vasodilatation and on the cell proliferation.
4. Altogether, our initial idea was to generate anti-angiogenic NP. Our result suggests that we obtained the opposite. Nonetheless, we ended up in a situation that mimic the contradictory results described in the different clinical trials using cilengitide or other anti-angiogenic therapies. Our NPs may thus help to understand the very complicated networks of stimuli/cell responses that are generated *in vivo* when a (RGD or anti-NRP1) peptide reaches a target cell already engaged in multiple interactions with ECM components. It is well known that multivalency will affect the ligand activity and, in addition, this ligand may reach its receptor as a free and soluble molecule or as an ECM-bound growth factor that will not diffuse freely nor be internalized easily once engaged with its receptor. Because we are working with 50

nm large NPs, we generate intermediate forms of presentation that we need to better characterize in order to control their activity *in vivo*.

5. Mixed NP actually blocks their target receptors very efficiently but they activate specific pathways that promote cell survival *in vitro* (on endothelial cells) and stimulate cell proliferation *in vivo* (at least on tumor cells). These mixed nanocarriers could now be loaded with small inhibitors of key signaling events (such as AKT, IGF1R/IR, EGFR, mTOR...) and could present strong killing effects. Thus we should investigate the impact of co-treatments based on the injection of mixed NP containing inhibitors.

## 10 Materials and Methods

Table 11. Cell lines tested in this study

<b>Cell line</b>	<b>Description</b>	<b>Source or Reference</b>	<b>Media</b>
<b>3T3</b>	Mouse embryo fibroblast cell line	ATCC	DMEM+10% FBS
<b>4T1</b>	Mouse mammary gland cancer cell line	ATCC	RPMI+10% FBS
<b>A549</b>	Human lung carcinoma cell line	ATCC	RPMI+10% FBS
<b>EA.hy926</b>	The human umbilical vein cell line derived from fusing human umbilical vein endothelial cells with the human lung carcinoma cell line A549; wt p53	Dr. Annie Molla; (Edgell et al., 1983)	DMEM+10% FBS
<b>H358</b>	Human lung bronchioalveolar carcinoma cell line; Non-small cell lung cancer cell line	ATCC	RPMI+10% FBS
<b>HDMEC</b>	Human dermal microvascular endothelial cells (pooled donor)	LONZA (#2516)	EGM-2 MV BulletKit (LONZA #3202)
<b>HMEC-1</b>	Human microvascular endothelial cell line immortalized by the large T antigen of SV40	Dr. Béatrice EYMIN; (Ades et al., 1992)	DMEM+10% FBS+ 1mM sodium pyruvate
<b>HUVEC</b>	Human umbilical vein endothelial cells (pooled donor)	LONZA (#2519A)	EGM-2 BulletKit (#LONZA 3162)
<b>M21</b>	Human melanoma cell line	Dr. Julien Gravier, MGH Boston, USA	DMEM+10% FBS
<b>M21L</b>	Human melanoma cell line lack of alpha v gene expression	(Felding-Habermann)	DMEM+10% FBS

		et al., 1992)	
<b>MDA-MB-231</b>	Human mammary gland adenocarcinoma cell line	ATCC	DMEM+10% FBS
<b>PANC-1</b>	Human pancreas epithelioid carcinoma cell line	ATCC	DMEM+10% FBS
<b>SKBR3</b>	Human mammary gland adenocarcinoma cell line	ATCC	McCoy's+10% FBS
<b>TSA</b>	Ts/Apc (mouse mammary carcinoma model)	Lollini, P. L., et al. (1995). Hum. Gene Ther. 6:743 – 752	RPMI+10% FBS
<b>U87</b>	Human glioblastoma cell line	ATCC	DMEM+10% FBS

Table 12. Primary antibodies tested in this study

<b>Antibody</b>	<b>Description</b>	<b>Reference</b>	<b>Application</b>
<b>VEGFR1</b>	Mouse monoclonal to VEGF Receptor1	Abcam #66184	WB
<b>VEGFR2</b>	Rabbit monoclonal to VEGFR2	CST #2479	WB
<b>Nrp1</b>	Rabbit monoclonal to Neuropilin-1	Abcam #81321	WB
<b>Nrp2</b>	Mouse monoclonal to Neuropilin-2	Santa Cruz #13117	WB
<b>p-VEGFR1 (Y1213)</b>	Rabbit antibody recognizes phosphorylated VEGFR1 at tyrosine1213 (no indication about the clonal type)	Millipore #MAB07-758	WB
<b>p-VEGFR2 (Y1175)</b>	Rabbit monoclonal to VEGFR2 (phospho tyrosine1175)	CST #2478	WB
<b>p-VEGFR2 (Y1054/1059)</b>	Rabbit polyclonal to VEGFR2 (phospho tyrosine1054 and 1059)	Abcam #5473	WB
<b>p-VEGFR2 (Y1214)</b>	Rabbit polyclonal to VEGFR2 (phospho tyrosine1214)	Invitrogen #44-1052	WB
<b>p-IGF-I R <math>\beta</math> (Y1135/1136)/ Insulin R <math>\beta</math> (Y1150/1151)</b>	Rabbit monoclonal to IGF-I (phospho tyrosine1135 and 1136) and insulin receptor (phospho tyrosine1150 and 1151)	CST #3024	WB
<b>p-EGFR (Y1068)</b>	Rabbit monoclonal to EGFR (phospho tyrosine1068)	CST #3777	WB
<b>p-AKT (S473)</b>	Rabbit monoclonal to AKT (phospho serine473)	CST #4060	WB, IH
<b>p-AKT (T308)</b>	Rabbit monoclonal to AKT (phospho threonine308)	CST #13038	WB
<b>p-GSK-3 <math>\beta</math> (S9)</b>	Rabbit monoclonal to glycogen	CST	WB

	synthase kinase-3 $\beta$ (phospho tyrosine1175)	#9336	
<b><math>\beta</math>-actin</b>	Mouse monoclonal to $\beta$ -actin	Santa Cruz #47778	WB
<b>Tubulin</b>	Mouse monoclonal to tubulin	Santa Cruz #23948	WB
<b>p-FAK (Y397)</b>	Rabbit monoclonal to FAK (phospho tyrosine397)	Epitomics #YE090604	WB
<b>p-eNOS (S1177)</b>	Rabbit polyclonal to endothelial nitric-oxide synthase (phospho serine1177)	CST #9571	WB
<b>AKT</b>	Rabbit monoclonal to AKT	CST #4691	WB
<b>p-Src (Y418)</b>	Rabbit polyclonal to Src (phospho tyrosine418)	Invitrogen #44660G	WB
<b>p-PKC (T 505)</b>	Rabbit polyclonal to PKC (phospho threonine 505)	CST #9374	WB
<b>p-p38 (Y180/Y182)</b>	Mouse monoclonal to p38 (Stress-Activated Protein Kinases) (phospho tyrosine180 and 182)	Millipore #MABS64	WB
<b>GSK-3 <math>\beta</math></b>	Rabbit monoclonal to glycogen synthase kinase-3 $\beta$	CST #9315	WB
<b>Cleaved-Caspase3</b>	Rabbit polyclonal to cleaved caspase-3 (Asp175)	CST #9661	WB
<b>PARP</b>	Rabbit polyclonal to PARP	Santa Cruz #7150	WB
<b>p-ERK (T202/Y204)</b>	Rabbit monoclonal to p44/42 MAPK (Erk1/2) (phospho tyrosine202 and 204)	CST #4370	WB, IH
<b>ERK</b>	Rabbit monoclonal to p44/42 MAPK (Erk1/2)	CST #4695	WB

<b>Ki67</b>	Rabbit polyclonal to Ki67	Abcam #66155	IH
<b>CD31</b>	Rat monoclonal to mouse CD31	BD #550274	IH
<b>Integrin <math>\alpha_v\beta_3</math></b>	Mouse monoclonal to integrin $\alpha_v\beta_3$	Millipore #MAB1976	FACS
<b>Nrp1</b>	Mouse IgG1 recognizes human CD304 (BDCA-4/Neuropilin-1) antigen	MACS # 130-090- 900	FACS
<b>IGF-1R<math>\beta</math></b>	Rabbit polyclonal to IGF-1R $\beta$	Santa Cruz #713	WB
<b>p-Met (Y1234/1235)</b>	Rabbit polyclonal to Met (phospho tyrosine1234 and 1235)	CST #3126	WB

Table 13. Chemicals tested in this study

<b>Chemical</b>	<b>Working concentration</b>	<b>Source or Reference</b>
<b>VEGF<sub>165a</sub></b>	20/100/200ng/ml	R&D systems #293-VE-010
<b>Collagen I (Rat Tail)</b>	1.33ug/cm <sup>2</sup>	Corning #354236
<b>Matrigel</b>	300ul/well (24 well plate)	Corning #356237
<b>Wortmannin</b>	0.2uM	CST #9951s
<b>R 1507</b>	100nM	Dr. Amandine Hurbin
<b>Linsitinib</b>	1uM	Dr. Amandine Hurbin
<b>Sorafenib</b>	1uM	Dr. Amandine Hurbin
<b>NPs</b>	10/100/1000 pM	Prof. Gilles Subra

### **Preparation of NPs**

All NPs were dissolved in PBS at a stock concentration of 8mg/ml (around 200nM NPs) and stored at -20 °C. They were diluted to the required concentration with corresponding cell culture medium when needed. Prior to treatment, all NPs were sonicated for 3 cycles of 2 min with 2 seconds interval of gentle vortex.

Since introducing PEG2000 or PEG3000 to silica NPs will significantly increase their molecular weight (MW), in order to equilibrate all NPs at the same working concentrations (pM), we used fluorescence spectrometry to equilibrate the final quantities. Importantly, since the absorbance at the excitation wavelength should be around 0.1 or less (otherwise the fluorescence signal might not be proportional to the NP's concentration), I always performed gradient dilutions of each NPs down to 1.6 mg/ml (5x dilution of stock solution), then dilute another 1000 times for fluorescence studies. Finally, we used naked-NPs' fluorescence to homogenize the amounts of type A, B and C NPs as well as PEG-NP.

### **Cell Culture**

All cells were maintained in American Type Culture Collection recommended cell culture media and conditions, which are listed in Table 11. Cells were all cultured at 37°C in a humidified atmosphere containing 5% CO<sub>2</sub>.

### **Cell Viability Assay**

The cell viability was measured *in vitro* according to MTS-based cell viability assay (Promega). We tested the viability of HUVEC cells in the presence of different concentrations of NPs with or without 1% Full medium (Lonza) or VEGF (20ng/ml, R&D systems) at different times. The indicated treatments are described in the main text. After treatment, the cell medium was aspirated and cells were washed with PBS. Then, 10 µl of WST-1 reagent was added to each well. The plates were mixed gently and the cells were incubated at 37°C for 2 to 4 hours. After the incubation period, the plates were mixed gently on an orbital shaker for one minute and the absorbance of each sample was measured at 492 nm using Beckman Coulter AD 340s (Fullerton, CA, USA).

### **Western Blotting**

Western blotting was performed as previously described [165]. 300,000-50,000 cells were planted in 6-well plate for 24 hours followed by NPs' treatments, which were indicated in the main text. The working medium volume is 1ml /well. Since HUVEC are very sensitive, all medium must be pre-warmed, and the maximum serum-starvation time is 20 hours. For *in vitro* cells samples, 10-20 µg of protein were loaded onto SDS-polyacrylamide gel (8% or 12%), or NuPAGE 4-12% gel (Life technologies, USA). For *in vivo* tumor tissue samples, 40 or 60 µg of proteins were loaded. Antibodies were listed in Table 12. The intensity of each band was measured by Image J (NIH software). Time-course exposure of proteins to chemiluminescence was used to perform semi-quantification of signal, as indicated in the main text.

### **Particle binding efficiency Assay by FACS**

After sonication of NPs for 3 cycles of 2 min, they were added in adherent HUVEC cells at indicated concentrations at 37°C in 5% CO<sub>2</sub>. Samples were rinsed thoroughly 3 times with PBS, and harvested with 0.05% trypsin-EDTA. Cells were then transferred to full medium for analysis by flow cytometry (BD Biosciences).

### **NRP1 receptor quantitative determination by FACS**

After NPs' incubation at 37°C for 1hour, HUVEC cells were rinsed gently twice with PBS and incubated in 5mM EDTA (Gibco) for 5min on ice. Hanks (Gibco) buffer with 1% FBS (Gibco) was then added. After centrifugation, cells were incubated with 1%FBS in Hanks for 5 min on ice, followed by staining with APC anti-Nrp1 (Miltenyi Biotec, Auburn, CA) for 10min with shaking in the dark on ice. After washing twice, cells were resuspended in 400ul Hanks buffer for analysis by flow cytometry.

### **Immunohistochemical labeling**

Tumor slices (7 µm) were placed at room temperature, fixed in acetone for 10 min and washed twice in TBS with 0.1% Tween 20 (TBS/T). Endogenous peroxidases were blocked with 1% H<sub>2</sub>O<sub>2</sub>/ ethanol, and slices were rinsed in distilled water and TBS/T for 5 min. Tumor

sections were blocked with 2% rabbit serum diluted in TBS for 20 min and rinsed for 5 min in TBS/T. CD31 and Ki67 were labeled respectively with anti-CD31 antibody (#550274 at 1/500; BD Biosciences) and anti-Ki67 antibody (#66155 at 1/250; Abcam) for 2 hours; p-AKT and p-ERK were labeled respectively with anti-pAKT antibody (#4060 at 1/50; Cell Signaling Technology) and anti-pERK (#4370 at 1/200; Cell signaling Technology) overnight. They were incubated with secondary rabbit anti-rat antibody #P0450 at 1/200 or secondary antibody against p-AKT (goat anti-rabbit HRP #P0448; 1/200; DAKO, San Antonio) or secondary antibody against p-ERK (goat anti rabbit HRP #P0448; 1/200; DAKO, San Antonio) for 1 hour. The labeling was detected with DAB for 5 min (#K3467; Dako, San Antonio) and rinsed with water for 5 min. Cell nuclei were stained with Gill's hematoxylin for 2–3 sec and washed with water for 5min. Samples were dehydrated with 2 baths of 100% ethanol and one with xylene before the addition of mounting medium (M-GLAS, #1.03973.001; Merck Millipore). Images were taken using AxioImager M2 microscope, and quantified by Image J (NIH software).

### **Animals**

Female Naval Medical Research Institute (NMRI) nude mice (5wk-old) weighting  $24.0 \pm 0.5$  g were purchased from Janvier (Le Genest). Before the beginning of the experiment, the animals were acclimatized in a temperature-controlled environment for 1 wk. Facility rooms were maintained at constant temperature (25°C), humidity (30–50% relative humidity), and 12-h light: dark illumination cycle. Access to food and tap water was available ad libitum. Experiments were carried out following Institut National de la Santé et de la Recherche Médicale guidelines regarding the fair treatment of animals with approval of the Comité d'Éthique en Expérimentation Animale de Grenoble.

### **Tumor implantation and treatment**

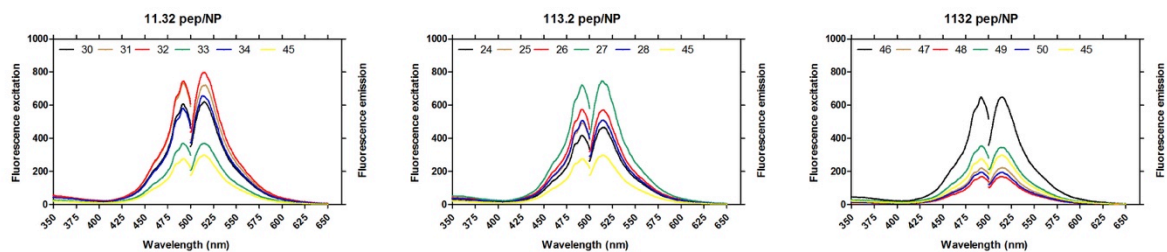
5 million U87MG cells, suspended in 100 $\mu$ L PBS, were injected subcutaneously into female NMRI nude mice (6 weeks old). After 5 weeks, the animals were randomized into 2 groups (n=4 per group). The first group was continuously administered for 2days: PEG-NPs (n=2; 8mg/ml; 200ul i.v; daily) and RGD/ATW-NPs (n=2; 8mg/ml; 200ul i.v; daily). The second group was continuously administered for 4 days with the same treatment. After 1 hour of the final i.v injection of NPs in each group, mice were sacrificed. The subcutaneous tumors

were excised and cut into two. One part was frozen for WB, another part was frozen for IH studies.

### **Statistical analyses**

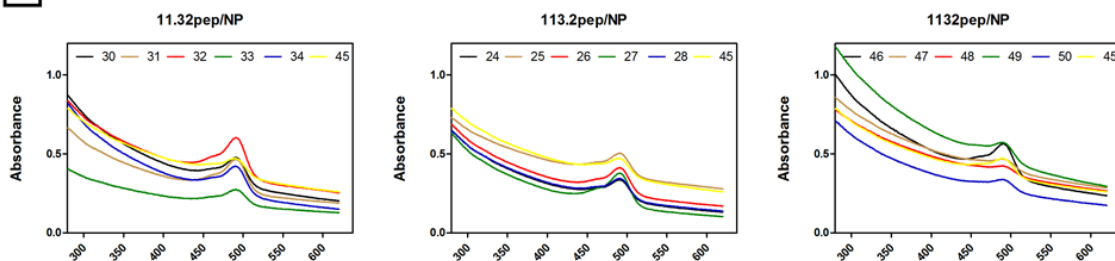
The statistical significance of the mean values among different groups was determined using one-way ANOVA, followed by Student's t test. Two-tailed Pearson correlation coefficient was performed using GraphPad Prism 6. The heatmap for the western blot signal data set was generated by Heatmap builder software (kindly provided by Dr. Euan Ashley, Stanford School of Medicine).

# 11 Appendix



Excitation spectrum—detection at 512 nm  
Emission spectrum—excitation at 494 nm

5X



50X

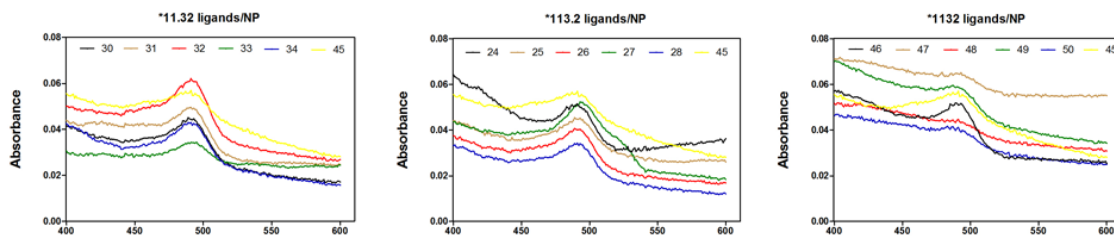


Fig. 88: Fluorescence spectrometry and absorbance spectrum studies

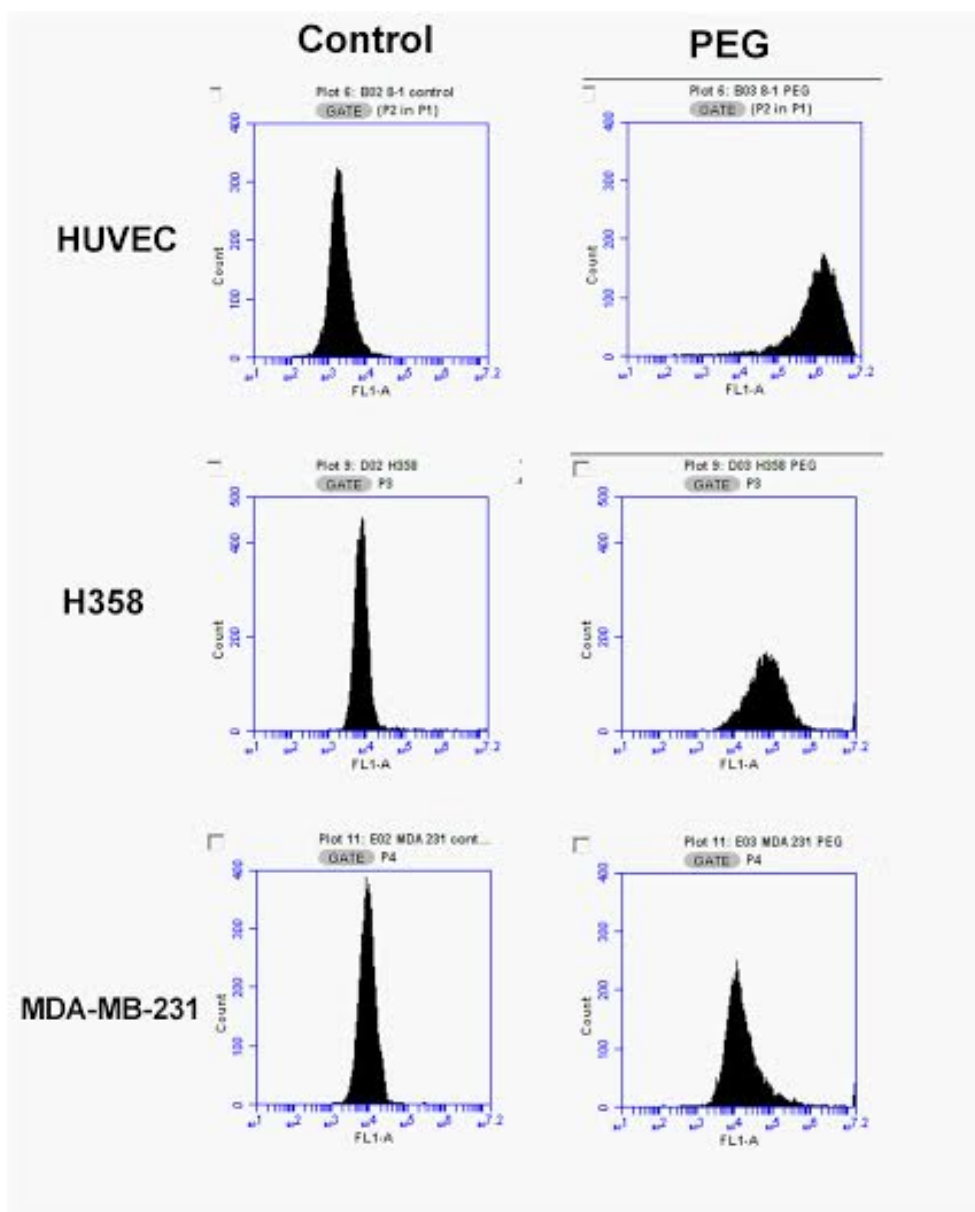


Fig. 89 Binding efficiency studies of type A Fluorine-PEG-NP on HUVEC, H358 and MDA-MB-231 cells. Flow cytometry analysis of HUVEC, H358 and MDA-MB-231 cells incubated with the Fluorine-PEG-NP for 30 min at 37°C in 5% CO<sub>2</sub>.

	%N	%C	%O	%H	DLS(PDI)	TGA	zeta
A <sup>3</sup>	0.91	5.39	6.17	1.65	79(0.12)	12.5	-28
A <sup>6.25</sup> <sub>0/100</sub>	0.92	5.56	X	X	75(0.13)	12.8	-26
A <sup>6.25</sup> <sub>25/75</sub>	0.91	5.40	X	X	79(0.15)	12.3	-30
A <sup>6.25</sup> <sub>50/50</sub>	0.90	5.39	X	X	76(0.13)	12.4	-26
A <sup>6.25</sup> <sub>75/25</sub>	0.92	5.43	X	X	80(0.12)	12.5	-24
A <sup>6.25</sup> <sub>100/0</sub>	0.93	5.56	X	X	79(0.13)	12.8	-23
A <sup>1.5</sup> <sub>0/100</sub>	0.98	5.89	6.10	1.70	76(0.12)	12.5	-24
A <sup>1.5</sup> <sub>25/75</sub>	0.99	5.70	6.16	1.63	81(0.10)	12.6	-24
A <sup>1.5</sup> <sub>50/50</sub>	1.01	5.90	5.99	1.85	79(0.14)	12.4	-28
A <sup>1.5</sup> <sub>75/25</sub>	0.95	5.75	6.23	1.92	80(0.16)	12.7	-29
A <sup>1.5</sup> <sub>100/0</sub>	0.98	5.91	6.18	1.79	75(0.16)	12.5	-23
A <sup>25</sup> <sub>0/100</sub>	1.96	7.02	6.13	1.66	75(0.15)	15.7	-28
A <sup>25</sup> <sub>25/75</sub>	1.92	7.32	6.35	1.83	77(0.12)	16.5	-26
A <sup>25</sup> <sub>50/50</sub>	1.80	7.13	5.26	1.87	76(0.12)	14.3	-28
A <sup>25</sup> <sub>75/25</sub>	1.71	7.55	6.33	1.94	80(0.14)	15.6	-26
A <sup>25</sup> <sub>100/0</sub>	1.93	7.18	6.45	1.85	77(0.13)	17.8	-24
B <sup>3</sup>	0.93	8.16	8.74	2.31	82(0.108)	18.3	-22
B <sup>6.25</sup> <sub>0/100</sub>	1	8.13	8.53	2.26	X	X	X
B <sup>6.25</sup> <sub>25/75</sub>	0.96	8.16	8.26	2.07	X	X	X
B <sup>6.25</sup> <sub>50/50</sub>	1.03	8.19	8.42	2.29	85(0.123)	X	-20
B <sup>6.25</sup> <sub>75/25</sub>	1.01	8.22	8.34	2.53	X	X	X
B <sup>6.25</sup> <sub>100/0</sub>	1.06	8.10	8.18	2.19	X	X	X
B <sup>1.5</sup> <sub>0/100</sub>	0.96	8.15	8.41	2.09	X	X	X
B <sup>1.5</sup> <sub>25/75</sub>	1.03	8.09	8.44	2.34	X	X	X

B <sup>2.5</sup> <sub>90/50</sub>	0.99	8.18	8.29	2.22	79(0.108)	X	-23
B <sup>2.5</sup> <sub>75/25</sub>	0.99	8.05	8.60	2.54	X	X	X
B <sup>2.5</sup> <sub>100/0</sub>	1.05	7.99	8.52	2.18	X	X	X
B <sup>25</sup> <sub>0/100</sub>	1.06	8.13	8.23	2.12	X	X	X
B <sup>25</sup> <sub>25/75</sub>	1.12	8.26	8.44	2.26	82(0.12)	X	-20
B <sup>25</sup> <sub>50/50</sub>	1.03	8.73	8.70	2.02	81(0.10)	X	-16
B <sup>25</sup> <sub>75/25</sub>	1.03	8.61	8.70	2.08	82(0.12)	X	-23
B <sup>25</sup> <sub>100/0</sub>	1	8.39	8.83	2.13	86(0.10)	X	-23
C <sup>2.5</sup> <sub>0/100</sub>	X	X	X	X	X	X	X
C <sup>2.5</sup> <sub>25/75</sub>	0.98	8.36	8.95	2.16	X	X	X
C <sup>2.5</sup> <sub>50/50</sub>	1.06	8.16	8.65	2.36	84(0.16)	19.6	-19
C <sup>2.5</sup> <sub>75/25</sub>	1.16	8.39	8.79	2.35	X	X	X
C <sup>2.5</sup> <sub>100/0</sub>	1.15	8.43	8.66	2.46	83(0.12)	19.4	-15
C <sup>25</sup> <sub>0/100</sub>	1.03	8.32	8.83	2.28	X	X	X
C <sup>25</sup> <sub>25/75</sub>	1.08	8.65	8.55	2.50	X	X	X
C <sup>25</sup> <sub>50/50</sub>	1.01	8.55	8.65	2.49	80(0.13)	18.7	-21
C <sup>25</sup> <sub>75/25</sub>	1.15	8.53	8.67	2.13	X	X	X
C <sup>25</sup> <sub>100/0</sub>	1.01	8.22	8.79	2.26	83(0.16)	19.1	-21

Table 14 Chemical characterization of different NPs (A/B/C<sup>x</sup><sub>y/z</sub>) by J. Ciccione (Cope from PhD thesis of Dr. Jeremy Ciccione). A, B, C indicate the type of NP, x indicates the overall peptides' loading efficiency described in the main text, and y/z indicates the ratio of ligands.

## 12 References:

1. Hanahan, D. and R.A. Weinberg, *The hallmarks of cancer*. Cell, 2000. **100**(1): p. 57-70.
2. Hanahan, D. and R.A. Weinberg, *Hallmarks of cancer: the next generation*. Cell, 2011. **144**(5): p. 646-74.
3. Carmeliet, P. and R.K. Jain, *Principles and mechanisms of vessel normalization for cancer and other angiogenic diseases*. Nat Rev Drug Discov, 2011. **10**(6): p. 417-27.
4. Nagy, J.A., et al., *Heterogeneity of the tumor vasculature*. Semin Thromb Hemost, 2010. **36**(3): p. 321-31.
5. Srichai, M.B. and R. Zent, *Integrin Structure and Function*. 2010: p. 19-41.
6. Takada, Y., X. Ye, and S. Simon, *The integrins*. Genome Biol, 2007. **8**(5): p. 215.
7. De Franceschi, N., et al., *Integrin traffic - the update*. J Cell Sci, 2015. **128**(5): p. 839-52.
8. Israeli-Rosenberg, S., et al., *Integrins and integrin-associated proteins in the cardiac myocyte*. Circ Res, 2014. **114**(3): p. 572-86.
9. Babbitt, C.J., et al., *Modulation of integrins and integrin signaling molecules in the pressure-loaded murine ventricle*. Histochem Cell Biol, 2001. **118**(6): p. 431-9.
10. Bridgewater, R.E., J.C. Norman, and P.T. Caswell, *Integrin trafficking at a glance*. J Cell Sci, 2012. **125**(Pt 16): p. 3695-701.
11. Roca-Cusachs, P., T. Iskratsch, and M.P. Sheetz, *Finding the weakest link: exploring integrin-mediated mechanical molecular pathways*. J Cell Sci, 2012. **125**(Pt 13): p. 3025-38.
12. Goksoy, E., et al., *Structural basis for the autoinhibition of talin in regulating integrin activation*. Mol Cell, 2008. **31**(1): p. 124-33.

13. Wegener, K.L., et al., *Structural basis of integrin activation by talin*. Cell, 2007. **128**(1): p. 171-82.
14. Wegener, K.L. and I.D. Campbell, *Transmembrane and cytoplasmic domains in integrin activation and protein-protein interactions (review)*. Mol Membr Biol, 2008. **25**(5): p. 376-87.
15. Serini, G., et al., *Besides adhesion: new perspectives of integrin functions in angiogenesis*. Cardiovasc Res, 2008. **78**(2): p. 213-22.
16. Desgrosellier, J.S. and D.A. Cheresh, *Integrins in cancer: biological implications and therapeutic opportunities*. Nat Rev Cancer, 2010. **10**(1): p. 9-22.
17. Weis, S.M. and D.A. Cheresh, *alphaV integrins in angiogenesis and cancer*. Cold Spring Harb Perspect Med, 2011. **1**(1): p. a006478.
18. Byron, A., et al., *Anti-integrin monoclonal antibodies*. J Cell Sci, 2009. **122**(Pt 22): p. 4009-11.
19. Schnell, O., et al., *Imaging of integrin alpha(v)beta(3) expression in patients with malignant glioma by [18F] Galacto-RGD positron emission tomography*. Neuro Oncol, 2009. **11**(6): p. 861-70.
20. Xiong, J.P., et al., *Crystal structure of the extracellular segment of integrin alpha Vbeta3*. Science, 2001. **294**(5541): p. 339-45.
21. Xiong, J.P., et al., *Crystal structure of the extracellular segment of integrin alpha Vbeta3 in complex with an Arg-Gly-Asp ligand*. Science, 2002. **296**(5565): p. 151-5.
22. Buerkle, M.A., et al., *Inhibition of the alpha-nu integrins with a cyclic RGD peptide impairs angiogenesis, growth and metastasis of solid tumours in vivo*. Br J Cancer, 2002. **86**(5): p. 788-95.
23. Haier, J., et al., *Inhibition of tumor progression and neoangiogenesis using cyclic RGD-peptides in a chemically induced colon carcinoma in rats*. Clin Exp Metastasis, 2002. **19**(8): p. 665-72.

24. Ogawa, M., et al., *Direct electrophilic radiofluorination of a cyclic RGD peptide for in vivo  $\alpha(v)\beta3$  integrin related tumor imaging*. Nucl Med Biol, 2003. **30**(1): p. 1-9.
25. Jin, Z.H., et al., *Noninvasive optical imaging of ovarian metastases using Cy5-labeled RAFT-c(-RGDfK-)<sub>4</sub>*. Mol Imaging, 2006. **5**(3): p. 188-97.
26. Jin, Z.H., et al., *In vivo noninvasive optical imaging of receptor-mediated RGD internalization using self-quenched Cy5-labeled RAFT-c(-RGDfK-)<sub>4</sub>*. Mol Imaging, 2007. **6**(1): p. 43-55.
27. Susanna Castel, R.P., Francesc Mitjans, Jaume Piulats, Simon Goodman, and F.H. Alfred Jonczyk, Senén Vilaró, and Manuel Reina, *RGD Peptides and Monoclonal Antibodies, Antagonists of  $\alpha v \beta 3$  Integrin, Enter the Cells by Independent Endocytic Pathways*. LABORATORY INVESTIGATION, 2001. **81**(12).
28. Cressman, S., et al., *Binding and Uptake of RGD-Containing Ligands to Cellular  $\alpha v \beta 3$  Integrins*. International Journal of Peptide Research and Therapeutics, 2008. **15**(1): p. 49-59.
29. Alanko, J., et al., *Integrin endosomal signalling suppresses anoikis*. Nat Cell Biol, 2015. **17**(11): p. 1412-21.
30. Muller, P.A., et al., *Mutant p53 drives invasion by promoting integrin recycling*. Cell, 2009. **139**(7): p. 1327-41.
31. Koch, S., et al., *Signal transduction by vascular endothelial growth factor receptors*. Biochem J, 2011. **437**(2): p. 169-83.
32. Merdzhanova, G., et al., *The transcription factor E2F1 and the SR protein SC35 control the ratio of pro-angiogenic versus antiangiogenic isoforms of vascular endothelial growth factor-A to inhibit neovascularization in vivo*. Oncogene, 2010. **29**(39): p. 5392-403.
33. Plein, A., A. Fantin, and C. Ruhrberg, *Neuropilin regulation of angiogenesis, arteriogenesis, and vascular permeability*. Microcirculation, 2014. **21**(4): p. 315-23.

34. Sawano, A., et al., *Flt-1 but not KDR/Flk-1 tyrosine kinase is a receptor for placenta growth factor, which is related to vascular endothelial growth factor*. *Cell Growth Differ*, 1996. **7**(2): p. 213-21.
35. Cao, Y., et al., *VEGF exerts an angiogenesis-independent function in cancer cells to promote their malignant progression*. *Cancer Res*, 2012. **72**(16): p. 3912-8.
36. Ellis, L.M. and D.J. Hicklin, *VEGF-targeted therapy: mechanisms of anti-tumour activity*. *Nat Rev Cancer*, 2008. **8**(8): p. 579-91.
37. Parker, M.W., et al., *Function of members of the neuropilin family as essential pleiotropic cell surface receptors*. *Biochemistry*, 2012. **51**(47): p. 9437-46.
38. Shintani, Y., et al., *Glycosaminoglycan modification of neuropilin-1 modulates VEGFR2 signaling*. *EMBO J*, 2006. **25**(13): p. 3045-55.
39. Yaqoob, U., et al., *Neuropilin-1 stimulates tumor growth by increasing fibronectin fibril assembly in the tumor microenvironment*. *Cancer Res*, 2012. **72**(16): p. 4047-59.
40. Pellet-Many, C., et al., *Neuropilins: structure, function and role in disease*. *Biochem J*, 2008. **411**(2): p. 211-26.
41. Hillman, R.T., et al., *Neuropilins are positive regulators of Hedgehog signal transduction*. *Genes Dev*, 2011. **25**(22): p. 2333-46.
42. Ge, X., et al., *Phosphodiesterase 4D acts downstream of Neuropilin to control Hedgehog signal transduction and the growth of medulloblastoma*. *Elife*, 2015. **4**.
43. Chaudhary, B., et al., *Neuropilin 1: function and therapeutic potential in cancer*. *Cancer Immunol Immunother*, 2014. **63**(2): p. 81-99.
44. Panigrahy, D., et al., *Regulation of soluble neuropilin 1, an endogenous angiogenesis inhibitor, in liver development and regeneration*. *Pathology*, 2014. **46**(5): p. 416-23.

45. Fassold, A., et al., *Soluble neuropilin-2, a nerve repellent receptor, is increased in rheumatoid arthritis synovium and aggravates sympathetic fiber repulsion and arthritis*. *Arthritis Rheum*, 2009. **60**(10): p. 2892-901.
46. Yang, S., et al., *Circulating soluble neuropilin-1 in patients with early cervical cancer and cervical intraepithelial neoplasia can be used as a valuable diagnostic biomarker*. *Dis Markers*, 2015. **2015**: p. 506428.
47. Parker, M.W., et al., *Structural basis for VEGF-C binding to neuropilin-2 and sequestration by a soluble splice form*. *Structure*, 2015. **23**(4): p. 677-87.
48. Abbasi, O., et al., *Soluble VEGFR1 concentration in the serum of patients with colorectal cancer*. *Surg Today*, 2015. **45**(2): p. 215-20.
49. Ock, C.Y., et al., *The distinct signatures of VEGF and soluble VEGFR2 increase prognostic implication in gastric cancer*. *Am J Cancer Res*, 2015. **5**(11): p. 3376-88.
50. Clegg, L.W. and F. Mac Gabhann, *Site-Specific Phosphorylation of VEGFR2 Is Mediated by Receptor Trafficking: Insights from a Computational Model*. *PLoS Comput Biol*, 2015. **11**(6): p. e1004158.
51. Mac Gabhann, F. and A.S. Popel, *Targeting neuropilin-1 to inhibit VEGF signaling in cancer: Comparison of therapeutic approaches*. *PLoS Comput Biol*, 2006. **2**(12): p. e180.
52. Imoukhuede, P.I. and A.S. Popel, *Expression of VEGF receptors on endothelial cells in mouse skeletal muscle*. *PLoS One*, 2012. **7**(9): p. e44791.
53. Napione, L., et al., *Unraveling the influence of endothelial cell density on VEGF-A signaling*. *Blood*, 2012. **119**(23): p. 5599-607.
54. Goel, H.L. and A.M. Mercurio, *VEGF targets the tumour cell*. *Nat Rev Cancer*, 2013. **13**(12): p. 871-82.
55. Jubb, A.M., et al., *Neuropilin-2 expression in cancer*. *Histopathology*, 2012. **61**(3): p. 340-9.

56. Jubb, A.M., et al., *Neuropilin-1 expression in cancer and development*. J Pathol, 2012. **226**(1): p. 50-60.
57. Holmqvist, K., et al., *The adaptor protein shb binds to tyrosine 1175 in vascular endothelial growth factor (VEGF) receptor-2 and regulates VEGF-dependent cellular migration*. J Biol Chem, 2004. **279**(21): p. 22267-75.
58. Koch, S. and L. Claesson-Welsh, *Signal transduction by vascular endothelial growth factor receptors*. Cold Spring Harb Perspect Med, 2012. **2**(7): p. a006502.
59. Duval, M., et al., *Vascular endothelial growth factor-dependent down-regulation of Flk-1/KDR involves Cbl-mediated ubiquitination. Consequences on nitric oxide production from endothelial cells*. J Biol Chem, 2003. **278**(22): p. 20091-7.
60. Zhang, Z., et al., *VEGF-dependent tumor angiogenesis requires inverse and reciprocal regulation of VEGFR1 and VEGFR2*. Cell Death Differ, 2010. **17**(3): p. 499-512.
61. Smith, G.A., et al., *VEGFR2 Trafficking, Signaling and Proteolysis is Regulated by the Ubiquitin Isopeptidase USP8*. Traffic, 2016. **17**(1): p. 53-65.
62. Fearnley, G.W., et al., *VEGF-A isoforms program differential VEGFR2 signal transduction, trafficking and proteolysis*. Biol Open, 2016.
63. Lemmon, M.A. and J. Schlessinger, *Cell signaling by receptor tyrosine kinases*. Cell, 2010. **141**(7): p. 1117-34.
64. Simons, M., *An inside view: VEGF receptor trafficking and signaling*. Physiology (Bethesda), 2012. **27**(4): p. 213-22.
65. Ballmer-Hofer, K., et al., *Neuropilin-1 promotes VEGFR-2 trafficking through Rab11 vesicles thereby specifying signal output*. Blood, 2011. **118**(3): p. 816-26.
66. Zhang, X. and M. Simons, *Receptor tyrosine kinases endocytosis in endothelium: biology and signaling*. Arterioscler Thromb Vasc Biol, 2014. **34**(9): p. 1831-7.

67. Soldi, R., et al., *Role of alphavbeta3 integrin in the activation of vascular endothelial growth factor receptor-2*. EMBO J, 1999. **18**(4): p. 882-92.
68. Byzova, T.V., et al., *A mechanism for modulation of cellular responses to VEGF: activation of the integrins*. Mol Cell, 2000. **6**(4): p. 851-60.
69. Reynolds, A.R., et al., *Stimulation of tumor growth and angiogenesis by low concentrations of RGD-mimetic integrin inhibitors*. Nat Med, 2009. **15**(4): p. 392-400.
70. Ellison, T.S., et al., *Suppression of beta3-integrin in mice triggers a neuropilin-1-dependent change in focal adhesion remodelling that can be targeted to block pathological angiogenesis*. Dis Model Mech, 2015. **8**(9): p. 1105-19.
71. Robinson, S.D., et al., *Alphav beta3 integrin limits the contribution of neuropilin-1 to vascular endothelial growth factor-induced angiogenesis*. J Biol Chem, 2009. **284**(49): p. 33966-81.
72. Montenegro, C.F., et al., *Blocking alphavbeta3 integrin by a recombinant RGD disintegrin impairs VEGF signaling in endothelial cells*. Biochimie, 2012. **94**(8): p. 1812-20.
73. Nam, J.O., et al., *FAS1 domain protein inhibits VEGF165-induced angiogenesis by targeting the interaction between VEGFR-2 and alphavbeta3 integrin*. Mol Cancer Res, 2012. **10**(8): p. 1010-20.
74. Sugahara, K.N., et al., *Tumor-penetrating iRGD peptide inhibits metastasis*. Mol Cancer Ther, 2015. **14**(1): p. 120-8.
75. Zanella, S., et al., *Synthesis, Characterization, and Biological Evaluation of a Dual-Action Ligand Targeting alphavbeta3 Integrin and VEGF Receptors*. ChemistryOpen, 2015. **4**(5): p. 633-41.
76. Hanahan, D. and J. Folkman, *Patterns and emerging mechanisms of the angiogenic switch during tumorigenesis*. Cell, 1996. **86**(3): p. 353-64.

77. Hurwitz, H., et al., *Bevacizumab plus irinotecan, fluorouracil, and leucovorin for metastatic colorectal cancer*. *N Engl J Med*, 2004. **350**(23): p. 2335-42.
78. Jain, R.K., et al., *Lessons from phase III clinical trials on anti-VEGF therapy for cancer*. *Nat Clin Pract Oncol*, 2006. **3**(1): p. 24-40.
79. Brooks, P.C., R.A. Clark, and D.A. Cheresh, *Requirement of vascular integrin alpha v beta 3 for angiogenesis*. *Science*, 1994. **264**(5158): p. 569-71.
80. Brooks, P.C., et al., *Integrin alpha v beta 3 antagonists promote tumor regression by inducing apoptosis of angiogenic blood vessels*. *Cell*, 1994. **79**(7): p. 1157-64.
81. Hood, J.D., et al., *Tumor regression by targeted gene delivery to the neovasculature*. *Science*, 2002. **296**(5577): p. 2404-7.
82. Hersey, P., et al., *A randomized phase 2 study of etaracizumab, a monoclonal antibody against integrin alpha(v)beta(3), + or - dacarbazine in patients with stage IV metastatic melanoma*. *Cancer*, 2010. **116**(6): p. 1526-34.
83. Uronis, H.E., et al., *A Phase I/biomarker study of bevacizumab in combination with CNTO 95 in patients with advanced solid tumors*. *Cancer Chemother Pharmacol*, 2015. **75**(2): p. 343-52.
84. Williams, R., *Discontinued in 2013: oncology drugs*. *Expert Opin Investig Drugs*, 2015. **24**(1): p. 95-110.
85. Robinson, S.D. and K.M. Hodivala-Dilke, *The role of beta3-integrins in tumor angiogenesis: context is everything*. *Curr Opin Cell Biol*, 2011. **23**(5): p. 630-7.
86. Bridges, E.M. and A.L. Harris, *The angiogenic process as a therapeutic target in cancer*. *Biochem Pharmacol*, 2011. **81**(10): p. 1183-91.
87. Grothey, A. and E. Galanis, *Targeting angiogenesis: progress with anti-VEGF treatment with large molecules*. *Nat Rev Clin Oncol*, 2009. **6**(9): p. 507-18.
88. Hong, T.M., et al., *Targeting neuropilin 1 as an antitumor strategy in lung cancer*. *Clin Cancer Res*, 2007. **13**(16): p. 4759-68.

89. Liang, W.C., et al., *Function blocking antibodies to neuropilin-1 generated from a designed human synthetic antibody phage library*. J Mol Biol, 2007. **366**(3): p. 815-29.
90. Pan, Q., et al., *Blocking neuropilin-1 function has an additive effect with anti-VEGF to inhibit tumor growth*. Cancer Cell, 2007. **11**(1): p. 53-67.
91. Xin, Y., et al., *Pharmacokinetic and pharmacodynamic analysis of circulating biomarkers of anti-NRP1, a novel antiangiogenesis agent, in two phase I trials in patients with advanced solid tumors*. Clin Cancer Res, 2012. **18**(21): p. 6040-8.
92. Weekes, C.D., et al., *A phase I study of the human monoclonal anti-NRP1 antibody MNRP1685A in patients with advanced solid tumors*. Invest New Drugs, 2014. **32**(4): p. 653-60.
93. Patnaik, A., et al., *A Phase Ib study evaluating MNRP1685A, a fully human anti-NRP1 monoclonal antibody, in combination with bevacizumab and paclitaxel in patients with advanced solid tumors*. Cancer Chemother Pharmacol, 2014. **73**(5): p. 951-60.
94. Gagnon, M.L., et al., *Identification of a natural soluble neuropilin-1 that binds vascular endothelial growth factor: In vivo expression and antitumor activity*. Proc Natl Acad Sci U S A, 2000. **97**(6): p. 2573-8.
95. Lu, Y., et al., *Identification of circulating neuropilin-1 and dose-dependent elevation following anti-neuropilin-1 antibody administration*. MAbs, 2009. **1**(4): p. 364-9.
96. Xin, Y., et al., *Anti-neuropilin-1 (MNRP1685A): unexpected pharmacokinetic differences across species, from preclinical models to humans*. Pharm Res, 2012. **29**(9): p. 2512-21.
97. Ruoslahti, E., *Tumor penetrating peptides for improved drug delivery*. Adv Drug Deliv Rev, 2016.
98. Sugahara, K.N., et al., *Tissue-penetrating delivery of compounds and nanoparticles into tumors*. Cancer Cell, 2009. **16**(6): p. 510-20.

99. Yan, F., et al., *Molecular imaging-guided photothermal/photodynamic therapy against tumor by iRGD-modified indocyanine green nanoparticles*. J Control Release, 2016. **224**: p. 217-28.
100. Binetruy-Tournaire, R., et al., *Identification of a peptide blocking vascular endothelial growth factor (VEGF)-mediated angiogenesis*. EMBO J, 2000. **19**(7): p. 1525-33.
101. Starzec, A., et al., *Structure-function analysis of the antiangiogenic ATWLPPR peptide inhibiting VEGF(165) binding to neuropilin-1 and molecular dynamics simulations of the ATWLPPR/neuropilin-1 complex*. Peptides, 2007. **28**(12): p. 2397-402.
102. Barr, M.P., et al., *A peptide corresponding to the neuropilin-1-binding site on VEGF(165) induces apoptosis of neuropilin-1-expressing breast tumour cells*. Br J Cancer, 2005. **92**(2): p. 328-33.
103. Starzec, A., et al., *Antiangiogenic and antitumor activities of peptide inhibiting the vascular endothelial growth factor binding to neuropilin-1*. Life Sci, 2006. **79**(25): p. 2370-81.
104. Wu, D., et al., *Anti-tumor effects of a novel chimeric peptide on S180 and H22 xenografts bearing nude mice*. Peptides, 2010. **31**(5): p. 850-64.
105. Kamarulzaman, E.E., et al., *Molecular modelling, synthesis and biological evaluation of peptide inhibitors as anti-angiogenic agent targeting neuropilin-1 for anticancer application*. J Biomol Struct Dyn, 2016: p. 1-20.
106. Kamarulzaman, E.E., et al., *New Peptide-Conjugated Chlorin-Type Photosensitizer Targeting Neuropilin-1 for Anti-Vascular Targeted Photodynamic Therapy*. Int J Mol Sci, 2015. **16**(10): p. 24059-80.
107. Jarvis, A., et al., *Small molecule inhibitors of the neuropilin-1 vascular endothelial growth factor A (VEGF-A) interaction*. J Med Chem, 2010. **53**(5): p. 2215-26.

108. Yue, B., et al., *Knockdown of neuropilin-1 suppresses invasion, angiogenesis, and increases the chemosensitivity to doxorubicin in osteosarcoma cells - an in vitro study*. Eur Rev Med Pharmacol Sci, 2014. **18**(12): p. 1735-41.
109. Li, X., et al., *RNA interference targeting NRP-1 inhibits human glioma cell proliferation and enhances cell apoptosis*. Mol Med Rep, 2011. **4**(6): p. 1261-6.
110. Schuch, G., et al., *In vivo administration of vascular endothelial growth factor (VEGF) and its antagonist, soluble neuropilin-1, predicts a role of VEGF in the progression of acute myeloid leukemia in vivo*. Blood, 2002. **100**(13): p. 4622-8.
111. Avallone, A., et al., *A randomized phase 3 study on the optimization of the combination of bevacizumab with FOLFOX/OXXEL in the treatment of patients with metastatic colorectal cancer-OBELICS (Optimization of BEvacizumab scheduLIng within Chemotherapy Scheme)*. BMC Cancer, 2015. **16**(1): p. 69.
112. Nishino, K., et al., *A randomized phase II study of bevacizumab in combination with docetaxel or S-1 in patients with non-squamous non-small-cell lung cancer previously treated with platinum based chemotherapy (HANSHIN Oncology Group 0110)*. Lung Cancer, 2015. **89**(2): p. 146-53.
113. Vasudev, N.S. and A.R. Reynolds, *Anti-angiogenic therapy for cancer: current progress, unresolved questions and future directions*. Angiogenesis, 2014. **17**(3): p. 471-94.
114. Ribatti, D., *Tumor refractoriness to anti-VEGF therapy*. Oncotarget, 2016.
115. Wong, P.P., et al., *Dual-action combination therapy enhances angiogenesis while reducing tumor growth and spread*. Cancer Cell, 2015. **27**(1): p. 123-37.
116. Cho, K., et al., *Therapeutic nanoparticles for drug delivery in cancer*. Clin Cancer Res, 2008. **14**(5): p. 1310-6.
117. Matsumura, Y. and H. Maeda, *A new concept for macromolecular therapeutics in cancer chemotherapy: mechanism of tumoritropic accumulation of proteins and the antitumor agent smancs*. Cancer Res, 1986. **46**(12 Pt 1): p. 6387-92.

118. Maeda, H., *Toward a full understanding of the EPR effect in primary and metastatic tumors as well as issues related to its heterogeneity*. Adv Drug Deliv Rev, 2015. **91**: p. 3-6.
119. Dufort, S., L. Sancey, and J.L. Coll, *Physico-chemical parameters that govern nanoparticles fate also dictate rules for their molecular evolution*. Adv Drug Deliv Rev, 2012. **64**(2): p. 179-89.
120. Bertrand, N., et al., *Cancer nanotechnology: the impact of passive and active targeting in the era of modern cancer biology*. Adv Drug Deliv Rev, 2014. **66**: p. 2-25.
121. Karageorgis, A., et al., *An MRI-based classification scheme to predict passive access of 5 to 50-nm large nanoparticles to tumors*. Sci Rep, 2016. **6**: p. 21417.
122. Hirsjarvi, S., et al., *Effect of particle size on the biodistribution of lipid nanocapsules: comparison between nuclear and fluorescence imaging and counting*. Int J Pharm, 2013. **453**(2): p. 594-600.
123. Cabral, H., et al., *Accumulation of sub-100 nm polymeric micelles in poorly permeable tumours depends on size*. Nat Nanotechnol, 2011. **6**(12): p. 815-23.
124. Sykes, E.A., et al., *Investigating the impact of nanoparticle size on active and passive tumor targeting efficiency*. ACS Nano, 2014. **8**(6): p. 5696-706.
125. Ciccione, J., et al., *Unambiguous and Controlled One-Pot Synthesis of Multifunctional Silica Nanoparticles*. Chemistry of Materials, 2016. **28**(3): p. 885-889.
126. Xu, S., et al., *Targeting receptor-mediated endocytotic pathways with nanoparticles: rationale and advances*. Adv Drug Deliv Rev, 2013. **65**(1): p. 121-38.
127. Danhier, F., A. Le Breton, and V. Preat, *RGD-based strategies to target alpha(v) beta(3) integrin in cancer therapy and diagnosis*. Mol Pharm, 2012. **9**(11): p. 2961-73.

128. Zhong, Y., et al., *Ligand-directed active tumor-targeting polymeric nanoparticles for cancer chemotherapy*. *Biomacromolecules*, 2014. **15**(6): p. 1955-69.
129. Benezra, M., et al., *Multimodal silica nanoparticles are effective cancer-targeted probes in a model of human melanoma*. *J Clin Invest*, 2011. **121**(7): p. 2768-80.
130. Phillips, E., et al., *Clinical translation of an ultrasmall inorganic optical-PET imaging nanoparticle probe*. *Sci Transl Med*, 2014. **6**(260): p. 260ra149.
131. Morlieras, J., et al., *Functionalization of small rigid platforms with cyclic RGD peptides for targeting tumors overexpressing alphavbeta3-integrins*. *Bioconjug Chem*, 2013. **24**(9): p. 1584-97.
132. Diou, O., et al., *RGD decoration of PEGylated polyester nanocapsules of perfluorooctyl bromide for tumor imaging: influence of pre or post-functionalization on capsule morphology*. *Eur J Pharm Biopharm*, 2014. **87**(1): p. 170-7.
133. Ragelle, H., et al., *Intracellular siRNA delivery dynamics of integrin-targeted, PEGylated chitosan-poly(ethylene imine) hybrid nanoparticles: A mechanistic insight*. *J Control Release*, 2015. **211**: p. 1-9.
134. Zitzmann, S., V. Ehemann, and M. Schwab, *Arginine-glycine-aspartic acid (RGD)-peptide binds to both tumor and tumor-endothelial cells in vivo*. *Cancer Res*, 2002. **62**(18): p. 5139-43.
135. Danhier, F., O. Feron, and V. Preat, *To exploit the tumor microenvironment: Passive and active tumor targeting of nanocarriers for anti-cancer drug delivery*. *J Control Release*, 2010. **148**(2): p. 135-46.
136. Kim, D., A.D. Friedman, and R. Liu, *Tetraspecific ligand for tumor-targeted delivery of nanomaterials*. *Biomaterials*, 2014. **35**(23): p. 6026-36.
137. Jencks, W.P., *On the attribution and additivity of binding energies*. *Proc Natl Acad Sci U S A*, 1981. **78**(7): p. 4046-50.

138. Kibria, G., et al., *Dual-ligand modification of PEGylated liposomes shows better cell selectivity and efficient gene delivery.* J Control Release, 2011. **153**(2): p. 141-8.
139. Hong, S., et al., *The binding avidity of a nanoparticle-based multivalent targeted drug delivery platform.* Chem Biol, 2007. **14**(1): p. 107-15.
140. Li, M.H., et al., *Evaluating binding avidities of populations of heterogeneous multivalent ligand-functionalized nanoparticles.* ACS Nano, 2014. **8**(6): p. 5600-9.
141. Ko, H.Y., et al., *A multimodal nanoparticle-based cancer imaging probe simultaneously targeting nucleolin, integrin alphavbeta3 and tenascin-C proteins.* Biomaterials, 2011. **32**(4): p. 1130-8.
142. Hayashi, Y., et al., *Multifunctional Envelope-Type Nano Device: Evolution from Nonselective to Active Targeting System.* Bioconjug Chem, 2015. **26**(7): p. 1266-76.
143. Kluza, E., et al., *Synergistic targeting of alphavbeta3 integrin and galectin-1 with heteromultivalent paramagnetic liposomes for combined MR imaging and treatment of angiogenesis.* Nano Lett, 2010. **10**(1): p. 52-8.
144. Singh, S.R., et al., *Intravenous transferrin, RGD peptide and dual-targeted nanoparticles enhance anti-VEGF intraceptor gene delivery to laser-induced CNV.* Gene Ther, 2009. **16**(5): p. 645-59.
145. Kluza, E., et al., *Dual-targeting of alphavbeta3 and galectin-1 improves the specificity of paramagnetic/fluorescent liposomes to tumor endothelium in vivo.* J Control Release, 2012. **158**(2): p. 207-14.
146. Dong, J., et al., *Stable IgG-like bispecific antibodies directed toward the type I insulin-like growth factor receptor demonstrate enhanced ligand blockade and anti-tumor activity.* J Biol Chem, 2011. **286**(6): p. 4703-17.
147. Bostrom, J., et al., *Variants of the antibody herceptin that interact with HER2 and VEGF at the antigen binding site.* Science, 2009. **323**(5921): p. 1610-4.
148. Chiu, G.N., et al., *Modulation of cancer cell survival pathways using multivalent liposomal therapeutic antibody constructs.* Mol Cancer Ther, 2007. **6**(3): p. 844-55.

149. Domingo-Espin, J., et al., *RGD-based cell ligands for cell-targeted drug delivery act as potent trophic factors*. *Nanomedicine*, 2012. **8**(8): p. 1263-6.
150. Schwab, E.H., et al., *Nanoscale control of surface immobilized BMP-2: toward a quantitative assessment of BMP-mediated signaling events*. *Nano Lett*, 2015. **15**(3): p. 1526-34.
151. Benezra, M., et al., *Ultrasmall integrin-targeted silica nanoparticles modulate signaling events and cellular processes in a concentration-dependent manner*. *Small*, 2015. **11**(14): p. 1721-32.
152. Rapraeger, A.C., *Synstatin: a selective inhibitor of the syndecan-1-coupled IGF1R- $\alpha$ v $\beta$ 3 integrin complex in tumorigenesis and angiogenesis*. *FEBS J*, 2013. **280**(10): p. 2207-15.
153. Parsons, J.T., *Focal adhesion kinase: the first ten years*. *J Cell Sci*, 2003. **116**(Pt 8): p. 1409-16.
154. Janostiak, R., et al., *Mechanosensors in integrin signaling: the emerging role of p130Cas*. *Eur J Cell Biol*, 2014. **93**(10-12): p. 445-54.
155. Fujiwara, K., *Platelet endothelial cell adhesion molecule-1 and mechanotransduction in vascular endothelial cells*. *J Intern Med*, 2006. **259**(4): p. 373-80.
156. Collins, C., et al., *Localized tensional forces on PECAM-1 elicit a global mechanotransduction response via the integrin-RhoA pathway*. *Curr Biol*, 2012. **22**(22): p. 2087-94.
157. Nilius, B. and G. Droogmans, *Ion channels and their functional role in vascular endothelium*. *Physiol Rev*, 2001. **81**(4): p. 1415-59.
158. Miyamoto, S., S.K. Akiyama, and K.M. Yamada, *Synergistic roles for receptor occupancy and aggregation in integrin transmembrane function*. *Science*, 1995. **267**(5199): p. 883-5.

159. Conner, S.D. and S.L. Schmid, *Regulated portals of entry into the cell*. Nature, 2003. **422**(6927): p. 37-44.
160. Sigismund, S., et al., *Endocytosis and signaling: cell logistics shape the eukaryotic cell plan*. Physiol Rev, 2012. **92**(1): p. 273-366.
161. Duncan, R. and S.C. Richardson, *Endocytosis and intracellular trafficking as gateways for nanomedicine delivery: opportunities and challenges*. Mol Pharm, 2012. **9**(9): p. 2380-402.
162. Leventis, P.A. and S. Grinstein, *The distribution and function of phosphatidylserine in cellular membranes*. Annu Rev Biophys, 2010. **39**: p. 407-27.
163. Sarrazin, S., W.C. Lamanna, and J.D. Esko, *Heparan sulfate proteoglycans*. Cold Spring Harb Perspect Biol, 2011. **3**(7).
164. Kay, J.G. and S. Grinstein, *Phosphatidylserine-mediated cellular signaling*. Adv Exp Med Biol, 2013. **991**: p. 177-93.
165. Busser, B., et al., *Amphiregulin promotes BAX inhibition and resistance to gefitinib in non-small-cell lung cancers*. Mol Ther, 2010. **18**(3): p. 528-35.

**Title:** Definition of bifunctional theranostic molecules for cancer treatment

**Key words:** cancer; angiogenesis; integrin; neuropilin; VEGFR; nanomedicine; signaling

Tumor angiogenesis refers to the ability of a tumor to stimulate new blood vessels formation. Angiogenesis strongly depends on cell surface receptors and integrin activation to promote tumor progression, local invasion and dissemination. Integrins (especially integrin  $\alpha_v\beta_3$ ) and Neuropilin-1 (NRP1), a co-receptor of VEGFR2, are over-expressed in the tumor vasculature and by tumor cells, and their expression has been correlated with tumor progression. Importantly, integrin  $\alpha_v\beta_3$  and NRP1 can physically and functionally interact.

The use of dual targeted drugs that block the integrin  $\alpha_v\beta_3$  and the NRP1 receptor simultaneously is thus expected to augment the anti-angiogenic and anti-tumor activities, as compared to each “mono-therapy” separately. During my PhD studies, in collaboration with the group of chemists leaded by Pr G. Subra, we generated different batches of bifunctional cRGD/ATWLPPR peptides coated nanoparticles (NPs) targeting integrin  $\alpha_v\beta_3$  and NRP1 simultaneously. We introduced different ratio of cRGD and ATWLPPR peptides (100/0, 25/75, 50/50, 75/25 and 0/100), and we also increased the amount of total ligands on the surface of the silica NPs. Systematic studies including molecules' affinity, selectivity, and biological activity as well as anti-angiogenic and anti-tumoral effects were performed on primary endothelial cells (ECs), immortalized ECs and several tumor cells. NPs properties were also evaluated *in vivo* in a mouse tumor model. We report here that these NPs present highly variable biological activities in ECs and tumor cells depending on the peptides ratio, surface coating of the NPs and on their concentration. In particular, “elevated” concentrations of NPs, which actually correspond to usual concentrations of peptides, can activate an unexpected IGF1-R/IR-AKT signaling pathway that could lead to a counter-productive pro-angiogenic activity (agonist instead of antagonist). This could mimic the conflicting results obtained in clinical trials using Cilengitide, an RGD-presenting peptide, and thus provide new areas of investigations and new possibilities to design active nano-drugs.

This work can thus participate to the general effort of our research community to design efficient targeted anti-angiogenic therapies that could be applied in particular for cancer treatment.

**Titre :** Définition de molécules théranostiques bifonctionnelles pour le traitement du cancer

**Mots clés :** cancer; angiogénèse; intégrine; neuropiline; VEGFR; nanomédecine; signalisation

L'angiogénèse tumorale réfère à la capacité d'une tumeur à stimuler la formation de nouveaux vaisseaux sanguins. L'induction de l'angiogénèse dépend notamment de la présence de certains récepteurs exprimés à la surface de cellules endothéliales et tumorales. Ces récepteurs sont impliqués dans la formation de nouveaux vaisseaux sanguins mais aussi dans la progression des tumeurs, l'invasion locale des tissus avoisinants et la formation de métastases. Nous nous intéressons ici essentiellement aux récepteurs de type intégrines (et surtout l'intégrine  $\alpha_v\beta_3$ ) ou neuropiline-1 (NRP1).

Les intégrines sont des récepteurs transmembranaires décrits initialement parce qu'ils permettent aux cellules d'adhérer et de se déplacer sur la matrice extracellulaire (ECM) en particulier parce qu'elles se lient à la séquence tri-peptidique RGD, mais elles interviennent aussi directement et indirectement dans les échanges biochimiques entre les cellules et leur micro-environnement. NRP1 est un corécepteur du VEGF (vascular endothelial growth factor). Pour cela, NRP1 s'associe au récepteur principal VEGFR2, surexprimé dans les tumeurs et dont l'expression a été corrélée avec l'angiogénèse. Il est très important de noter que l'intégrine  $\alpha_v\beta_3$  et le récepteur NRP1 peuvent interagir physiquement et fonctionnellement. Notre hypothèse de travail est alors qu'en bloquant la fonction de ces 2 récepteurs nous pourrions augmenter l'efficacité des thérapies anti-angiogéniques anti-tumorales.

Nous avons généré des nanoparticules de silices bifonctionnelles car elles présentent à leur surface à la fois des peptides cycliques cRGD ciblant l'intégrine  $\alpha_v\beta_3$  et ATWLPPR qui cible NRP1. Nous avons testé des ratio différents de peptides cRGD et ATWLPPR (100/0, 25/75, 50,75/50/25 et 0/100), et nous avons aussi optimisé le nombre total de ces ligands/NP. Nous avons analysé l'affinité des différentes molécules, leur sélectivité et activité biologique ainsi

que leurs propriétés anti-angiogéniques et anti-tumorale en particulier sur des cellules endothéliales humaines (ECs) et sur des lignées de cellules tumorales.

Notre étude suggère que ces nanoparticules bifonctionnelles présentent un grand potentiel si leur composition est soigneusement définie. En particulier, elles peuvent présenter des activités extrêmement variables voir opposées suivant la nature et composition de leur surface et de la concentration à laquelle les NPs sont utilisées. En effet, à « haute concentration » en NP, ce qui correspond en fait à une faible concentration en peptides, nous montrons qu'il est possible d'obtenir un effet « pro-angiogénique » lié au recrutement d'autres récepteurs de facteurs de croissance (IGF1-R/IR) qui a priori ne devaient pas intervenir dans notre système, mais semblent pouvoir être fonctionnellement liés aux intégrines et/ou NRP1 en réponse aux particules présentant les 2 peptides cRGD et ATWLPPR. Ces résultats contribuent à expliquer certains échecs thérapeutiques des agents anti-angiogéniques mais nous permettent aussi de proposer des solutions attractives pour la définitions nouveaux agents thérapeutiques.